THE UNIVERSITY
of EDINBURGH

The Role of ANLN in Post Ischaemic Angiogenesis

Ben Cathcart

Submitted for the degree of Doctor of Philosophy

University of Edinburgh 2019

Abstract:

Angiogenesis is a key physiological process by which new blood vessels are dynamically formed in Endothelial cell (EC) driven processes. The identification of new potential genes of interest in ECs can help to further understand the underlying mechanisms of angiogenesis and help develop new therapeutic strategies for cardiovascular disease. One such gene identified in the Caporali lab is Anillin (ANLN) an F-actin binding protein with functions in cytokinesis, asymmetric cell division and potential roles in migration and proliferation in multiple cell types.

We identified that ANLN was highly upregulated in the ECs of a mouse model of hind limb ischaemia. *In vitro* modulation of ANLN expression with siRNA and ANLN-EGFP lentivirus in HUVECs identified an effect of ANLN expression on multiple aspects of EC function including, migration wound healing and barrier function. A correlation between ANLN expression and tubulogenesis assay performance was observed associating ANLN with an early model of sprouting angiogenesis. A potential regulatory mechanism of ANLN by ZFP36 RNA binding proteins was identified in vascular inflammation and ischaemia *in vivo* and *in vitro*. Based on *in vitro* observations, ANLN expression was investigated in the ECs of the developing vasculature, and in a model of vascular injury using the *anln:anln-eGFP* x *flk:mcherry* reporter zebrafish. ANLN was not associated with the 24 hpf developing vasculature in the trunk, CNS or tail of the fish however there was a strong band of *Anln*$^{+ve}$ cells near the developing trunk vasculature and caudal artery plexus. A micro point laser injury of the caudal artery was developed; with injuries being recoverable 24 hours post injury and causing association of neutrophils with injury sites. Anln was not observed in ECs of the caudal artery after laser injury, however, increased Anln^{+ve} cells are observed in mechanical injury of the tail fin identifying Anln expression in a response to injury. Hypomorphic modulation of *anln* expression by morpholino injection of *flk:gfp* embryos did not alter the vascular morphology of the 2-3 dpf zebrafish vasculature.

This data for the first time associates ANLN with the EC response to the angiogenic response in ischaemia. Although our zebrafish study was mostly negative a new method for inducing vascular injury in zebrafish was developed and there was a novel application of an *anln:anln-eGFP* zebrafish for the investigation of ANLN in vascular regeneration. Our vascular injury model for the investigation of ANLN can be improved by utilising a mechanical method of vessel injury for further studies. Application of vascular specific CRISPR/CAS9 mutation of

ANLN expression may improve identification of a vascular phenotype in zebrafish, which was not observed with morpholino injection. Further *in vitro* experiments should focus on ANLN-EGFP in sprouting angiogenesis models and investigating a potential nuclear role of ANLN.

Lay abstract:

Cardiovascular disease is the leading cause of death world-wide, this is caused by the blockage of blood vessels, leading to heart attacks and poor blood flow in the legs. Both of these conditions can cause life changing health effects and death. In response to these diseases, the body needs to grow new blood vessels from existing vessels to supply tissues that are not receiving enough blood flow. This process is referred to as “angiogenesis” (new blood vessel formation) and is guided by a specialist cell called the endothelial cell.

In my PhD I investigated the effect of a protein called Anillin on endothelial cell function in angiogenesis. It was found that altering levels of Anillin altered the movement and general function of endothelial cells in cell based experiments that mimic angiogenesis.

Zebrafish embryos were used to identify Anillin expression in a live model of angiogenesis and blood vessel injury. The zebrafish embryos used had fluorescent blood vessels and a modified fluorescent version of Anillin, this allowed identification of Anillin’s location in individual endothelial cells. There was no association of fluorescent Anillin with the developing blood vessels in the embryos. A new method for investigating blood vessel injury was created, using a laser to damage a large blood vessel in the embryo and observing it recover. There was no association of fluorescent Anillin with the recovering injured vessels, but this may be due to the weak detectable Anillin fluorescence.

In conclusion further research can be used to identify ANLNs role in endothelial cells in angiogenesis. We could further investigate potential interactions of ANLN with other proteins to identify how it functions in angiogenesis to try and develop new therapies for cardiovascular disease. The new zebrafish vessel injury can be used to investigate how blood vessels develop and regenerate.

DECLARATION

The thesis herein is solely my own work. Apart from where stated the experiments were performed entirely by me. I confirm that this work has not been previously submitted for any other degree.

…….

Contributions:

Here in are contributions to the work in this thesis, with the location and contributor named, and the contributor referenced in the relevant figure legend.

Location	Contributor	Data
Chapter 3	L. Rose A. Caporali	Figure 3.3.1B+C Figure 3.3.2A, 3.3.5A+C, 3.3.7C, 3.3.8A
Chapter 4	L. Rose	Figure 2.2.1A+B, 2.2.2A+B

Acknowledgements:

I have enjoyed the support of numerous people throughout my PhD. I would like to thank my primary supervisor Andrea Caporali for his guidance throughout the project. I would like to thank the input of my second supervisor Marco Meloni and Chairperson Matthew Bailey for their input in my annual reviews. I would like to say a huge thanks to my third supervisor Sonja Vermeren for her practical advice during my PhD project and the support she gave me during my thesis write up.

I would like to thank my collaborator Lucia Poggi for providing the zebrafish line and molecular tools for the zebrafish portion of this project.

I would like to thank Carl Tucker, the students of the Denvir group, and Lisa Ni Challaigh for their vital advice in the zebrafish facility. Included in this are the CALM microscopy facility staff, particularly Charlotte Buckley who supported me through training and advice.

I would like to thank my fellow PhD Vlad Miscianinov and Andrea Martello for their companionship during our times in the lab together. I would like to thank David Mellis for his continued support during the later period of my PhD.

Finally I would like to acknowledge the support of my family and friends over the years.

Contents

Chapter 1:

Introduction

1.1 The function and structure of the cardiovascular system:

The cardiovascular system is a key collection of tissues and organs that evolved in response to the limitations of diffusion in the supply of oxygen and the removal of the waste products of respiration (Siddall 2004). Vertebrate species possess a collection of large and small blood vessels supplying the organs with oxygenated blood and removing deoxygenated blood (Monahan-Earley et al. 2013).

Blood vessels carry blood flow from the heart and are made up mainly of four cells types, endothelial cells (ECs), vascular smooth muscle (VSMC), pericyte and, occasionally neuronal cells. These cells are organised into 4 vessel categories. Arteries and arterioles carry oxygenated blood whereas veins and venules carry deoxygenated blood (Lake 1985). The arterioles are adapted for carrying high pressure blood and feature a thick external tunica adventitia consisting of connective tissues and a thick medial layer of concentric smooth muscle cells, that maintain an elastic quality (Lake 1985). They lead into a large network of capillaries consist of endothelial cells with only a sparse covering of pericytes. The capillaries maintain the homeostasis of tissues by allowing the passive transport of metabolites into the tissues and waste products of respiration away for excretion (Lake 1985). Veins and venules are adapted to carry low pressure blood and are similarly structured to the arteries, except that they contain valves that protrude into the lumen to prevent backflow. The integrity of these vascular structures is a key component of homeostasis, disruption of their integrity results in numerous adverse clinical disorders.

1.2 Cardiovascular disease:

Currently the second leading cause of death globally, cardiovascular disease is associated with many contributing factors including obesity, old age, and diabetes (Hennekens & Gaziano 1993). Cardiovascular disease begins with atherosclerosis, where lipid plaques develop in the vessels. Atherosclerotic plaque number and size increase with age and are used as an overall indicator of cardiovascular health (Ross 1999; Lang & Insull 1970). These plaques arise from an initial insult to the endothelial cell (EC) layer and the deposition of lipids between the intimal and medial layers of the vessel, referred to as atherosis (Steinbrecher et al. 1984). This results in a raised plaque which increases in size exhibiting a dense lipid core. Neutrophil accumulation induces a focal point of inflammation, an external sclerosis is formed by vascular smooth muscle cell (VSMC) proliferation (Newby & Zaltsman 1999). VSMC proliferation generates a fibrous cap covering the lipid core which partially occludes the vessel. Inflammation and cell death can lead to rupture of the fibrous cap, allowing exposure of the lipid core to circulating platelets, and eventually resulting in thrombus formation (Falk 1992). Thrombi can induce the complete occlusion of a vessel and result in a critical loss of blood flow defined as Ischaemia, causing damage to the supplied tissue (*Figure 1.1*).

Ischaemic heart disease is caused by atherosclerotic plaque formation in the descending coronary arteries (Vlodaver & Edwards 1971). Plaque rupture results in acute ischaemia of the heart muscle causing myocardial infarction (Fuster et al. 1992). There is rapid damage to the cardiomyocytes induced by hypoxia, reactive oxygen species and inflammation resulting in death of the ischaemic portion of the heart muscle. Due to the low regenerative capacity of the heart, dead cells are replaced by fibroblasts resulting in a reduction of its contractility and pathological muscle remodelling (Fuster et al. 1992). This results in the progression to eventual heart failure as the heart becomes unable to maintain normal cardiac output resulting in disability and death (Cohn 1996). Peripheral artery disease (PAD) is major symptom of systemic atherosclerosis with 12% of the adult population suffering from this condition (Caporali et al. 2018). PAD initially results in acute pain caused by

transient ischaemia in the lower limb and this can progress to critical limb ischaemia. Critical limb ischaemia is the acute loss of blood flow to the lower limbs resulting in insufficient perfusion of skeletal muscle (Ouriel 2001). This results in EC dysfunction, chronic inflammation and tissue necrosis, eventually requiring the amputation of affected limbs.

Typical care consists of initial anti-thrombotic treatment to remove thrombi and vein grafting or stent insertion to stabilise unstable atherosclerotic plaques (Hlatky et al. 2004). Vein grafting uses a non-diseased vein typically from the lower limb, grafted onto the diseased artery to bypass the occluded vessel. While this treatment is very effective in the short-term, the procedure can have catastrophic failure within one year of surgery giving it a limited long term life span (De Vries et al. 2016). Stenting is the insertion of a cylindrical drug eluting metal construct into the affected arteries to forcibly open the artery and prevent further atherosclerosis and reduce thrombus formation (Mattichak et al. 2008). These approaches whilst effective as immediate treatments to stabilise ischaemic disease, don't improve overall cardiovascular health or aid the formation of new blood vessels. There is therefore a clinical need for new therapeutic approaches that improve the body's natural process for blood vessel formation to stabilise ischaemic disease.

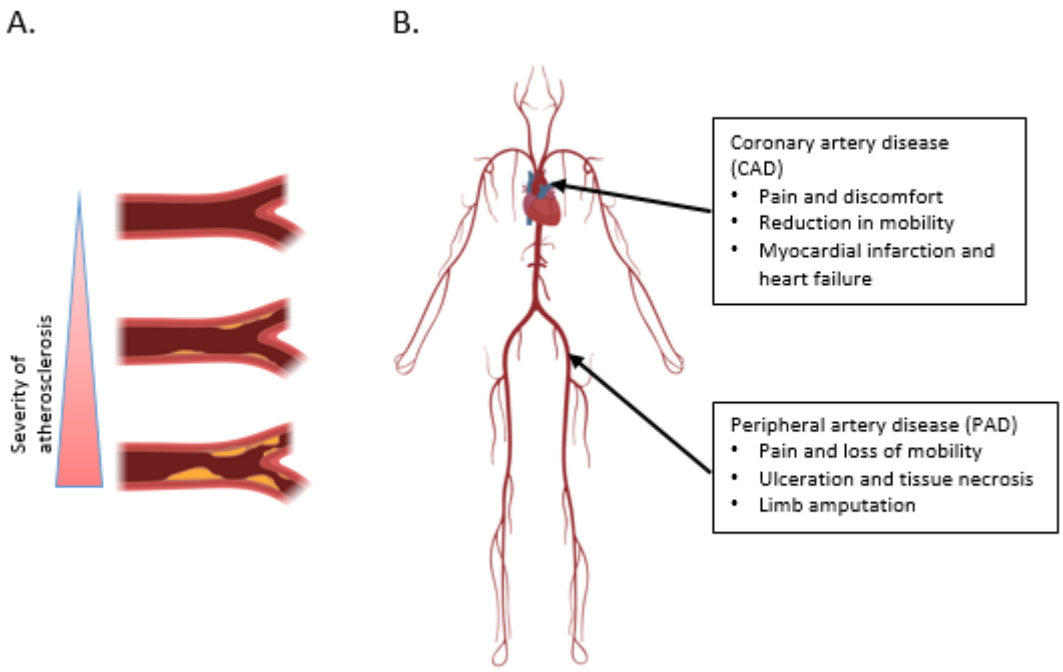

Figure 1.1: The progression of Atherosclerosis leads to common ischaemic diseases

(A) Cardiovascular disease caused by increasing atheroma formation in the arteries reducing blood flow and creating chronic ischaemia. (B) Plaque ruptures result in critical ischaemia in key tissues including the heart and peripheral lower limbs leading to coronary and peripheral artery disease.

1.3. Cardiovascular Development:

The blood vessels form early on in embryonic development, and this process is referred to as vasculogenesis. During gastrulation of the embryo, at E6.5-7 haemangioblasts arise from the mesoderm in the blood islands of the yolk sac (Drake & Fleming 2000). These cells differentiate into the early haematopoietic stem cells and angioblasts, the angioblasts form tube like structures and differentiate into the early ECs. The ECs coalesce to form a primitive vascular plexus, a primitive lumen, and they begin to secrete an extracellular matrix. This early vascular plexus connects to the pre-contractile heart tube (Patel-Hett & D'Amore 2011). The differentiation of these primitive vessels into a more complicated network containing arteries and veins is controlled by multiple signalling mechanisms and this has been described in detail as observed in zebrafish in section 1.12.

1.4 The Angiogenesis process:

The sprouting of new vessels from mature vascular networks is defined as angiogenesis (Folkman 1971) (*Figure 1.2*). At rest, blood vessels are quiescent, forming a confluent barrier of ECs. EC junctions consist of VE-cadherin (VCAD) and adherens junctions that maintain vascular homeostasis and promote resistance to secreted factors that alter vascular structures (*table 1*) (Ehling et al. 2013; Giannotta et al. 2013).

Table 1 Key angiogenic factors:

Factor	nomenclature	Function	reference
Vascular endothelial growth factor	VEGF A-E	Guides EC migration, promotes proliferation survival and increases vessel permeability	(Blanco & Gerhardt 2013)
Fibroblast growth factor	FGF, FGF	Promotes capillary morphogenesis and vessel lumenisation	(Carmeliet & Jain 2011)
Tumour necrosis factor α	TNF-α	Stimulates inflammatory response and growth factor release from tissues.	(Klagsbrun & D'amore 1991)
Transforming growth factor-beta	TGFβ 1-3	Promotes mural cell attachment and extra cellular matrix degradation.	(Pardali et al. 2010)
Angiopoietins	ANG-1,2	Alters vessel stability by regulating permeability and mural cell attachment.	(Augustin et al. 2009)
Platelet derived growth factor B	PDGF-B	Promotes vessel maturation by influencing mural cell recruitment.	(Gaengel et al. 2009)

After ischaemic insult or wound repair, the ECs become activated by hypoxia or inflammatory mediators released by the surrounding tissues. Secretion of matrix metalloproteinases (MMP), including MMP1/2, allows for digestion of the

extracellular matrix (ECM) followed by ANG-2 stimulation and detachment VSMCs and pericytes (Blasi & Carmeliet 2002; Eble & Niland 2009; Augustin et al. 2009). Growth factors stored in the ECM are liberated during ECM degradation and affect the initial increase in EC motility (Arroyo & Iruela-Arispe 2010).

VEGF is the most important growth factor in angiogenesis (*table 2*). VEGF is secreted by the surrounding tissue and acts on the exposed ECs to promote sprouting angiogenesis, this is driven by a VEGF concentration gradient in the tissue (Gerhardt et al. 2003). ECs located at the highest concentration of VEGF become tip cells that migrate along the VEGF gradient (Gerhardt et al. 2003). Neighbouring ECs at lower VEGF concentrations become proliferating stalk cells that make the body of the new vessel. The differences in tip and stalk cell behaviour is affected by different VEGF signalling. VEGFR2 mediates the majority of VEGF signalling by receptor tyrosine kinase activation in combination with its co receptor NRP-1/2 (Takahashi & Shibuya 2005). VEGFR1, expressed mainly by the stalk cell acts as an antagonist of VEGF activity, alternatively spliced soluble VEGFR1 is secreted by stalk cells to sequester free VEGF (Kendall & Thomas 1993; Chappell et al. 2009; Roberts et al. 2004). Tip/stalk cell designation is referred to as dorsal lateral inhibition, a process where adjacent cells can influence the phenotype of neighbouring cells.

Table 2 Key VEGF signalling components in angiogenesis:

Signalling component	Role	References
Vascular endothelial growth factor (VEGF)	Soluble ligand of VEGF receptors, present in multiple isoforms (VEGF-A-E) and splice variants with VEGF-A mediating most of its effects in angiogenesis.	(Tischer et al. 1991)
Vascular endothelial growth factor receptor 2 (VEGFR2)	Receptor of VEGF and the main mediator of angiogenic signalling controlling EC proliferation, survival and migration.	(Waltenberger et al. 1994)
Neuropilin 1/2 (NRP-1/2)	Acts a co-receptor with VEGFR1 and VEGFR2 to enhance VEGF signal transduction.	(Soker et al. 1998)
Vascular endothelial growth factor receptor 1 (VEGFR1)	High affinity receptor for VEGF-A but with low receptor tyrosine kinase activity, acts as a sink for VEGF to maintain VEGF gradients in angiogenesis.	(Waltenberger et al. 1994)

There is a significant interplay between Notch and VEGF signalling in controlling dorsal lateral inhibition as shown in *figure 1.2*. Notch signalling is a highly conserved intercellular contact mediated receptor ligand interaction that is involved in cell fate and tissue development (Karsan 2005). In dorsal lateral inhibition VEGFR2 receptor signalling upregulates Dll4 notch ligand in the newly defined tip cells (Lobov et al. 2007). Dll4 interacts with the Notch receptor on stalk cells and suppresses VEGFR2 and NRP1/2 expression while upregulating VEGFR1 (Eilken & Adams 2010). Expression of the Notch ligand JAGGED on stalk cells antagonises Dll4 activation of Notch on the tip cell, thus, enhancing VEGFR2 expression and suppressing VEGFR1 expression (Kofler & Simons 2015). This dynamic interaction between VEGF and Notch signalling helps to maintain the tip/stalk cell behaviour and allows orderly angiogenesis. Leading edge tip ECs form extensive filopodia driven by VEGFR2

activation of CDC42 driving migration towards the chemoattractant VEGF (De Smet et al. 2009). Stalk cells supported by FGF2 expression proliferate forming intercellular connections and begin to generate the ECM to provide structural support to the new vessel (Du et al. 2016).

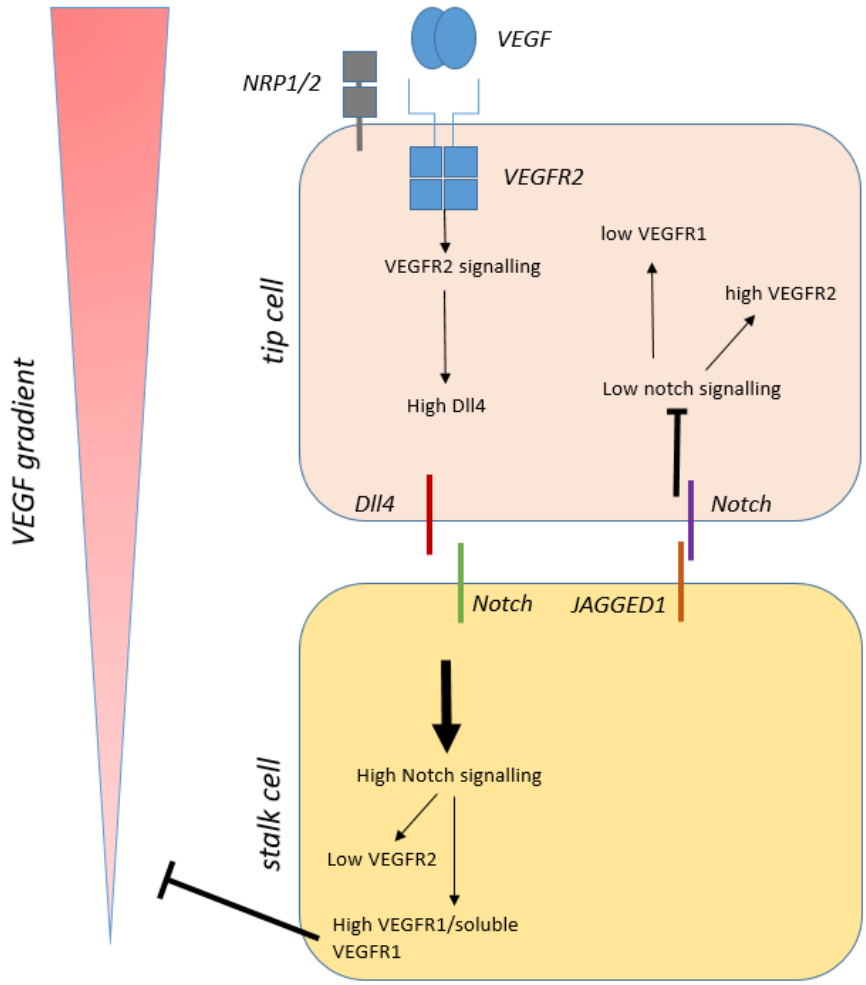

Figure 1.2 Dorsal lateral inhibition by VEGF and Notch signalling drives EC migration and proliferation:

VEGF secreted by surrounding tissues acts on VEGFR2 on ECs closest to the highest VEGF concentration. Activation of VEGFR2 and its co-receptor activate downstream signalling pathways to generate the migratory tip cell phenotype which is the leading migrating EC. High VEGFR2 signalling increases Dll4 Notch ligand integration in to the membrane which activates the Notch receptor on neighbouring proliferative stalk cells. This suppresses VEGFR2 expression in the stalk cell and promotes VEGFR1 and soluble VEGFR1 expression, VEGFR1 sequesters VEGF from the surrounding cells maintaining a polarising VEGF gradient. Simultaneously JAGGED1 Notch ligand antagonises Dll4 Notch signalling in the tip cell suppressing Notch mediated expression of VEGFR1. This paradigm maintains the distinct migratory tip cell and the proliferative stalk cell to allow for organised angiogenesis. Adapted from (Blanco & Gerhardt 2013)

As new networks are formed, tip cell filopodia interact to form branching vessels and the two vessels anastamose by forming VE-cadherin rich connections (Fantin et al. 2010). Lumenisation of the new vessel occurs through apical-basal polarisation of ECs, wherein, parallel stalk cells connected by apical VE-cadherin junctions integrate negatively charged glycoproteins into the apical EC membrane (Strilić et al. 2009). The negatively charged apical membrane gives a repulsive signal which encourages lumenisation of the new vessel with EC architecture modulated by VEGF activation of Rho kinase (ROCK) (Zeeb et al. 2010). Secretion of tissue inhibitors of metalloproteinases (TIMPs) allows for regeneration of the ECM and establishment of EC junctional integrity (Stetler-Stevenson & Seo 2005). Vessel quiescence is encouraged by VSMC and pericyte recruitment supported by the secretion of ANG-1, PDGF-B, S1P and TGF-β by ECs (Krump-Konvalinkova et al. 2005; Allende & Proia 2002; Lindblom et al. 2003). After stabilisation of the new vessel, blood flow begins to the ischaemic or injured area (*figure 1.3*).

In ischaemia and inflammation, neutrophils and macrophages of the immune system have key roles in angiogenesis (Campbell 2015). Factors like VEGF and TNF-α are released by macrophages and neutrophils in ischaemia, impacting on EC migration (Stark et al. 2013; Gong & Koh 2010). Neutrophil secretion of MMPs assists in basement matrix degradation promoting increased EC motility, in ischaemia and inflammation the loss of neutrophil presence is a hallmark of new vessel quiescence (Ardi et al. 2007). Tip cell fusion events at sites of anastomosis are mediated in part by macrophages which associate with the junction between two new vessels. This improves cell to cell communication before VE-cadherin mediated filopodia interaction and vessel fusion (Liu et al. 2016; Fantin et al. 2010).

The transcription factor hypoxia induced factor 1 (HIF-1α) is a key regulator of angiogenesis. HIF-1α controls a number of key genes in the EC response to O_2 deprivation by binding to hypoxia response elements in target genes (Semenza 2012). MMP-2 and associated metalloproteinases are direct targets of HIF-1α leading to an initial increase in EC motility in early angiogenesis (Shweiki et al. 1992; Krock et al. 2011). Other important targets include VEGF-A, VEGFR1, PDGF-B, ANG-1, and, ANG-

2 with further control of genes involved in autophagy and PH regulation (Semenza 2012). Partial knockout of HIF-1α in mice results in an impaired angiogenesis in hind limb ischaemia and reduced limb perfusion (Bosch-Marce et al. 2007).

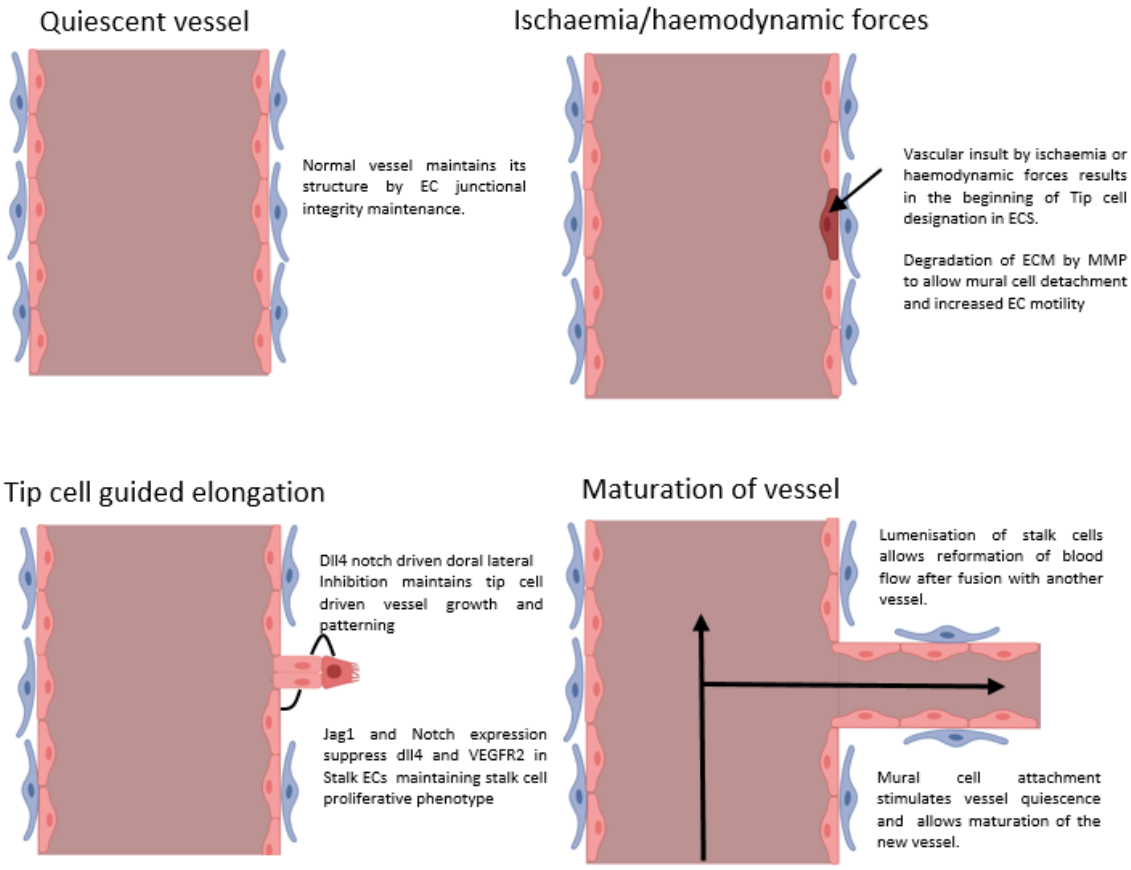

Figure 1.3: Haemodynamic forces and ischaemia induces sprouting angiogenesis:

Quiescent vessels exhibit very little proliferation and cell migration but upon ischaemic challenge or haemodynamic stresses sprouting begins. Vessel dilation followed by tip cell selection allows for sprouting of a new vessel with dorsal-lateral inhibition by VEGF/Notch signalling maintaining tip and stalk cell heterogeneity. After fusion with another sprouting vessel lumenisation occurs and vessel quiescence is supported by mural cell attachment and restoration of EC junctional integrity (Potente et al. 2011).

1.5 The failure of endogenous angiogenesis in cardiovascular disease:

Failure of endogenous angiogenesis to provide an adequate response in cardiovascular disease is a key area of interest to develop therapies to improve the clinical outcome in ischaemic conditions (Dragneva et al. 2013).

In critical PAD, limb loss is attributed to a failure of vessel collateralisation of the ischaemic limb for a number of reasons (Scholz et al. 2002; Ziegler et al. 2010). Atherosclerotic plaques form throughout the vessels of the lower limb leading to a gradual decrease in blood pressure and increased hypoxia (Dragneva et al. 2013). This condition leads to maximal vasodilation of arterioles and EC resistance to vasodilatory stimuli. Increased reactive oxygen species and inflammation leads to EC dysfunction in capillaries (Coats & Wadsworth 2005). EC dysfunction in the micro vessels leads to small thromboses and the gradual accumulation of oedema, promoting fibrosis of tissue and gradual necrosis. The resulting ischaemic condition worsens and due to encroaching irreparable necrosis removal of the affected limb is required (Dragneva et al. 2013).

The lack of appropriate angiogenesis in coronary artery disease is observable clinically through the prevalence of angina (Ischaemic pain in the heart) and heart failure in cardiovascular disease patients (Henry et al. 2014; Henry et al. 2013). Although there is an angiogenic response to ischaemia in the heart, continued insufficient reperfusion can lead to pathological ventricular remodelling resulting in reduced cardiac output increasing the chance of death (Taggart 2012; Kobayashi et al. 2017). Therefore there is an insufficiency of endogenous angiogenesis in conjunction with regular therapies to sufficiently perfuse myocardial infarction (Taggart 2013; Taggart et al. 2006)

Metabolic disease, particularly diabetes, can exacerbate EC dysfunction and produce unique challenges in treating ischaemic disease as well as producing new complications like diabetic retinopathy (Rosberger 2013). EC dysfunction induced by diabetes mainly affects the architecture and function of the micro vessels, by causing a loss of control of the numerous growth factors controlling angiogenesis induced by

hyperglycaemia (J. Wang et al. 2010). Long term diabetic conditions result in increased expression of VEGF and VEGFR2. Simultaneously a reduction in VEGF sensing is observed through a reduced activation of VEGFR1 (Waltenberger et al. 2000; Sasso et al. 2005). Altered expression of VEGF and VEGF receptors results in signalling imbalances, impairing new vessel formation (Sasso et al. 2005). Excess systemic VEGF causes an increase in vascular permeability by disrupting EC junctional integrity, resulting in tissue oedema (Adamis et al. 1999; Weis & Cheresh 2005). Vascular dysfunction is worsened by chronic inflammation associated with diabetes and the expression of inflammatory cytokines (Ziyadeh et al. 2000).

1.6 Therapeutic angiogenesis

The main outcome intended from angiogenic therapy is to promote the formation of new blood vessels to ischaemic tissue to treat the aforementioned ischaemic conditions mentioned in section 1.2 (Folkman 1971). Approaches using the growth factors FGF-2, VEGF, IGF, ANG-1 and EGF to modulate angiogenesis in ischaemic conditions have had limited success (Lazarous et al. 1997; Ferrara & Alitalo 1999). Due to the complex nature of angiogenesis, applying one growth factor to stimulate vessel growth or repair is unlikely to provide lasting treatment (Chu & Wang 2012). In PAD, improving micro vessel density of skeletal muscle by VEGF treatment has had no effect on the overall perfusion of the limb due to a continued lack of large vessel collateralisation (Scholz et al. 2002). Pre-clinical studies in PAD animal models have shown an improvement of vascularisation after growth factor treatments (*table 3*). However human clinical trials have not produced a significant improvement in post ischaemic angiogenesis (*table 4*). Furthermore, treatment of diabetic patients with VEGF or EGF could complicate diabetic retinopathy and nephropathy by enhancing vascular permeability (Welch et al. 2009).

Table 3: Post-ischaemic angiogenesis is improved in animal models of ischaemia (Caporali et al. 2018).

Growth factors	Animal model	Effect	Reference
VEGF	PIG MI	Increased neo angiogenesis and improved myocardial function.	(Choi et al. 2006)
FGF2	PIG MI	Enhanced arteriogenesis within the ischaemic area	(Horvath et al. 2002)
HGF	Rabbit HLI	Increased blood flow and arteriogenesis	(Taniyama et al. 2001)
ANG-1	Mouse MI	Increase in capillary density, reduction in infarct size, and increased heart performance	(Takahashi et al. 2003)
IGF-1	Mouse MI	Increased capillary density	(Dobrucki et al. 2010)

Table 4: Growth factor treatment in humans does not improve clinical outcomes of MI or PAD (Caporali et al. 2018).

Disease/patient number	Growth factor/vector	Primary outcome	Trial reference
PAD/60	FGF-2/SeV	Walking performance	NCT02276937
PAD/500	HGF/PI	Time to major amputation	NCT02144610
MI/41	HGF	Time 1mm ST depression during exercise stress testing	NCT01757223

1.7 Anillin - a new target in angiogenesis?

In order to improve current treatments of cardiovascular disease there is a requirement for the identification of novel genes that regulate regenerative angiogenesis in the response to ischaemia. Previous studies by Andrea Caporali have identified numerous genes that may have key roles in early regenerative angiogenesis. Analysis of microarray data from hind limb ischaemic adductor muscle and ECs overexpressing the P75 neurotrophin receptor 2, a negative regulator of angiogenesis, identified actin cytoskeletal reorganisation and cytokinesis as key gene clusters affected by ischaemia (GSE34675+GSE9910). ECs undergo major structural changes in early sprouting and lumenisation of the newly formed vessel with cytoskeletal remodelling being required for this process. Among the listed genes, the F-actin binding protein Anillin (ANLN) was highlighted in all the considered datasets. Therefore, we have further explored the role of ANLN in ischaemia-induced angiogenesis.

Human ANLN is an 1124 amino acid protein that is highly conserved across multiple species. Found in all cell types, ANLN is heavily associated with the cell cycle and in particular the completion of cytokinesis (Rogers et al. 2003). ANLN was first identified in 1989 by Miller et al in *D.melanogaster* by actin filament affinity chromatography as a unique actin binding protein and cloned by Field et al (Field & Alberts 1995; Miller et al. 1989). The general structure of ANLN consists of a large protein ~1100-1200 amino acids in length with an N-terminal region consisting of myosin and actin binding domains with a nuclear localisation site (Piekny & Glotzer 2008). The C-terminal domain referred to as the Anillin homology region (AHR) contains a Pleckstrin homology (PH) domain (Piekny & Glotzer 2008). ANLN has been shown to have multiple binding partners in the formation of the contractile ring at the cleavage furrow in cytokinesis (*table 5*). These associated binding partners include key regulators of actomyosin contractility in the cleavage furrow as shown in *figure 1.4*. These include Rho GTPases, particularly RhoA, which when bound to GTP in its active state at the central spindle acts through downstream signalling effectors to mediate

actin bundling. ECT2 a Guanine nucleotide exchange factor (GEF) activates RhoA during cleavage furrow ingression by increasing the concentration of GTP bound RhoA (Miller 2011). Actin filament formation and depolymerisation is mediated by septins and formins. RhoA activates Rho kinase (Rock) which phosphorylates non muscle myosin light chain 2, initiating contraction of the contractile ring. The activity of RhoA in contractile ring formation and contraction is moreover regulated by GTPase activating proteins (GAPS), with p190RhoGAPA thought to regulate RhoA inactivation in this context (Miller 2011).

Table 5: Known ANLN binding partners

Protein	species	Role	Reference
APC^{cdh15}/cyclosome	*H. Sapiens*	Degrade ANLN after the cell cycle	(Zhao & Fang 2005)
Importin α/β	*D. Melanogaster* *H. Sapiens*	Maintains ANLN localization in the nucleus through a RAN dependent mechanism	(Chen et al. 2015; Silverman-Gavrila et al. 2008)
mDia2	*H. Sapiens*	Actin crosslink regulator in cytokinesis	(Watanabe et al. 2010)
CD2AP	*D.Melanogaster* *H. Sapiens*	Intercellular bridge stability Stabilisation of podocyte foot processes	(Haglund et al. 2010) (Hall et al. 2018)
Non-muscle myosin light chain 2	*X. Laevis*	Contraction at the equatorial plane of cell division Contractile ring formation in epithelial cell junctions	(Reyes et al. 2014)
F-actin	*L. Xenopus*	Crosslinking F-actin in the cleavage furrow Contractile ring formation in Epithelial junctions	(Reyes et al. 2014)
RacGAP500C	*D. Melanogaster*	Crosslink the central spindle to the contractile ring	(D'Avino 2009)
P-190RhoGAPA	*H. Sapiens*	Inactivates RhoA in the contractile ring	(Manukyan et al. 2015)
RhoA	*H. Sapiens*	Stabilising RhoA to F-actin and myosin to the contractile ring	(Piekny & Glotzer 2008)
RhoG	C.*Elegans*	Actin polymerisation in filopodia extension in neurite outgrowth	(Tian et al. 2015)
ECT2 (GEF)	*H. Sapiens*	Activates RhoA in the contractile ring	(Mikawa et al. 2008)
Septins (peanut, sep 2 +5) Septins (Sept 2, 6 ,9 and 11)	*D.melanogaster* *H. Sapiens*	Link F-actin and septins for cleavage furrow stabilisation	(D'Avino 2009; Liu, Gregory D Fairn, et al. 2012)

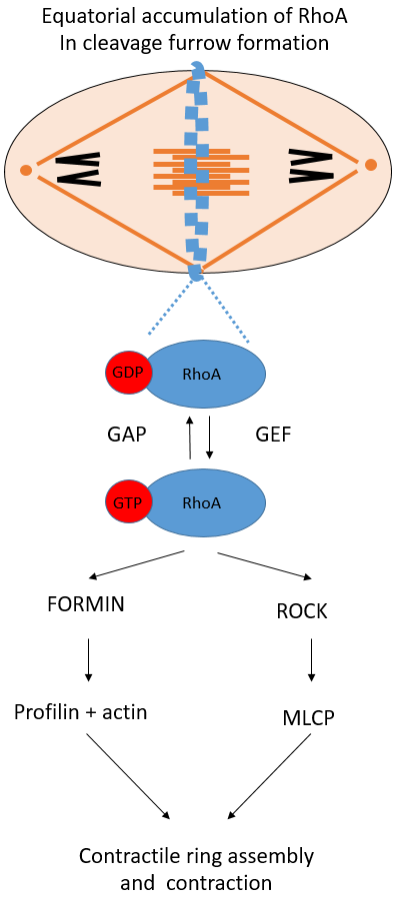

Figure 1.4: Contractile ring formation and contraction requires RhoA initiated assembly:

In contractile ring formation and contraction RhoA is regulated at the cleavage furrow by GAPs and GEFs. RhoA-GTP mediates actin filament bundling through formins and stimulates actin contraction through ROCK-mediated phosphorylation of MLC2. Cleavage furrow contraction and ingression results in the completion of cytokinesis

Initial investigations of ANLN in *D.melanogaster* identified a unique role for ANLN in controlling the contractile ring in cytokinesis and embryogenesis. Several ANLN mutants, so-called *scraps* mutants, have been shown in Drosophila to cause maternal sterility that can be rescued by ANLN cDNA injection (Schüpbach & Wieschaus 1991; Field et al. 2005). Mutations of the ANLN sequence in the AHR resulted in embryonic lethality due to a failure of cellularisation and gastrulation of the embryo (Field et al. 2005). This was attributed to a failure of localisation of ANLN with F-actin, myosin-2 and septins, reducing the stability of intracellular bridges. Altered cleavage furrow ingression caused by contractile ring failure destabilised new plasma formation during cellularisation of the embryo (Straight et al. 2005).

Further investigations of ANLN in human cell lines have identified further functions of the AHR in contractile ring stabilisation during cytokinesis. There is an enrichment of phosphatidylinositol-4,5-bisphosphate ($PI(4,5)P_2$) in the plasma membrane at the cleavage furrow, which is preferentially bound by the ANLN PH domain (Liu, Gregory D Fairn, et al. 2012). Mutation of the $PI(4,5)P_2$ binding site in the PH domain results in loss of ANLN from the cleavage furrow, causing destabilisation of the contractile ring and a loss of symmetric cell division (Liu, Gregory D Fairn, et al. 2012). Fusion of ANLN with other $PI(4,5)P_2$ targeting PH domains restores ANLN localisation to the cleavage furrow, however, cytokinetic defects remain. This is attributed to the loss of ANLN mediated stabilisation of septins 2, 9 and 11 at the cleavage furrow (Liu, Gregory D Fairn, et al. 2012) . Therefore the AHR is required not only for ANLN localisation to the cleavage furrow and the stabilisation of F-actin, but also for septin localisation to the cleavage furrow (Liu, Gregory D Fairn, et al. 2012).

A simplified schematic for ANLN expression and localisation dynamics in mammalian cytokinesis is shown in *figure 1.5A*. ANLN expression increases during G1-G2 phases of the cell cycle, accumulating in the nucleus by a Ran dependent mechanism mediated by importin-β2 (Chen et al. 2015; Beaudet et al. 2017). Here importin-β2 binds to ANLNs nuclear localisation sites (NLS) and transports it through the nuclear

pore into the nucleus, the small GTPase Ran then binds importin-β2 dissociating ANLN (Cavazza & Vernos 2016). ANLN is sequestered in the nucleus during interphase to prevent adverse interactions of ANLN with the cytoskeleton (Chen et al. 2015). After the dissolution of the nuclear membrane ANLN is localised to peripheral cortical stress fibres of the cell (Kinoshita et al. 2002). In anaphase, ANLN localises to the cleavage furrow for contractile ring formation, with association of its PH domain with $PI(4,5)P_2$ resulting in improved actin accumulation and the formation of the contractile ring. Association of ANLN allows for the interaction of F-actin, MLC2 and active RhoA regulated by ECT2 and P-190RhoGAPA activity (Mikawa et al. 2008). ANLN remains at the cleavage furrow until cytokinesis has been completed and only then transported back to the nucleus. Degradation is mediated the anaphase promoting complex (APC^{cdh1}), APC^{chd1} is responsible for the degradation of multiple cell cycle associated proteins after M phase to arrest the cell cycle (Zhao & Fang 2005).

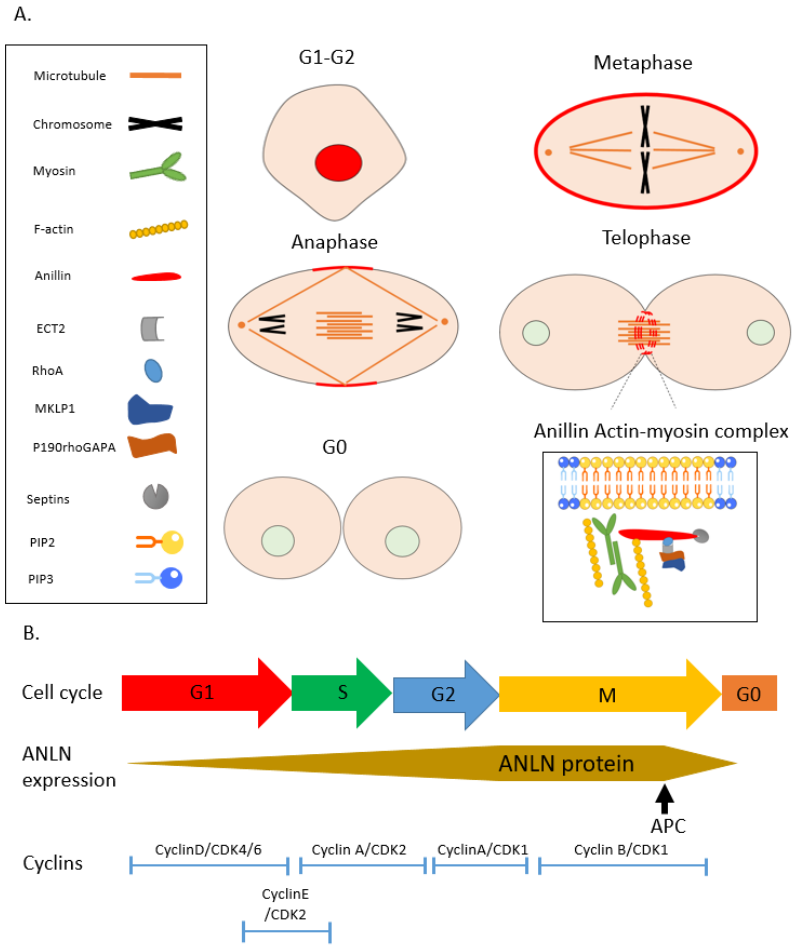

Figure 1.5: ANLN function and localisation during the cell cycle and cleavage furrow ingression:

(A) ANLN expression increases and is localised to the nucleus during G1-G2 phases, dissolution of the nuclear membrane encourages ANLN localisation to the cell cortex. In metaphase gradually restricting to the equator to regulate contractile ring formation in anaphase restricting till the completion of cytokinesis where in interphase ANLN is rapidly. The ANLN actin-myosin complex functions by allowing the interaction of ANLN, F-actin, RhoA and numerous septins facilitated by ANLN with localisation maintained by interaction of ANLNs PH domain with PIP_2 in the cell membrane (Piekny & Glotzer 2008). (B) Schematic of the cell cycle showing the individual cell cycle stages and associated cyclins. ANLN accumulates in G1-G2 until degradation by the anaphase promoting

Outside of its role in cytokinesis, ANLN has been associated with multiple cell phenotypes that may help with identifying a potential role of ANLN in ECs during angiogenesis. ANLN homologues in *C. elegans* have been shown to perform vital roles in neuronal cell development (Tian et al. 2015; Fotopoulos et al. 2013). ANLN is present in three isoforms, Ani-1-3 in *C. elegans*, all of which have been identified as having individual functions, unlike in vertebrates. Ani-1 silencing causes a range of cytokinetic defects, key of which is a misalignment of neuroblast cell division resulting in serious embryonic phenotypes (Fotopoulos et al. 2013). Further in development ANLN has been associated with neurite outgrowth and migration of Q-cell neuroblasts, here ani-1 localises to the leading edges of migrating Q-cell neuroblasts. The proposed mechanism was a myosin independent stabilisation of leading edge lamella protrusions by an interaction between Ani-1 and RhoG for the regulation of actin filament assembly (Tian et al. 2015). Ani-2 has a role in antagonising the effect of Ani-1, Ani-2 lacks the n-terminal actin/myosin domain, and has been suggested to compete with Ani-1 to regulate the contractile ring (Chartier et al. 2011; Pacquelet et al. 2015). *C.Elegans* ani-1-2 lack the NLS site, so they may have different cellular functions and distribution to vertebrate ANLN (Maddox et al. 2005).

In cancer cells, ANLN expression can be upregulated 2-6 fold in multiple human tumours which is associated with an increase of tumour migration and metastasis (Hall et al. 2005). In ovarian cancer, high ANLN expression was associated with a decrease in survival amongst patients compared to groups with low ANLN expressing tumours (Suzuki et al. 2005). Silencing of ANLN with shRNA has been shown to markedly reduce the proliferative and migration capacity of breast cancer cell lines *in vitro* (Zhou et al. 2015). This was due to a dysregulation of the cell cycle, ANLN silenced cells expressed less cyclin D1 and had an increase in cdc2 phosphorylation (*see figure 1.5B*). This caused the arrest of the cell cycle and accumulation in the G2/M stage (Zhou et al. 2015). Similarly, ANLN silencing in human non-small cell lung cancer cell lines has been shown to impair cell migration and proliferation whereas overexpression increases these factors (Suzuki et al. 2005). Interestingly an

association between PI3K-activity and the nuclear localisation of ANLN showing a potential nuclear effect of ANLN in cancer invasiveness (Suzuki et al. 2005).

ANLN has also been associated with cell-cell junction integrity in epithelial cell lines which may be relevant to EC junctions. ANLN silencing in *Xenopus* oocyte epithelial cell layers has been shown to reduce integrity of cell-cell junctions. Silencing of ANLN strongly disrupts claudin 5 distribution and β-catenin localisation at the cell to cell junction (Reyes et al. 2014). Rho activity is also disturbed resulting in an increased number of shorter, more intense bursts at the cell-cell junction. Interestingly, ANLN overexpression causes a severe contractile phenotype resulting in an increased localisation of P-MLC2 at the cell-cell junctions and the formation of aberrant contractile rings (Reyes et al. 2014). Investigations in human epithelial cell lines have demonstrated similar functional phenotypes. In human epithelial cells, ANLN exclusively localises to the nucleus during interphase. ANLN silencing resulting in an overall severe general cellular phenotype characterised by cell-cell junctional disorganisation without loss of expression of common junctional proteins despite there being no association of ANLN at the cell-cell junction (Wang et al. 2015).

Unique interactors with ANLN have been investigated in renal familial focal segmental glomerulosclerosis (FSGS). FSGS is the gradual damage to individual glomeruli resulting in renal failure, usually manifesting between 35 and 75 years of age. A missense mutation located at R431C in ANLN was identified using genome wide association and exome sequencing in families with the inherited disorder. One particular kindred that had a high prevalence of the disorder carried the R431C mutation of ANLN (Gbadegesin et al. 2014). ANLN was upregulated in FSGS patient biopsies and overexpression of R431C mutant ANLN increases the migration and motility of immortalised podocytes. Further investigation identified the mutant as the interaction site ANLN with CD2AP, a key component of the structural foot processes of podocytes (Gbadegesin et al. 2014). The mutant form of ANLN results in the uncoupling of ANLN from CD2AP causing hyper activation of the PI3K/AKT/mTOR signalling pathway (Hall et al. 2018). This signalling pathway controls aspects of the cell cycle, proliferation and survival. Overexpression of mutant R431C mutant ANLN

results in endoplasmic reticulum stress and apoptosis in cultured immortalised podocytes (Hall et al. 2018). Inhibition of mTOR with rapamycin reduced pro migratory phenotypes and ER-stress induced apoptosis in podocytes (Hall et al. 2018).

The relevance of ANLN to the regenerative response in cardiovascular disease has been explored in myocardial infarction (Livet et al. 2007). Hesse et al produced a CAG-ANLN-EGFP reporter mouse for the investigation of ANLN in the cell cycle dynamics of mouse embryonic development which reported a nuclear localisation of ANLN-eGFP in cells in S/G2 phase (Hesse et al. 2012). ANLN was moreover found to act as a mitotic marker in pluripotent stem cells and importantly marked endoreduplication in myocardial injury. Transmural myocardial injury of the CAG-ANLN-eGFP mouse identified ANLN positive cells in the border zone of myocardial injury. Analysis of cardiomyocytes via flow cytometry showed that ANLN-eGFP positive cardiomyocytes had an increased DNA content compared to ANLN negative cells (Hesse et al. 2012). Supporting this, ANLN one of the top 5 upregulated genes in RNA sequencing of injured/non-injured zebrafish cardiomyocytes (Kang et al. 2016).

1.8 RNA binding proteins a potential regulatory mechanism of ANLN in CV disease?

Post transcriptional regulation is the process of regulating gene expression at the mRNA transcript level and is mediated by multiple biological mechanisms. A key post transcriptional regulatory mechanism is RNA binding protein modulation of mRNA stability as shown in *figure 1.6*.

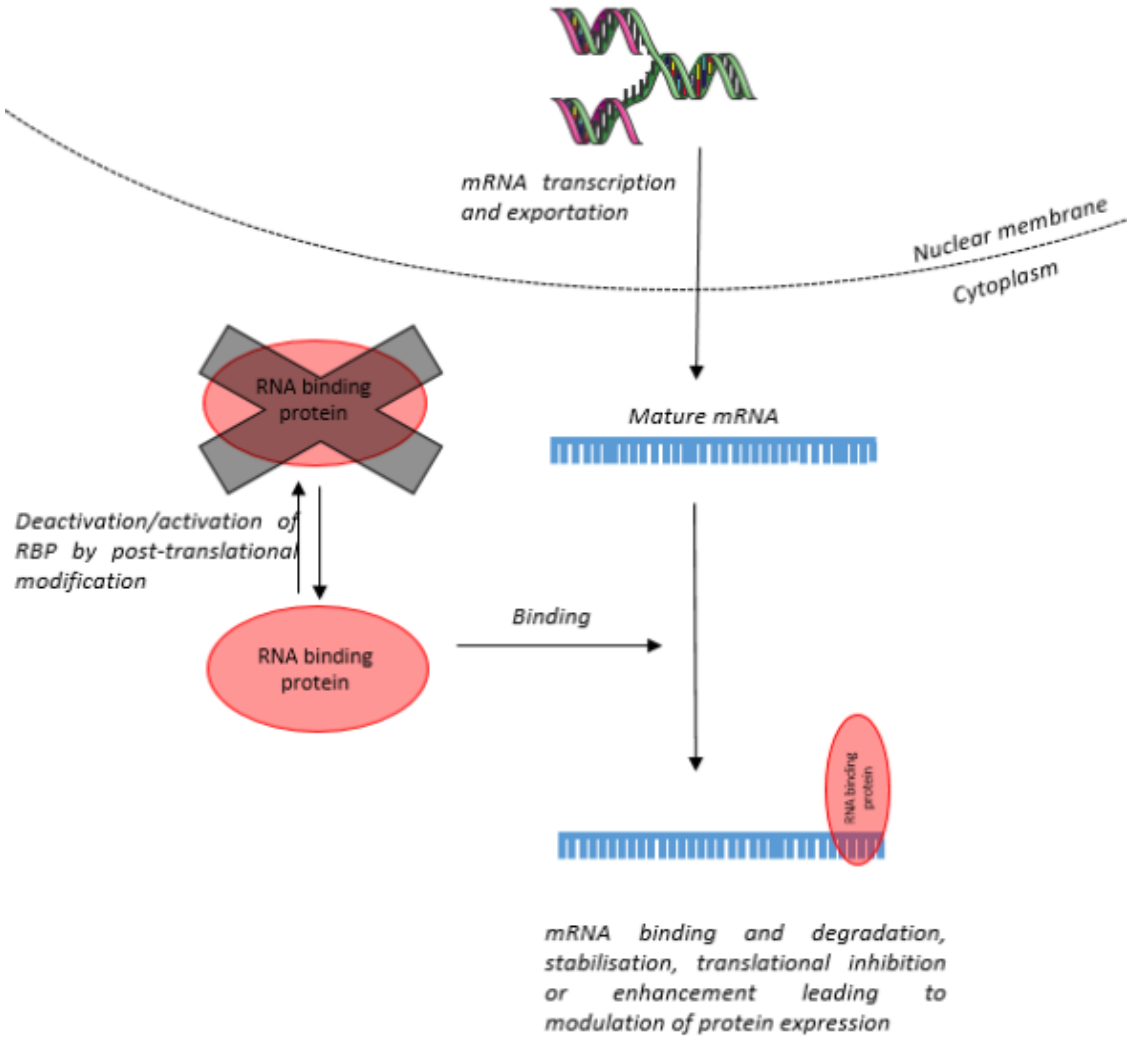

Figure 1.6: RNA binding proteins regulate the translation of protein from mRNA;

RBPs expressed in the cytoplasm are activated/deactivated by phosphorylation through numerous signalling pathways. When active RBPs can bind to the 3'UTR of multiple target genes to mediate mRNA stability and the translational efficiency of proteins in target pathways. (Sanduja et al. 2012)

RNA binding proteins (RBPs) are a diverse group of proteins which have been observed to suppress and facilitate the expression of target genes in cardiovascular cell types. RBPs attach to adenylate uridylate rich elements (ARE) in the 3'UTR of mRNA transcripts and induce either degradation or stabilisation of the mRNA transcript. The ANLN 3'UTR contains multiple ARE sequences in its 3'UTR making it a potential target of RBPs as shown in *figure 1.7*. Multiple RNA binding protein families have been identified to function in cardiovascular cell types. RBPs which induce degradation of mRNA include AUF1, ZFP36, QKR1 and KSRP, mRNA stabilising RBPs include HuR, PAIP2 and AUF1. These RBPs control the expression of multiple genes in embryogenesis, inflammation and cell growth in multiple cell types.

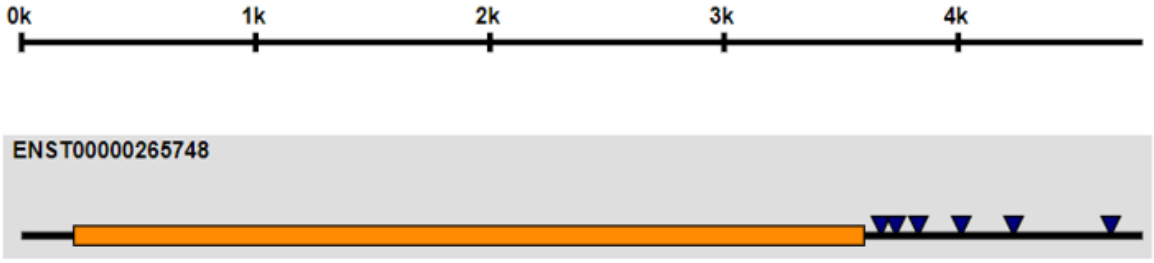

Figure 1.7: The ANLN 3'UTR contains multiple ATTTA sites for regulation by RNA binding proteins: Screening of the ANLN 3'UTR contains using AREsite identified ANLN as having multiple ATTTA ARE elements for targeting by RNA binding proteins. (Fallmann et al. 2016)

RBPs are known to play key roles in cardiovascular development and EC function in health and disease. In the maintenance of normal EC cell junction behaviour VE-Cadherin and β-catenin mRNAs are stabilised by the binding of QKR1 RBP to the 3'UTR enhancing mRNA translation (De Bruin et al. 2016). QKR1 is highly expressed in the endothelium and the loss of QKR1 results in an overall increase in vascular permeability and a reduction of EC barrier function. In the EC response to ischaemia the transcription factor hypoxia inducible factor 1α and VEGF are controlled by multiple RBPs; HUR and PTB have been shown to improve the translation of these key genes in angiogenesis (Galbán et al. 2008). Conversely, the degradation of these factors is mediated by ZFP36 family RBPS during angiogenesis and this assists in regulating the EC response to growth factor stimulation. The interplay between RNA

binding protein regulation of target genes in disease can be affected inflammatory status. For example in ECs ZFP36 regulation of VEGF stability is suppressed by TNF-α leading to increased HUR and PTB translational enhancement of VEGF (Dean et al. 2001).

1.9 ZFP36 family RNA binding proteins:

The ZFP36 RBP family consisting of ZFP36, ZFP36L1 and ZFP36L2 are key regulators of angiogenesis (Bell et al. 2006). This family has overlapping targets and functions at similar time points in development and in the response to cytokines and chemokine expression in inflammation and cell growth. There are three main constituents of the ZFP36 RBPs family in humans, each have a highly conserved core RNA binding domain featuring a tandem zinc finger domain *figure 1.8* (Lai et al. 2014). These domains function to bind the highly conserved ARE elements in the 3'UTR of target genes (Lai et al. 2014).

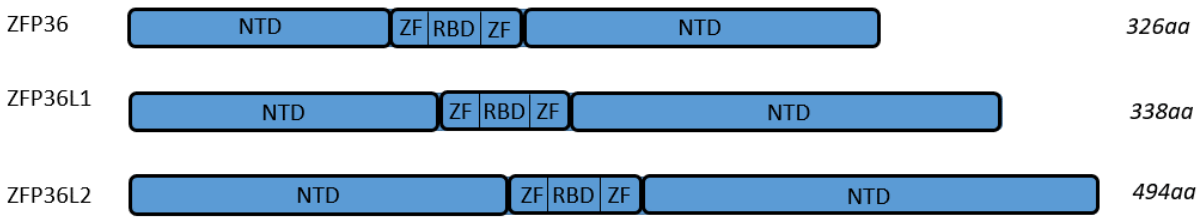

Figure 1.8: Representation of the homologous protein structure of the three members of the human ZFP36 family showing the N terminal domain (NTD) and C terminal domain (CTD) which function as activators of the zinc finger (ZF) RNA binding as well as inhibited mRNA deadenylation and decay.

Although the different members of the family exhibit a highly conserved structure they respond differently to growth factor stimuli to regulate multiple genes (Hacker, Valchanova, Adams & Munz 2010; Lai et al. 2014; Hudson et al. 2004; Blackshear et al. 2005). ZFP36 was first identified as an inducible protein by sequencing of cDNA from insulin stimulated mouse fibroblasts (Blackshear et al. 2005). Shortly thereafter the human ZFP36 sequence was described and found to be a potent regulator of TNF-α mRNA stability (Taylor et al. 1996). ZFP36L1 and ZFP36L2, the second and third

members of the family were identified after their cDNA sequence was cloned from TPA treated fibroblasts (Varnum et al. 1991). The sequence and structural similarity of these proteins with ZFP36 were noted particularly the 67 amino acid RNA binding domains (Varnum et al. 1991; Bustin et al. 1994). Screening for the optimum binding sites of ZFP36 RBPs found the ideal ARE UUAUUUAUU sequence, although partially complete binding sites can allow binding of ZFP36 family RBPs (Blackshear et al. 2003). ZFP36 mRNA mediation of decay each zinc finger domains binds to a UAUU subsite in the binding site (Hudson et al. 2004). The ZFP36 RBPs function through the binding to the 3'UTR of target transcripts and remove the polyA tail as shown in *figure 1.9* by promoting association of the deadenylase complex leading to destabilisation of the mRNA transcript (Blackshear 2002; Sandler et al. 2011). Following mRNA destabilisation the RBP mRNA complex is transported into organelles for processing. ZFP36 mRNA complexes in exosomes undergo 3' 5' degradation by endonuclease digestion (Garneau et al. 2007). ZFP36 mRNA complexes in P-bodies undergo rapid decapping of the 5' 7- methyl guanosine cap by DCP-1 resulting in 5' to 3' degradation by XRN-1 nuclease (Cougot et al. 2004; Mitchell & Tollervey 2000).

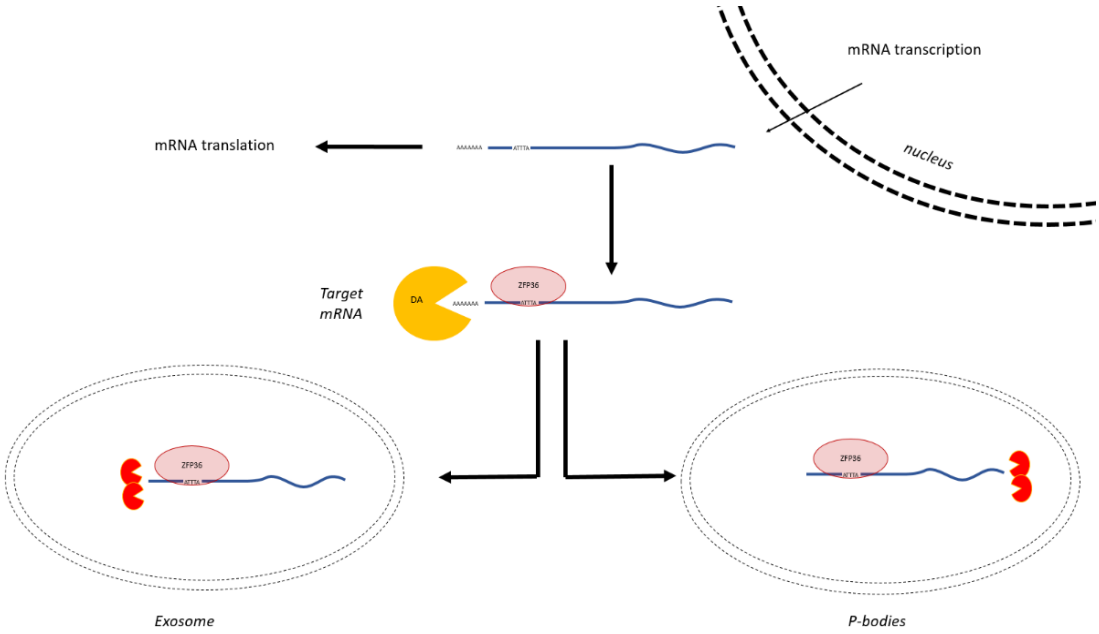

Figure 1.9: ZFP36 regulates mRNA transcripts through ARE mediated decay

Processed mRNA transcripts are exported from the nucleus where ZFP36 family RBPs bind to ARE elements in the 3'UTR. Recruitment of the deadenylase complex (DA) removes the polyA tail to destabilise the mRNA transcript. ZFP36 bound transcripts are then localised to exosomes where the transcript is degraded by 3' to 5' nucleases. In P-bodies the 5' end is decapped followed by 3' to 5' degradation of the transcript.

Normal regulation of ZFP36 RBP mediated mRNA decay is maintained by the phosphorylation of several residues of ZFP36 family RBPs controlled by multiple cell signalling pathways. This process is well described in macrophages, where ZFP36 regulation of inflammatory gene expression is associated with an increased activation of MKP-1 following a peak of p38-MAPK activity a key regulator of inflammatory signalling mRNA stability (Cao et al. 2006). The overlap of gene expression from P38-MAPK, activation expression and targets of ZFP36 shows a significant regulatory role of ZFP36 in controlling inflammation. Phosphorylation controls binding of the RBP to RNA transcripts by multiple mechanisms, downstream of p38-MAPK MK2 phosphorylates ZFP36 at Ser52 and Ser178 (Chrestensen et al. 2004). Phosphorylation results in association of ZFP36 with the 14-3-3 complex greatly reducing the RNA binding efficiency of ZFP36 (Chrestensen et al. 2004). Subcellular localisation is altered by association with 14-3-3 resulting in exclusion of ZFP36 from P bodies and stress granules further improving mRNA stability. To stop the inflammatory response PP2A dephosphorylates ZFP36 at Ser52 and Ser178 resulting in a loss of 14-3-3 interaction and recovery of RNA binding efficiency and the suppression of inflammation through mRNA degradation (Sun et al. 2007). There is presence of an auto-regulatory loop by which ZFP36 regulates the DUSP-1 3UTR the phosphatase responsible for dephosphorylating and inactivating p38 MAPK. Therefore suppression of ZFP36 activity leads to an increased deactivation of p38MAPK in a negative feedback loop mechanism.

Similar mechanisms are present in other members of the ZFP36 family of RBPs, ZFP36L1 is phosphorylated heavily by AKT/PKB a constituent of the PI3K pathway. Phosphorylation of Ser92 and Ser203 results in the protection from degradation by improving association with the 14-3-3 complex and preventing mRNA degradation (Benjamin et al. 2006). Enhancement of ZFP36L1 RNA binding efficiency can be initiated by the cAMP signalling pathway. Phosphorylation of Ser54 and Ser334 by PKA increases the half-life of ZFP36L1 and improves the binding and degradation of ZFP3l61 target mRNA (Rataj et al. 2016). ZFP36L2 doesn't currently have any reported

phosphoserine residues that regulate its function although it is presumed there are several present on its structure.

ZFP36 knockout mice exhibit a moderate phenotype having a 2-5 fold reduction in weight than controls and exhibit overall poor health. This is associated with an increase in inflammation causing an enlarged spleen, lymph nodes and atrophied thymus. ZFP36L1 knockout mouse embryos exhibit embryonic lethality at E9.5 due to cardiac outflow tract and multiple vascular abnormalities. These phenotypes produced were attributed to high VEGF-A production from embryonic fibroblasts causing overall vascular disorganisation (Bell et al. 2006; Stumpo et al. 2004). Tissue specific knockouts of ZFP36L1 and ZFP36L2 identified ZFP36L1 as a regulator of key transcription factors controlling the cell survival, maturation and migration of B cells in a ZFP36L1 Cre-Lox mouse (Newman et al. 2017).

ZFP36 and ZFP36L1 have been shown to regulate the differentiation of quiescent stem cell populations in development and regeneration (McClelland et al. 2017). In the response to injury of skeletal muscle, populations of quiescent satellite stem cells differentiate to replace damaged or injured myofibers (Hausburg, Doles, Clement, Cadwallader, Hall, Blackshear, Lykke-andersen, et al. 2015). MAPK inactivation of ZFP36 and stabilisation of the target mRNA myoD, allows for the differentiation and cell fusion into the myofibers (Hausburg, Doles, Clement, Cadwallader, Hall, Blackshear, Lykke-andersen, et al. 2015; Busse et al. 2008).

ZFP36 and ZFP36L1 are key mediators of multiple angiogenic genes and control targets such as HIF1-α and VEGF expression in ECs (Hacker et al. 2010). ZFP36L1 appears to have a more important vascular phenotype than ZFP36 in knockout mouse lines. VEGF is a target of both ZFP36 and ZFP36L1 which means dysregulation of VEGF is not the main cause of vascular malformation. Dll4, the notch ligand responsible for tip stalk cell designation and controlling blood vessel branching and density, has been shown to be strong target of ZFP36L1 which can explain the strong vascular phenotype of ZFP36L1 knockout (Desroches-castan et al. 2011). Given that the ANLN

3'UTR contains ARE elements (*figure 1.7*), there may be a regulatory mechanism of post transcriptional regulation of ANLN by ZFP36 RBPs in angiogenesis.

1.10 Zebrafish in medical research:

It was decided to use zebrafish as our model organism for the investigation of ANLN in angiogenesis. Zebrafish have become a valuable tool in the investigation of gene function in development, organogenesis and regeneration. This is owing to their small size, high fertility and their translucent embryos; these features were first utilised by George Streisinger thirty years ago (Grunwald & Streisinger 1992). Large scale screening studies in zebrafish embryos and mapping of their genome has identified multiple zebrafish homologues and orthologues of mammalian genes (Howe et al. 2013; Haffter & Nusslein-Volhard 2003). The zebrafish genome has at some point duplicated, some of these duplications have been lost and some have drifted from the original function (Postlethwait et al. 1998). Despite the duplication of the zebrafish genome the number of chromosomes remains similar to humans (Postlethwait et al. 2000). The rapid achievement of embryonic landmarks and the ease of imaging has led to a near requirement for the use of zebrafish in some areas of biology.

The relative ease of genetic modification of the zebrafish embryo and the volume of viable single cell stage embryos created allows for the generation of multiple different transgenic lines using a number of different techniques. Microinjection of morpholinos is a readily used technique to mediate transient interference of genes in vivo (Timme-Laragy et al. 2012). Morpholinos are small DNA oligos which can bind to the kozac sequence or splice sites in the mRNA transcript, this interferes with protein expression. Morpholinos however can produce a wide array of off target effects which can cause misleading phenotypes (Timme-Laragy et al. 2012). Using CRISPR-Cas9 to replace all previous forms of genetic interference is increasingly common. CRISPR-Cas9 originated as a bacterial immune response against viral infection. It was first identified to function in *S.thermopilus,* where resistance to bacteriophages had been acquired through integration of viral DNA with the Cas9

enzyme and excision of viral DNA from the host genome (Barrangou et al. 2007). Of the three CRISPR-Cas9 mechanisms present in bacteria, type 2 is the method currently most used for genome editing. It requires three components, (i) a complementary RNA (crRNA) which is reciprocal to the target gene locus, (ii) a trans-activating crRNA (tracrRNA), which is complementary to the crRNA and (iii) the Cas9 enzyme. Cas9 associates with the crRNA and tracrRNA and facilitates association of nucleases which initiate a doublestrand break of the target locus. For genome editing purposes, the crRNA and tracrRNA can be combined into a short guide RNA (sgRNA); when paired with a recombinant Cas9 enzyme this can be injected into single cell embryos to direct targeted double stranded breaks of loci of interest in the genome (Jinek et al. 2012). The only requirement of target sites is the presence of a 2-5 nucleotide protospacer adjacent motif (PAM) sequence. PAMs are specific to different recombinant Cas9 enzymes wand must directly follow the sgRNA sequence to allow recognition of the site (Swarts et al. 2012). The similarity between multiple zebrafish genes make zebrafish an ideal model for investigating mammalian gene function. However a caveat of zebrafish research is the lack of available antibodies for zebrafish proteins. This makes traditional methods such as Western blot and immunostaining challenging.

1.11 Zebrafish in Cardiovascular research:

In cardiovascular research the zebrafish has become increasingly popular. Within the first 24 hours of its life, the zebrafish embryo develops a contracting heart tube and the beginnings of the early vascular system and blood flow (Isogai et al. 2001). These features, along with the ability of the early embryo to receive oxygen by diffusion, means that the use of severe cardiovascular injuries or knockout lines have ethical advantages in zebrafish embryos over adult mice.

1.12 Zebrafish Vasculogenesis:

Angiogenesis as previously described in section 1.4 refers to the development of blood vessels from existing vascular networks. In early embryonic development the initial vascular cords form through vasculogenesis, this process is the *de novo* creation of blood vessel by the coalescence of endothelial cell progenitors (Lawson & Weinstein 2002).

This process is well described in the zebrafish embryo, as shown in *figure 1.10.* Vasculogenesis occurs after the formation of the neural tube and somites from the initial embryonic layers. The developing neural tube and notochord release the soluble factor sonic the hedgehog (shh). SHH stimulates the release of VEGF from the somites encouraging the migration of $VEGFR2^{+ve}$ angioblasts from the lateral plate mesoderm to the trunk of the embryo, these cells form the intermediate cell mass (ICM) (Lawson & Weinstein 2002; Lawson et al. 2002). The angioblasts stimulated by VEGF from the somites and notch signalling from the notochord begin to generate early vascular structures. These structures become the developing dorsal aorta (DA) and pericardinal vein (PCV) through changes in gene expression controlling arterial venous designation. ECs of the early DA are stimulated by VEGF activation of VEGFR2 activation of notch, Ephrin B2 (EPHB2) expression drives arterial designation.(Ellertsdóttir et al. 2010) The development of the PCV from the early vascular cords is caused by expression of the EPHB2 receptor Ephrin B4 (EPHB4), ephrin signalling between the arterial and venous side assists in early venous designation (Ellertsdóttir et al. 2010). The formation of the main trunk vasculature is

completed by ~1dpf and is capable of carrying blood flow, further developmental angiogenesis follows to create the microvasculature.

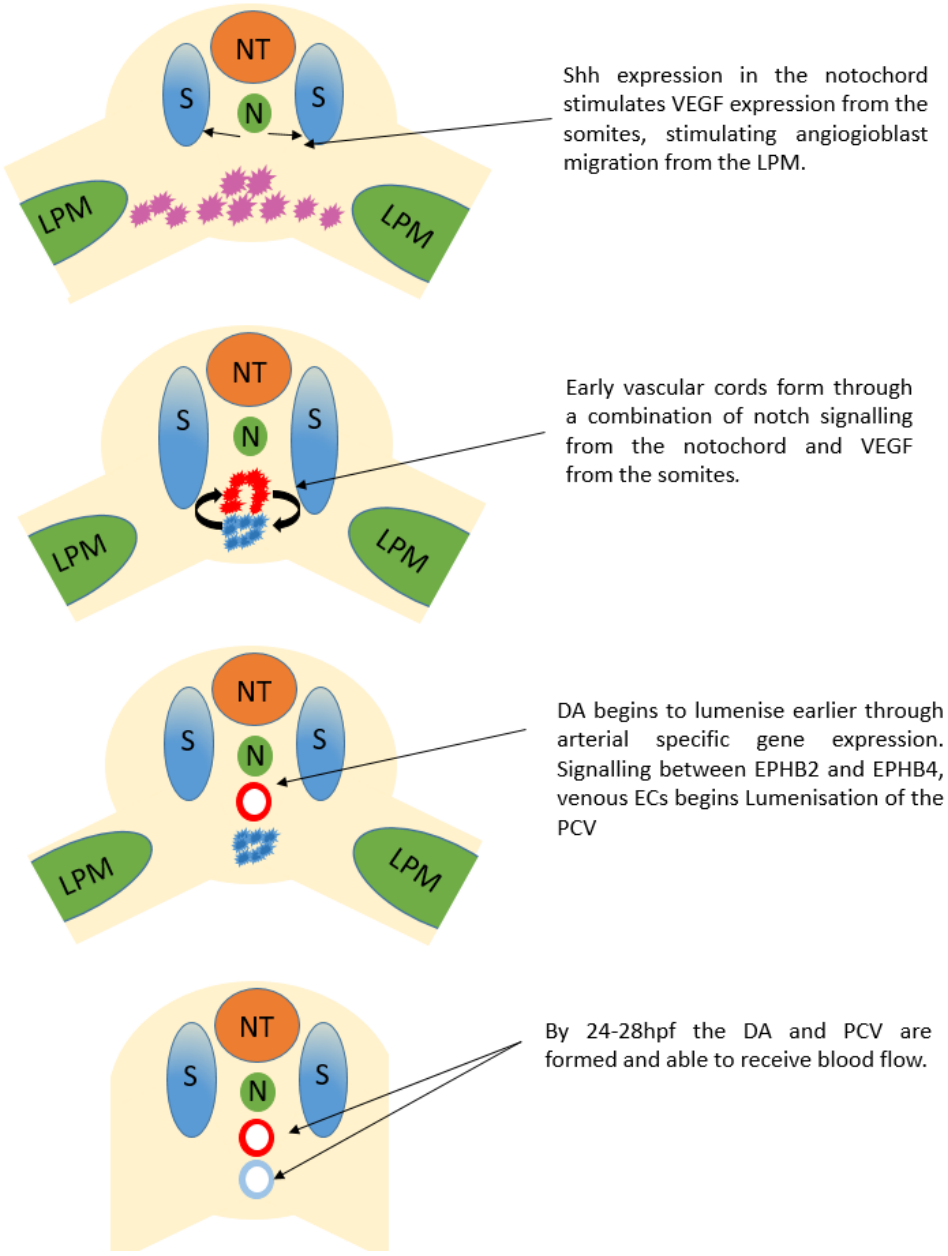

Figure 1.10: Arterial/venous definition in vasculogenesis in the zebrafish trunk:

Axial slice schematic of the 14-28 hpf zebrafish embryo. Showing the generation of the dorsal aorta and pericardinal vein (PCV) by signalling events from the notochord (N) located inferior to the neural tube (NT), and the somites (S). Angioblasts migrate from the lateral plate mesoderm (LPM) to produce the initial vascular cords before undergoing arterial venous designation into the dorsal aorta (DA) and pericardial vein (PCV). Adapted from (Lawson & Weinstein 2002)

The general architecture of the zebrafish embryo arteriovenous system is similar to mammalian embryos, with the embryo forming distinct arteries and veins early in development (Isogai et al. 2001). The complexity of the vasculature increases rapidly between 1-5dpf as shown in figure 1.11. Between the somites of the embryo, the intersegmental vessels (ISV) form in two waves of angiogenesis (Isogai et al. 2003). The first wave occurs at ~22-28hpf where sprouting angiogenesis from the DA produces vessels along the somite boundaries creating the segmental arteries. At the dorsal roof of the embryo the sprouting ECs merge to form the dorsal longitudinal anastomotic vessel (DLAV) (Kamei et al. 2006). The second wave of sprouting occurs between 28-32 hpf where sprouting angiogenesis from the PCV produces the segmental veins. Increasing EC density and mural cell attachment continue to develop the ISVs into mature vessels (Isogai et al. 2003). The development of the CNS, gill and gastro intestinal vessels also rapidly develop between 1-5 dpf as shown in *figure 1.11* (Isogai et al. 2001).

1.13 Investigating zebrafish vasculature:

Multiple transgenic lines have been generated that permit the in-depth investigation of the developing zebrafish vasculature. Key to this are lines which express fluorescent reporters like mCherry or GFP under the control of EC specific reporters, such as *fli-1* or *flk-1 (*VEGFR2*)*, to fluorescently mark vascular structures throughout development and adulthood (Y. Wang et al. 2010; Lawson & Weinstein 2002). In addition, certain transgenic lines and knockouts have been shown to affect EC function *in vivo*. These include the cloche mutant, which results in the failure of EC development and a complete absence of vasculature (Stainier et al. 1995). The *mindbomb* mutant, a mutant of an E3 ubiquitin ligase required for efficient Dll4/Notch signalling, produces strong haematopoietic and EC lineage phenotypes (Itoh et al. 2003; Yoo et al. 2006; Bingham et al. 2003). These (and other) lines have been used successfully to image the developing vasculature in a manner which is not possible with traditional rodent based models (Kamei & Weinstein 2005).

Investigation of inflammatory cell involvement in cardiovascular development and injury is another key facet of zebrafish research. Zebrafish embryos generate innate immune cells (macrophages and neutrophils) by 2 dpf, whereas adaptive immunity develops later (Le Guyader et al. 2008). Several lines utilising fluorescent proteins to mark macrophages with the *mpeg* promoter and neutrophils with the *mpx* promoter have been developed (Renshaw et al. 2006; Ellett et al. 2011). These lines have been used to visualise the behaviour of immune cells in zebrafish development and injury repair.

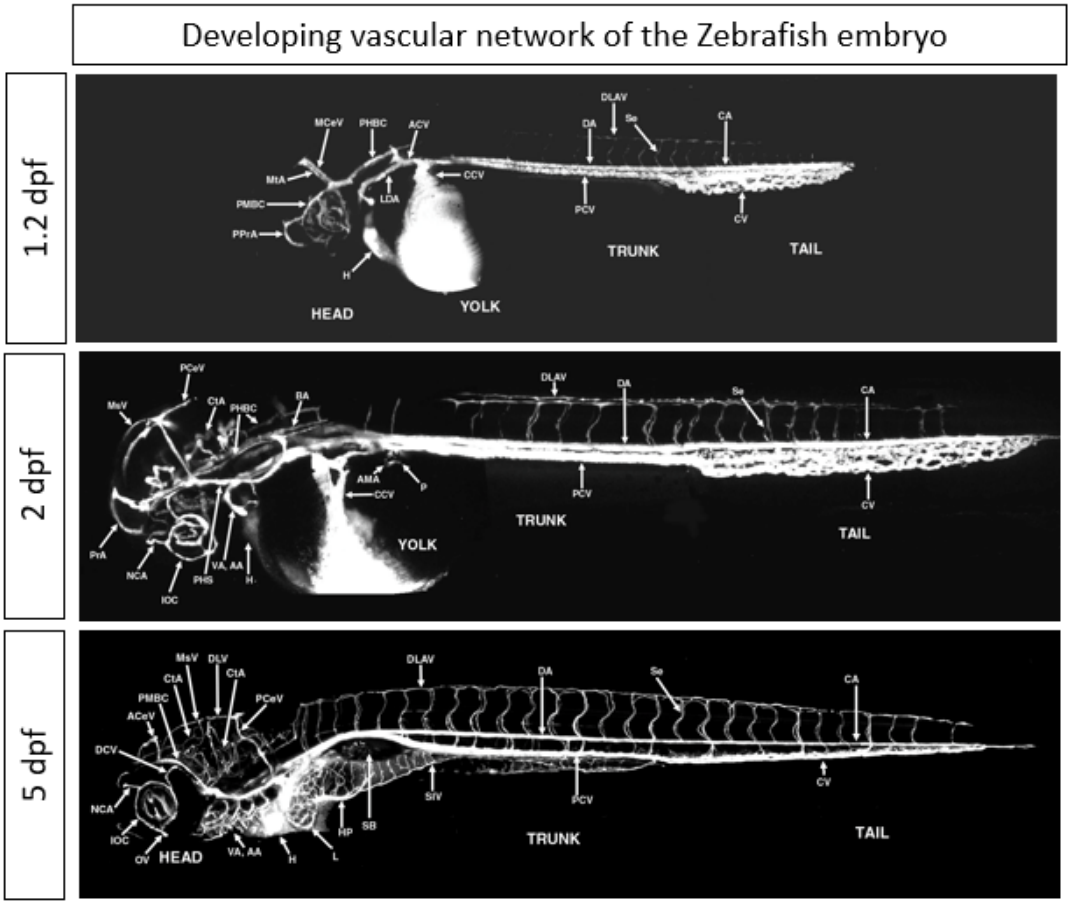

Figure 1.11: The vascular anatomy of the zebrafish embryo between 1-5 dpf:

From 2-4 dpf there is rapid maturation and expansion of the vascular network. Maturation is particularly noted in the trunk and caudal artery/vascular plexus and increasing network density in the CNS, GI tract and gill between 2 and 5 dpf. taken from (Isogai et al. 2001)

1.14 Models of cardiovascular injury in zebrafish:

Several experimental injury models have been developed to study the cardiovascular response and model myocardial infarction and tissue regeneration in the zebrafish embryo. Such techniques have also been used to investigate the regenerative capacity of the heart. For example, cryoinjury in adult zebrafish demonstrated the remarkable capacity for heart regeneration. These studies used super chilled metal probes applied to the exposed heart in conjunction with fluorescent reporters to successfully demonstrate myocardial regeneration and neovascularisation (González-Rosa et al. 2011; Marín-Juez et al. 2016). In the embryo, cryoinjuries of the heart have been overtaken by laser injury models. Laser injury of the embryonic heart were shown to produce a reproducible trauma that induces cardiomyocyte apoptosis, reduced cardiac outflow and stimulates regenerative processes (Matrone et al. 2014; Matrone et al. 2013; Matrone et al. 2015).

Exploration of vascular injury or the vascular response in regeneration has been carried out successfully to investigate the revascularisation of the adult zebrafish tail fin (Hlushchuk et al. 2016). However applying this to the developing embryo is more difficult because the vascular network is less developed than in the adult fish. Still, laser injuries of embryonic vessels have been used to study different aspects of vascular development, and to investigate thrombus formation and resolution in the embryonic fish (Watson et al. 2013). Laser induced thrombus formation identified the flow dependent maturation of the intersegmental vessels, identifying the role of blood flow in zebrafish vascular development and patterning (Watson et al. 2013; Gray et al. 2007). Laser injuries can moreover successfully ablate single vessels in the cerebrovascular system of the developing embryo. Ablation of single vessels has identified macrophage mediated blood vessel anastomosis (Liu et al. 2016). Mechanical injury models of larger vessels of the embryonic fish have also been developed and were instrumental in identifying the EC response in wound healing and inflammation (Clay & Coughlin 2015).

1.15 The *anln:anln-eGFP* zebrafish and asymmetric cell division in embryonic development:

To investigate *Anln* expression in the developing zebrafish vasculature we imported a fluorescent reporter of *Anln* expression. Dr Lucia Poggi of the University of Trento developed this BAC based fluorescent reporter zebrafish expressing full length eGFP tagged *Anln* under the zebrafish *anln* promoter (zebrafish lines designated by the nomenclature (*promoter:coding sequence*)) (Paolini et al. 2015). This zebrafish was used extensively for investigating the asymmetric cell divisions in retinal progenitor cell development and differentiation. This model suggested that *anln* is highly expressed in the early neuroepithelium, marking asymmetric cell divisions of retinal ganglion cells (*figure 1.12*). *Anln* expression was found to decline throughout retinal development, simultaneously the expression of *Ath5* (a marker of retinal ganglion cell maturity) was seen to increase. In $Ath5^{-/-}$ embryos *Anln* expression does not decrease during development and retinal ganglions cells do not develop (Paolini et al. 2015). *Anln* was observed to control asymmetric cell division in retinal ganglion cell progenitor differentiation, supporting this, interference of *Anln* expression with morpholinos reduced the number of $Ath5^{+ve}$ retinal ganglion cells (Paolini et al. 2015). Furthermore, *anln-eGFP* marked the mitotic potential of retinal cell and progenitor cell populations within the cell layers of the pre-juvenile zebrafish retina (Malo et al. 2017). This *anln:anln-eGFP* reporter fish was proposed to be useful for investigating the asymmetric cell divisions and the progression of the cell cycle in regeneration (Malo et al. 2017).

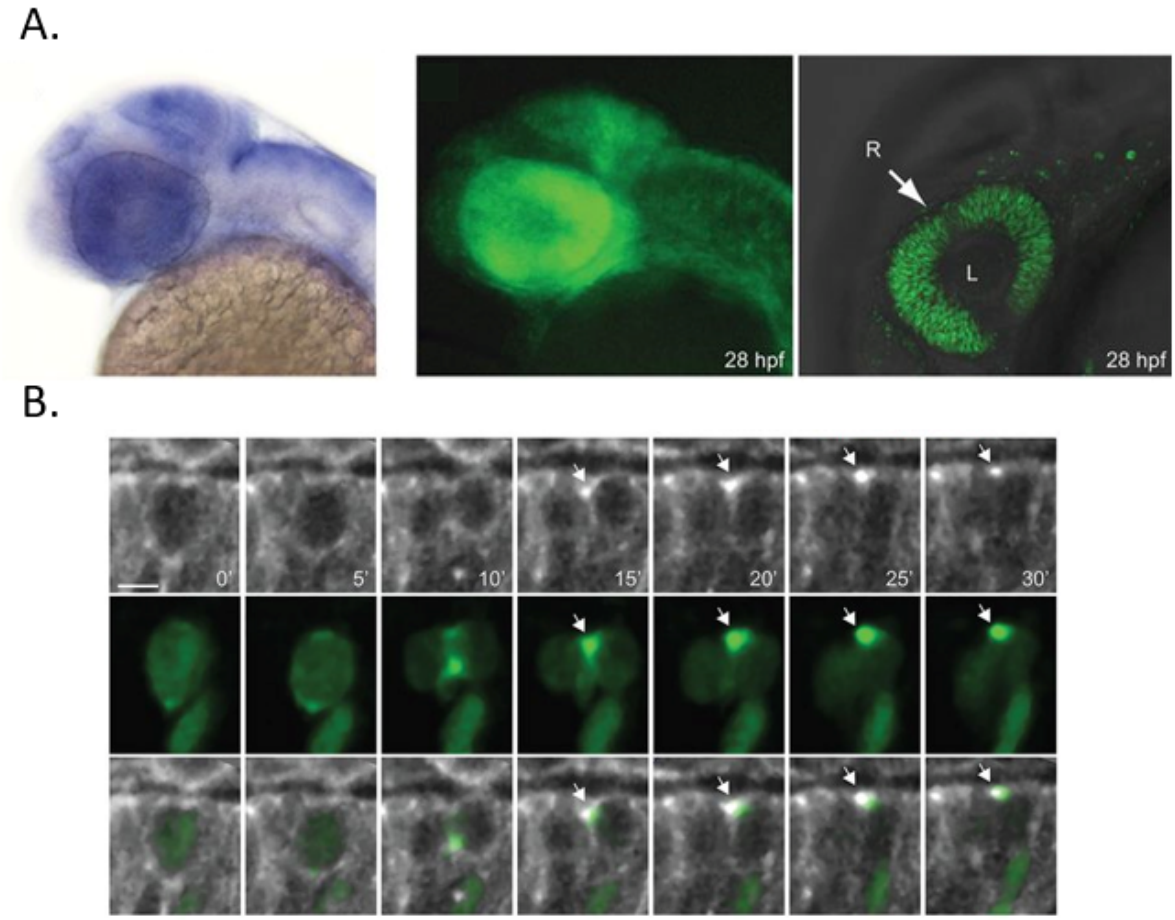

Figure 1.12: The *anln:anln-eGFP* zebrafish marks asymmetric cell division in retinal development

(A) The anln:anln-eGFP fluorescent reporter marks matches an anln mRNA in situ hybridisation showing high *Anln* expression in the retina . (B) Confocal imaging of the retinal cell layers identified *Anln* association with asymmetric cell divisions of retinal ganglion cells (Paolini et al. 2015).

Asymmetric cell division is a key process in eukaryotic invertebrate development where smaller daughter cells are produced by a larger parent cell (Knoblich 2008). This process is observed in budding yeast reproduction, where budding of the daughter cells from the mother cell is controlled by asymmetric gene expression, driving asymmetric placement of the cleavage furrow. This process is less common in vertebrates, particularly in embryogenesis, where cell divisions are typically symmetrical. Important regulators of asymmetric cell division observed across species include NUMB, PROSPERO and BRAT (Knoblich 2008). In vertebrate tissues, asymmetric cell division is rather associated with the differentiation of two individual daughter cells of separate lineages from progenitor cell types as investigated by Paolini and Malo et (Paolini et al. 2015; Malo et al. 2017). Outside of neuronal cell development, asymmetric cell division is also associated with the generation of multiple cell lineages in development, and in disease, by regulating self-renewal and tissue regeneration (Berika et al. 2014). Asymmetric cell division in haematopoiesis (controlled by Notch) regulates the self-renewal and differentiation of haematopoietic progenitors. Loss of Notch expression is associated with asymmetric haematopoietic cell differentiation, whereas increased Notch expression is associated with symmetric self-renewal of progenitor populations (Duncan et al. 2005; Schroeder 2007). Different inheritance of NUMB is thought to be associatewith altered levels of Notch signalling in daughters cells; NUMB was shown to act as a tissue specific repressor of NOTCH signalling in other cell types (Knoblich 2008).

In *C.elegans,* asymmetric cell division is key to early embryonic development, where embryonic cell lineages are generated from initial asymmetric cell divisions after fertilisation of the egg. ANLN has been associated with the establishment of cell polarity in early C*.Elegans* embryogenesis and cytokinesis. Here, the *C.elegans* orthologue of LKB1 (PAR4) has been shown to regulate the placement and activity of the ANLN orthologue ani-2 (Chartier et al. 2011). Loss of PAR4 results in inappropriate ani-2 localisation and dysfunctional acto-myosin contractility in asymmetric cell division (Chartier et al. 2011).

The relevance of asymmetric cell division to EC development and blood vessel formation has not been fully explored, however, recent investigations in zebrafish by Costa et al has shown asymmetric cell division in angiogenesis (Costa et al. 2016). The control of collective EC migration in angiogenesis in the mouse is influenced by baso-lateral inhibition between tip and stalk cell ECs (Phng & Gerhardt 2009). This is heavily influenced by asymmetric cell division and the differential inheritance of cell products to produce these two separate cell types (Costa et al. 2016). Imaging of zebrafish intersegmental vessels at 22-28hpf have identified fundamental differences in cell size between tip and stalk cells during angiogenesis (Costa et al. 2017; Costa et al. 2016). Asymmetric placement of the centriole allows for different post-mitotic inheritance of VEGFR machinery. This is a requirement of tip/stalk cell designation, allowing for efficient collective cell migration in angiogenesis (Costa et al. 2017; Costa et al. 2016).

Investigation of ANLNs expression in early vascular development or injury of the zebrafish embryo may identify a role of ANLN in angiogenesis.

1.16 Hypothesis:

ANLN is a new important target in ECs in cardiovascular disease. This thesis therefore examined the hypothesis that "ANLN is an important mediator of angiogenesis *in vivo* and *in vitro*".

1.17 Aims:

I sought to identify whether ANLN could affect EC function in angiogenesis *in vivo* and *in vitro* by addressing three separate questions. Hence my three aims were:

1. Investigate the effects of ANLN in post ischaemic angiogenesis.
2. Identify a potential post transcriptional mechanism for the regulation of ANLN *in vitro* and *in vivo* RBP.
3. Investigate the expression and role of ANLN in ECs *in vivo* using a zebrafish model of vascular development and injury.

Chapter 2: Methods

2.1 techniques for in vitro studies

2.1.1 Cell culture:

All cell culture was carried out at 37 ºC with 20% and 5% CO_2 in a humidified incubator, cell lines used and media are listed in *table 1.* For simulation of inflammation conditions, HUVECs had media supplemented with the addition of 10ng/ml IL-1β (Peprotech, 200-01B).

Table 1: cell lines used in in vitro studies:

Cells	media
Human vein umbilical ECs (HUVEC) (Lonza, C2517A	EGM-2 (EBM2+EGM bullet kit) (Lonza, CC-3162)
HEK293T (ATCC®, CRL-11268)	DMEM (10% FBS+1% Pen-Strep+2.5 mM glutamine) (Lonza)

1.1.2 SiRNA transfection:

Transfections were carried out using RNAimax lipofectamine transfection reagent (Thermofischer, 13778075). $1x10^5$ HUVEC were added to a 6 well dish and transfected with RNAimax according to the manufacturer's protocol with Optimem low serum media (Thermofisher, 3195062) using the siRNA and concentrations listed in *table 2*. The media was changed ~16 hours post transfection and transfections left for 48 hours before use in experiments.

Table 2: siRNA used in in vitro experiments

siRNA	manufacturer (order number)	Experimental concentration
All stars negative control	Quiagen (SI03650318)	10nm
ANLN	Quiagen (SI00122710)	10nm
ZFP36L1 1	Ambion (SI2089)	10nm
ZFP36L1 2	Ambion (SI2091)	10nm
ZFP36 1	Ambion (SI2026)	20nm
ZFP36 2	Ambion (SI2027)	20nm

2.1.3 Lentivirus production and transfection:

Lentivirus particles containing ZFP36 and EGFP coding sequences in the pRRL vector were obtained from Luccia Montorsi produced as described in Montorsi et al. 2016. Two lentiviral vectors were purchased from Cyagen^{TM}, an ANLN-EGFP and control EGFP plasmid [(pLV[Exp]-Neo-CMV>ClaI/EGFP(ns)/XbaI:hANLNSbfI)+(pLV[Exp]Puro CMV>EcoRV/ORF_91bp/XmaI/XbaI:IRES:EGFP/ClaI)]. After lentiviral plasmid DNA production and purification (see section 2.1.21), plasmid preparations were given to Pamela Brown of Edinburgh University Core facilities for packaging as per established methods (Collins et al. 2009).

$1x10^5$ HUVECs were plated in each well of a 6 well dish and transfected by incubation with 10 M.O.I. of lentiviral particles in EGM-2 containing 8µg/ml polybrene (Sigma, TR-1003) overnight. Media was replaced with fresh EGM-2 and the cells used in downstream assays.

2.1.4 Cell sorting:

ANLN-EGFP and EGFP control HUVECS were detached using trypsin (Thermofisher, 25200056) and resuspended in EGM-2 media in sterile FACS tubes (BD Biosciences, 352008). Cells were sorted on a FACS ARIA 2 (100µm nozzle) cell sorter, the live populations were gated from cell debris using BD FACS DIVA software and $EGFP^{+ve}$ cells collected in a FACS tube containing EGM-2 media. Post sorting cells were centrifuged at 300g at R.T and the FACS buffer and media aspirated away, the cell pellet was washed two times with PBS at R.T. The cell pellet was resuspended in EGM-2 and added to a T75 for further culture at standard cell culture conditions.

2.1.5 Matrigel assay:

In vitro angiogenesis assays were performed via the matrigel tubulogenesis assay. Matrigel was thawed on ice overnight and pipetted to the bottom of a 96 well plate (Corning, CLS3595) and solidified for half an hour at 37ºC. $1x10^4$ HUVEC were added to each well and incubated at 37ºC for 5-6 hours before being fixed with R.T 4% PFA for 10 minutes, PFA was replaced with PBS and images taken on a Leica inverted

microscope. Images were analysed with FIJI with the angiogenesis analyser plugin (NIH, Image J).

For live imaging matrigel was plated in a μ-angiogenesis slide (Ibidi). Live imaging data was acquired using a Zeiss wide field observer inverted microscope. Images were taken every 15 minutes, images were exported as high quality tiff format and compiled in FIJI.

2.1.6 Barrier function and wound healing assay:

Using the electric cell impedance (ECIS) based assay system (Applied Biophysics) the barrier function and migration capacity of HUVEC were measured. 8W10PET+ chambers (Applied Biophysics) for barrier function or 8W2LE chambers (Applied Biophysics) were coated with 1.5mM homo-cysteine and 10 μg/ml fibronectin and 0.2% gelatine. $6x10^4$ HUVECS were added to each well of the ECIS assay chambers. For barrier function experiments, assay chambers were left to equilibrate for 24 hours before the acquisition of data; following a further 24 hours post data collection the peak resistance for each chamber was taken and used for analysis. For wound healing assays the assay chambers were left to equilibrate for 24 hours before the application of an electrical wound at the parameters 20000mV for 30 seconds. Measurements were acquired up to 24 hours post injury and used to calculate the rate of wound closure post injury.

2.1.7 Cell cycle staining:

First, sub-confluent HUVECs were detached using Trypsin/EDTA, pelleted at 300G and washed three times with PBS. 10mls of ice cold 70% Ethanol *v/v* was then added to the pellet dropwise with gentle vortexing to disrupt the cell pellet into a homogenous solution, this was then stored at -20°C. For propidium Iodide (PI) staining. The fixed cells were allowed to gently equilibrate to R.T for 15 minutes before being centrifuged at 1500 *g* for 5 minutes then washed once in PBS followed by centrifugation at 1500 *g* for 5 minutes. PBS was aspirated and the cells were stained by addition of 200 μls per $3x10^5$ cells of staining solution containing 25 μg/ml PI and 30 μg/ml RNAse A (Sigma, 10109134001) in PBS, this was incubated at 37°C shielded

from light for 30 minutes. Samples were transferred to FACS tubes and analysed on a 5LSR Fortessa flow cytometer (BD biosciences). The cells were gated to generate cell cycle histograms by identification of the cells and exclusion of doublet cells, histograms were generated showing the relative intensity of PI stain. The individual peaks were gated to obtain counts of cells in the G_0/G_1, S and G_2M phases.

2.1.8 Cell proliferation assay:

Cellular proliferation assays was analysed by measuring via Edu (Thermofisher, E11087) incorporation. $1x10^4$ HUVECs per well were plated into a 96 well plate (Corning), after 24 hours the media were replaced with EGM-2 containing 10µM of EdU. This was incubated overnight before being fixed in 4% PFA for 15 minutes, cells were washed 3 times with PBS before being permeabilized with 0.5% Triton X-100 in PBS for 5 minutes. Staining for Edu incorporation was carried out using the Click-iT EdU alexa fluor 594 imaging kit (Thermofisher, C10339) according to the manufacturer's instructions. Images of each well were taken and on an inverted digital microscope the percentage of EdU^{+ve} nuclei against total nuclei were quantified using ImageJ.

2.1.9 Transwell filter migration assay:

6.5 mm transwell filter inserts (Corning, 3422) were coated with 10 µg/ml fibronectin and 0.2% gelatin (both manufacturers) and left to dry. HUVECs were starved in supplement free EGM-2 media for 6 hours and then detached with trypsin/EDTA and resuspended in migration media (EGM-2 without addition of growth factors supplemented with 0.5% BSA). EGM-2 supplemented with 20 ng/ml VEGF-A (Peprotech, 100-20) or its vehicle (PBS) was added to the wells of a 24 well plate (Corning, 3422), and $5x10^4$ HUVECs were added into each insert. Inserts were incubated for 3 hours in a humidified tissue culture incubator. Then, cells on the upper layer were scraped off using a cottons swab before fixing the transwells in ice-cold methanol for 10 minutes. HUVEC nuclei were stained using 1:5000 DAPI (sigma,

D5942) in PBS and then washed 3 times with PBS. The filter was cut from the insert and mounted on a glass slide using fluoromount (Sigma, F4680) and a coverslip. Images were taken on a Leica inverted microscope and images quantified with the ImageJ cell counter plugin.

1.10 Immunocytochemistry:

HUVECs were cultured on sterile 25 mm glass coverslips coated with 10 µg/ml fibronectin and 0.2% gelatin at a density of $5x10^4$ cells per well. Coverslips were fixed with 4% PFA (Fischer, 28908) at RT for 15 minutes. Coverslips were washed 3 times with PBS and permeabilized in PBS with 0.5% Triton X-100 (Sigma, T8787) for 15 minutes. Coverslips were blocked for one hour in 3% BSA in PBS. Following blocking, primary antibody (see *table 3*) was added to each coverslip in 1% BSA in PBS at 4°C overnight. Following primary antibody incubation staining solution was removed and coverslips washed 3 times with PBS. Secondary antibody incubations (*see table 3*) were carried out in 1% BSA in PBS for one hour at RT. Secondary antibody solution was removed and the coverslips were washed 3 times with PBS, this was followed by staining with DAPI and Phalloidin (see *table 3*) in PBS at RT for 5 minutes. Coverslips were mounted with Fluoromount™ (Sigma, F4680) on glass slides (Surgipath, 08001E) and left to set in the dark overnight at 4°C. Images were taken using a Zeiss LSM 780 confocal microscope.

Table 3: antibodies used in immunocytochemistry

Antibody and supplier	Clone	dilution
Anti-ANLN (Abcam, ab154337)	Polyclonal	1:125
Anti-EGFP (Abcam, ab6556)	Polyclonal	1:2000
Phalloidin conjugated to Alexa-Fluor 594nm (life technologies, A12381)	-	1:200
DAPI (Sigma, D9542)	-	1:1000
Anti-rabbit conjugated Alexa-Fluor 488nm (Life Technologies, A11072)	Polyclonal	1:500

2.1.11 Western blot sample preparation:

Protein sample concentration was assayed by BCA assay as per manufacturer's protocol (Thermofischer, 23225) in a 96 well plate (Corning). Samples were prepared in loading buffer (0.5% bromophenol blue, 2% β-mercaptoethanol, 10% glycerol (w/v) and 2% SDS) and heated to 95°C for 2 minutes.

2.1.12 SDS page and western blot:

Reduced samples and corresponding molecular weight markers (Thermofischer, 26616) were separated on 8/10% acrylamide gels; resolving gel (30% *v/v* Protogel (30% acrylamide *w/v* 0.8 % Bis-acrylamide *w/v)* (National diagnostics, EC-890) + 0.375M Tris-HCl pH 8.8+0.1% SDS +0.33% ammonium persulfate (10% *w/v*) + 0.1% TEMED), stacking (13% protogel *v/v*, 0.1M Tris-HCl pH 6.8, 0.1%SDS + 0.5% ammonium persulfate (10% *w/v)* + 0.1% TEMED). Gels were poured using a mini-protean stacking system (Bio-Rad, 1653303) and ran in an electrophoresis chamber in tris-glycine-SDS buffer (25mM Tris, 200mM glycine, 0.1% SDS) for 40 minutes at 65 volts followed by 1.5 hours at 95 volts. Proteins were transferred onto PVDF membranes in tris-glycine-methanol buffer (25mM Tris, 200mM Glycine and 10% Methanol) at 60mA overnight at 4°C.

After transfer membranes were stained with Ponceau S stain (Sigma, P7170) to confirm transfer, followed by washing in 0.03% *w/v* trichloroacetic acid in ddH_2O (Sigma, T6399). Membranes were then blocked in TBST (Tris-buffered saline pH 7.4 supplemented with 0.1% tween) and 5% non-fat milk for one hour at RT. The membrane was then incubated overnight in primary antibody (see *table 4*) at 4°C in TBST with 4% milk.

The primary antibody solution was removed and retained for future use and the membranes washed 3 times in TBST. Membranes were then incubated in the corresponding HRP linked secondary antibody in TBST with 4% milk for 1 hour at RT. Membranes were washed 3 times in TBST before being developed with Immobilon™ Western Chemiluminescent HRP Substrate (EMD Millipore, WBKLS0500) for 5 minutes. Excess development solution was removed by capillary action and the membrane was sealed in a development cassette with cling film. Signal was captured

by exposing CL-Xposure film (Thermofischer; 34089) to the membrane in a dark room. Film was developed using an automated processor (Konica, SRX-101A). Molecular weights were marked on the film after exposure and films scanned using an office scanner (Xerox).

Table 4: Antibodies used in Western blot:

Antibody and supplier	Clone	Concentration
Rabbit anti-ZFP36L1 (CST, 2119s)	Polyclonal	1:1000
Rabbit anti-ZFP36 CST (CST, 14030)	monoclonal	1:1000
Rabbit anti-EGFP (Abcam, ab6556)	Polyclonal	1:1000
Goat anti-ANLN (Abcam, ab5910)	Polyclonal	1:1000
Mouse anti-beta actin (Sigma, A3516)	Monoclonal	1:50000
Sheep anti-mouse HRP (Sigma A5906)	Polyclonal	1:5000
Goat anti-rabbit Sigma HRP (A0545)	Polyclonal	1:5000

2.1.13 RNA-extraction:

RNA extraction was carried out using the MiRneasy kit (Qiagen: 217084). RNA was extracted by addition of Qiazol (Quiagen: 79306) to cultured cells. Homogenates were incubated for 5 minutes and vortexed before the addition of 140µls of chloroform. Samples were vortexed and then centrifuged for 15 mins at 12000g at 4°C, the supernatant was removed leaving protein residue and phenol. The upper aqueous phase was transferred into a new tube (~600µl by volume) and 1.5 volume of 70% ethanol was added and mixed thoroughly. The sample was added to an RNeasy® Mini Spin Column and all on column steps were performed as per the MiRNAeasy protocol.

2.1.14 DNA/RNA quantification:

DNA and RNA samples were thawed on ice and 1.5µls added to a nanodrop. The RNA/DNA concentration was quantified in the sample for downstream application in cDNA generation or Biochemical assays.

2.1.15 Reverse transcription polymerase chain reaction (RT-PCR) by genomic DNA wipeout:

The QuantiTect Reverse Transcription Kit (QIAGEN, Cat. # 205311) kit and protocol were used for this process. 500 ng of RNA extract was added to RNAse free water to a volume of 12µl in PCR tubes and placed on ice. Then, 2µl of 7xgDNA wipeout buffer was added to each sample and mixed thoroughly by pipetting. The RT-PCR master mix per sample was made as; 1µl Quantiscript RT enzyme, 1 µl Quantiscript RT primer mix, 4µl of Quantiscript RT buffer 5x.

Each PCR tube was added to the thermocycler using the following protocol; 2 minutes 42°C, 4 minutes hold at 4°C (addition of 6µls of master mix followed by thorough mixing by pipetting), 30 minutes at 42°C, incubation for 3 minutes at 95°C, cDNA was stored frozen at -20°C.

2.1.16 qPCR protocol:

Power SYBR® Green PCR Master Mix (Applied Biosystems, Cat. # 4367659) was used for the following qPCR protocol. Primers were supplied by Life Technologies and sequences are listed in *table 5*. Sample mixes consisted of 5µls Power SYBR green PCR master mix, 3µls of RNase-free water and 1 µl of 10µM primer mix.

The lightcycler™ protocol used is as follows; melting 95°C, 15 seconds, annealing 65°C, 30 seconds; extension 72°C for 30 seconds. Quantification was performed using the $2^{-\Delta Ct}$ method using the house keeping gene 18s.

Table 5: qPCR primers:

Primer name	sequence
ZFP36	Forward: CAAGTAATCCCCTTTTCCAG Reverse: CACCATCATGAATACTAGC
ZFP36L1	Forward: TTATGGAAGGGTAACAAGC Reverse: TGGTTCTGGTGGAACTTG
ANLN	Forward: ATAGCAGCAGTGTTAAGCAGG Reverse: AACCAAAGACCCATCACAGC
VEGF	Forward: ATCTGCATGGTGATGTTGGA Reverse GGGCAGAATCATCACGAAGT
18s	Forward: CCAGTAAGTGCGGCTCATAT Reverse: CCGAGGGCCTCACTAACC

2.1.17 Cloning:

The sequences were selected from the UCSC genome browser (https://genome.ucsc.edu/) and primers designed on Primer3 primers and manufactured by Sigma Custom oligos, see *table 6*. PCR reactions were carried out using 1x Q5 reaction buffer (NEB: B90275), Q5 High Fidelity polymerase 0.02U/µl, 200µM dNTPs (NEB: B90275), 0.5µM forward, 0.5µM reverse primer and 1µl template cDNA. Reactions were ran on a thermocycler with the following protocol, Denaturation at 98°C for 30 seconds, 25-30 cycles of 98°C for ten seconds then 63°C for 30 seconds then 72°C for 30 seconds followed by a final extension at 72°C for 2 minutes and a final hold at 4°C.

Table 6: primers for insert preparation

Sequence name	Forward	Reverse
ANLN 3'UTR	CATGCTATCTAGAGGTTTTTGATG	TTCCTTTAGACATTTACAGGTATTTATTT
ZFP36L1 coding sequence	TAAGCTTATGACCACCACCCTCGT	TTCTAGATTAGTCATCTGAGATGGAAAGTC

2.1.18 DNA gel electrophoresis:

PCR products were mixed with 10X loading buffer (100mg orange G, 15 ml glycerol and 35 ml H_2O) and DNAse free water, then ran on a 1.2% ultrapure agarose (Thermofishers) gel incorporating Gel Red (Biotium) in TAE buffer (0.04M Tris-acetate and 0.001M EDTA) at 95V at 4°C. The gel was imaged using a trans illuminator and the corresponding molecular weight bands cut from the gel using a scalpel, transferred to a DNAse free tube for processing and stored frozen at -20°C.

2.1.19 Restriction digests:

PCR products and plasmids [pMIR or pCDNA3.1 (Thermofisher, AM5795+V79020)] were digested to produce sticky ends using Spe1 (NEB: R01335), HindIII (NEB: R70025) or XbaI (NEB: R0145S), using NEB2 buffer (NEB: R90275) at 37°C for 2 hours as per the manufacturers protocol. The digestion products were purified by chloroform phenol extraction; products were made up to 300 µls with H_2O, 150µls of Phenol and chloroform were added and the solution vortexed. This was incubated at room temperature for 2 minutes then on ice for 2 minutes. This was then centrifuged at 13000 *g* at 4°C and the upper aqueous layer removed and added to 3x volumes of 100% ethanol and 1:10 *v/v* 3M sodium acetate. This was vortexed and frozen at -80°C. Samples were thawed on ice and centrifuged at 13000g for 30 minutes and the supernatant discarded. The pellet was washed in 70% ethanol, allowed to dry and then resuspended in DNAse free H_2O.

2.1.20 DNA gel extraction:

DNA gel extractions were performed using the QIAquick Gel Extraction Kit (Qiagen, 28704). First, excised DNA bands were suspended in 3 times the gel weight of QG buffer and heated at 50°C until the agarose gel had dissolved. Following this, one volume of isopropanol was added to the sample and mixed thoroughly by pipetting. Then the entire sample was added to a QIAquick column and centrifuged for 1 minute at 13000 *g*. Following this all on column steps were carried out as per manufacturer's

instructions. DNA was eluted by addition of 30µls of DNase free water to the column and centrifugation at 13000 *g*.

2.1.21 DNA ligation and bacterial transformation:

Ligations were performed using a rapid ligation kit (Roche: 11635379001) using 3-10x molar insert-to-plasmid ratio, as described in the manufacturers protocol. 2µls of ligation mixture were mixed gently with 50 µls of NEB-5α Bacteria (NEB; P/N: C2988J) on ice and the mixture was left on ice for 30 minutes before being heat shocked at 42oC for 45 secs and placed on ice for 2 minutes. Bacteria were added to 1 ml of LB broth (1% *w/v* Tryptone, 0.5% *w/v* bacto-yeast extract 170 mM $NaCl_2$ PH 7.0 NaOH) and placed on a shaker for one hour at 37°C. The bacteria were spread onto plates (Corning) containing LB agar with 100µg/ml ampicillin (manufacturer). Colonies were selected and grown in 10 ml LB broth with 100 µg/ml ampicillin. Miniprep (Quiagen: 27104) extractions were performed as per manufacturers protocol and selected colonies were sequenced by Reliance Biosciences. One selected colony was grown in 300 ml of LB broth with 100µg/ml ampicillin overnight, bacteria were pelleted and maxi prep extractions (Thermofisher, K210006) were performed as per the manufacturer's instructions.

2.1.23 Calcium phosphate transfection:

300µM $CaCl_2$ containing ANLN-LUC plasmid, ZFP36/ZFP36L1/control plasmid and CMV-β-galactosidase plasmid (Clontech, 631712) was left at room temperature for 15 minutes. This solution was then diluted 1:1 *v/v* by dropwise addition to 37°C HEPES buffer (270mM NaCl, 10mM KCl, 12 mM D-Glucose, 25 mM HEPES, 1.5mM Na_2PO_4 pH 7.06) while being vortexed. DNA solution containing 20ng of ANLN-Luc plasmid, 20ng ZFP36/ZFP36/PcDNA3.1 and 100 ng β-galactosidase was added to $4x10^5$ HEK293 with fresh DMEM in a 24 well plate (corning). The media was replaced after 24 hours and the cells re-suspended after 48 hours in luciferase lysis buffer (Promega, E1910).

2.1.22 Luciferase assay:

The cell lysates were centrifuged at 12000 *g* at 4°C and a BCA assay performed as per manufacturer's instructions (Thermofisher, 23225). 2µg of each lysate was added per well of a 96 well plate (Corning,3610) and 100µl of luciferase substrate (Promega:E151A) was added to each well simultaneously using a multipipette. The plate was read in luminescent plate reader (Tecan, infinite). To normalise the transfection, a β-galactosidase enzyme assay (Promega, E2000) was carried out in parallel in a 96 well plate (Corning, 3610) according to the manufacturer's protocol. The optical density (420 nm) was read in a plate reader (molecular devices, Spectramax) and the values obtained used to normalise the results of the luciferase assay.

2.1.23 RNA immunoprecipitation (RIP):

The Magna RIP kit (Millipore, 17:700) was used to extract RNA bound to ZFP36L1/ZFP36 from HUVEC cell lysates as per the manufacturer's protocol. $6x10^6$ HUVEC were used per RIP with 5µg anti-ZFP36L1/ZFP36 antibody (Santa Cruz, 79151/14030). 10% of the input lysate was retained for downstream analysis. The beads and input lysate had bound RNA extracted by phenol:chloroform extraction as previously described in section 2.1.19 and RNA samples were stored at -80°C. cDNA was produced as described in section 2.2.15 and analysed by qPCR, CT values were normalised to 10% of the input lysate to determine the target transcript enrichment.

2.2 techniques for in vivo studies:

2.2.1 Immunohistochemical DAB stain:

Hind limb ischaemic adductor muscles were harvested at day 7 and fixed in 10% buffered formalin (Sigma, HT501128) for 16h at 4°C before embedding in paraffin blocks. 4µm paraffin embedded skeletal muscle tissue sections were cut and baked onto glass slides.

Tissue sections were rehydrated gradually by incubation of slides in the following solvent gradient, 2 times 5 minute incubations in Xylene, 5 minutes in 100% ethanol, 5 minutes in 85% ethanol, 5 minutes in 50% ethanol. The slides incubated in 3% Hydrogen peroxide (sigma, H1009) in distilled water for 20 minutes followed by two 5 minute washes in phosphate buffered saline-tween (0.05% Tween) to block endogenous peroxidases. Antigen retrieval was carried out in 10mm sodium citrate buffer, samples were boiled for 5 minutes in a microwave on the fast cook setting, followed by another 10 minutes of heating on low. Samples were allowed to cool to RT before being blocked with 10% goat Serum for 30 minutes at RT. Slides were incubated overnight in primary rabbit anti-ANLN diluted (Abcam, Ab154337) to 1:125 in 5% goat serum. Primary antibody solution was removed and the slides washed in three 5 minute washes in PBST. After washing slides were incubated in biotinylated secondary goat anti rabbit antibody (DAKO, BA1000) diluted to 1:200 in 5% goat serum for 45 minutes at RT. Secondary antibody solution was removed and the slides were washed in three 5 minute washes in PBS-Tween. The section was covered in Elite ABC all in one reagent (Vector, Vector PK7100) and incubated for 30 minutes in the dark. ABC solution was removed and the slides washed in three 5 minute washes in PBST. The section was covered in peroxidase substrate DAB kit solution (Vector, SK4100), the brown stain was allowed to develop and the reaction stopped at the first sign of positive signal by washing the slides for 5 minutes in ddH_2O. After DAB stain development samples were counterstained with 0.5% light green counterstain (Genetex, GTX73306). Samples were dehydrated in a reverse solvent gradient and

mounted with cover glass using DPX mounting media (Sigma, 06522) and left overnight at RT.

Slides were imaged using a Nanozoom XR with NDP viewer 3.1 (Hamamatsu). Images were exported at 20x digital zoom Tiffs and the average number of $ANLN^{+ve}$ ECs counted per vessel.

2.3 zebrafish production:

2.3.1 Zebrafish maintenance and husbandry:

All zebrafish maintenance and experimentation were carried out in accordance to home office guidelines under the project licence: and personal licence: Zebrafish were maintained in system water at 28.5°C and were fed three times daily a mixture of either dry food or brine shrimp as in accordance with the University of Edinburgh husbandry policies. Zebrafish used are listed in *table 7*

Table 7: Zebrafish lines utilised:

Zebrafish line	Phenotype description	Source
WIK	Wild type	Dr Carl Tucker (CBS aquatics university of Edinburgh)
*flk:*mcherry	*Flk:*mcherry express mcherry in ECs.	Professor John Mullins (CVS University of Edinburgh)
*fli1:*eGFP	*Fli1:*eGFP express eGFP in ECs.	Dr Martin Denvir (CVS University of Edinburgh
*fli1:*eGFP x *mpx*:mcherry	*fli1:*eGFP: *mpx*:mcherry express eGFP in ECs and mcherry in neutrophils.	Dr Martin Denvir (CVS University of Edinburgh)
anln:anln-eGFP	*anln:anln*-eGFP fish express *Anln-eGFP* fusion protein under the *anln* promoter globally.	Dr Luccia Poggi (University of Trento)

2.3.2 Zebrafish embryo production:

Transgenic embryos were produced by pair mating in breeding tanks, WIK embryos were produced using a mass embryo production system (MBK installations ltd). Zebrafish were maintained in E3 media (5 mM NaCl, 0.17 mM KCl, 0.33 mM $CaCl_2$, 0.33 mM $MgSO_4$, 10^{-5} % Methylene Blue) in 90mm dishes in a 28.5°C incubator with daily water changes and maintenance.

2.4 Zebrafish experimental techniques:

2.4.1 Anaesthesia protocol:

Zebrafish were anaesthetised by suspension of embryos in system water containing 0.02% tricaine until fully unresponsive.

2.3.4 Morpholino mediated gene expression interference:

Morpholinos were used to modulate the expression of a*nln* as described in Paolini et al. 2015. Lyophilised morpholinos were reconstituted to 1 nM concentration with 300 µls of DNAse free dH20 and gentle mixing via pipetting.

Table 8: Morpholinos used in injections:

Morpholino	manufacturer	Sequence	Target
Control	Gene tools	CCTCTTACCTCAGTTACAATTTATA	No genomic target
ATG morpholino	Gene tools	GTACGCTACAAGCTGAAAGTAAAGT	Kozac sequence of ANLN
Splice morpholino	Gene tools	TTTCACAAAAAGCTCTCACCTCGGT	Exon 2 of ANLN pre-mRNA

2.4.3 Microinjection:

Micropipettes (WPI, IB100F-4) were pulled on a micropipette puller (Sutter's, instruments) with settings; heat 580, pull 250, velocity 50, time 125ms. Microinjection needles were loaded with injections solutions containing 8ng/µl morpholino (*see table 8*) and 0.01% phenol red (Sigma,143-74-8). 1nl of each morpholino solution was injected in zebrafish embryos at the one cell stage, damaged embryos were removed after ~4 hours and the viable embryos had E3 media changed daily prior to being imaged.

2.4.4 Zebrafish mRNA extractions

Zebrafish mRNA extractions were carried out essentially as detailed in section 2.1.13, except that an additional initial homogenisation step was carried out. 30 embryos were anaesthetised and media was removed before the addition of 700µls QIAzol followed by storage at -80°C. Samples were defrosted on ice and added to an RNase free 2ml tube containing 2 metal beads (fisher, 15505809) samples were homogenised with a benchtop homogeniser (Retsch, mm301) for 2 minutes at 30 Hz. The homogenate was then processed using the standard miRNAeasy kit protocol (Qiagen, 217084).

2.4.5 Zebrafish QPCR:

This was carried out essentially as described in section 2.1.16, using the primers listed in *table 9.*

Table 9: Zebrafish QPCR primers

Primer	sequence
Beta actin	F: GATCTTCACTCCCCTTGTTCA R: GGCAGCGATTTCCTCATC
elf1α	F: CCTTCGTCCCAATTTCAGG R: CCTTGAACCAGCCCATGTT
ANLN	F: CGTGGCGAGTGTGTGTATGT R: CTCTCCGCCATCTTCTTCTG

2.4.6 Laser Injury induction:

Embryos were anaesthetised with tricaine by established methods and then mounted on a glass coverslip; excess water was wicked away with tissue paper. Fish were orientated on a glass cover slide using the brightfield of an inverted microscope (Nikon, TE62000), using the 40x objective lens the caudal artery was brought into focus. The eye piece shutter was closed and the embryos were treated with pulses of

unattenuated 455nm micropoint laser (Andor). Fish were rehydrated by addition of E3 media with Tricaine before being imaged.

2.4.7 Tail fin injury:

Embryos were anaesthetised using the established tricaine method. Fish were orientated using forceps and a small transection of the tail fin of the zebrafish embryo cut using a size 11 scalpel (Swann Morton, W260). The anatomical end of the notochord was identified visually and by pigment location; with the help of these markers, the same degree of injury was induced in all fish. Fish were then imaged using Spinning disk microscopy at 4 and 24 hours post injury time points post injury. Images were exported and analysed using FIJI (ImageJ, NCBI).

2.4.8 SgRNA production for CRISPR/CAS9:

The sgRNA core sequence was taken from CHOPCHOP using the experimental design parameters of Xu et al. 2015. The T7/SP6 sequence and universal primer sequence were added onto the ~20 nucleotide core sequence, these are listed in *table 10.*

Table 10: sgRNA sequences for CRISPR/CAS9 generation yet:

Promoter	gRNA sequence	Universal sequence	purification
SP6(ATTTAGGTGACACTATA)	GAAGGGGGATGGCTTGGAGG	GTTTTAGAGCTAGAAATAGC	Desalt
T7(TAATACGACTCACTATA)	GGACGCCTCTGTTAACTCT	GTTTTAGAGCTAGAAATAGC	Desalt
T7(TAATACGACTCACTATA)	GGGGTCGAGCACAGAACTCT	GTTTTAGAGCTAGAAATAGC	Desalt
T7(TAATACGACTCACTATA)	GGGGATGGATCCATTCACCG	GTTTTAGAGCTAGAAATAGC	Desalt
T7(TAATACGACTCACTATA)	GGGGATGGATCCATTCACCG	GTTTTAGAGCTAGAAATAGC	HPLC

2.4.8 sgRNA annealing and *in vitro* transcription:

The sgRNA templates were produced by annealing of a sgRNA oligo (see *table 10*) to the universal tracRNAoligo: 5'AAAAGCACCGACTCGGTGCCACTTTTTCAAGTTGATAA-CGGACTAGCCTTATTTTAACTTGCTATTTCTAGCTCTAAAAC 3' by Q5 polymerase. Reactions were carried out using Q5 reaction buffer 1x (NEB: B90275), Q5 high fidelity polymerase 0.02U/µl, 200µM dNTPs (NEB: B90275), 0.5µM oligo and 0.5µM TRACR oligo. Annealing reactions were ran on a thermocycler (Techne, Thermal personal) with the following protocol; denaturing 98^{o}C 2 mins, annealing 50^{o}C 10 mins, extension 72^{o}C 10 mins. Annealed templates were quality checked by agarose gel electrophoresis as previously described in *section 2.1.18*.

The sgRNA was transcribed from templates by addition of 3µls gRNA template to a T7/SP6 mMessage machine *in vitro* transcription reaction according to the manufacturer's protocol (AMBION, AM1340/AM144). 1µl of completed reactions were suspended in RNase free water and orange G buffer to a volume of 10 µls. Samples were then ran in a 1.2 % agarose gel as previously described in section *2.1.18*.

2.5 Zebrafish Microscopy techniques:

2.5.1 Epifluorescent microscopy:

Zebrafish anaesthetised by established tricaine method were aligned on a glass cover slide in a drop of E3 media in 0.5% w/v methylcellulose (Sigma, M7140). Images were acquired on a Leica M205FCA epifluorescent microscope with a 1x planpo objective lens using filter sets ET GFP2 and ET mcherry (Leica, 232FL349303, 232FL349306). Images were acquired with LASX software and exported in Tiff format; quantification was performed using FIJI (NIH, ImageJ).

2.5.2 Andor Spinning disk confocal microscopy:

First, a 35 mm round cover glass was attached to a custom mounting dish with vacuum grease (Thorlabs, SG10). Zebrafish were anaesthetised via established method and added in system water to the glass cover slip, excess system water was removed and molten 0.5% agar was added to the coverslip and individual fish were manipulated with forceps to the desired position.

After mounting fish on the microscope stage images were taken using 10x and 20x air objective lenses (Zeiss, UPLFLN10X2/UPLSAPO20X) with Channel 488 (300 ms exposure) and 561 (100ms exposure). Images were acquired with IQ3 software (Andor) and exported as the TIFF image format; images were compiled in FIJI (NIH, ImageJ). For live imaging, E3 media containing tricaine was added on top of mounted fish in a heated and humidified stage (Oko-lab) utilised to maintain the temperature at 28°C.

2.5.3 Confocal microscopy:

First, a 35 mm round cover glass was attached to a custom mounting dish with vacuum grease; anaesthetised fish were mounted in 0.5% Agar. For this, zebrafish were anaesthetised via established method and added in system water to the glass cover slip, excess system water was removed and molten 0.5% agar was added to the coverslip and individual embryos were manipulated with forceps to the desired position. To obtain serial Z-stacks and tile scanned images of zebrafish embryos, a Leica SP8 confocal microscope was used. Images were acquired with a HC PLAAPO 10X CS2 (Leica) and HC PLAPO 20X CS2 (Leica) objective lenses. The following detector sets were used HYD1 (498-550nm) HYD2 (571nm-650nm) with lasers used 488nm (8%) laser 561 nm (2%) laser.

Images were acquired using LAS X software (Leica) and images saved as .LIF files before being exporter to TIFF format with ImageJ. Tile scanning was performed by scanning through the entire Z-stack and setting the highest and lowest points, followed by gating of the entire embryo for stack acquisition through spiralisation.

2.5.4 Selective plane illumination microscopy (SPIM):

Zebrafish embryos were anaesthetised by established tricaine method and placed in molten 0.5% Agar in E3 media (no methylene blue). Embryos were mounted in custom syringe mounts by pulling on the plunger to orientate the embryo in fluorinated ethylene propylene tubing (Adtech, TW01), the agar was left to solidify.

Embryos in syringe mounts were placed in the SPIM microscope stage and images acquired using a 16x NIKON CFI plan fluor objective (N16LWD-PF) with a Vortran Versalase multiple wavelength system as the light source, using 2 lasers 488 nm and 561 nm. Data was collected through two QI-Click Mono CCD cameras (Q-Imaging Inc.). Lasers were set to pulse and scan, the acquisition of each wavelength was acquired independently (40ms exposure and 100 ms exposure). Z-stack projections were produced and recorded through a custom SPIM control software written in the C programming language (Johnathan Taylor, University of Glasgow). Images were exported as multi-layer tiffs and concatenated and compiled using ImageJ.

2.6 Statistics:

All statistical analyses were carried out using Prism 5 (Graph pad) and are detailed in the corresponding figure legends.

Chapter 3:

Does ANLN effect EC function?

3.1 Introduction:

As stated in chapter 1 cardiovascular disease is one of the leading causes of death world-wide, in western countries an increasing elderly population and poor diets have created a health crisis. Critical limb ischaemia and coronary artery are the leading causes of ischaemic injury, disability, and death in cardiology patients. In these conditions chronic ischaemia and inflammation leads to EC dysfunction, disrupting natural regeneration and angiogenesis, resulting in poor prognoses and eventual death.

Identification of new potential therapeutic targets in the natural angiogenic response to injury or ischaemia is essential for future drug discovery. In the Caporali lab initial studies have identified numerous potential angiogenic targets of interest in improving the vascular response to injury (Caporali & Emanueli 2011; Caporali et al. 2011). Comparison of microarray datasets from sorted mouse hind limb ischaemic ECs and HUVEC overexpressing the P75 NTR (a negative regulator of angiogenesis) has identified numerous genes in cell motility, the cell cycle and actin remodelling as key potential mediators of angiogenesis (Caporali et al. 2012; Caporali et al. 2015). Investigating genes controlling these processes is essential to understanding early angiogenesis (Silvestre et al. 2013). ANLN was a robust gene identified in these *in vivo* and *in vitro* datasets as a gene of interest in the EC angiogenic response to ischaemia (Caporali et al. 2012; Caporali et al. 2011).

ANLN is an F-actin binding protein which is associated with the cleavage furrow formation during cytokinesis in all cell types as laid out in chapter 1. Here ANLN acts as a structural component of the cytoskeleton to allowing the association of F-actin with RhoA to regulate the ingression of the cleavage furrow and the orderly completion of the cell cycle (Piekny & Maddox 2010). Outside of these key roles ANLN has been a gene of interest in other aspects of cell function in numerous cell types (Piekny & Maddox 2010; Dorn et al. 2010). ANLN expression has been associated with pro migratory and invasiveness phenotypes in lung, breast and prostate cancers, $ANLN^{+ve}$ tumour biopsies result in a poor prognostic survival of clinical patients

(Suzuki et al. 2005; Zhou et al. 2015). In embryonic development of the CNS ANLN is associated with migrating neuroblasts, where, ANLN localises toward the leading filopodia of neurite outgrowth helping to stabilise the interaction between F-actin and RhoG (Tian et al. 2015; Fotopoulos et al. 2013). ANLN has been identified as a potential regulator of cell to cell junction integrity in epithelial cells (Reyes et al. 2014; Wang et al. 2015). Here ANLN was suggested to have interactions with multiple signalling pathways by acting as a structural component for the interaction of the cytoskeleton with cell to cell junction proteins (Reyes et al. 2014; Wang et al. 2015).

ANLN has been identified as a highly upregulated in both tail fin and myocardial regeneration in zebrafish and its expression is of interest in marking mitotic cells or the regenerative response in these injuries (Kang et al. 2016; Malo et al. 2017). ANLN has never been investigated in ECs in angiogenesis and it would be of advantage to identify its potential effect on EC phenotypes and behaviours particularly the EC response to ischaemia.

3.2.1 Hypothesis:

Experiments were carried out with the hypothesis that ANLN is required for normal EC function and that ANLN is required for the response to ischaemia *in vivo,* to be investigated with the following aims.

3.2.2 Aims:

1. Investigate the expression of ANLN in ischaemic angiogenesis using *in vivo* hind limb ischaemia
2. Investigate a possible role for ANLN in ischaemic angiogenesis using *in vitro* techniques to assess EC function after ANLN expression modulation

3.3 Results:

3.3.1 There is an association between ANLN expression and Ischaemia in ECs:

To investigate the expression of ANLN in the endothelial response to ischaemic insult a hind limb ischaemia surgery was performed in mouse. ANLN expression was assayed by QPCR in $CD31^+$ $CD45^-$ ECs sorted from ischaemic hind limb muscle. This demonstrated an increase of ANLN expression from 3-15 days post ischaemia compared to the mRNA from whole muscle as shown in *figure 3.3.1B+C* (***= P<0.001 *=P<0.05 Two-way Anova with post-hoc Bonferroni). As detailed in *figure 3.3.1A* the response of the tissue and blood vessels in the skeletal muscle changes over the time course of the experiment, with the peak proliferation of ECs occurring at ~7 days post-ischaemia. Therefore, at 7 days post ischaemia we stained for ANLN in sectioned hind limb ischaemic muscle to identify ANLN expression in the vessels. DAB staining of Ischaemic muscle tissue 7 days post ischaemia seen in *figure 3.3.1D+E* showed an increased expression of ANLN in the vessels compared to non-ischaemic muscle tissue (*= P<0.01 t-test). These experiments suggested an association between ANLN expression and ECs *in vivo* during ischaemia.

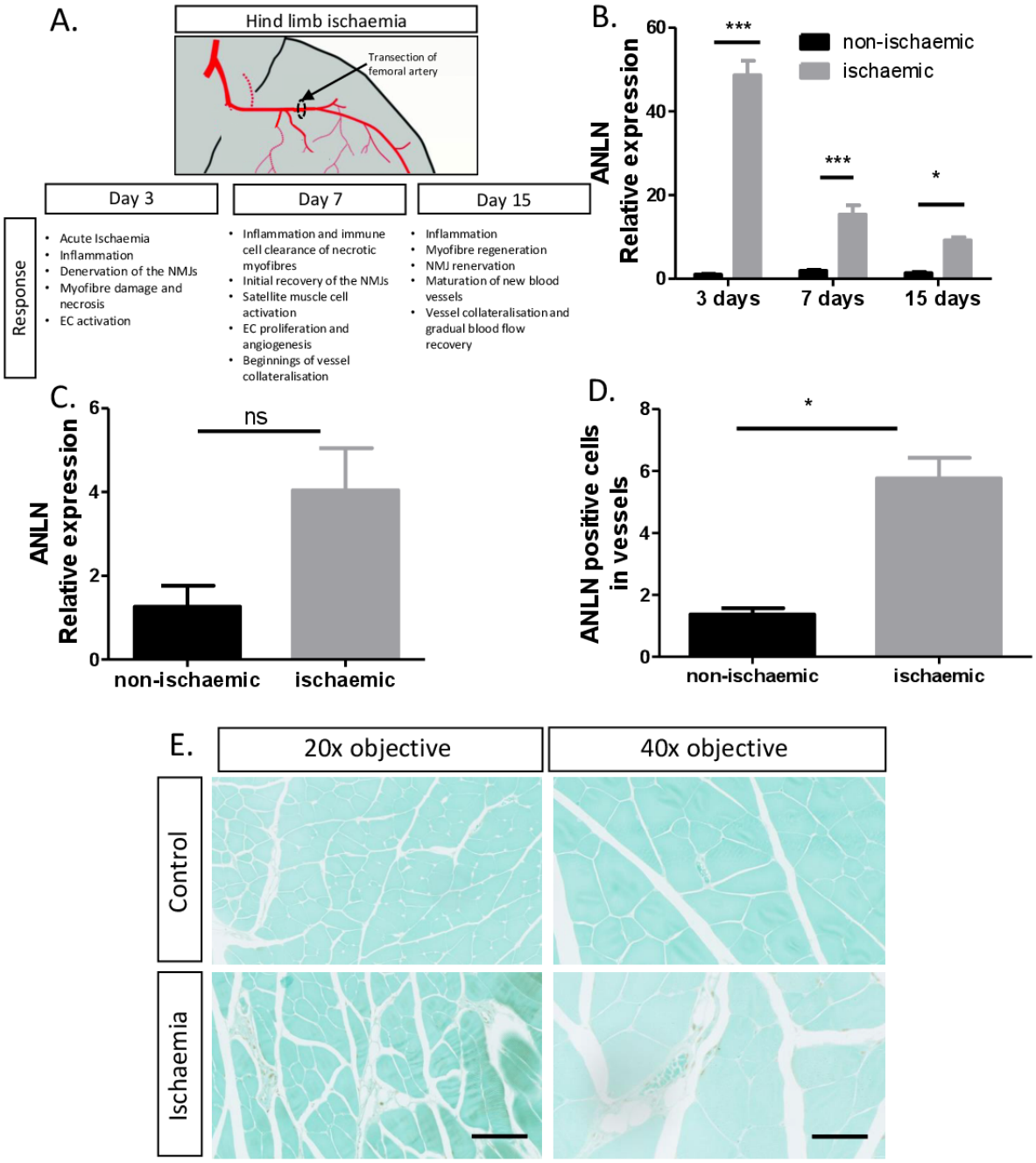

Figure 3.3.1: ANLN expression is increased in the ECs of mouse hind limb ischaemia muscle:
(A) Timeline of the response of the skeletal muscle and blood vessels to femoral artery transection induced ischaemia over 3, 7 and 15 days (adapted from Jia et al. 2011 and Mohiuddin et al. 2019). (B) ANLN mRNA expression is significantly increased between 3, 7 and 15 days post ischaemia in $CD31^{+}CD45^{-}$ ECs sorted from hind limb ischaemia (n=4 ***=P<0.001, **=P<0.01 by 2 way). (C) Shows a trend for an increase of ANLN mRNA expression in whole ischaemic muscle tissue compared to control non-ischaemic muscle 7 days post ischaemia (n=4, ns=P>0.05 by t-test) (D) Quantification of the average ANLN positive ECs per vessel in non-ischaemic and ischaemic muscle tissue (n=3, *= P<0.05 by t-test).) (E) 20x and 40x objective representative images of control and ischaemic muscle tissue DAB stained for ANLN expression (scale bars=100µm+50µms). (B+C) QPCR performed by L. Rose)

3.3.2 ANLN-EGFP can be successfully overexpressed and WT localisation is conserved in ECs

HUVECS were transfected with control or ANLN siRNA resulting in a reduction of ANLN mRNA expression as shown in *figure 3.3.2A-B*. A loss of ANLN mRNA expression results in a loss of WT ANLN signal in the nucleus of transfected HUVECs (*figure 3.3.2C*).

To identify the effect of ANLN overexpression on EC function and ANLN localisation in ECs an ANLN-EGFP lentivirus was produced. Inverted microscope images of HUVEC after treatment with ANLN-EGFP or control GFP lentivirus showed that ANLN-EGFP has a nuclear localisation compared to dispersed cytosolic control EGFP expression. Transduction with 10 M.O.I. of ANLN-EGFP lentivirus gives a visibly lower transduction efficiency than an equivalent control EGFP lentivirus. Flow analysis of HUVEC after treatment with the lentivirus showed was 50% less ANLN-EGFP^{+ve} ECs than the equivalent EGFP control (**=P<0.01, t-test). To obtain pure ANLN-EGFP overexpressing populations, cells were sorted using FACS, the gating strategy is shown in *figure 3.3.3B*.

Confocal microscopy of ANLN-EGFP transduced HUVEC shown in *figure 3.3.4A* after staining for EGFP, DAPI and phalloidin confirms the nuclear localisation of ANLN-EGFP, furthermore, cortical and mid-body localisation can be seen in mitotic cells confirming ANLN-EGFP functionality. Western blot of lysates from sorted ANLN-EGFP and control EGFP transduced HUVEC showed a band of ~160kda in size after staining with both anti-GFP and anti-ANLN antibody (*figure 3.3.4B*). These experiments suggest that functional ANLN can be overexpressed successfully and visibly retain WT ANLN localisation *in vitro*.

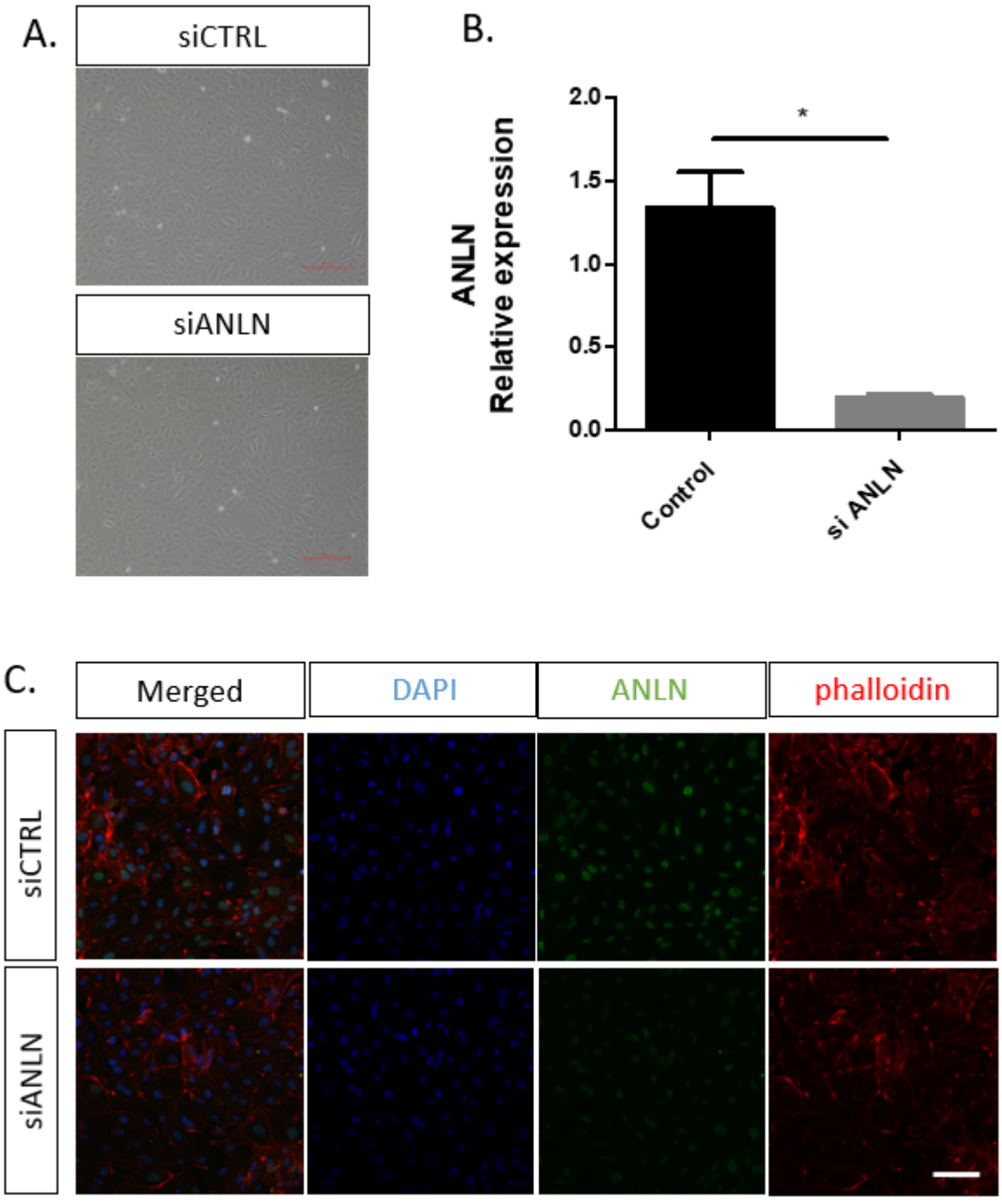

Figure 3.3.2 WT ANLN expression is nuclear in ECs *in vitro*:
(A) Brightfield images of HUVECS 48 hours after transfection with 10 nm ANLN or control siRNA. (B) QPCR of HUVEC mRNA 48 hours after transfection with 10nm siANLN shows a concurrent decrease in ANLN mRNA (n=3 *=P<0.05 t-test). (C) Immunocytochemistry of HUVECS after transfection with 10nm Control/siANLN showing staining for DAPI, ANLN and phalloidin demonstrating a reduction of ANLN expression in the nuclei of siANLN transfected cells (scale bars=100µm). ((A) preliminary data from A.Caporali)

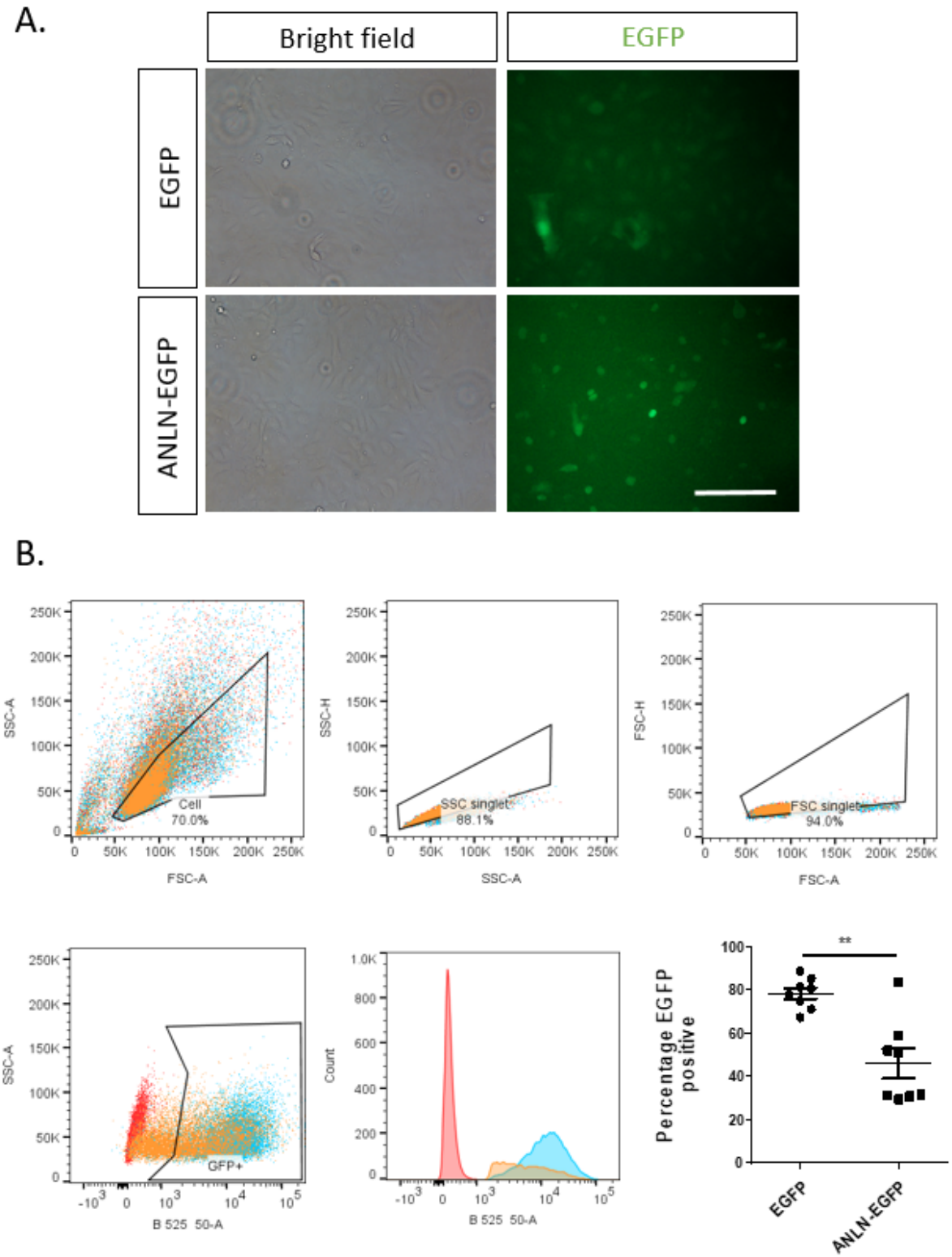

Figure 3.3.3 Cell sorting is required to obtain a pure population of ANLN-EGFP overexpressing ECs: (A) Lentiviral overexpression of ANLN-EGFP in HUVEC produces a low efficiency of ANLN-EGFP^{+ve} nuclei in ECs compared to EGFP control detected by brightfield and epifluorescence (scale bar=50µm). (B) Flow analysis of ANLN-EGFP/EGFP expressing ECs identified a significantly lower expression of ANLN-EGFP compared to EGFP control. (n=8 error bars=S.E.M**=P<0.01 t-test).

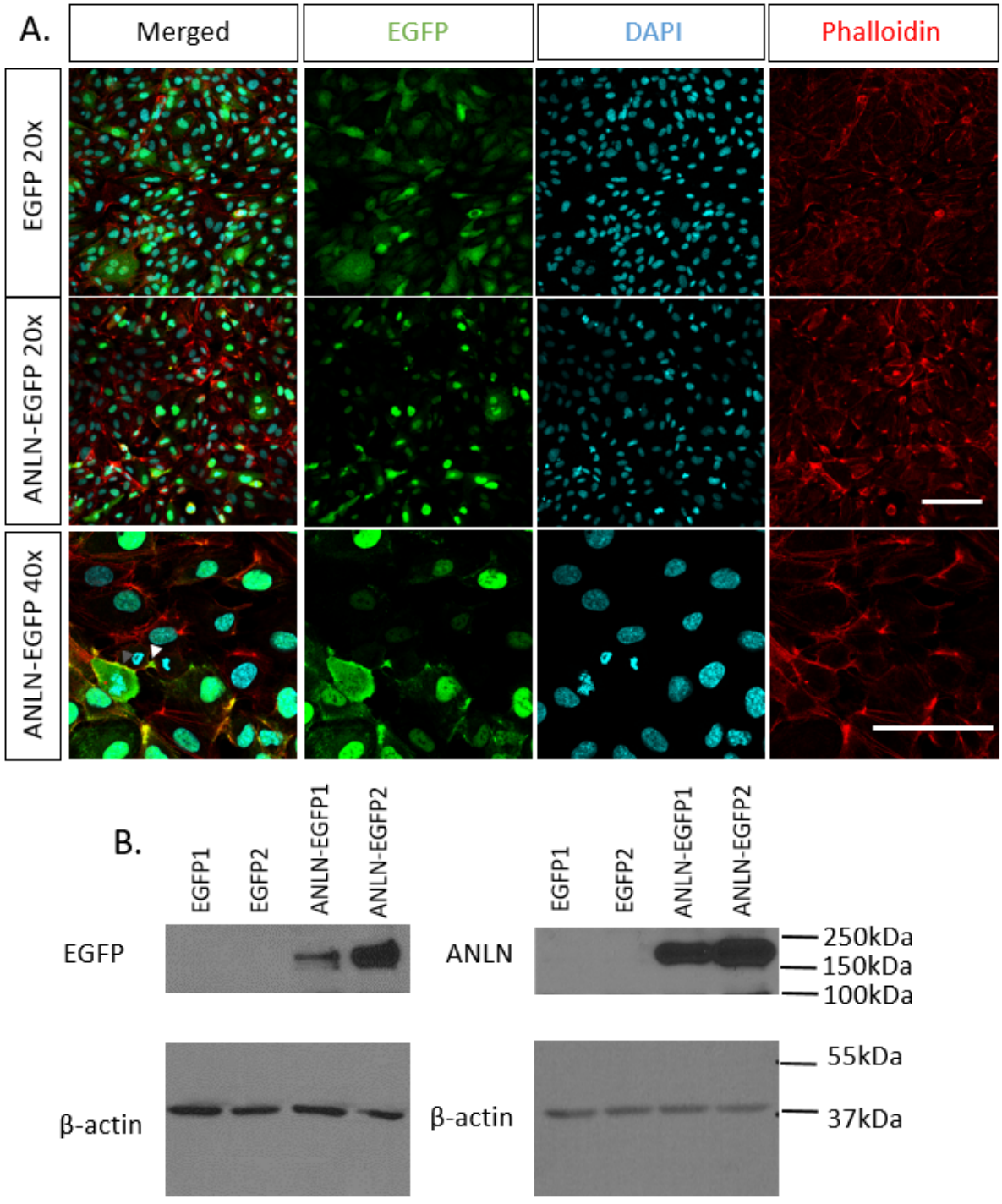

Figure 3.3.4: Overexpression of ANLN-EGFP in ECs produces functional full length ANLN:
(A) Localisation of ANLN-EGFP fusion protein in HUVEC showing (indicated by arrows) a nuclear localisation of the ANLN-EGFP (20x and 40x objective) and with cortical (grey arrow) and cleavage furrow (white arrow) localisation during cell division (scale bars=100µm). (B) Western blot of HUVEC lysates after ANLN-EGFP overexpression showing the molecular weight of ANLN-EGFP after detection with an anti-EGFP antibody and anti-ANLN antibody at ~160 kDa.

3.3.3 ANLN expression affects tubulogenesis in HUVECS:

To investigate the effect of ANLN expression on an in vitro model of angiogenesis, tubulogenesis assays were carried out on HUVEC after treatment with ANLN siRNA or ANLN-EGFP lentivirus as shown in *figure 3.3.6A-D*. These showed that ANLN silencing significantly reduced the total length of the tubule network formed by the ECs, however, ANLN-EGFP overexpression significantly increased the total length of the tubule network. After completion of tubule formation ANLN-EGFP expression appeared to remain distributed mainly to the nucleus as seen in *figure 3.3.6B*.

Given the effect of ANLN-EGFP overexpression on tubulogenesis live imaging was used to determine the localisation of ANLN-EGFP during tubulogenesis. However, the weak ANLN-EGFP signal and drift of the microscope focus after one hour causes difficulty in observation of localisation as shown in *figure 3.3.6*. These experiments suggested an involvement of ANLN in ECs in a sprouting angiogenesis like condition.

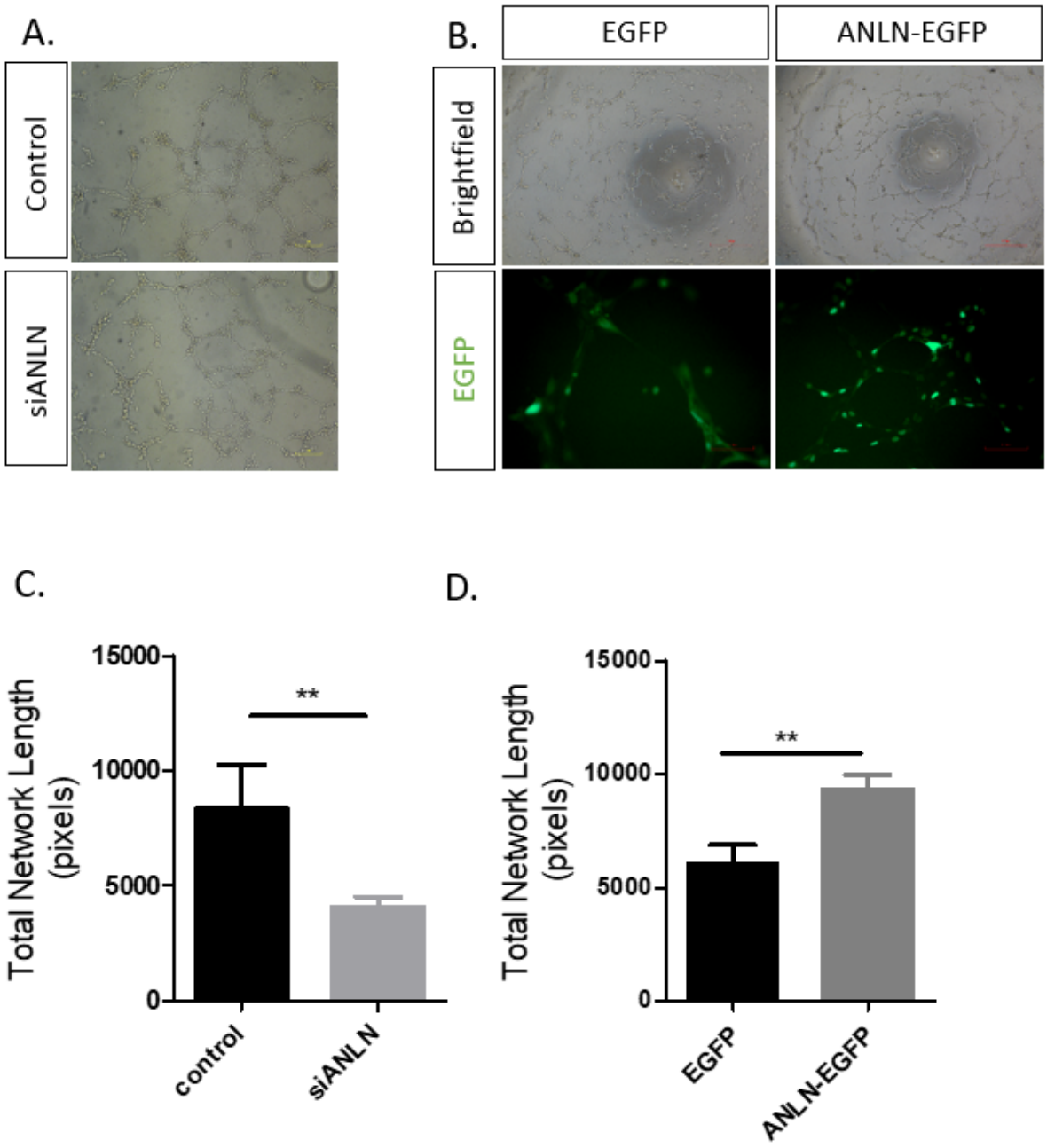

Figure 3.3.5: ANLN silencing and overexpression affect *in vitro* matrigel tubulogenesis assay performance:

(A) Brightfield images of matrigel tubule networks of HUVEC after treatment of HUVEC with 10nm control or ANLN siRNA. (B) Brightfield and fluorescent images of matrigel tubule networks of HUVEC after treatment with ANLN-EGFP or EGFP lentivirus. (C-D) Quantification of matrigel tubule networks showing a significant decrease of total network length after silencing and a significant increase in total network length after overexpression. (n=3, **=P<0.01 t-test). ((A+C) preliminary data from A. Caporali)

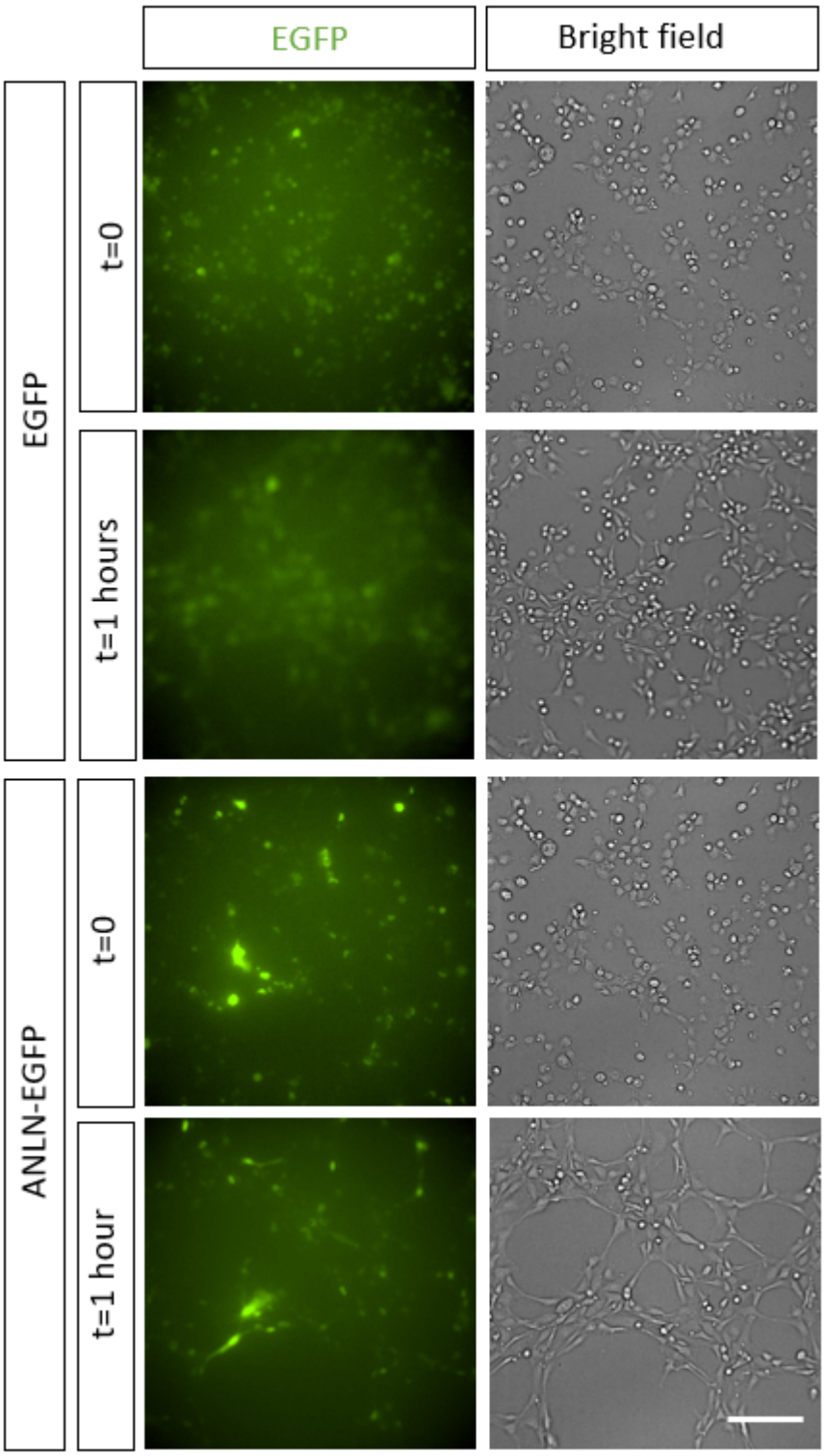

Figure 3.3.6 It was not possible to determine ANLN localisation in *in vitro* matrigel tubulogenesis assays of HUVEC after ANLN-EGFP overexpression:
Brightfield and fluorescent live imaging of tubulogenesis assays of EGFP and ANLN-EGFP transduced HUVEC plated on matrigel in a µ-angigogenesis slide. Time points show the drift of the focus during time-course experiment making tracking of individual cells difficult (Representative scale bar = 100µm)

3.3.4 Silencing of ANLN expression has a significant effect on EC cell to cell junctions and migration:

ANLNs effect on other aspects of EC function were determined by trans-well filter migration assay and impedance based ECIS chamber assays as shown in *figures 3.3.7-3.3.8*.

ECIS chamber assays were used to determine the effect of ANLN on the wound healing capacity and cell to cell junctional integrity of HUVECS (*figures3.3.7 A-D)*. ANLN silencing significantly reduced the integrity of EC cell to cell junctions and wound healing capacity of HUVECS (*=P<0.05 t-test). Transwell migration assays showed that ANLN silencing in HUVECS treated with siRNA compared to control significantly reduced the ability of ECs to migrate towards VEGF without affecting basal migration (*figure 3.3.8 A)*. *Figures 3.3.7A+B* and *3.3.8B* show that there was no difference in EC performance after ANLN-EGFP overexpression in either transwell or ECIS assays (t-test= P>0.05).

These assays suggested that ANLN silencing has a greater effect on EC migration, wound healing and basal cell to cell junctional integrity than ANLN-EGFP overexpression.

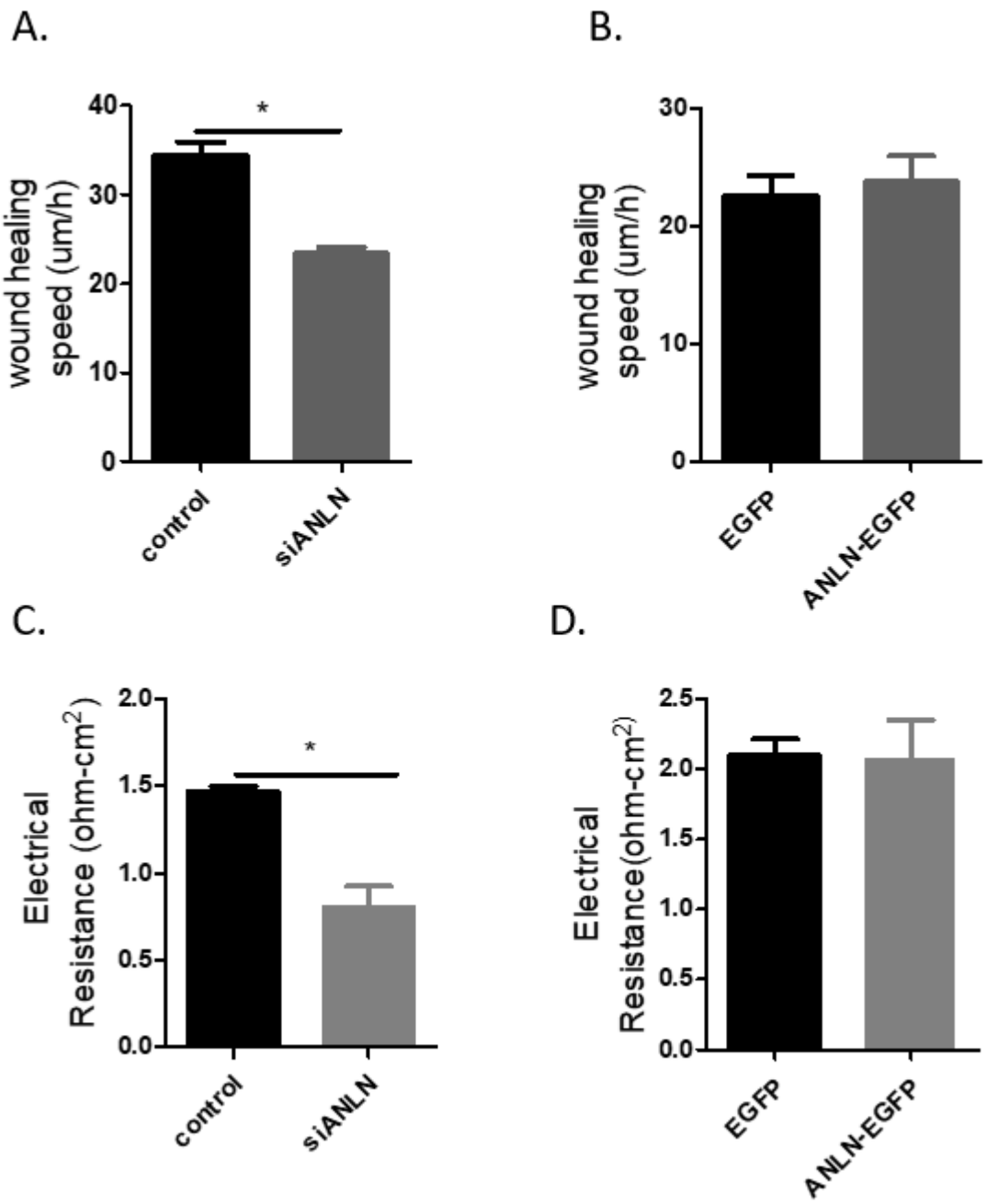

Figure 3.3.7 ANLN silencing reduces wound healing and cell to cell junction integrity but overexpression has no effect:

(A-B) The wound healing velocity of cultured HUVEC by ECIS electric wound application after silencing of ANLN or ANLN-EGFP overexpression, showing a significant decrease in wound healing speed after ANLN silencing. (C-D) The resistance of a cultured monolayer of HUVEC indicative of cell to cell junctional integrity after treatment with ANLN siRNA or ANLN-EGFP overexpression, showing a significant decrease in barrier integrity after ANLN silencing. (Error bars = SEM, n=3, significance *=P<0.05 by t-test). ((C) Preliminary data from A. Caporali)

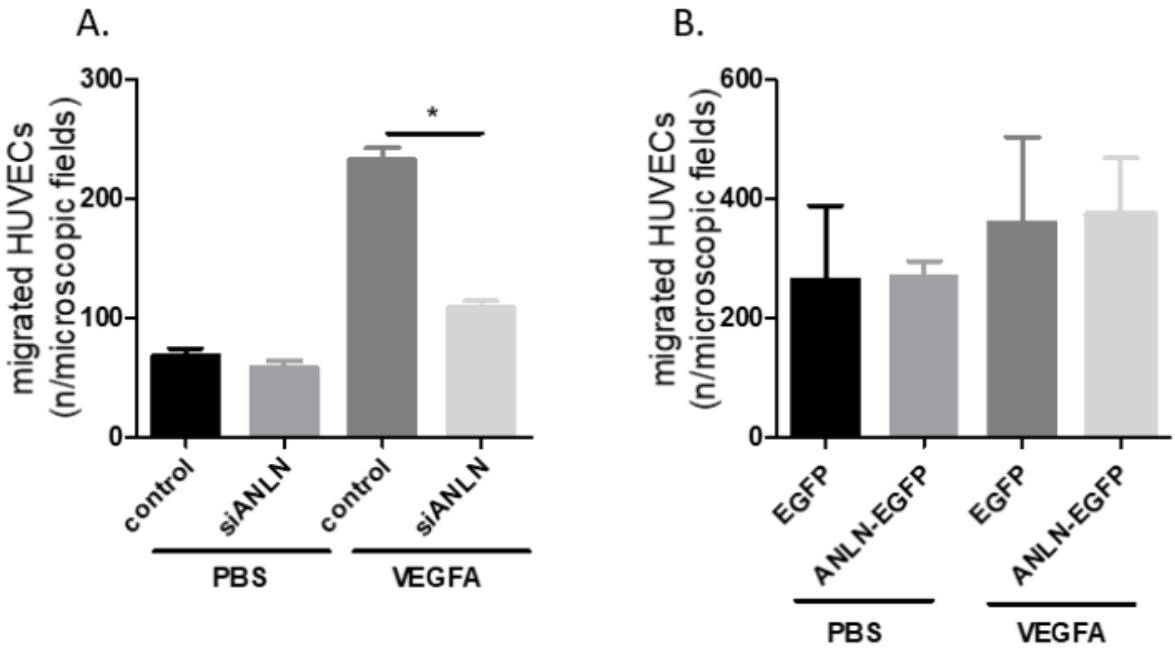

Figure 3.3.8: ANLN silencing reduces EC migration towards VEGF but overexpression has no effect:
(A) Shows the number of migrated HUVEC through transwell filter towards 25ng/ml VEGFA or PBS vehicle after treatment with control siRNA or ANLN siRNA. (B) Shows the number of migrated HUVEC through transwell filter towards 25ng/ml VEGFA or PBS vehicle after EGFP or ANLN-EGFP overexpression. (n=3 error bars=SEM, *=P<0.05 one way ANOVA). ((A) preliminary data from A. Caporali)

3.3.5 ANLN expression modulation does not affect proliferation or cell cycle progression in ECs:

EDU incorporation and propidium iodide (PI) staining was used to investigate the effect of ANLN on the cell cycle dynamics and proliferative capacity of HUVECs shown in *figures 3.3.9-3.3.10*. *Figure 3.3.9 A+B* shows the incorporation of EDU into HUVEC after treatment with ANLN siRNA or ANLN-EGFP overexpression, neither conditions significantly affected the overnight proliferation of HUVECS (ns=P>0.05 t-test). Similarly, there was no difference in the distribution of the cells in each cell cycle stage, as assayed by PI staining in either HUVECS treated with ANLN siRNA or ANLN-EGFP overexpression as shown in figure *3.3.10 A+B* (ns=P>0.05 t-test). This data suggested that neither of these assays could detect cell cycle defects in either condition.

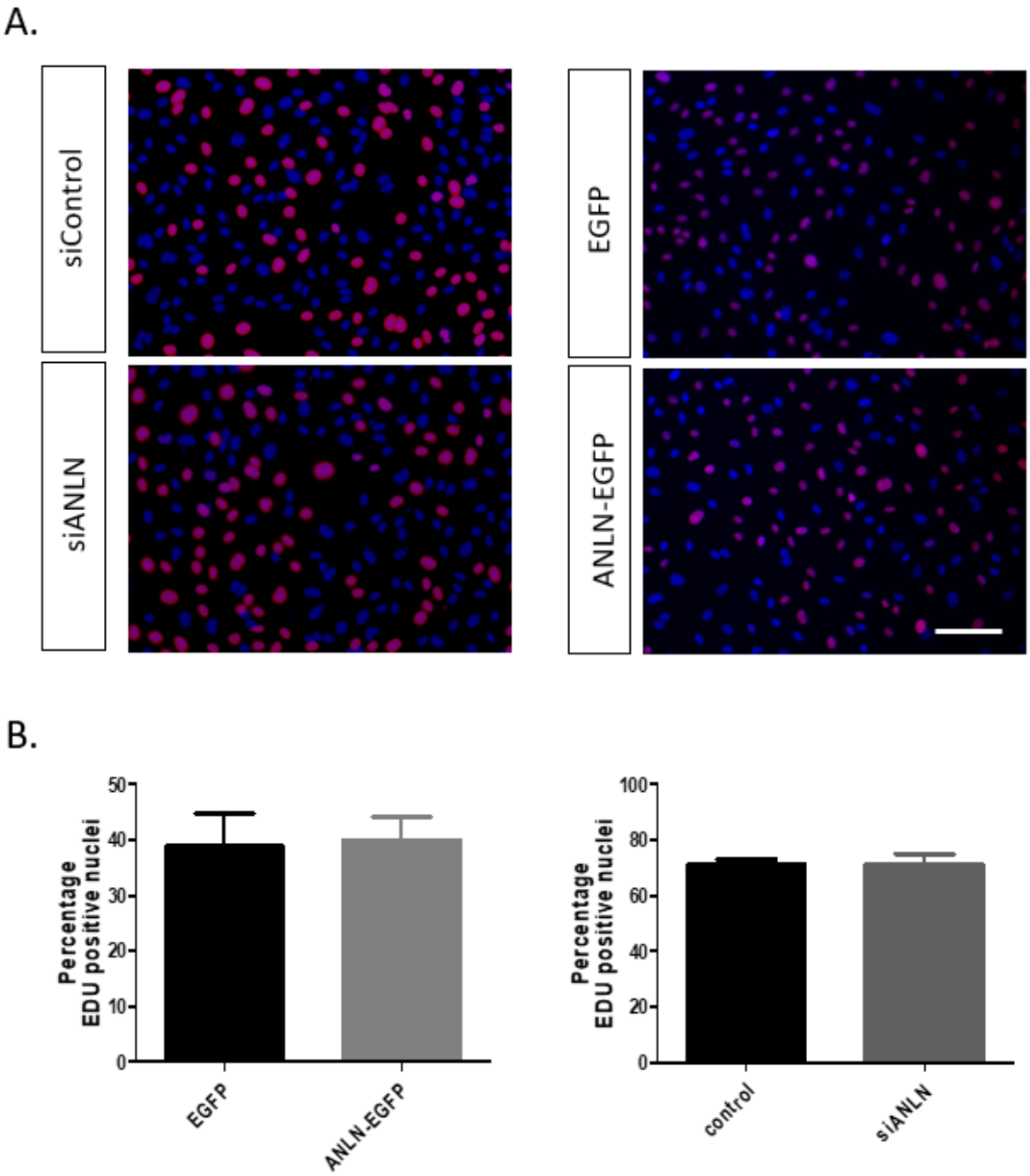

Figure 3.3.9: ANLN silencing or overexpression has no effect on EC proliferation:
(A) Merged images of DAPI stained and EDU positive nuclei (pink nuclei) showing the number of proliferating HUVECS after ANLN silencing or ANLN-EGFP overexpression. (B) Quantification of the percentage of EDU positive nuclei showed no difference in proliferation between control and either silencing or overexpression. (Silencing n=2 and overexpression n=3 error bars=S.E.M ns=P<0.05 t-test) representative scale bars = 100 µm.

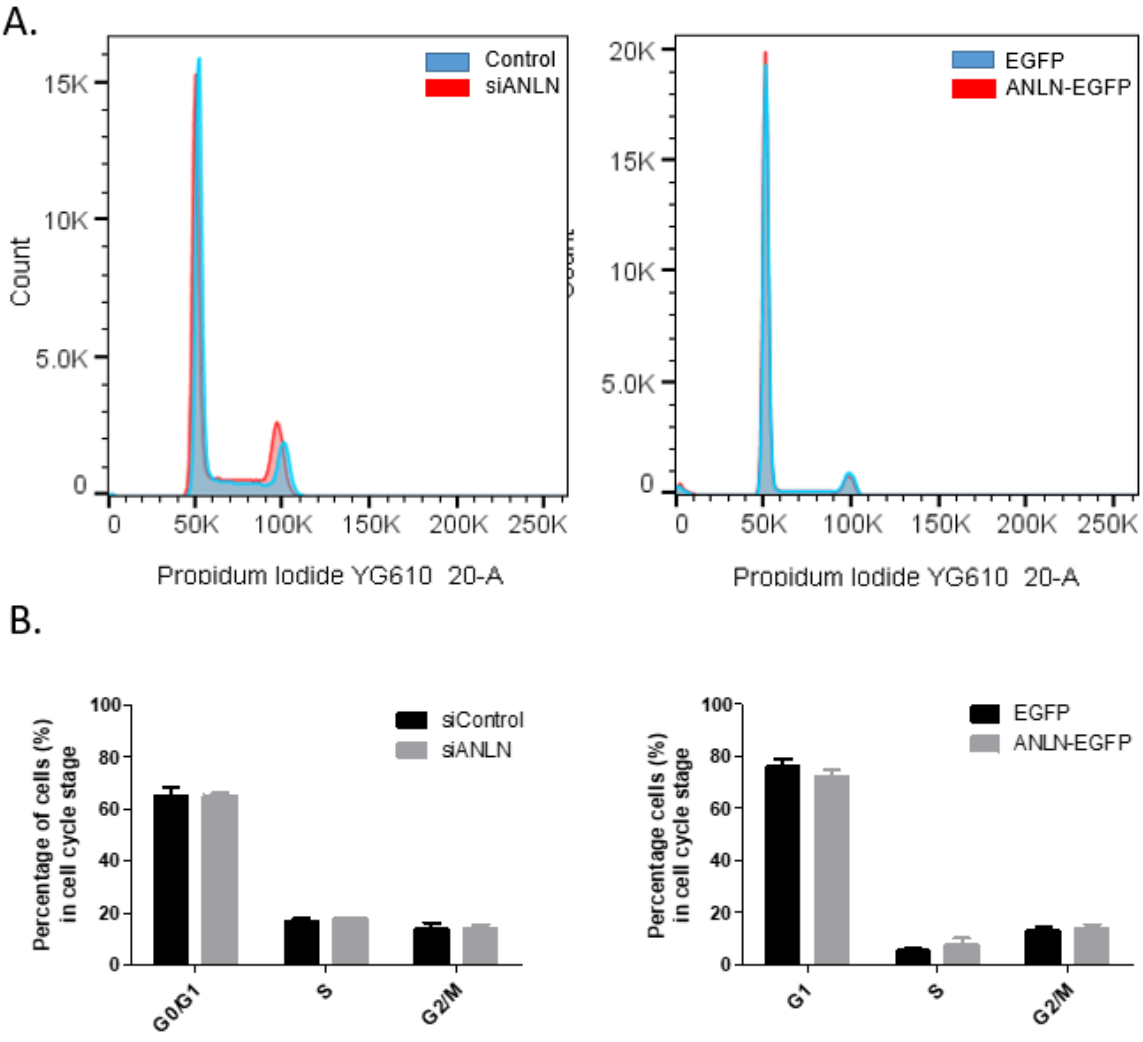

Figure 3.3.10: ANLN silencing or overexpression has no effect on EC cell cycle progression: (A) Flow diagrams of cell count in G0/G1, S and G2/M phase after flow cytometry of ANLN silenced and ANLN-EGFP overexpressed HUVEC stained with PI. (B) Quantification of cell number in each stage of the cell cycle showing no difference between control and either ANLN silenced or ANLN_EGFP overexpressed HUVEC showing no difference between groups. (silencing n=2 and overexpression n=3 error bars = S.E.M)

3.4 Discussion:

In this chapter, a role of ANLN in EC function in post ischaemic angiogenesis was investigated for the first time.

ANLN expression was increased in the ECs of skeletal muscle from a mouse model of hind limb ischaemia. This suggested an involvement of ANLN in the EC response to ischaemic injury as has been observed in mouse and zebrafish cardiomyocytes after myocardial cryoinjury (Kang et al. 2016; Hesse et al. 2012).

3.4.1 ANLN silencing has a more severe effect on EC performance than overexpression *in vitro*:

To identify the effect of ANLN expression on EC phenotypes *in vitro* siRNA and an ANLN-EGFP lentivirus were used to modulate ANLN expression. After transduction with ANLN-EGFP lentivirus cell sorting was required to enrich the ANLN-EGFP positive cells for use in functional assays. The distribution of overexpressed ANLN-EGFP was mainly nuclear which matched our own observations of endogenous ANLN and those made in most cell types (Wang et al. 2015; Zhou et al. 2015). ANLN-EGFP localisation was conserved and observed in the nucleus during interphase and associated with the cell cortex and cleavage furrow during cytokinesis (Piekny & Maddox 2010). This localisation helped confirm the functionality of the EGFP fusion ANLN as observed in other studies (Liu, Gregory D. Fairn, et al. 2012; Paolini et al. 2015).

The effect of ANLN expression on basic assays of EC function were polarised between the overexpression and silencing of ANLN. Wound healing and EC barrier function assays were inhibited by ANLN silencing confirming observations of the effect of ANLN on cell to cell junctions and cell motility in epithelial cells (Reyes et al. 2014; Wang et al. 2015). Migration towards a chemoattractant (in this case VEGF) was impaired by ANLN silencing, however, the basal migration was not affected. This observation may suggest an involvement of ANLN with stimulated migration that is not observed in basal migration. However, ANLN-EGFP overexpression had no effect on these assayss. It is possible that ANLN-EGFP overexpression may affect cell

junctions after EC treatment with a growth factor like VEGF which could be investigated using ECIS capacitance based assays. Further investigation of expression of the ANLN-EGFP reporter at the cell to cell junction of ECs would also identify a possible role of ANLN in the structural machinery of EC junctions. It is possible that very little ANLN is required to fulfil many of its cellular functions, in our western blot there was no endogenous ANLN found at the exposure that detected the overexpressed ANLN-EGFP. Thus, ANLN-EGFP overexpression may have no effect on certain aspects of EC function. It should be noted that proliferation was not blocked pharmacologically during migration or wound healings assays. As there is a proliferative component to wound healing and migration this may have contributed to the result. However, the cells were starved before the migration assays to reduce proliferation, and the time course for both the migration and wound healing assays were short (<6hours), therefore, the proliferation of ECs in this time frame should be minimal.

Interestingly, cell cycle progression and proliferation were not affected by modulating ANLN expression. This has been observed in podocytes where overexpression of WT ANLN does not affect proliferation (Gbadegesin et al. 2014). However multiple studies have observed binucleation and G2/M accumulation in cell lines after the silencing of ANLN (Zhang et al. 2018). However, this phenotype has only been observed in immortalised or cancer derived cell lines after ANLN silencing (Gbadegesin et al. 2014; Hall et al. 2018; Zhang et al. 2018). It is possible that ANLN silencing with our siRNA is not strong enough to induce this phenotype but may cause other effects on cell function. This phenotype may be more likely in immortalised cells that already have a dysregulation of the cell cycle than in primary cells like HUVECs. It is also possible that there is a degree of cell cycle dysfunction that is not detectable by EDU incorporation or PI stain after ANLN silencing. Therefore this should be investigated by qPCR for different cell cycle or cytoskeletal markers in both ANLN silenced and overexpressing HUVECs.

The low efficiency of ANLN-EGFP expression after lentiviral transduction could be a result of post translational regulation of ANLN-EGFP protein by APC^{cdh1}. This complex

is responsible for the ubiquitination and subsequent degradation of ANLN after the completion of the cell cycle (Zhao & Fang 2005). This has effect has been noted in a flt1/ANLN-EGFP mouse model where ANLN-EGFP was only detected in proliferative endothelial cells (Herz et al. 2018). Treatment of unsorted ANLN-EGFP HUVECS with a proteasome inhibitor like MG132 would determine this possibility. If the number of ANLN-EGFP positive cells increases after proteasome inhibition then ANLN-EGFP overexpression is being suppressed by APC^{cdh1} after mitotic exit.

It was not known what type of phenotype ANLN-EGFP overexpression in ECs would exhibit as ANLN expression is tightly controlled in terms of localisation and protein expression during the cell cycle (Piekny & Maddox 2010). The ANLN-EGFP protein produced had a very high atomic mass of 180Kda and the size of the plasmid is much larger than the control EGFP lentivirus. It would be easier to utilise a smaller tag such as a flag tag or his tag to reduce the size of the expressed protein and improve efficiency. However using another non-fluorescent tag would impair the ability to do live imaging of ANLN localisation *in vitro*. A fragment of ANLN tagged with GFP has been used by Liu et al where ANLN localisation was identified with an EGFP fusion to just the PH domain of ANLN (Liu, et al. 2012). Using this strategy may improve the expression of the fusion reporter. However, a fluorescent reporter of just the PH domain or the Actin myosin binding domain may reduce the relevance of the observed localisations compared to overexpression of endogenous ANLN.

It should be noted that a difference between our EC phenotype observed between silencing and overexpression may be partly caused by the usage of cell sorting to enrich ANLN-EGFP positive cells. There was a noticeable difference in baseline results for the cell cycle staining, proliferation, migration and wound healing between control siRNA and EGFP overexpression. HUVECS are not a homogenous population of cells, they are primary cells obtained from trypsin digest of umbilical cords (Davis et al. 2007). Cell sorting could have selected different populations of cells with slightly different phenotypes. In addition to this, the continued quality of the cultured HUVECs could also have been impaired due to the time spent in room temperature

flow buffer during cell sorting. Including an unsorted population of HUVECS in future *in vitro* assays would act as a control for this possibility.

3.4.3 ANLN may affect sprouting angiogenesis:

There was a correlation between tubulogenesis assay performance and ANLN expression modulation. Performance was improved in ANLN-EGFP overexpression and reduced in ANLN silencing experiments. Interestingly fluorescent images of the completed EC network showed that ANLN-EGFP remained nuclear after the tubule network formation. It was hoped that ANLN expression would be visible at sites of cell to cell contact or at the leading edge of the cell as has been observed in neurite outgrowth (Tian et al. 2015). Live imaging of tubulogenesis in ANLN-EGFP overexpressing HUVEC was attempted to determine changes in ANLN localisation. This has been observed in neuronal outgrowth where ANLN-EGFP associates with the leading edge of the cell (Tian et al. 2015). Normal 96 well cell culture plates did not produce high quality images for live imaging due to the menisci formation of matrigel and the plastic thickness. Another approach used μ-angiogenesis slides, this is a glass bottomed 15-well imaging slide. This used less matrigel to reduce menisci formation and create a thickness of 0.8 mm of matrigel to allow a smaller working distance between the objective lens and the cell layer. Imaging of tubulogenesis assays with this method were still insufficient due to drift of the microscopes focus caused by changing thickness of the matrigel layer. Using cell tracker dyes or lifeact-RFP lentivirus to pre-stain cells before the assay would give a stronger secondary signal to maintain focus on the imaged cells. These imaging issues could be addressed by performing tubulogenesis assays without matrigel, this would involve a co-culture of HUVECs and fibroblasts (Staton et al. 2009). The fibroblasts secrete a matrix which acts as a structural scaffold for tubule formation, these assays more closely resemble capillary beds than the more common matrigel based assay. This assay would be less high throughput but would allow for the generation of superior images (Staton et al. 2009).

However, in retinal angiogenesis assays from an flt1/ANLN-EGFP reporter mouse, ANLN expression was seen to be entirely nuclear in ECs (Herz et al. 2018). This study supports our observed localisation of ANLN in *in vitro* tubulogenesis, but still doesn't capture a dynamic change in ANLN localisation during EC sprouting.

Tubulogenesis is regarded as a sprouting angiogenesis like assay, being a potential predictor of EC cell function, however, it doesn't exactly model angiogenesis and multiple cell types can form tubules (Weavers & Skaer 2014; Pollack et al. 1998). To fully investigate sprouting angiogenesis *in vitro* it would be required to use spheroid cell culture to generate EC spheroids for embedding in 3D matrices. For this HUVECs or an equivalent EC cell type could be cultured in a low adhesion coated round bottom plate to allow spheroid formation (Heiss et al. 2015). EC spheroids would then be plated in a 3D matrix (collagen or matrigel), EC spheroids cultured in this manner form tip and stalk cells more similar to the process of angiogenesis than tubulogenesis. This would allow investigation of the effect of ANLN on dorsal lateral inhibition and tip cell formation *in vitro* (Heiss et al. 2015). Here ANLN-EGFP lentivirus can be used to investigate the formation of sprouting after ANLN-EGFP overexpression. Using siRNA to investigate the opposite effect may be problematic as HUVECS may not form spheroids after ANLN silencing. For this, a tamoxifen inducible shRNA lentivirus system may be more suitable for the investigation of sprouting after ANLN silencing. Validated sequences of ANLN shRNA are available, here, shRNA expression can be induced during sprouting to observe the effect of ANLN silencing on sprouting angiogenesis (Suzuki et al. 2005).

ANLN has been associated with asymmetric cell division in the differentiation of cell types in the zebrafish CNS and retina (Malo et al. 2017; Paolini et al. 2015; Fotopoulos et al. 2013). In zebrafish, asymmetric cell division of ECs is required for tip/stalk cell designation, this helps generate the different sprouting EC daughter cells (Costa et al. 2016). Even if ANLN expression is not associated with the leading edges of sprouting ECs its distribution at the cleavage furrow may affect EC sprouting (Fotopoulos et al. 2013; Dorn et al. 2010). Therefore, future experiments should also include identification of ANLN localisation in asymmetric cell division of ECs in sprouting

angiogenesis. An *anln:anln-eGFP* reporter zebrafish was imported for this purpose from Dr Lucia Poggi of the university of Trento.

3.4.3 Future investigations of ANLN signalling pathways:

Investigations of the signalling mechanisms of ANLN could be carried out using the ANLN-EGFP lentivirus. Using ANLN-EGFP HUVECs would produce a relatable result to ECs as ANLN has been shown to interact differently with binding partners in individual cell types (Gbadegesin et al. 2014; Haglund et al. 2010; Hall et al. 2018). These studies initially identified ANLN interactions with signalling pathways through unique localisations with the cytoskeleton outside of cytokinesis. These include interactions with CD2AP in podocyte foot process like structures in HEK293/podocytes, and, association *of C.elegans* homologue ani-1 with RhoG in the leading edge of migrating neurites in *C.elegans* (Tian et al. 2015; Gbadegesin et al. 2014; Hall et al. 2018).

We observed a nuclear localisation of ANLN, this has never been thoroughly investigated despite ANLN's expression in HUVECS being mainly nuclear in interphase (Piekny & Maddox 2010; Zhao & Fang 2005). High nuclear ANLN expression has been suggested to have an effect on cell size and metastatic potential in cancer (Magnusson et al. 2016; Suzuki et al. 2005). When localised to the nucleus ANLN could be interacting with short lived actin structures. The role of actin in the nucleus is a contentious issue, monomeric and filamentous actin is detected within the nucleus, however the function of these structures is still being determined (Misu et al. 2017). Nuclear actin polymerisation is regulated by multiple factors with 30 actin binding proteins being found within the nucleus which can prevent or facilitate actin polymerisation (Misu et al. 2017). A key effect of nuclear actin is its association with nuclear programming and transcriptional regulation where actin has been associated with the initiation of RNA polymerase 2 (Hofmann et al. 2004). High levels of monomeric actin shuttled into the nucleus by importin 9 and removed by exportin 6 has been shown to support active transcription (Stüven et al. 2003).

The cell response to serum response factor (SRF) has been shown to be induced partly by alterations to nuclear actin dynamics (Sotiropoulos et al. 1999). The formin mDIA2

(a binding partner of ANLN) has been shown to be involved in the polymerisation of nuclear actin in NIH3T3 cells stimulated by SRF (Watanabe et al. 2008; Watanabe et al. 2010; Baarlink et al. 2013). Here mDIA2 was seen to localise to the nucleus from the cytoplasm after SRF activation and was associated with polymerised nuclear F-actin structures (Baarlink et al. 2013). MDia2 stimulates the formation of short actin filaments promoting their stability and allowing the formation of the centromere by the association of CENP-A during the G1 phase (Liu et al. 2018). No studies have investigated the association of ANLN with its binding partners separately in the nucleus and the cytoplasm despite its mostly nuclear localisation out with cytokinesis (Piekny & Glotzer 2008). This could be investigated by using a nuclear fractionation in HUVECs overexpressing ANLN-EGFP or ANLN-flag and retaining the cytoplasmic fraction. Using a pulldown for the tagged ANLN in each fraction and SDS-page with western blotting of common ANLN binding partners would identify an association between ANLN and nuclear F-actin. Liquid chromatography with Mass spectrometry could be used with the products of the pull down to identify all enriched ANLN binding partners from both nuclear and cytoplasmic fractions. This approach would identify all novel interactors of ANLN in ECs, the nucleus and the cytoplasm.

3.5 Conclusions:

To conclude, we have identified a potential role of ANLN in ECs in the response to ischaemic injury. Comparison of ANLN overexpression and silencing phenotypes identified tubulogenesis as an assay affected by both ANLN silencing and overexpression. As this is a predictor of EC function in angiogenesis future studies should focus on identifying a role for ANLN in sprouting angiogenesis in a suitable *in vitro* or *in vivo* model. If a strong association between ANLN and EC sprouting is found then investigation of potential binding partners within this process is justified. This could be investigated by immunoprecipitation and mass spectrometry or western blot to elucidate specific binding partners of ANLN in angiogenesis.

Chapter 4:

Does the ZFP36 RNA binding protein family regulate ANLN expression?

4.1 Introduction:

Identifying a potential regulatory mechanism for ANLN in ischaemia is essential for understanding its role in the angiogenic response of ECs. The ANLN 3'UTR contains multiple adenylate-uridylate rich elements (ARE) in its 3'UTR that are targetable by RNA binding proteins (RBPs) (*figure 1.1.1*) (Fallmann et al. 2016).

A.

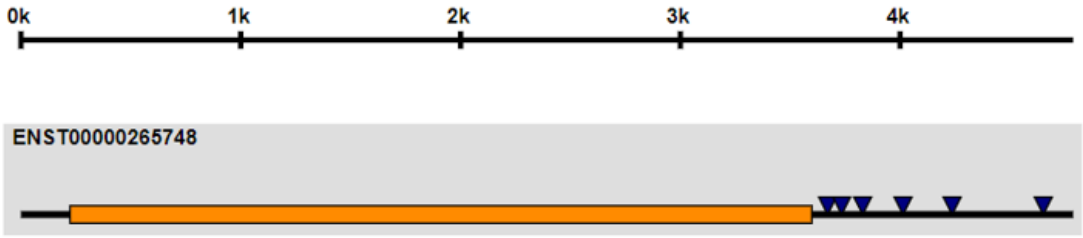

B.

C.

motif	Location
ATTTA	3665-3669
ATTTA	3735-3739
ATTTA	3828-3832
ATTTA	4011-4015
ATTTA	4237-4241
ATTTA	4652-4656

Figure 4.1.1: The ANLN mRNA transcript contains putative RBP binding sites:
Bioinformatic analysis data from AREsite showing that the ANLN mRNA transcript contains in its 3'UTR 6 AUUUA RBP binding sites. (A+B) shows the location of the ATTTA binding sites on the 3'UTR (C) Table of the exact base location of the RBP binding sites within the ANLN mRNA transcript. (Fallmann et al. 2016)

ZFP36 family RBPS are key regulators of mRNA expression in inflammation and cell growth, and they may target the ATTTA ARE sites in ANLNs the 3'UTR. The ZFP36 family RBPs consist of ZFP36, ZFP36L1 and ZFP36L2 with each protein having individual and overlapping targets (Blackshear et al. 2005; Hacker, Valchanova, Adams & Munz 2010).

ZFP36 RBPs knockout studies in mice have shown a significant effect on mouse development and the response to inflammation. ZFP36 knockout mice have a severe phenotype with very low body weights, increased inflammation, vascular dysfunction, arthritis, and defects in myelopoesis and haematopoiesis (Taylor et al. 1996). Endothelial cell dysfunction in ZFP36 knockout mice was attributed to an increase in inflammation and reactive oxygen species (Bollmann et al. 2014). ZFP36L1 knockout mice show embryonic lethality due to placental defects early in development, however, embryos have significant vascular disorganisation and cardiac out flow abnormalities. ZFP36L1 tissue specific knockouts in B-cells causes increases in B-cell precursor cells, whereas, knockout in T-cells results in thymus atrophy and T-cell based tumour formation (Hodson et al. 2010; Vogel et al. 2016). These different in vivo phenotypes point towards each RBP having independent targets in different cell types. The binding efficiency and stability of ZFP36 RBPs is controlled by their phosphorylation. Phosphorylation of ZFP36 RBPs is controlled by the ERK and PI3K pathway, controlling ZFP36 RBPs mediated mRNA degradation (Rataj et al. 2016; Benjamin et al. 2006).

In the EC response to ischaemia and hypoxia the expression of ZFP36 family RBPs have been shown to be amongst the most affected genes in *in vivo* and *in vitro* conditions (Kamphuis et al. 2007; Chamboredon et al. 2007; Desroches-castan et al. 2011). ZFP36 and ZFP36L1 regulate the key angiogenic genes HIF-1α, VEGF and Dll4 in ECs and may contribute to the control of angiogenic signalling *in vivo* (Desroches-castan et al. 2011; Chamboredon et al. 2007). In skeletal muscle regeneration ZFP36 RBPs have been shown to regulate satellite cell muscle quiescence and maturation into skeletal muscle myofibers (Busse et al. 2008; Hausburg, Doles, Clement, Cadwallader, Hall, Blackshear, Lykke-andersen, et al. 2015; Bye-A-Jee et al. 2018).

Therefore, there is a potentially important role of ZFP36 RBPs in the regenerative response of ECs in ischaemia.

There is an inverse correlation between ANLN expression and ZFP36 RBPs expression in the regeneration of zebrafish tail fin and myocardial injury, this suggests a potential regulatory mechanism (Kang et al. 2016b). Due to the presence of ARE regions in the 3'UTR of ANLN it was decided to investigate ANLN regulation by RNA binding protein in ECs.

4.2.1 Hypothesis

These experiments were performed under the hypothesis that ANLN had a post transcriptional regulatory mechanism by ZFP36 family RBPs in the EC response to Ischaemia.

4.2.2 Aims:

In this chapter I aimed to identify ZFP36 RBP regulation of ANLN by:

1. Identifying a potential regulatory mechanism between ANLN and ZFP36 RBPs in *in vivo* hind limb ischaemia and *in vitro* assays performed in ECs
2. Confirming binding of the ANLN transcript to ZFP36 RBPs through biochemical assays

4.3 Results:

4.3.1 There is an association between ANLN mRNA expression and RBP expression:

Using the online toolset AREsite (University of Vienna) the ANLN mRNA sequence was screened for putative RNA binding sites as shown in *figure 4.1.1.* This showed that the ANLN mRNA transcript contains 6 ATTTA sites in 3'UTR which can be the targeted by RNA binding proteins of the ZFP36 RBPs family, these sites had not been validated experimentally for RNA binding protein regulation before (Fallmann et al. 2016). In ECs sorted from hind-limb ischaemia there is an association between a down regulation of ZFP36 mRNA and ZFP36L1 mRNA (*figure 4.3.1A+B*) (*=P<0.05 **=P<0.01, Two way ANOVA with post hoc Bonferroni) matching a concurrent increase in ANLN mRNA (as detailed in chapter *3.1.1A+B*). Moreover, in vitro simulation of vascular inflammation using IL-1β stimulation of HUVEC demonstrated a down regulation of ANLN mRNA rapidly at 4 hours post stimulation and continued down regulation at 16 and 24 hour time points (***=P<0.001, Two way ANOVA with post hoc Bonferroni). This matches an increase in ZFP36L1 mRNA in HUVEC 4 hours post stimulation with IL-1β (*figure4.3.2A+B*) (**=P<0.01, T way ANOVA with post hoc Bonferroni). Western blot of lysates from HUVEC demonstrated that ZFP36L1 protein is induced at 4 hours post treatment after IL-1β stimulation (*figure4.2.2C*).

This data suggests that there is potential for ANLN regulation by ZFP36 RBPs, because of the presence of binding sites in its 3'UTR, and a regulatory association in hind limb ischaemic ECs and IL-1β stimulated HUVECS.

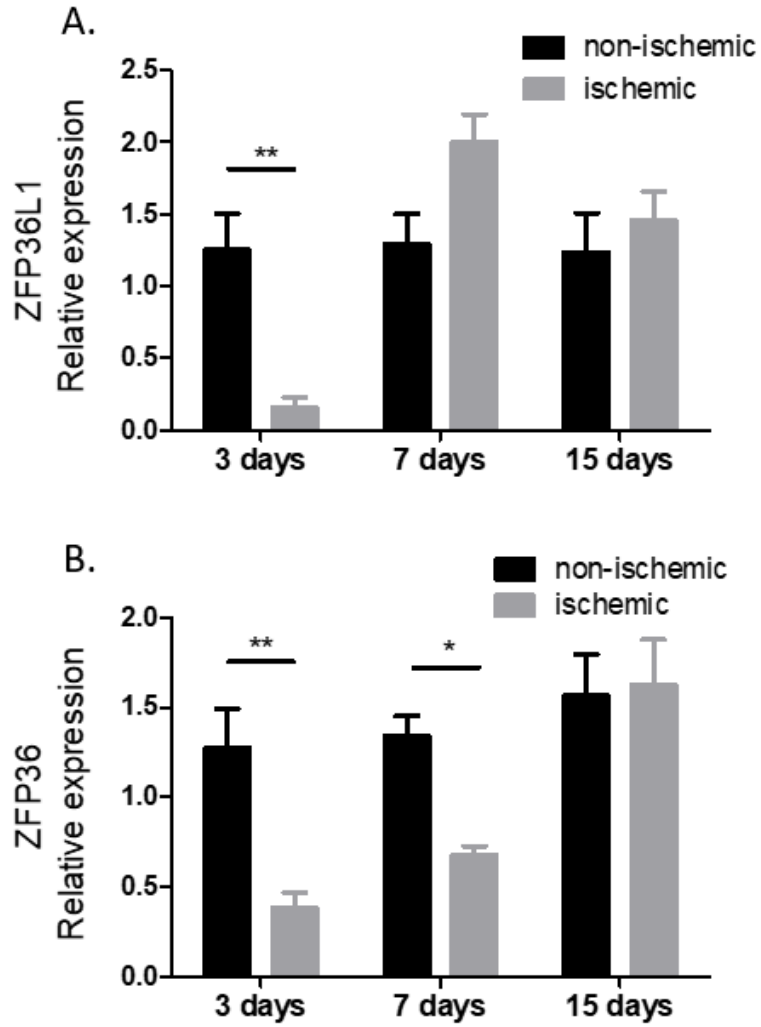

Figure 4.3.1 The expression of ZFP36 RBPs in ECs is altered during ischaemic injury:

Expression of (A) ZFP36L1 and (B) ZFP36 in endothelial cells ($CD31^{+}CD45^{-}$) sorted from adductor muscles after femoral artery ligation at the indicated time points. (n=4 **=P<0.01,*=P<0.01 by Two-way ANOVA with post-hoc Bonferroni test) (A+B qPCR by Lorraine Rose)

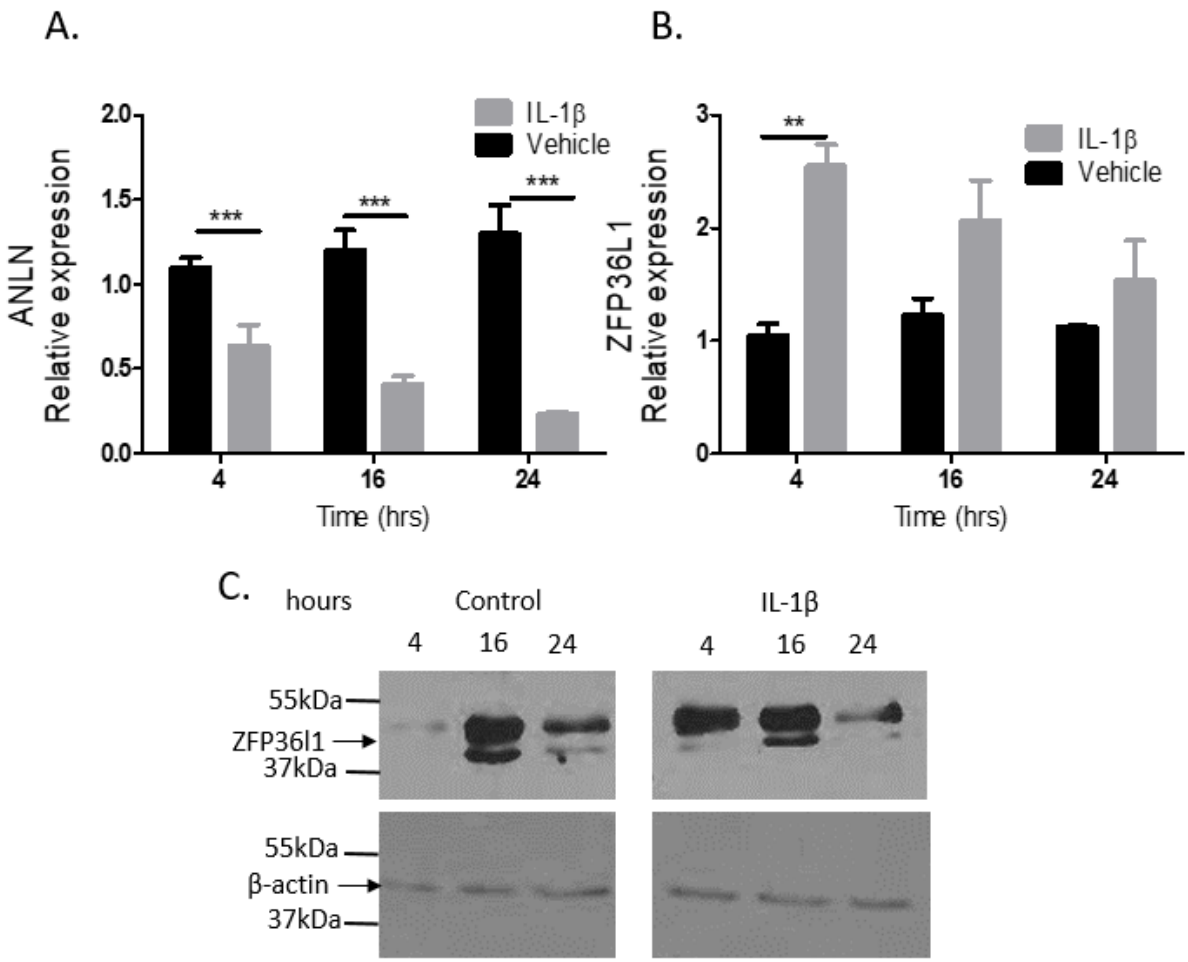

4.3.2 Association between ANLN with ZFP36 RBPs expression *in vitro*:

HUVEC were stimulated with IL-1 β (10 ng/ml) at indicate time points. The charts are showing: A) ANLN; and B) ZFP36L1 expression. (n=3 **=P<0.01,***=P<0.001 by Two-way ANOVA with post-hoc Bonferroni test). C) Western blot of HUVEC after IL-1β stimulation (10ng/ml) showing an induction of ZFP36l1 protein at 4 hours post stimulation. (A+B QPCR by Lorraine Rose)

4.3.2 ZFP36 RBP family expression modulation in endothelial cells:

To determine If ANLN mRNA stability was affected by ZFP36L1 expression, two anti-ZFP36L1 were used to silence ZFP36L1 in HUVEC. Western blot for ZFP36L1 in HUVEC protein lysates after transfection with ZFP36L1 siRNAs showed that only siZFP36L1 #1 successfully knocked down ZFP36L1 as shown in *figure 4.3.3A*. Q-PCR of HUVEC mRNA after transfection with siZFP36l1 #1 (*figure 4.3.3B)* showed a significant decrease of ZFP36L1 mRNA but no significant increase of ANLN mRNA (*= $P<0.05$ ns= $P>0.05$ t-test). This experiment was repeated with two anti-ZFP36 siRNA as shown in *figure 4.3.4A*, but again this did not significantly increase ANLN mRNA expression. To compensate for a potential redundant increase in one of either ZFP36 or ZFP36L1 after silencing transfections of HUVECs with both siRNAs were used, however, these did not cause an increase in ANLN mRNA (*figure 4.3.4B*).

These experiments suggested that silencing of ZFP36 RBPs did not improve ANLN mRNA stability.

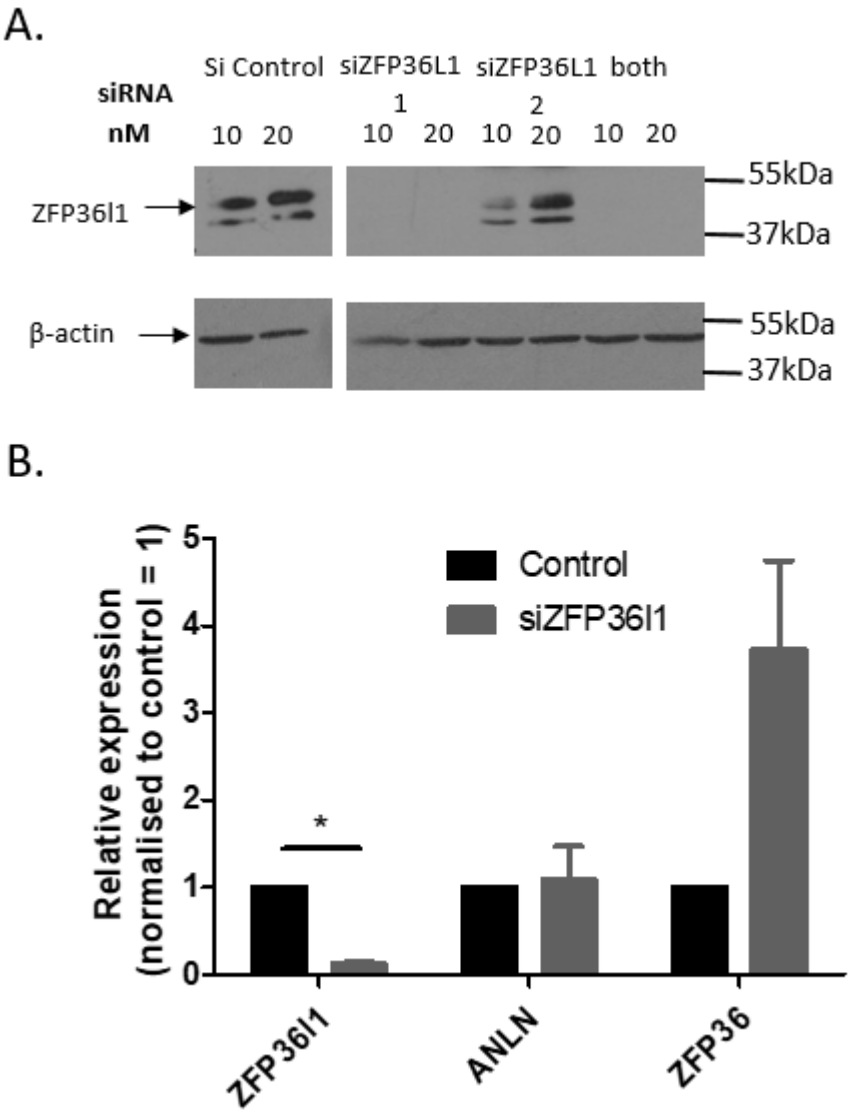

Figure 4.3.3: The ANLN mRNA transcript is not increased after ZFP36l1 silencing

(A)Western blot of lysates from siRNA transfected HUVEC: ZFP36L1 1# and #2 or both at 10nm or 20nm concentration. (B) qPCR showing ZFP36L1, ANLN and ZFP36 expression in HUVEC 48 hours after transfection with 10nm siZFP36L1 #1 (error bars=S.E.M, *=P<0.05 by t-test).

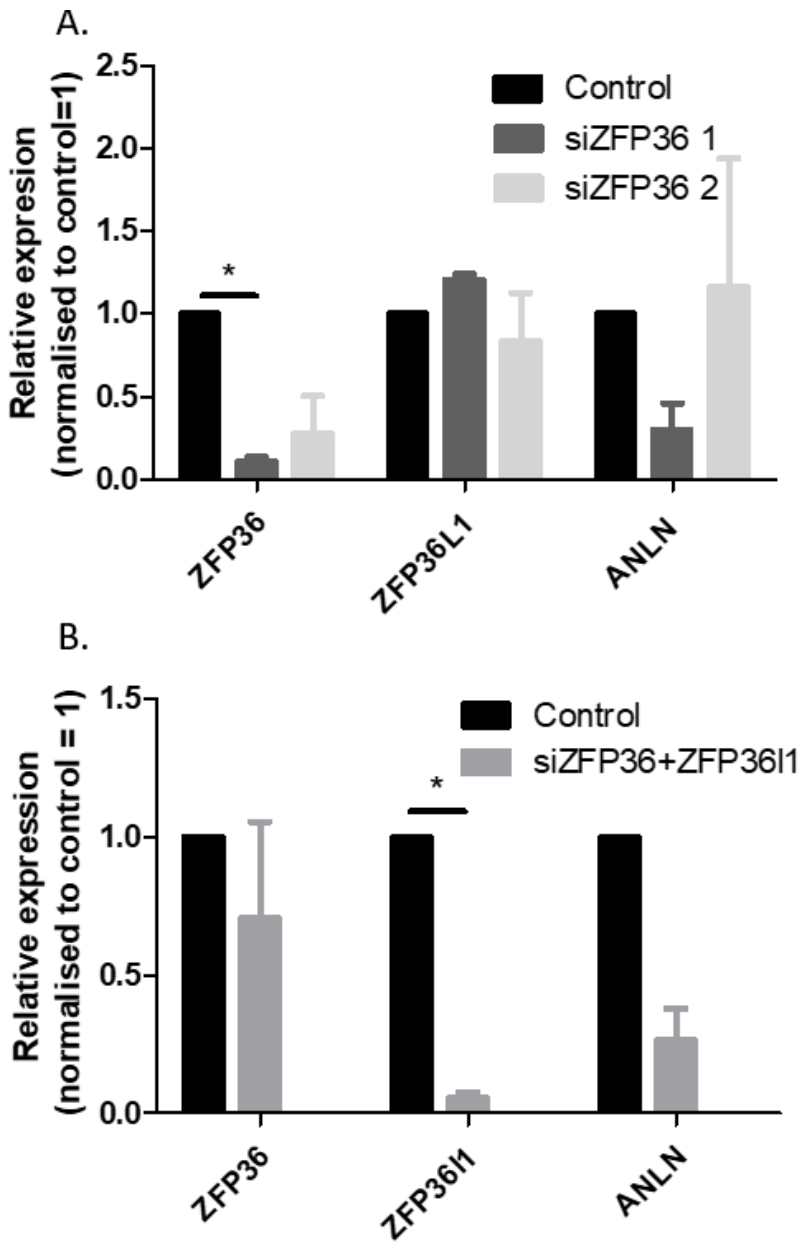

Figure 4.3.4: The ANLN expression is not effected by ZFP36 knock-down or ZFP36 RBPs family silencing

(A) qPCR showing the expression of ZFP36, ANLN and ZFP36L1 in HUVEC 48 hours after transfection with ZFP36 siRNAs (10nM); (B) qPCR showing the expression of ZFP36, ZFP36L1 and ANLN in HUVEC after transfection with both ZFP36 and ZFP36L1 siRNAs (error bars=S.E.M, *=P<0.05 by t-test).

4.3.3 Plasmid production for the validation of ANLN 3'UTR regulation by RBPs:

To confirm the direct binding of RBPs to the ANLN 3'UTR, a luciferase target validation had to be performed. This required the cloning of a plasmid containing the ANLN 3'UTR fused to a luciferase reporter. The insert was generated via RT-PCR producing a band of ~1.2kb in length (*figure 4.3.5A)*; this insert was ligated into the p-MIR luciferase plasmid, and restriction digest of the produced clones identified insert carrying clones as shown in *figure 4.3.5A*. Protein lysates of HEK293 transfected with the ANLN 3'UTR luciferase plasmid produce a luciferase signal after addition of luciferin, this showed that the plasmid is functional as shown in *figure 4.3.5C*. A plasmid for ZFP36 overexpression had already been received from Dr Lucia Montorsi so a corresponding plasmid for the overexpression of ZFP36L1 was generated (Montorsi et al. 2016). The insert for ZFP36L1 overexpression was generated via RT-PCR, producing a ~1 kb insert containing the coding sequence including the Kozac sequence. The insert was ligated into the pcDNA3.1 plasmid as shown in *figure 4.3.6A-B* and restriction digest of the plasmid identified multiple clones carrying the insert. Western blot for ZFP36L1 in protein lysates from HEK293 transfected with the ZFP36L1 plasmid produces a strong band at ~37kda confirming overexpression of ZFP36L1 protein as shown in *figure 4.3.6C*. The plasmids generated here were to be used for validation of the RBPs binding to the ANLN transcript.

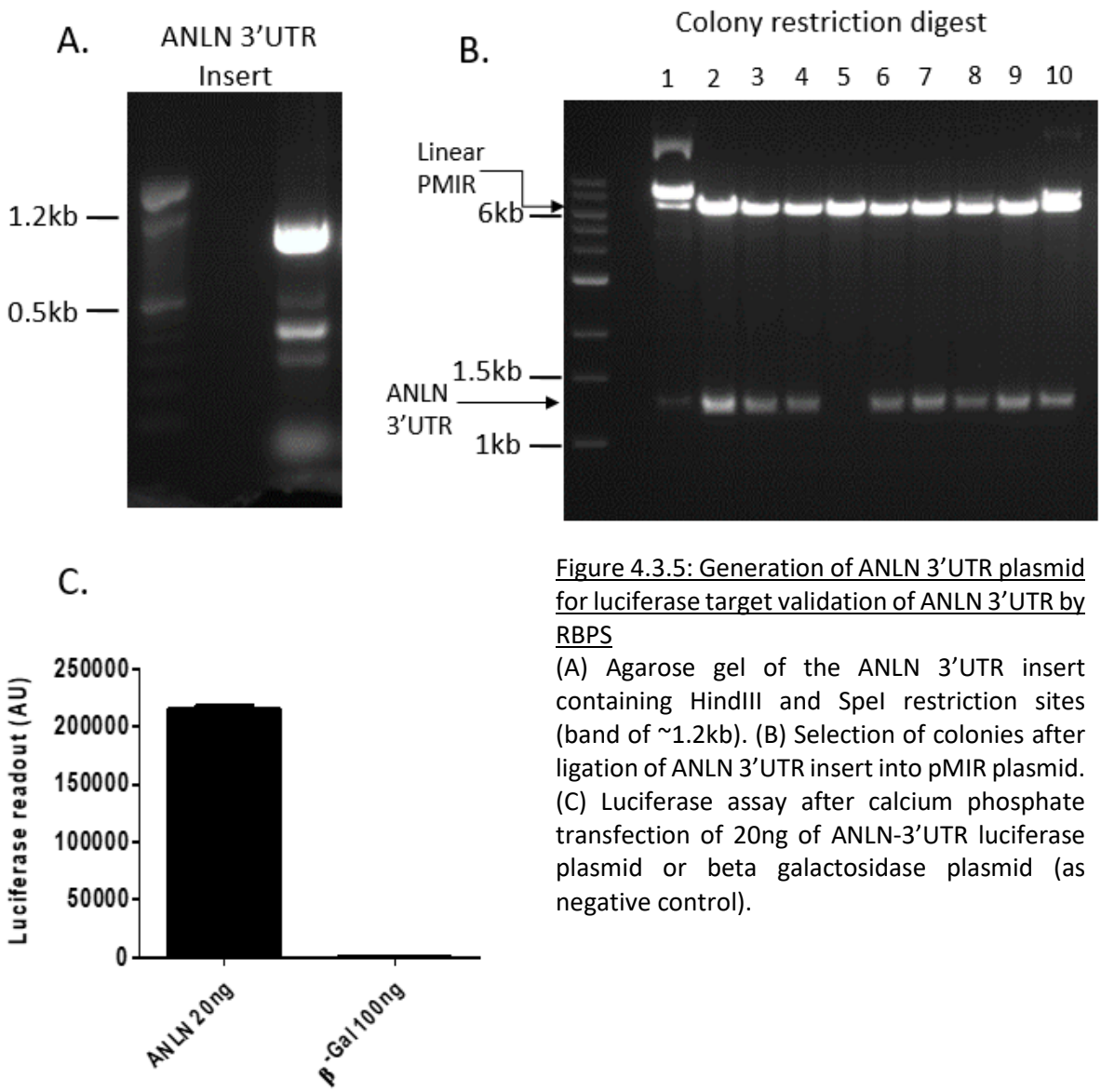

Figure 4.3.5: Generation of ANLN 3'UTR plasmid for luciferase target validation of ANLN 3'UTR by RBPS

(A) Agarose gel of the ANLN 3'UTR insert containing HindIII and SpeI restriction sites (band of ~1.2kb). (B) Selection of colonies after ligation of ANLN 3'UTR insert into pMIR plasmid. (C) Luciferase assay after calcium phosphate transfection of 20ng of ANLN-3'UTR luciferase plasmid or beta galactosidase plasmid (as negative control).

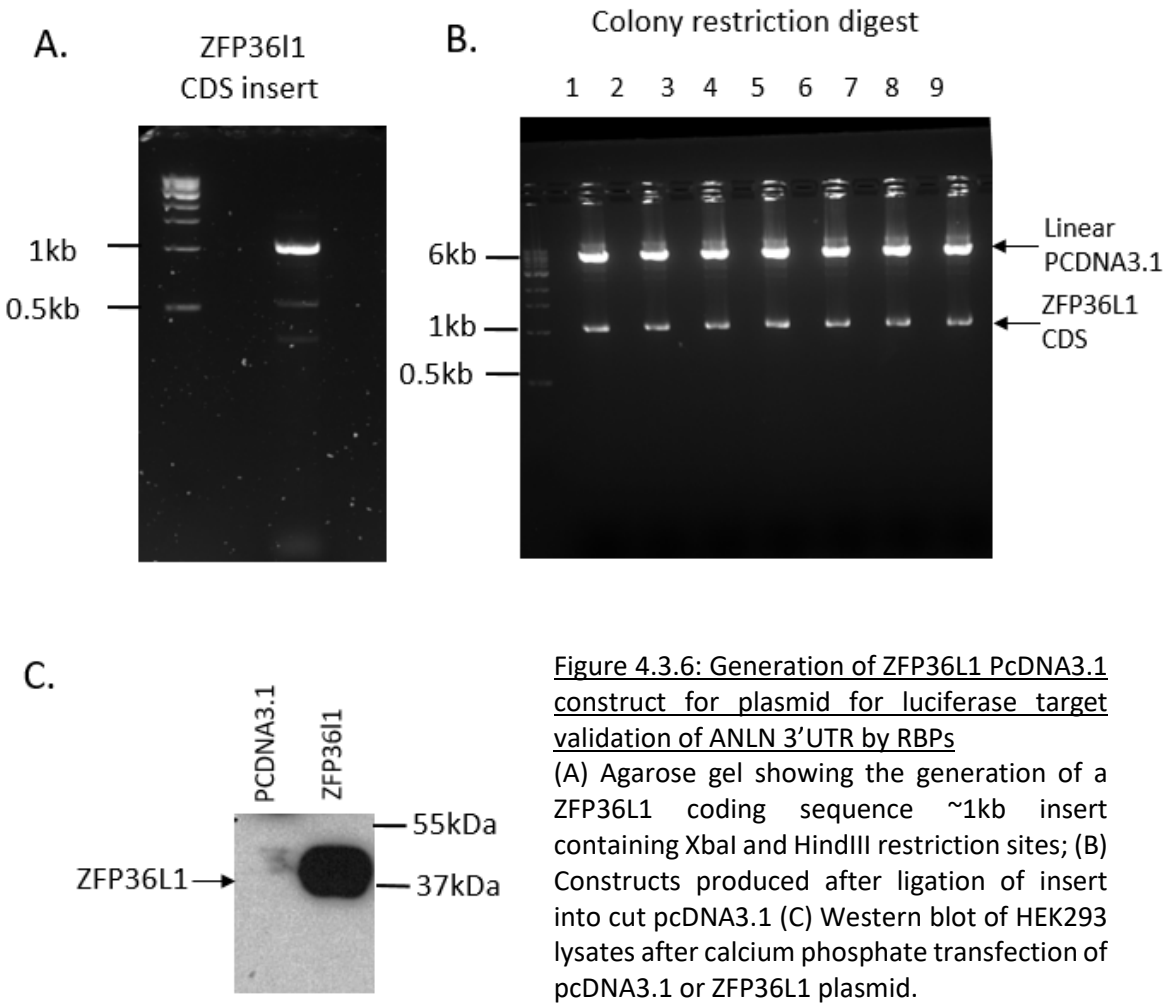

Figure 4.3.6: Generation of ZFP36L1 PcDNA3.1 construct for plasmid for luciferase target validation of ANLN 3'UTR by RBPs

(A) Agarose gel showing the generation of a ZFP36L1 coding sequence ~1kb insert containing XbaI and HindIII restriction sites; (B) Constructs produced after ligation of insert into cut pcDNA3.1 (C) Western blot of HEK293 lysates after calcium phosphate transfection of pcDNA3.1 or ZFP36L1 plasmid.

4.3.4 The ANLN 3'UTR is regulated by ZFP36 family RBPs

The biochemical interaction between ZFP36 family RBPs was confirmed by a 3'UTR luciferase assay. The ANLN 3'UTR-luciferase signal was regulated by RNA binding proteins when assayed with luciferin after co-transfection of the ANLN luciferin reporter plasmid with ZFP36 or ZFP36L1 plasmid in HEK293 (*figure 4.3.7A*). Overexpression of ZFP36 or ZFP36L1 significantly reduced the luciferase activity compared to a transfection with a control plasmid, pCDNA3.1 (***=P<0.01, one way ANOVA with post-hoc Bonferroni).

To demonstrate the binding of ANLN mRNA to ZFP36L1 and ZFP36, an RNA immunoprecipitation (RIP) for ZFP36L1 was performed on HUVEC protein lysates. QPCR of the mRNA products of the RIP showed that there was significant enrichment of the positive control mRNA VEGF in the ZFP36L1 pulldown compared to IgG, there was no significant enrichment of ANLN mRNA (**=P<0.01, ns=P>0.05, t-test) (*figure 4.3.7B*). However, there was a significant enrichment of both VEGF and ANLN mRNA on the ZFP36 RIP (**=P<0.01, *=P>0.05, t-test).

Finally, to confirm the post-transcriptional regulation of ANLN by ZFP36, ZFP36 was overexpressed in HUVECs. Overexpression of ZFP36 by lentivirus in HUVEC produced ~50KDa protein detectable by Western blot (*figure 4.3.8A*). QPCR analysis of mRNA from HUVEC transduced with ZFP36 lentivirus showed a trend for a reduction in ANLN mRNA expression (P>0.05=ns, t-test) as shown in *figure 4.3.8B*.

These experiments suggest that the reporter luciferase assay identified the ANLN 3'UTR as a potential target of ZFP36 and ZFP36L1. However the transcript was only enriched on the binding site of ZFP36 in a RIPs from HUVEC lysates.

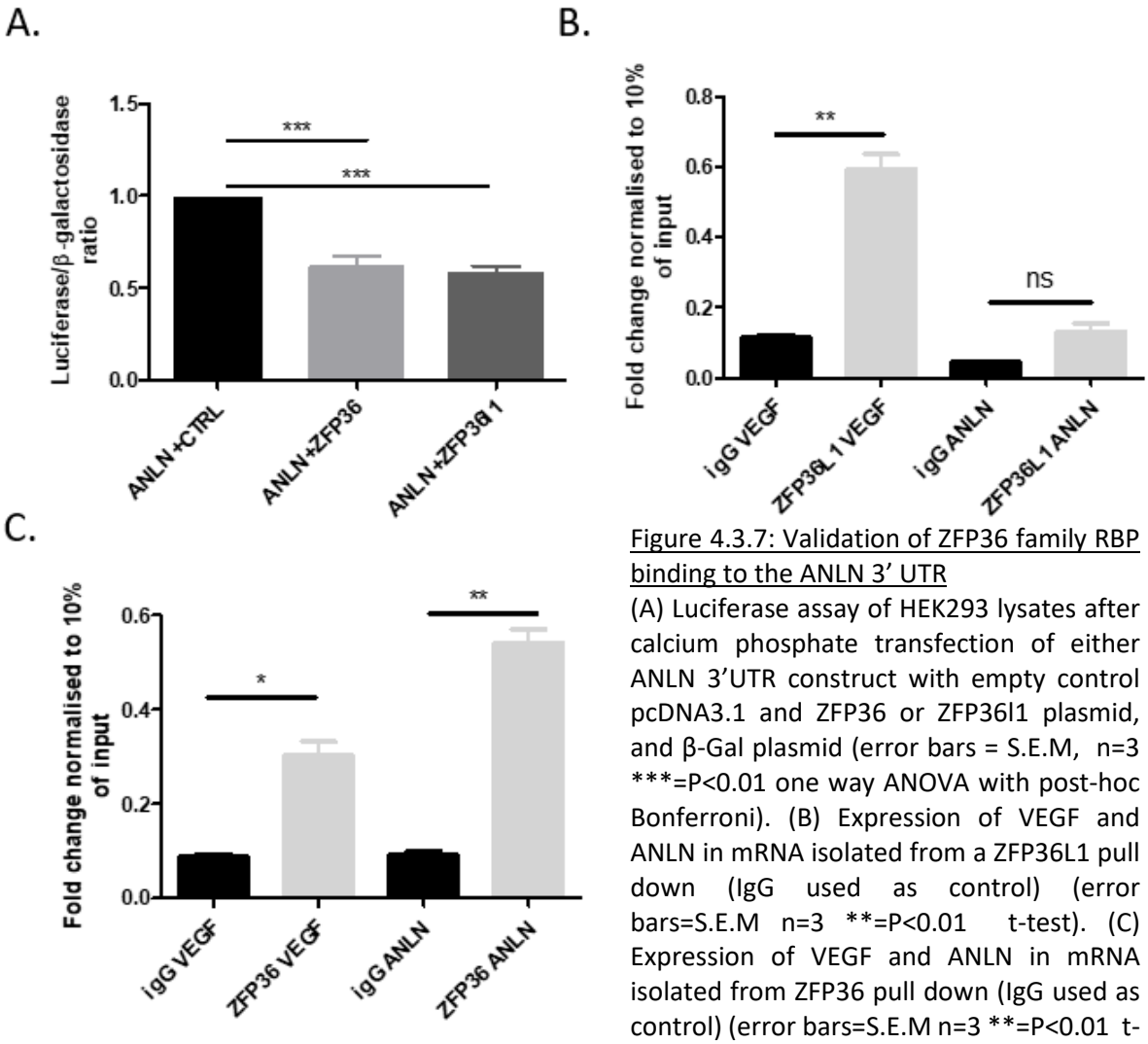

Figure 4.3.7: Validation of ZFP36 family RBP binding to the ANLN 3' UTR

(A) Luciferase assay of HEK293 lysates after calcium phosphate transfection of either ANLN 3'UTR construct with empty control pcDNA3.1 and ZFP36 or ZFP36l1 plasmid, and β-Gal plasmid (error bars = S.E.M, n=3 ***=P<0.01 one way ANOVA with post-hoc Bonferroni). (B) Expression of VEGF and ANLN in mRNA isolated from a ZFP36L1 pull down (IgG used as control) (error bars=S.E.M n=3 **=P<0.01 t-test). (C) Expression of VEGF and ANLN in mRNA isolated from ZFP36 pull down (IgG used as control) (error bars=S.E.M n=3 **=P<0.01 t-test).

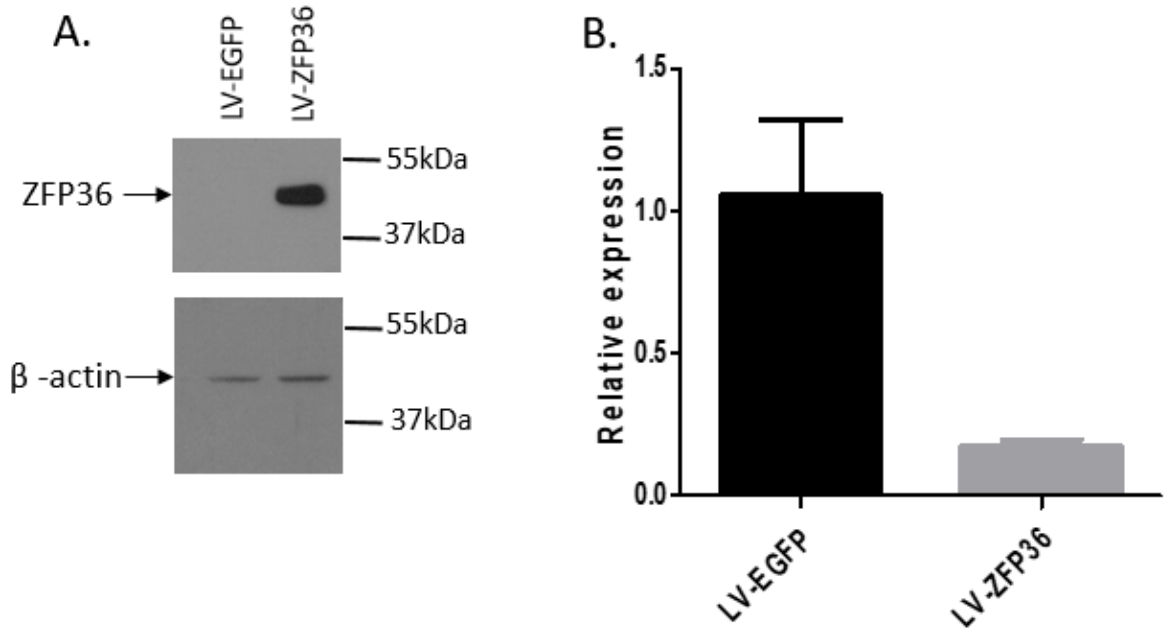

Figure 4.3.8: There is a trend for a reduction of ANLN mRNA after ZFP36 overexpression:
(A) Western blot for ZFP36 in HUVEC lysates after transduction with EGFP and ZFP36 lentivirus.
(B) Expression of ANLN after ZFP36 or EGFP overexpression in HUVEC (n=2 error bars =S.E.M).

4.4 Discussion:

In this chapter, for the first time, the post transcriptional regulation of ANLN in ECs by the ZFP36 RNA binding protein family was investigated.

4.4.1 There is a potential regulatory mechanism of ANLN by ZFP36 RBPS:

An increase of ANLN expression and a reduction in ZFP36/ZFP36l1 expression was shown in $CD31^{+}/CD45^{-}$ ECs sorted from mouse hind limb ischaemia at the 3 and 7 day time points. This suggested a regulatory association between ANLN mRNA levels and ZFP36 RBPs in proliferating or migrating ECs as expected at this experimental time point in ischaemia. As ZFP36 RBP expression is in part regulated by inflammatory stimuli it would be required to check the expression of the RBPs in ischaemic muscle. Confirmation of ZFP36 protein down regulation *in vivo* would be difficult, it is not feasible to collect enough protein from $CD31^{+}/CD45^{-}$ sorted ECs for western blot. Staining for ZFP36 RBPs in 7 day ischaemic muscle would identify ZFP36 RBP down regulation in ischaemic ECs, and could identify ZFP36 RBP expression in satellite muscle cell differentiation in post ischaemic skeletal muscle regeneration (Hausburg et al. 2015; Bye-A-Jee et al. 2018).

The mouse model of hind limb ischaemia induces tissue hypoxia and the activation of angiogenic and inflammatory response. To simulate vascular injury and inflammation *in vitro*, IL-1β stimulation of ECs has been used, as in other studies to model this condition (Merhi-Soussi et al. 2005). IL-1 beta stimulation of epithelial cells has been shown to induce ZFP36 RBP expression in a p38MAPK dependant mechanism (King et al. 2009). The observations match a regulatory mechanism whereby there was an observable increase of ZFP36L1 matching a concurrent drop in ANLN mRNA during IL-1 beta stimulation. The change in expression of ZFP36 RBPs could be controlled as in other cell types by phosphorylation and induction of protein expression through p38MAPK (King et al. 2009). In addition to ZFP36L1 protein induction at 4 hours, increased streaking of the protein band suggested an increase in phosphorylation of ZFP36L1. This could be investigated by western blotting of IL-1β stimulated HUVEC lysates with an anti phospho-ZFP36L1 antibody. This would

determine if ZFP36l1 is activated/de-activated by phosphorylation in IL-1β stimulation. Furthermore, modelling ischaemia *in vitro* using a hypoxia chamber (1% O_2) may better simulate the ischaemic expression of ZFP36 RBPs.

To understand the potential regulatory mechanism, ZFP36 RBPs were knocked down *in vitro* with siRNA, however, Silencing of ZFP36 RBPs with siRNA did not significantly increased ANLN expression in HUVECS. This was counter to observations of other targets of ZFP36 RBPs in the literature where HIF-1α and dll4 mRNA were significantly increased after ZFP36L1 or ZFP36 silencing (Chamboredon et al. 2007; Desroches-castan et al. 2011). There appeared to be a trend for the increase of ZFP36 expression after silencing of ZFP36L1. This could be a redundancy mechanism by which ZFP36 expression is increased to compensate for a loss of ZFP36L1. This has been observed in T cells where loss of ZFP36L1 leads to perturbed mouse thymus development, however, loss of ZFP36 was recovered by a redundant increase of ZFP36L1 expression to maintain normal gene expression (Hodson et al. 2010). Transfections with siRNA of both ZFP36 and ZFP36L1 did not produce the up-regulation of ANLN mRNA which was expected. Confirmation of a redundant increase of expression of either ZFP36 or ZFP36l1 could be confirmed by western blot in HUVEC lysates after silencing. Moreover, it should be recognised that a post translational regulatory mechanism of ANLN expression exists through APC^{cdh1} mediated ubiquitination and degradation (Zhao & Fang 2005). This mechanism functions to degrade ANLN and other cell cycle associated proteins after completion of the cell cycle (Zhao & Fang 2005). In the CAG-ANLN-EGFP mouse and flt1-ANLN-EGFP mouse, which function essentially as ANLN overexpression models, ANLN-EGFP is degraded rapidly by APC^{cdh1} in non-proliferating cells (Hesse et al. 2012; Herz et al. 2018). This mechanism may be affected by any treatment which affects proliferation, including; IL-1β stimulation and ZFP36 RBP overexpression/silencing. IL-1β stimulations and ZFP36 RBP interference could be used in ANLN-EGFP transduced HUVEC to determine their effect on ANLN-EGFP protein stability. Flow cytometry could be used to detect shifts in ANLN-$EGFP^{+ve}$ cell numbers of sorted and unsorted ANLN-EGFP transduced cells, this could identify changes in post-translational regulation of ANLN-EGFP protein.

Plasmids for investigating the regulation of ANLN were successfully produced. Overexpression of ZFP36 RBPs is possible despite the presence of auto regulatory ATTTA sites in their 3'UTR (Mukherjee et al. 2014). The ANLN 3'UTR was confirmed as a target of ZFP36 and ZFP36lL1 by luciferase assay in HEK293, confirming the RBP binding to one or multiple of the ARE sites on the ANLN 3'UTR. This effect was not due to changes in transfection efficiency as all transfections included the β-galactosidase plasmid as a control. The physical interaction of the ANLN mRNA transcript was confirmed by RNA immunoprecipitation. This showed that the positive control mRNA VEGF, was enriched compared to the control input lysate in ZFP36 and ZFP3L1. ANLN was only enriched compared to input in a ZFP36 but not in a ZFP36L1 pull down. ZFP36 and ZFP36L1 are homologous (particularly the zinc finger domains), but they have some key differences in surrounding domains, these differences may affect their regulation and target recognition (Ciais et al. 2013). The individual binding site on the 3'UTR was not confirmed, however, we could do this by site directed mutagenesis or a deletion of each of the 6 binding site present on the 3'UTR luciferase plasmid. Additionally we could include a mutant control RBP plasmid, this would be ZFP36 and ZFP36L1 with mutated zinc finger domains to prevent binding to the target ARE elements in the 3'UTR. It is possible that ANLN mRNA does bind to the ZFP36L1 active site, but this is undetectable in normal HUVEC lysates. We could use the approach of other studies, where flag tagged ZFP36 RBP plasmids were overexpressed in HEK293 to confirm the target transcript presence on the RIPs (Chamboredon et al. 2007). If this approach is used then mutated ZFP36 RBP plasmids could also be used as an additional negative control in ZFP36 RIPs. Although using HEK293 would remove some physiological relevance, the experiment would still demonstrate the biochemical interaction between the ANLN mRNA transcript and ZFP36L1. Again it would not be feasible to produce enough protein lysates from ECs sorted from hind limb ischaemic muscle to perform ZFP36 RBP RIPs with these cells.

Overexpression of ZFP36 in HUVECs by lentivirus caused a trend for a concurrent drop in ANLN mRNA compared to control. ZFP36 overexpressed HUVEC didn't survive multiple passages so this experiment may not accurately portray the true expression

of ANLN. This could be caused by ZFP36 overexpression down-regulating proliferative gene expression. This may lead to cell cycle suppression and cell death as has been reported in other cell types overexpressed with ZFP36 RBPs (Wegmüller et al. 2007; Suk et al. 2018). This may be a result of enhanced mRNA target repression seen in ZFP36 RBP overexpression, where, overexpression results in direct shuttling of ZFP36 bound mRNA from the nucleus to P-bodies. Although this is a normal mechanism of ZFP36 mediated RNA degradation, it is increased during overexpression of ZFP36 RBPs. The effect of ZFP36 RBP expression on the could be confirmed by staining for apoptotic markers via TUNEL staining or through staining of PCNA or Ki67 to determine if the cell cycle is being suppressed (Bologna-Molina et al. 2013). We only had a limited volume of ZFP36 lentivirus which restricted the amount of experiments we could perform at this point.

4.4.2 Future investigations of ZFP36 RBPs in angiogenesis:

The initial aim with the RBP protein hypothesis was to use an animal model for investigating the effects of RBP knockout on vascular regeneration after ischaemia. This was to be done by using an inducible endothelial specific Cre-lox knockout of either ZFP36 or ZFP36L1 in mice (Newman et al. 2017). However, this model wasn't obtainable due to time constraints in organising the importation and establishment of this mouse line.

Several studies showed that *in vitro* functional assays after ZFP36 RBP expression modulation are not necessarily representative of an *in vivo* phenotype. Some of the phenotypes induced *in vivo* by global RBP knockout may be a paracrine effect caused by increased growth factor release from surrounding cells. This effect has been hypothesised as a contributing factor to vascular disorganisation seen in ZFP36L1 knock outs (Bell et al. 2006). Cultured myeloid cells from ZFP36 knockout mice do not have a hyper proliferative phenotype as observed *in vivo*. Moreover, the endothelial dysfunction observed in ZFP36 knockout mice is attributed to a paracrine effect of increased overall inflammation and not a direct effect on ECs (Bollmann et al. 2014). The same effect is observed in fibroblasts obtained from ZFP36L1 knockout mice,

where there is no difference in cell proliferation or apoptosis compared to controls (Hacker, Valchanova, Adams, Munz, et al. 2010). Therefore for these experiments to be accurate, a vascular specific knockout of ZFP36 RBPs is required. This would eliminate a paracrine effect of cytokine or growth factor secretion from surrounding cells and demonstrate a true vascular phenotype.

Finally, the tools generated and utilised in this study can be used to identify ZFP36 RBP gene targets, particularly those of ZFP36L1. The ZFP36L1 RIP and siRNA could be used in HUVEC to generate samples for RNA sequencing to identify targets of ZFP36L1. This would allow for further investigation of RNA binding protein post transcriptional control of gene expression in angiogenesis (Vogel et al. 2016). Multiple potential targets expressed in tip stalk cell designation including, Apelin, Dll4 and Notch contain ZFP36 ARE elements. Identifying a regulatory mechanism of these genes by ZFP36L1 could explain the vascular defects associated with ZFP36L1 knockout mice (Fallmann et al. 2016).

4.5 Conclusions:

To conclude, the ANLN 3'UTR was a potential target of ZFP36 RBPs and there was a regulatory association *in vivo* and *in vitro* between ANLN and ZFP36 family RBPs in ECs. However ANLNs expression was not affected by the silencing of ZFP36 and ZFP36L1 RBPS and the transcript was not present on the binding site of ZFP36L1. The ANLN mRNA transcript was present on the ZFP36 binding site, however, because we couldn't obtain a ZFP36 RBP vascular specific knockout mouse model to carry out suitable *in vivo* experiments we decided to stop. Instead it was decided to focus the last part of the thesis on investigating the ANLN expression and function in vascular injury *in vivo*. If this RBP regulatory mechanism was to be continued in future, ZFP36 rather than ZFP36L1 should be focused on as the potential regulatory mechanism

Chapter 5:

Does Anln expression localise with endothelial cells during development or vascular injury in the zebrafish embryo?

5.1 Introduction

ANLN has been shown to profoundly affect the cleavage furrow, where its association with the contractile ring is required for successful cytokinesis to take place (Straight et al. 2005; Field & Alberts 1995). Importantly, ANLN is required for the correct placement of the mitotic centriole during cytokinesis (van Oostende Triplet et al. 2014). ANLN silencing in invertebrates has been shown to produce asymmetric cell division phenotypes resulting in a loss of asymmetry in embryogenesis (Piekny & Glotzer 2008). In mammalian cell lines, loss of ANLN is also associated with asymmetric cell division phenotypes (Liu, Gregory D. Fairn, et al. 2012).

Zebrafish are a powerful and versatile tool for investigating embryogenesis, angiogenesis, wound healing, and gene function as laid out in chapter 1. We investigated and acquired the *anln:anln-eGFP* zebrafish line which was generated by Dr Lucia Poggi of the University of Heidelberg, Germany, to allow us to conduct investigations of *anln* in zebrafish. This zebrafish line was generated by injection of a BAC plasmid containing the full zebrafish *anln* promoter with the coding sequence of *anln* fused to eGFP (Paolini et al. 2015). This generated a zebrafish that expresses a fluorescent reporter of Anln expression and cellular localisation. This line was used extensively for the investigation of Anln in the asymmetric cell division of zebrafish retina progenitor cells (Paolini et al. 2015; Malo et al. 2017). Asymmetric cell division is a well described cellular process whereby asymmetric placement of the centriole allows for polarised inheritance of cell products and changes in cell size (Berika, Marwa E Elgayyar, et al. 2014). This process is important in budding yeast reproduction where daughter cells bud from the parent cell (McFaline-Figueroa et al. 2011). In non-vertebrate organisms like *C. elegans* asymmetric cell division is associated with early embryonic development. The first division of the zygote is asymmetric to produce daughter cells that will produce embryonic layers through further asymmetric cell division (Berika, Marwa E Elgayyar, et al. 2014).

Although essential in invertebrates, it is less important in vertebrates where there is some evidence for this process in stem cell renewal and tissue maturation (Ettinger

et al. 2011; Dubreuil et al. 2007; Berika, Marwa E. Elgayyar, et al. 2014). Asymmetric cell division has been observed to mediate tip stalk cell designation in neoangiogenesis (Costa et al. 2016; Costa et al. 2017). During tip/stalk cell designation the leading EC or tip cell has a different migratory phenotype to the stalk cells that make up the rest of the developing vessel (Costa et al. 2016). In zebrafish, tip cells were found to be 1.8 to 1.9 times larger than stalk cells in volumetric analysis of 26-32hpf *flk:mcherry* intersegmental vessels (ISV) (Costa et al. 2016). Asymmetric placement of the centriole in ECs predicts the motility of produced daughter ECs (Costa et al. 2016). In this way asymmetric division was shown to affect the distribution of VEGF signalling components, with polarised localisation of VEGFR2 receptor in the leading tip daughter cell (Costa et al. 2017; Costa et al. 2016).

The *in vitro* data in chapter 3 showed that ANLN overexpression and silencing both affect EC tubulogenesis. Tubulogenesis was employed as a model of early sprouting angiogenesis, therefore it was decided to investigate Anln in the early vascular development of the zebrafish embryo. Furthermore, due to an association of ANLN expression with hind limb ischaemia in the mouse, a vascular injury model in zebrafish was developed to further investigate the association of ANLN with ECs in vascular injury.

5.2.1 Hypothesis:

The underlying hypothesis for this chapter was, that Anln localises to ECs during vascular development/injury and that interference with *anln* expression impairs the morphology of zebrafish blood vessels by impairing asymmetric cell division associated with tip/stalk cell designation.

This hypothesis was to be addressed by using the *anln:anln-eGFP* zebrafish provided by Dr Luccia Poggi using associated molecular tools and zebrafish lines (Paolini et al. 2015).

5.2.2 Aims:

In this chapter I aimed to;

1. Investigate *anln* expression in the zebrafish vasculature using the *anln:anln-eGFP and flk:mcherry* zebrafish lines
2. Develop a method for vascular injury of the zebrafish to observe if *anln:anln-eGFP* is expressed at the site of injury localised within ECS
3. Determine the effect of *anln* knock-down on the vascular morphology of *flk:eGFP* zebrafish.

5.3 Results

5.3.1 The *anln:anln-eGFP* transgene is weakly expressed from 24hpf

To investigate the expression of Anln in angiogenesis and vascular development in the zebrafish embryo, reporter zebrafish expressing *anln:anln-eGFP* were imported and raised to breeding age. The live *anln:anln-eGFP* embryos were screened by epifluorescence at the early stages of development after fertilisation. Representative images of the whole fish are shown in *figure 5.3.1A-B anln:anln-eGFP* fluorescence is visible in the cell mass of the early 32-cell and shield stage embryo (*figure 5.3.1A*). Later time points of the embryos between 24-72hpf exhibited no detectable expression of the *anln:anln-eGFP* transgene except for the yolk sack. This suggested that from ~24 hpf onwards the expression of *anln:anln-eGFP* required a more sensitive method of detection.

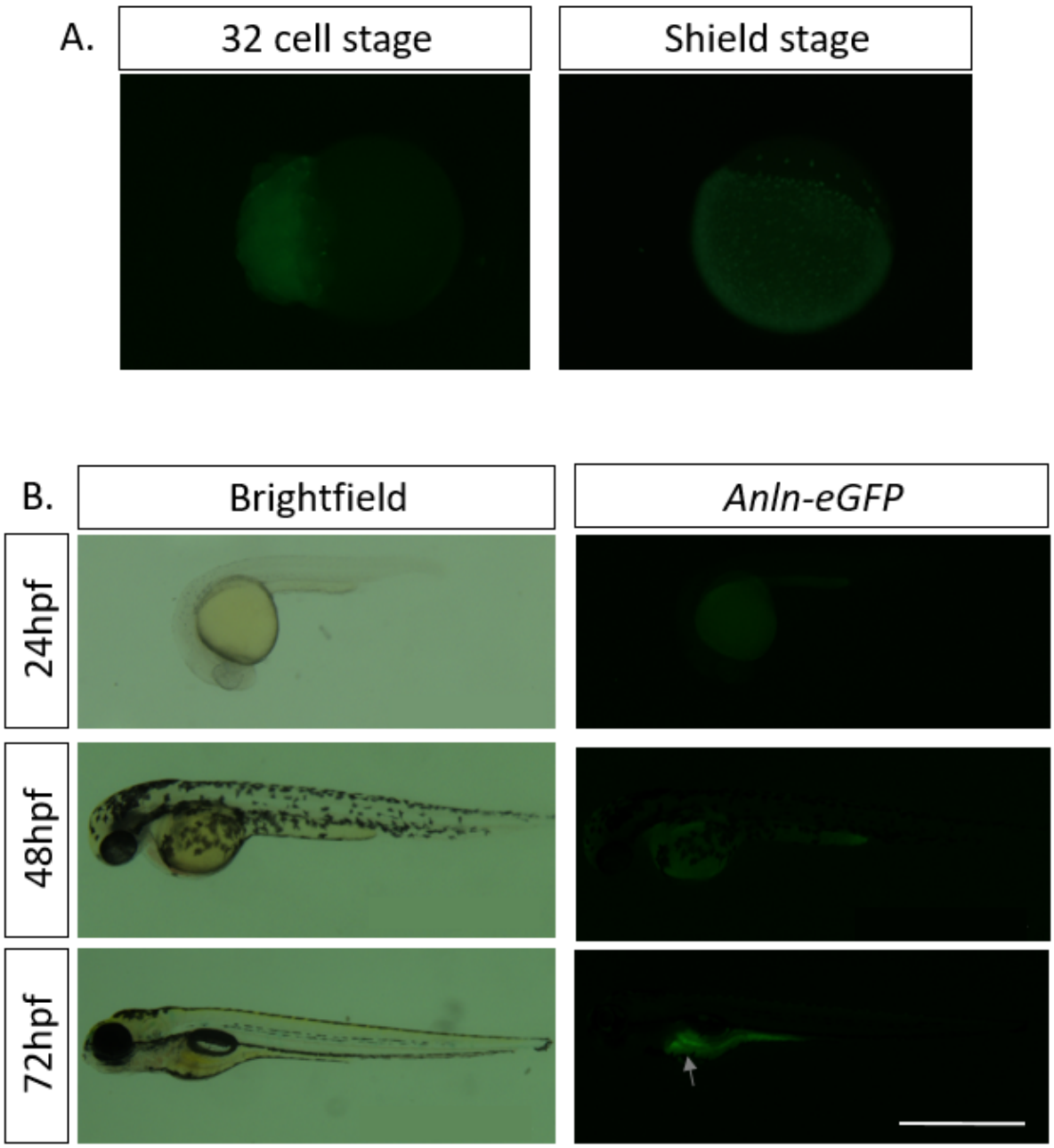

Figure 5.3.1: The *anln:anln-eGFP* transgene is not detectable with epifluorescence from 24 hpf:

(A) Weak *anln:anln-eGFP* fluorescence is visible via epifluoresence of the early cell mass embryonic stages up until the shield stage of embryonic development. (B) At later time points (24-72hpf) no detectable Anln-eGFP expression could be detected with epifluorescence, with only yolk sack auto fluorescence visible as indicated by grey arrow (scale bar=1mm).

5.3.2 The *anln:anln-eGFP* transgene expression is reduced with age of the fish embryo

Using a more sensitive detection method, 24-48 hpf *anln:anln-eGFP* embryos were screened by single plane illumination microscopy (SPIM) to determine *anln:anln-eGFP* expression throughout embryonic development of the zebrafish. In *figure 5.3.2* the expression of the *anln:anln-eGFP* transgene in the head eye and trunk of the embryonic fish is shown. This reveals *anln:anln-eGFP* transgene expression at 24 hpf is widespread in the dermis, head, eyes, and CNS of the developing embryo. In the trunk of the 24hpf fish two strong bands of GFP positive cells were found adjacent to the cloaca, that align anatomically with the notochord and developing vessels (*figure 5.3.3*). At 48hpf, *anln:anln-eGFP* expression is more restricted in these areas, with expression retained in the dermis and eye but lost in the CNS and trunk of the fish. This showed that between 24 hour and 48 hpf the *anln:anln-eGFP* transgene can be detected by SPIM imaging. During the 24-48hpf time points there is a concurrent significant decrease of *anln* mRNA as indicated by QPCR analysis of the whole fish embryo (**=P<0.01, t-test) (*figure5.3.3B*). This matched a reduction in expression of the transgene in the head, eye and trunk over these time points. For reference negative control images of *wik* (wild type) embryos please check supplementary *figure 1.*

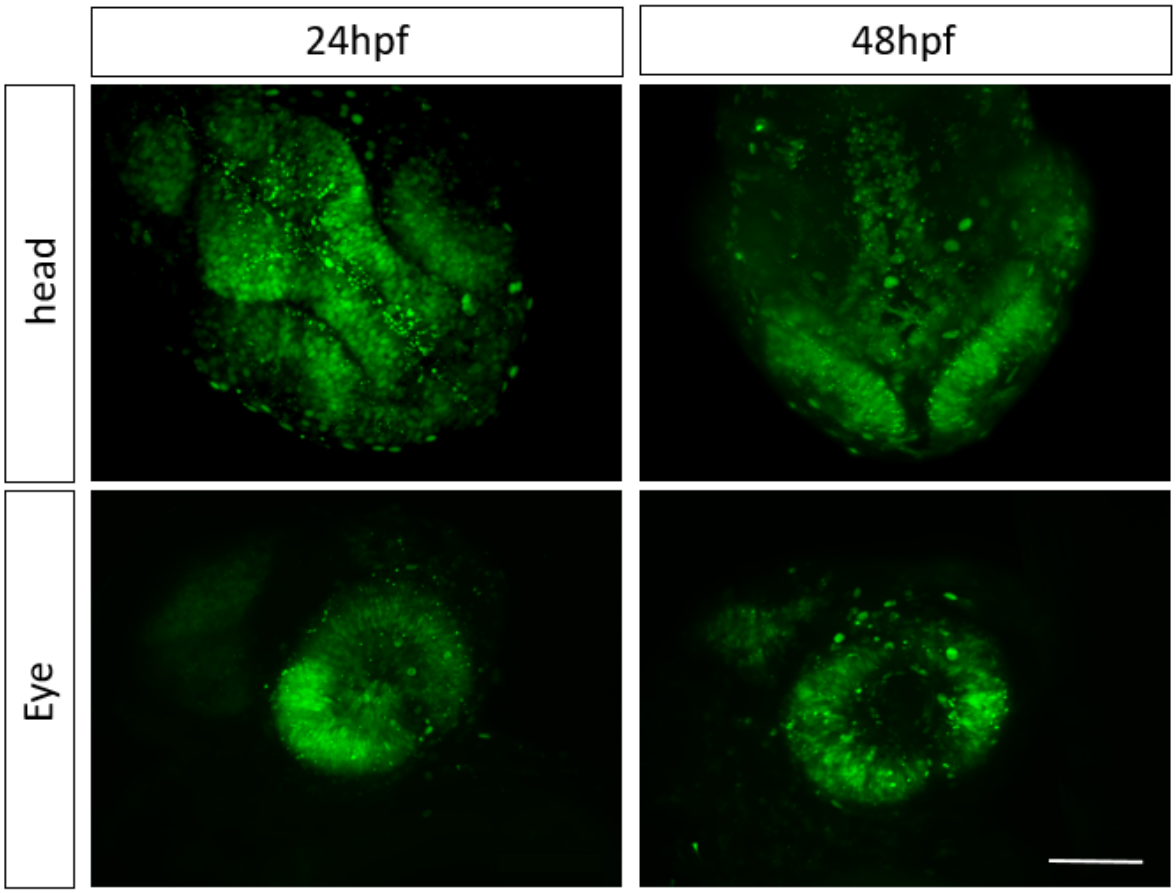

Figure 5.3.2: The *anln*:*anln-eGFP* fluorescence in the developing zebrafish embryo declines at 24-48hpf in the embryonic CNS and eye:

SPIM imaging of the 24-48 hpf *anln:anln-eGFP embryos* showing the head and eye of embryos. The *anln:anln-eGFP* transgene is widely expressed at 24hpf throughout the eye head and CNS while expression is reduced at 48 hpf (scale bar= 100µms).

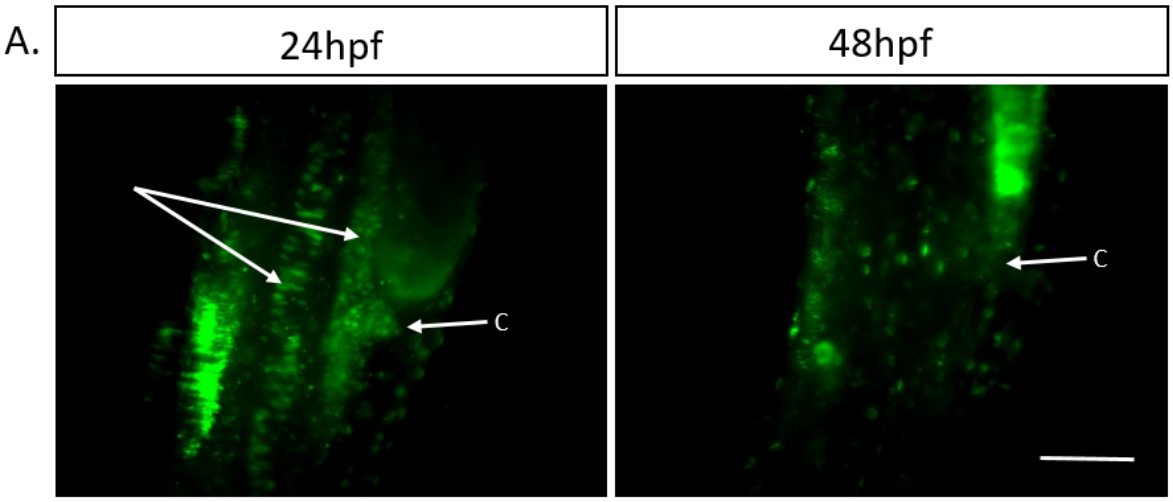

B.

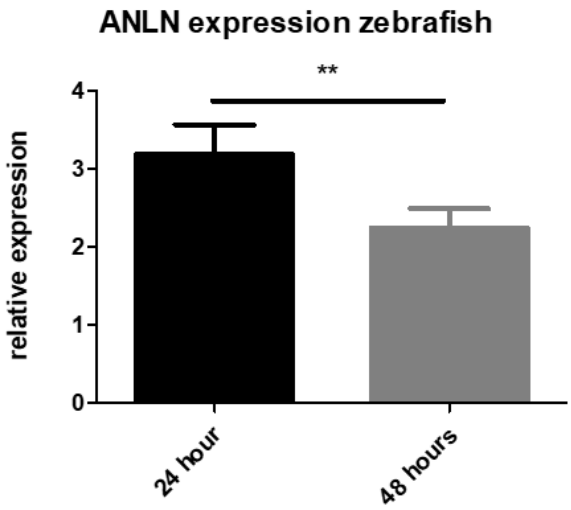

Figure 5.3.3: The expression of *anln:anln-eGFP* in the trunk declines between 24-48 hpf:

SPIM imaging of the 24-48 hpf *anln:anln-eGFP embryos* showing the trunk of the embryo. Indicating arrows mark the cloaca (C) of the developing fish. (A) *Anln-eGFP* is expressed in the trunk of the 24hpf zebrafish marking cells of developing embryonic tissues which is lost at 48hpf (scale bar= 100µms) (B) qPCR analysis of whole zebrafish embryos between 24-48 hpf detects a significant reduction in expression of ANLN mRNA between 24-48 hpf n=5 (groups of 30 embryos) (**=P<0.01 T-test).

5.3.3 *anln:anln-eGFP* signal does not co-localise with blood vessels at 24hpf

To determine whether expression of the *anln:anln-eGFP* transgene was associated with the developing blood vessels, *anln:anln-eGFP* fish were crossed with the *flk:mcherry* expressing zebrafish and offspring were analysed at regions of interest. SPIM microscopy was used to investigate the trunk, tail, and CNS of the resulting 24hpf *anln:anln-eGFPxflk:mcherry* zebrafish. Representative images are shown in *figure 5.3.4-5.3.6*. In the head, eyes, and CNS, the cerebrovascular system was developed and there appeared to be an association of the *anln:anln-eGFP* transgene with some cells of the vessels of the CNS in *figure 5.3.4A*. However, investigation of these cells in smaller Z-stacks and by manipulation of a 3D image showed that these cells were not associated with the vessels (*figure3.3.4B-C*). In the trunk and tail, vascular structures of the caudal artery plexus (CAP) and dorsal aorta (DA) were observed; an association, but no actual co-localisation of the *anln:anln-eGFP* transgene with these vascular structures was detected. A band of Anln-eGFP^{+ve} positive cells is positioned inferior and adjacent to the dorsal aorta but does not co-localise with the vessel; in the CAP there was an association of Anln-eGFP^{+ve} positive cells interspersed with the developing vessel, but again there was no co-localisation. These data identified that in the developing 24-48hpf fish at least in these regions of interest there is no co-localisation of the *anln:anln-eGFP* transgene expression with the developing blood vessels of the fish.

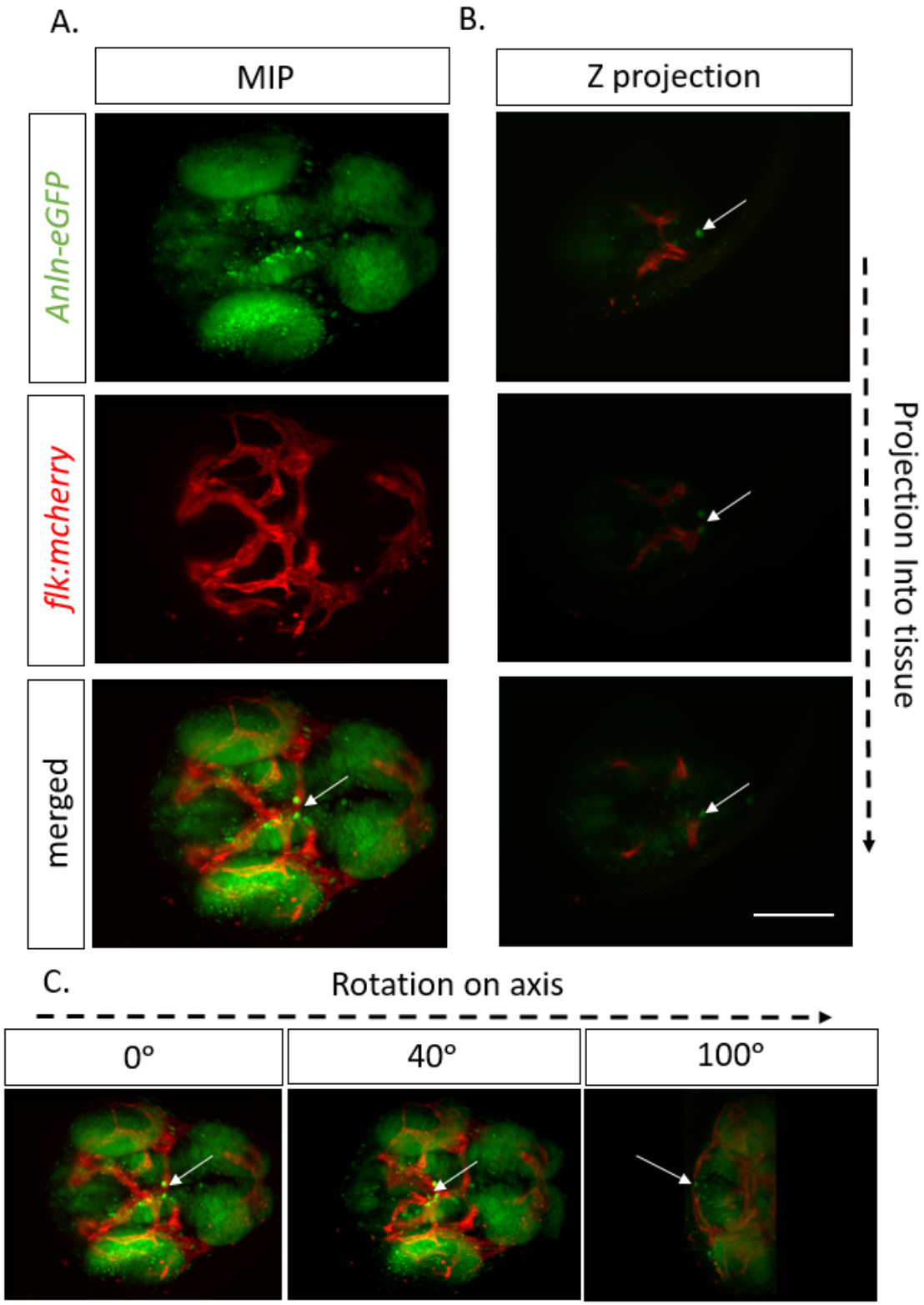

Figure 5.3.4: *anln:anln-eGFP* does not co-localise with the vessels in the 24hpf CNS: SPIM imaging identified no association of *Anln-eGFP*$^{+ve}$ *cells* with the blood vessels of the developing CNS of the 24 hpf *anln:anln-eGFP* x *flk:mcherry* zebrafish embryo. (A) Maximum intensity projection of a Z-stack of the CNS (showing potential co-localisation with arrows) (B) Individual z projections from the top of the z-stack (showing potential co-localisation with arrows) C. Rotation of a 3D MIP at 0, 40 and 100 degrees identified that potential co-localisations were in a different plane to the vessels of interest (scale bar= 100µms).

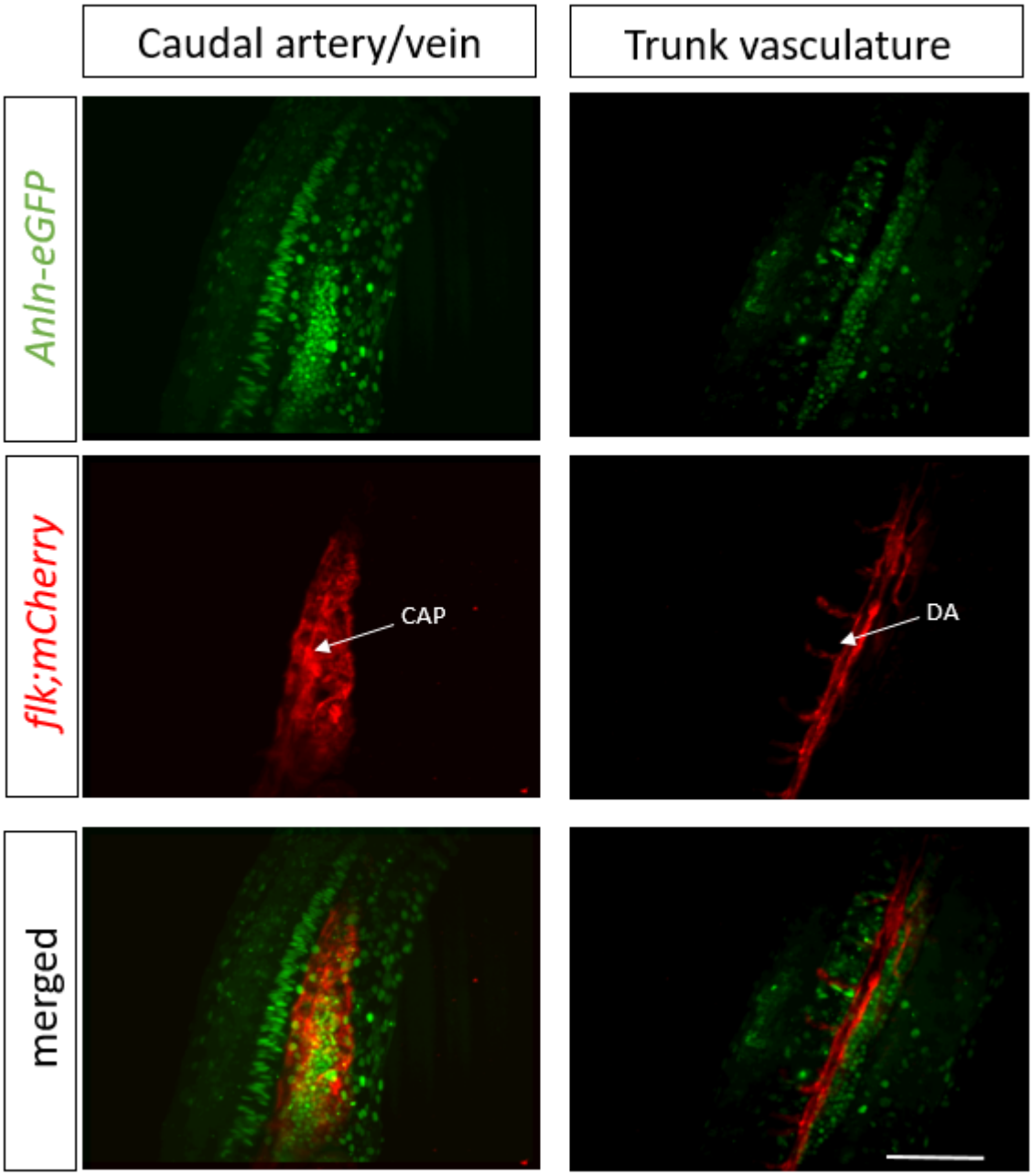

Figure 5.3.5: There is an association but no co-localisation of *anln:anln-eGFP* with the vessels in 24 hpf zebrafish embryo trunk and tail:

SPIM imaging showed an association but not co-localisation of Anln-eGFP^{+ve} cells with the vessels of the trunk and tail of 24 hpf *anln:anln-eGFP* x *flk:mcherry* zebrafish embryos. Arrows indicate the Caudal artery plexus (CAP) and Dorsal aorta (DA). (scale bar= 100µms).

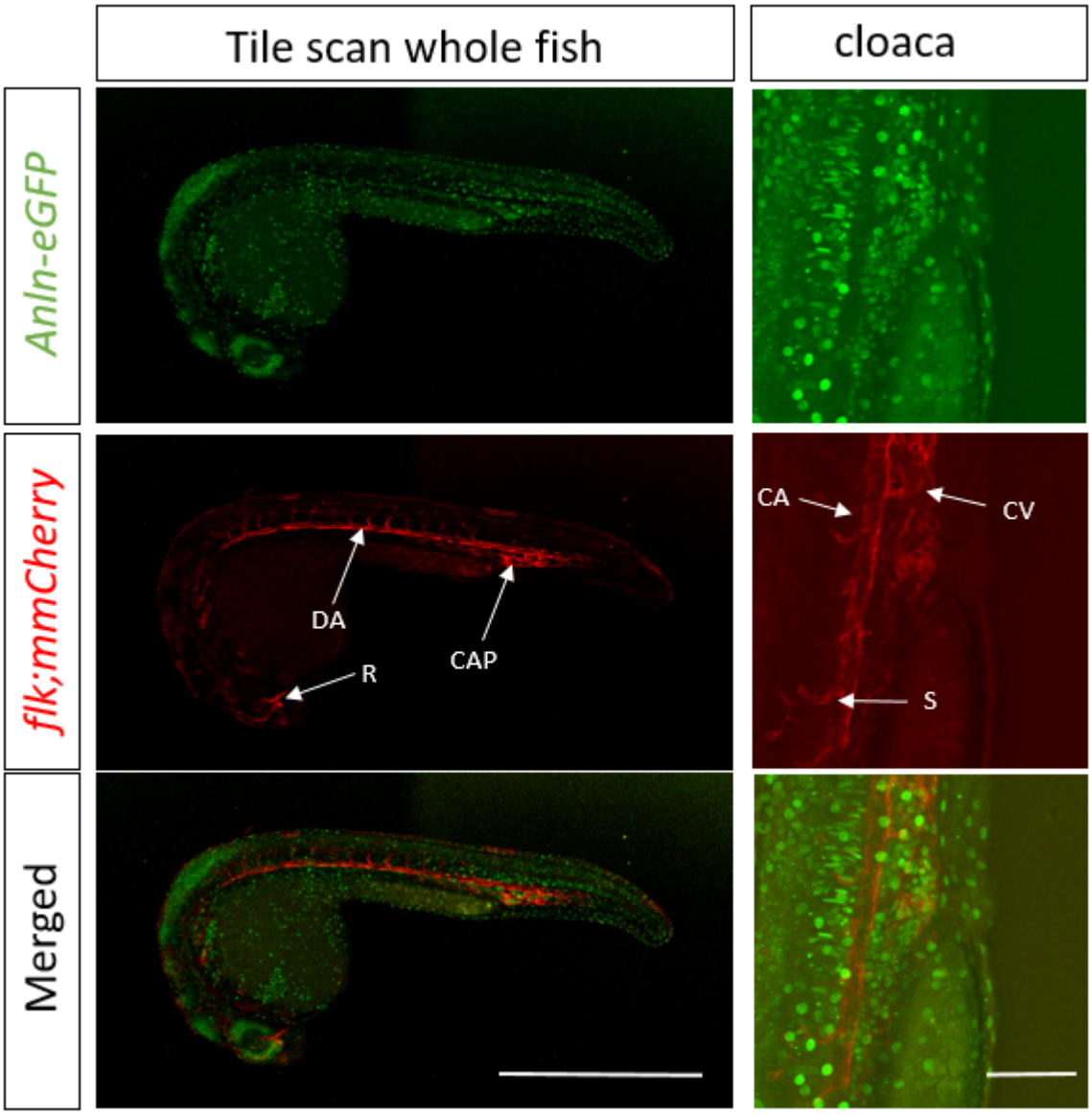

Figure 5.3.6 *anln:anln-eGFP* associates but does not co-localise with blood vessels in the 24 hpf zebrafish embryo:

Imaging with confocal microscopy identified Anln-eGFP localisation in the vasculature of the whole embryo. Individual sprouting ECs at the cloaca showed no co-localisation with *anln:anln-eGFP*. Tile scan of whole fish are shown. Arrows indicate the retina (R) dorsal Aorta (DA) and the caudal artery/vein plexus (CAP). Cloaca showing the developing caudal artery (CA) and cardinal vein (CV) with individual sprouting ECs (S) (representative scale bars =1mm and 50µm, respectively).

5.3.4 Micro point laser injury produces non-lethal injuries of the caudal artery

To investigate *Anln* expression in the EC response to injury, a protocol for vascular injury of the caudal artery in larval zebrafish was developed using a micro point laser system. *Figure 5.3.7A* shows representative images of the laser injury induced after 3 and 6 pulses of unattenuated laser power demonstrating a single clot at the site of injury. The clotting time of the blood after injury was dependent upon injury intensity, with a significant reduction in time for clot formation seen between embryos receiving 1, 3 or 6 pulses of the micro point laser ($P<0.001$=*** one way ANOVA with post hoc Bonferroni) as shown in figure *5.3.7B*. Survival was observed overnight as shown in figure 5.8 where there was no significant difference between uninjured and injured groups in overnight survival or blood flow recovery. These experiments demonstrated that laser injury of the caudal artery is possible in embryonic fish and that this type of injury is not final, with regeneration observed within 24 hours. These three intensities of laser injury were classified as either weak, moderate or severe based on the clotting times. To assess the impact of this type of laser injury on the vessel, time-lapse SPIM imaging was used to capture the recovery of the caudal artery in 48-72hpf and 72-96hpf *flk:gfp* larval fish after injury with 3 pulses of unattenuated laser (*figure 5.3.9+5.3.10*). The representative images shown demonstrate a temporary loss of fluorescence at the site of laser injury which fully recovered over a period of ~ 12 hours. I also employed f*lk:gfp x mpx:mcherry* fish, in which ECs are marked by green and neutrophils by red fluorescence, a line commonly used to assess regeneration and neutrophilic inflammation in response to wound healing, to determine if neutrophils associate with the caudal artery at the site of laser injury (*figure 5.3.11*). These experiments identified an association of neutrophils with the laser injury site in 2-3 dpf zebrafish. Interestingly, from 1 hpi injury neutrophils associated with the injury site leaving the injury site by 24 hpi, identifying immune cell localisation with the injury. To exclude the possibility that photo bleaching might be a component of these injuries, laser injury experiments were repeated using the *flk:mcherry* zebrafish (*figure 5.3.12*). The injuries observed were different in the *flk:mcherry* zebrafish with a gradual recovery of fluorescence and

visible EC motility in close proximity to the injury site. These experiments showed that the laser injuries did induce a loss of fluorescence in the *flk-eGFP,* but not the *flk:mcherry* line and that damage to the vessel causes localisation of inflammatory cells to the injury sites.

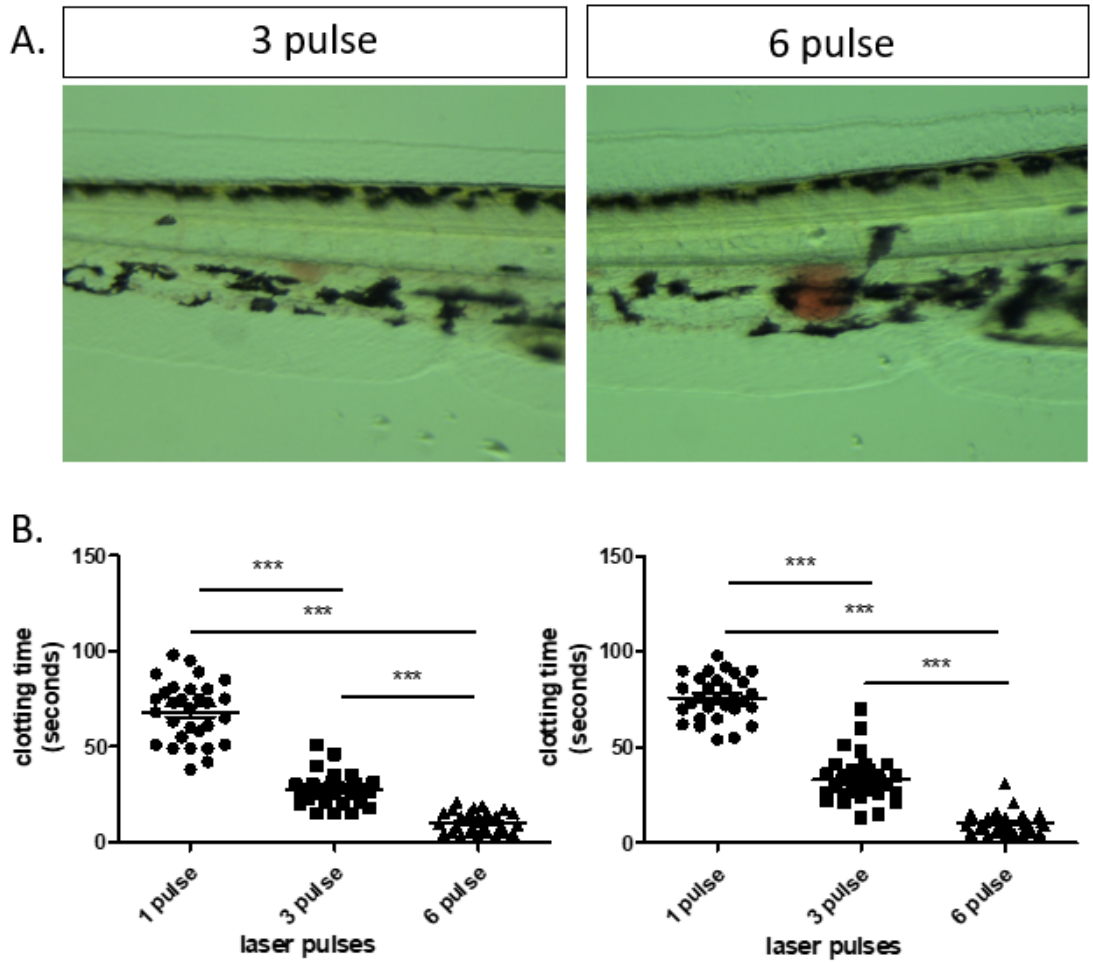

Figure 5.3.7: laser injury of the caudal artery induces a thrombus at the site of injury:
(A) 3-6 pulses of un-attenuated micro point laser focused on the caudal artery of 48hpf zebrafish induces a thrombus at the site of injury. (B) In 48-72hpf embryos the time for thrombus formation of the caudal artery after laser injury was measured, indicating a faster thrombus formation with increased laser pulse number (n=30) (Error bars=SEM ***=P<0.001 ANOVA with post hoc Bonferroni).

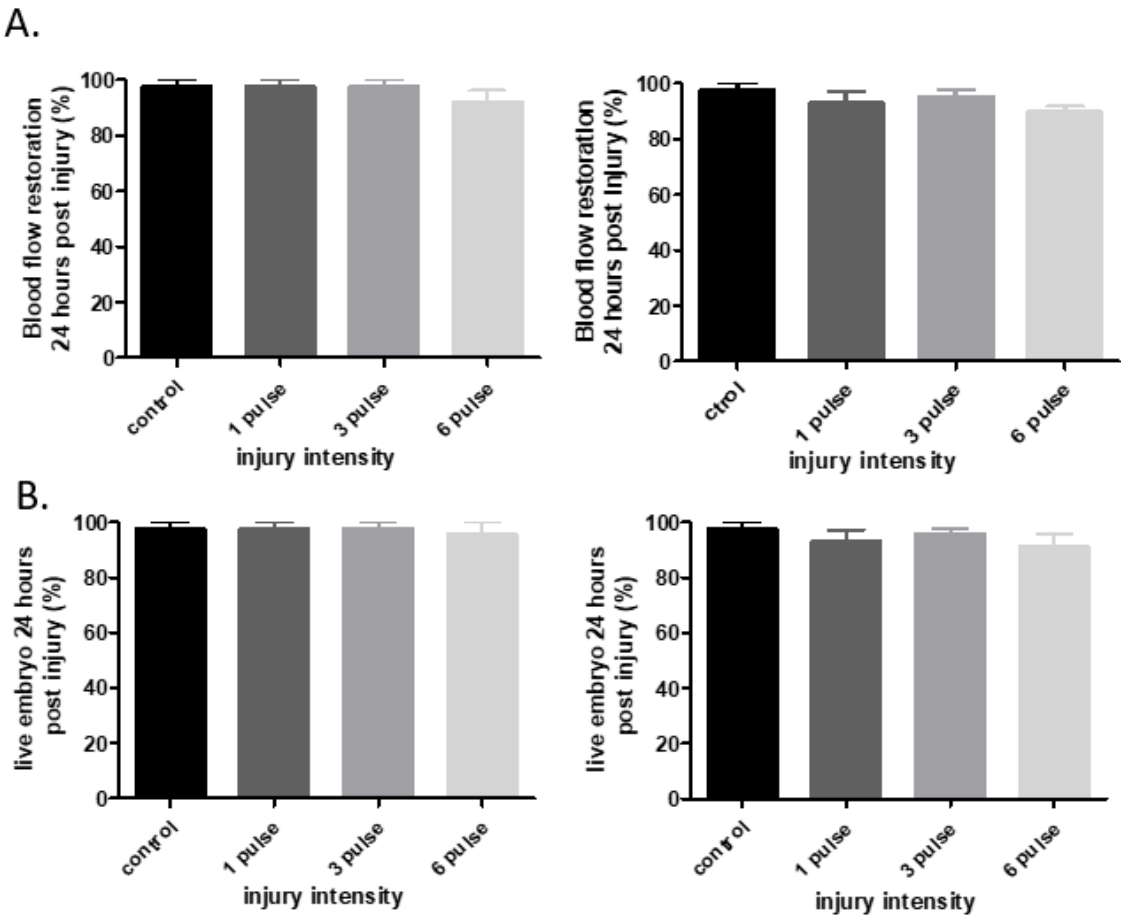

Figure 5.3.8 – Embryonic zebrafish are highly resistant to laser injuries at 48-96 hpf: (A) There is a complete recovery of blood flow in 48-96 hpf WIK zebrafish after application of one, three and six pulses of un-attenuated micro point laser to the caudal artery. (B) There is a high rate of survival in 48-96 hpf WIK zebrafish embyros after application of one, three and six pulses of un-attenuated micro point laser to the caudal artery. (n=3 15 embryos per group) (error bars=SEM)

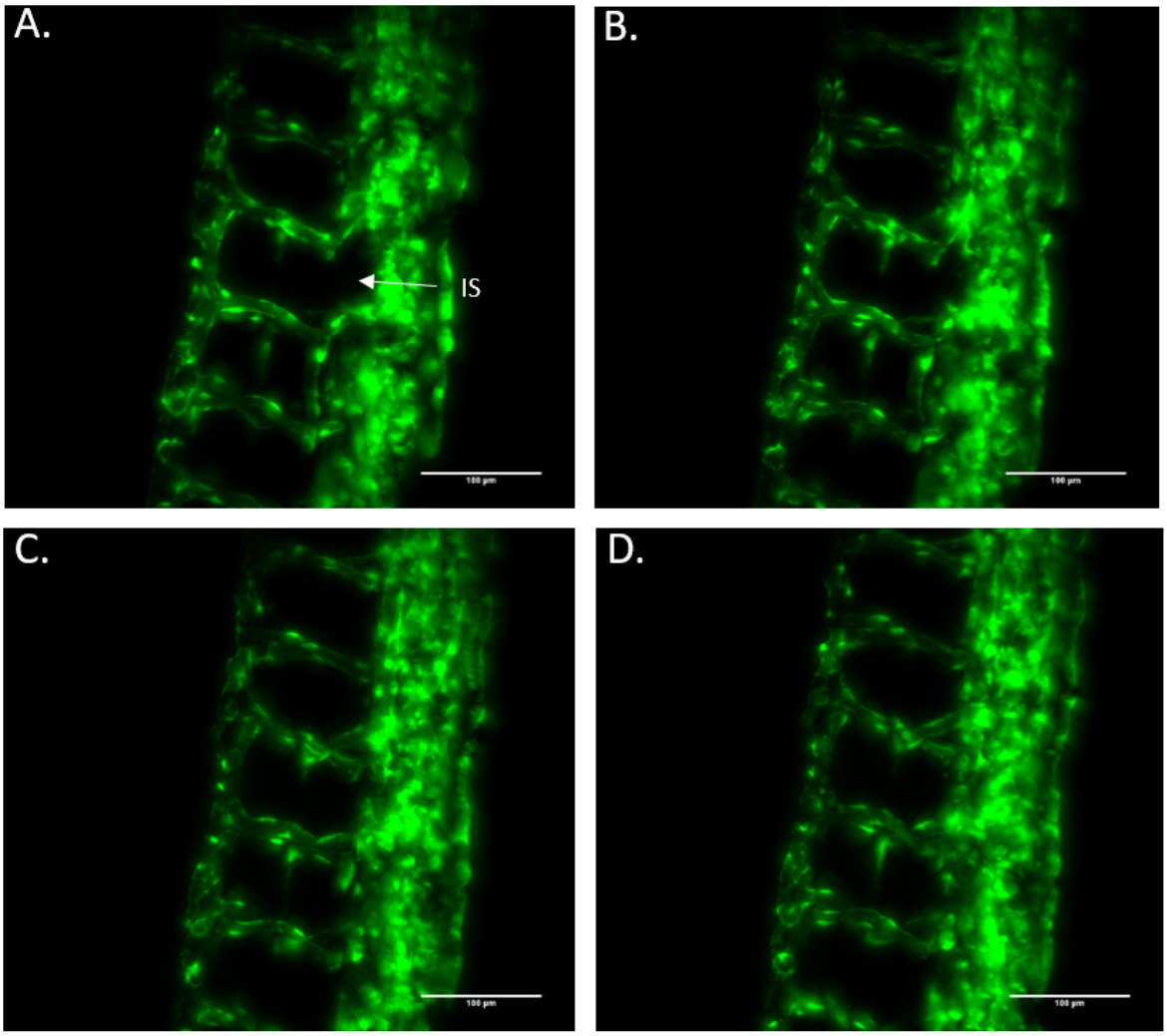

Figure 5.3.9: Green fluorescence recovers after laser injury of the caudal artery:
SPIM images of injured 48hpf *flk:GFP* zebrafish embryos after moderate micro point laser injury (3 pulses). Images show a gradual closing of the wound and recovery of fluorescence at the injury site injury 0, 5, 10, and 15 (A,B,C and D) hpi with arrows indicating the injury site (IS) (representative scale bars=100 µm).

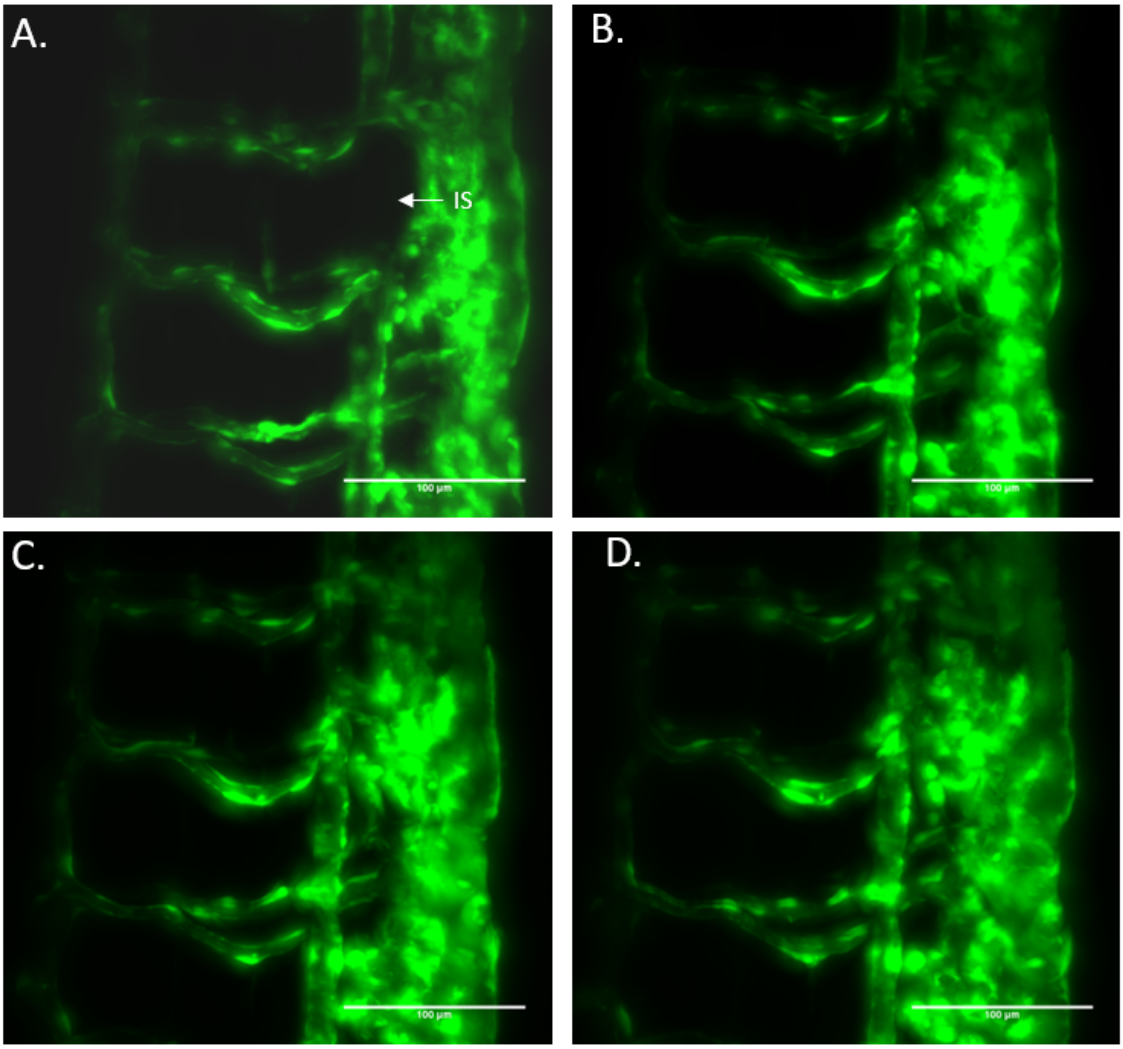

Figure 5.3.10 There is a recovery of fluorescence after laser injury of the caudal artery
SPIM images of injured 72hpf *flk:GFP* zebrafish embryos after moderate micro point laser injury (3 pulses). Images show a showing gradual closing and recovery of fluorescence at the injury site injury 0, 5, 10, and 15 (A,B,C and D) hpi with arrows indicating the injury site (IS) (representative scale bars=100 µm).

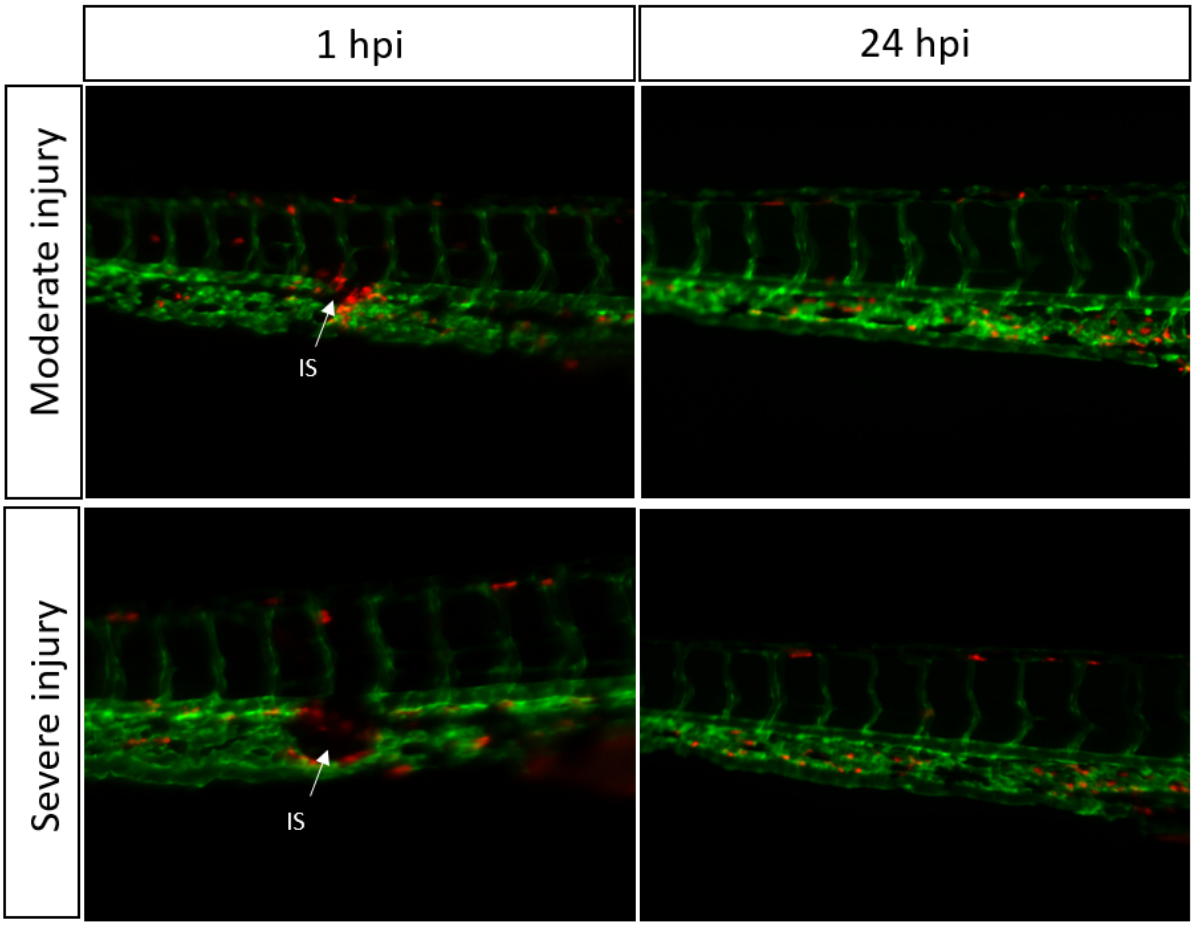

Figure 5.3.11: Neutrophils associate with laser induced injury of the caudal artery:
Epifluorescence images showing the lateral view of the 48hpf *flk:eGFP x mpx;mcherry* zebrafish embryo caudal artery after injury with moderate (3 pulses) and severe (6 pulses) micro point laser injury. Arrows indicate the injury site (IS), neutrophil association is observed 1hpi with loss of neutrophil association at 24hpi.

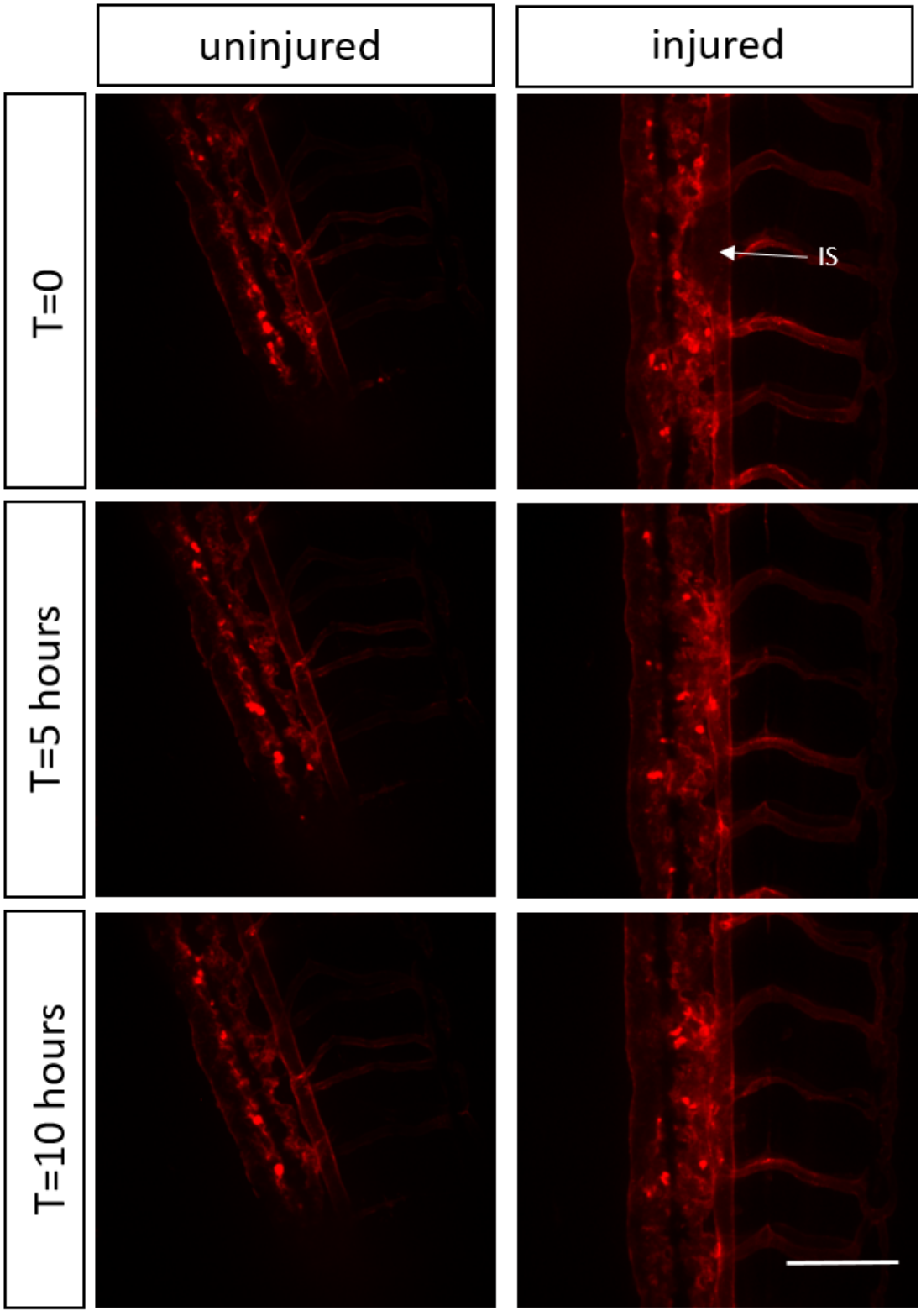

Figure 5.3.12: Moderate laser wounds of the caudal artery of *flk:mcherry* zebrafish heal within 10 hrs without loss of fluorescence

Time-lapse spinning disk microscopy of 48 hpf *flk:mcherry* embryos after moderate micro point laser injury (3 pulses) of the caudal artery. Images show recovery of the injury site (IS) with a minimal loss of fluorescence 0, 5 and 10 hpi in injured fish compared to uninjured fish (representative scale bars=100 µm).

5.3.5 *Anln-eGFP* expression is not induced by laser injury of the 48hf caudal artery:

Using the vascular injury model developed, the caudal artery of the 2-3 dpf *anln:anln-eGFPxflk:mcherry* zebrafish was injured with moderate laser injury and observed at 0 and 10 hours post injury. Representative images of these injuries are shown in *figure 5.3.13.* This identified no association of *anln:anln-eGFP* signal with the site of injury at either time point.

Next, a mechanical injury of the tail fin was used to stimulate a more severe injury response (*figure 5.3.14A-D*). Severing the tail fin of the developing 3-4 dpf zebrafish produced a significant increase of *anln* positive cells at the injury site (**=P<0.01). Dividing *Anln*$^{+ve}$ cells were observed in the tail of both injured and uninjured zebrafish. We concluded that although there was no association of *anln:anln-eGFP* with laser injury sites of the vessel there may be an association of Anln-eGFP^{+ve} cells with wound healing after more severe injuries of the tail fin.

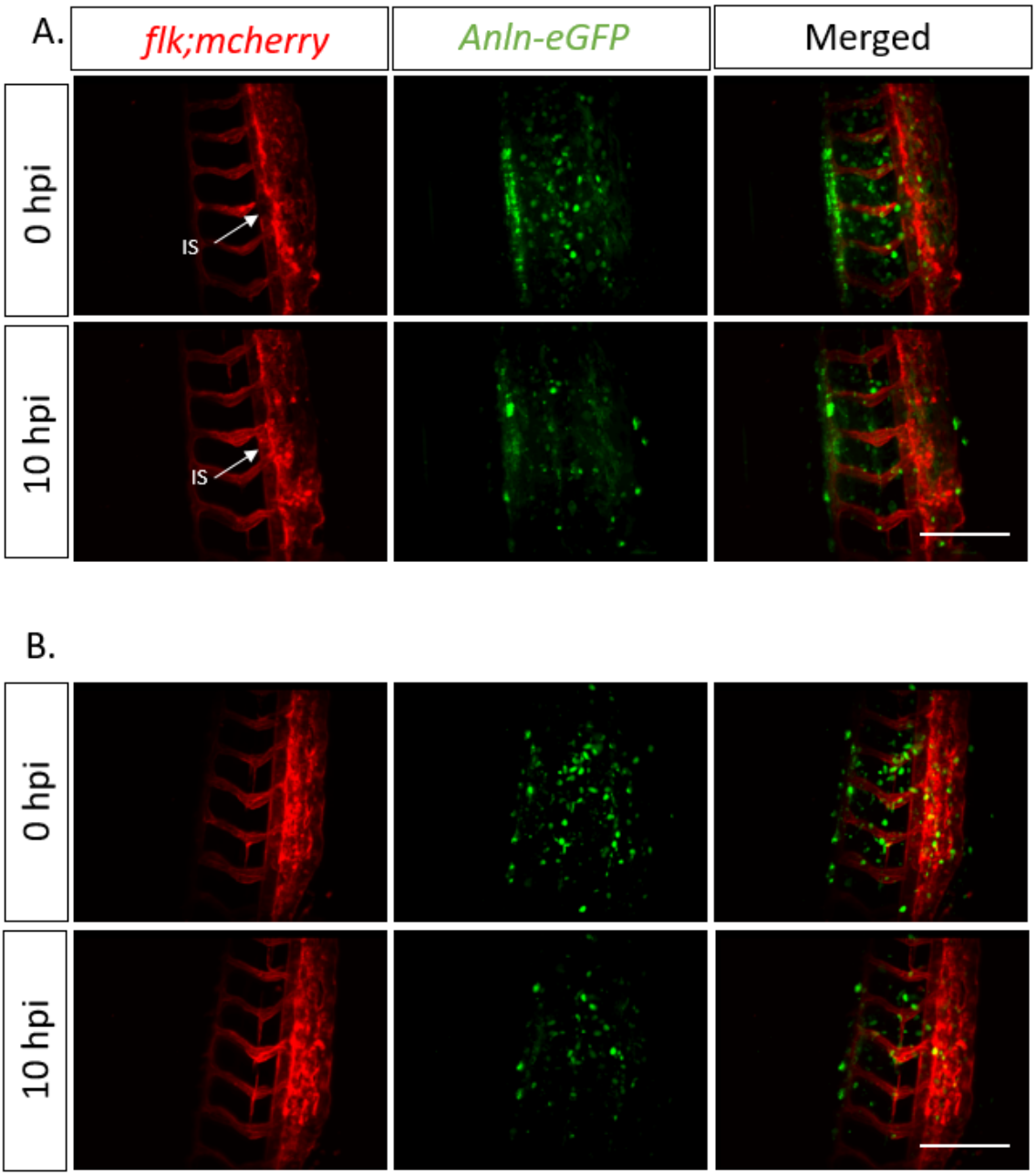

Figure 5.3.13: *Anln-eGFP* expression is not associated with Injury of the caudal artery with moderate laser injury of 48-72 hpf zebrafish embryo:
SPIM images of 48hpf *flk:mcherry x anln:anln-eGFP* after application of moderate micro point laser injury (3 pulses) 0 and 10 hpi. (A) Injured f*lk:mcherry x anln:anln-eGFP* fish with injury site indicated with arrow showing no association of (IS). (B) Uninjured *Flk:mcherry x anln:anln-eGFP* control (representative scale bars=100 µm).

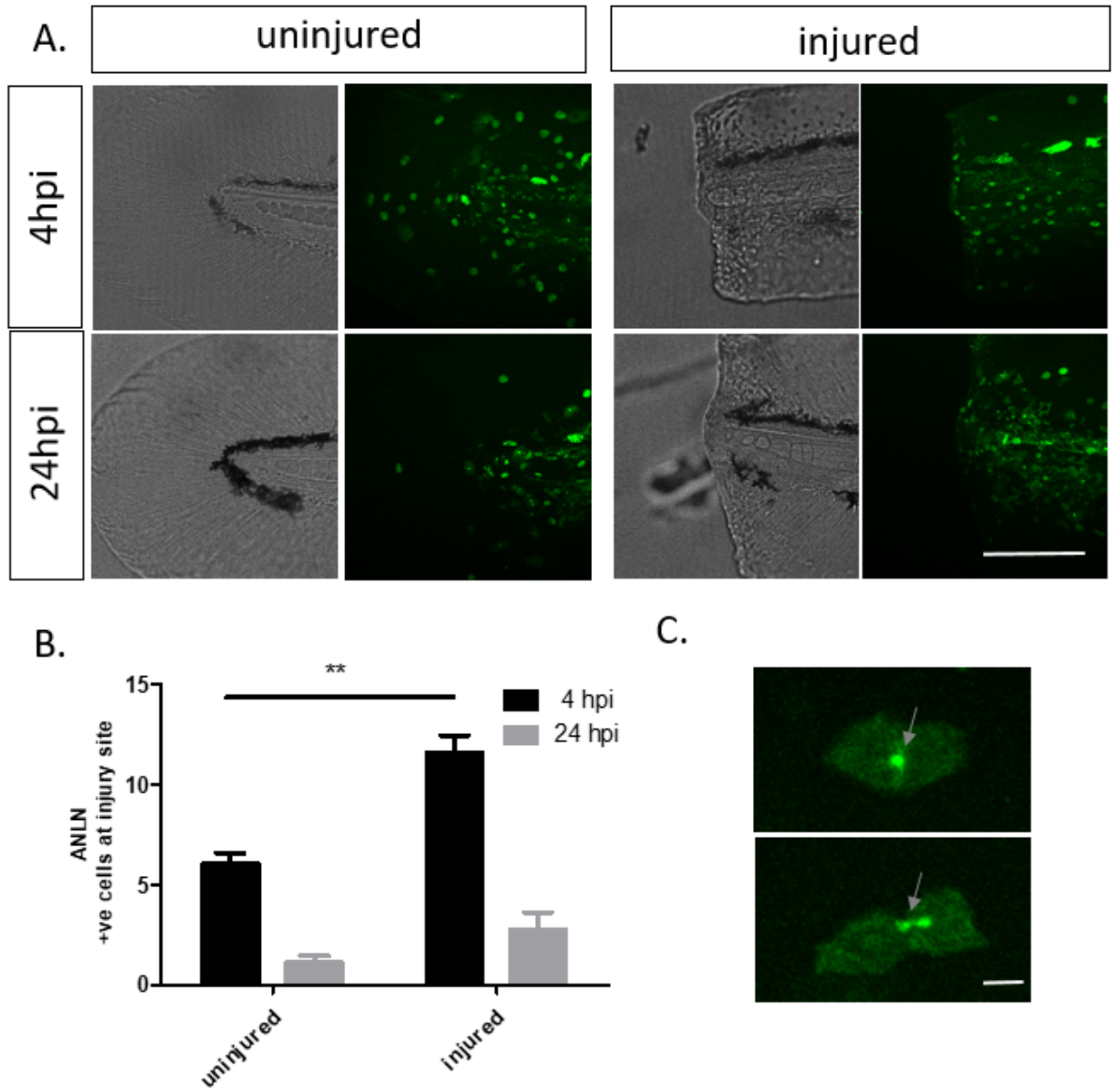

Figure 5.3.14 There is increased *anln:anln-eGFP* expression after tail fin injury:
(A) Spinning disk confocal images of 72-96hpf *anln*:*anln-eGFP* zebrafish embryo after mechanical tail fin injury (representative scale bars=100 µm). (B) Quantification of anln-EGFP positive cells on a 1500µm boundary site of 4 and 24 hours post tail injury (hpi) (n=10 error bars=SEM significance **=P<0.01 t-test). (C) *Anln-eGFP*$^{+ve}$ indicated by grey arrows present at the mid body of dividing cells present in the dermis of the tail fin injury site (scale bars =5µm).

5.3.6 Partial silencing of *anln* does not affect vascular development:

To further investigate the effect of *anln* expression on vascular development and regeneration, morpholinos were used that had already been shown to partially silence *anln* expression (Paolini et al. 2015). Partial silencing had to be used to prevent the generation of lethal phenotypes observed with global *Anln* knock out (Gbadegesin et al. 2014).

Injection with either control, splice or ATG targeting morpholinos did not cause any visible differences in overall vascular structure and no changes in ISV number at 48 or 72 hours post injection (*figure 5.3.15-5.3.17)*. The structure of the trunk vasculature including the DLAV, ISVs, caudal artery and caudal vein displayed no visible differences between groups and there were no differences in the length of the ISVs or caudal artery width between groups. Injection of the splice mRNA showed a trend for a ~30% reduction in *anln* mRNA 24hpi (n=2) as shown in *figure 5.3.15C* .These experiments showed that partially silencing *anln* with morpholino did not affect the vascular development of the zebrafish embryo.

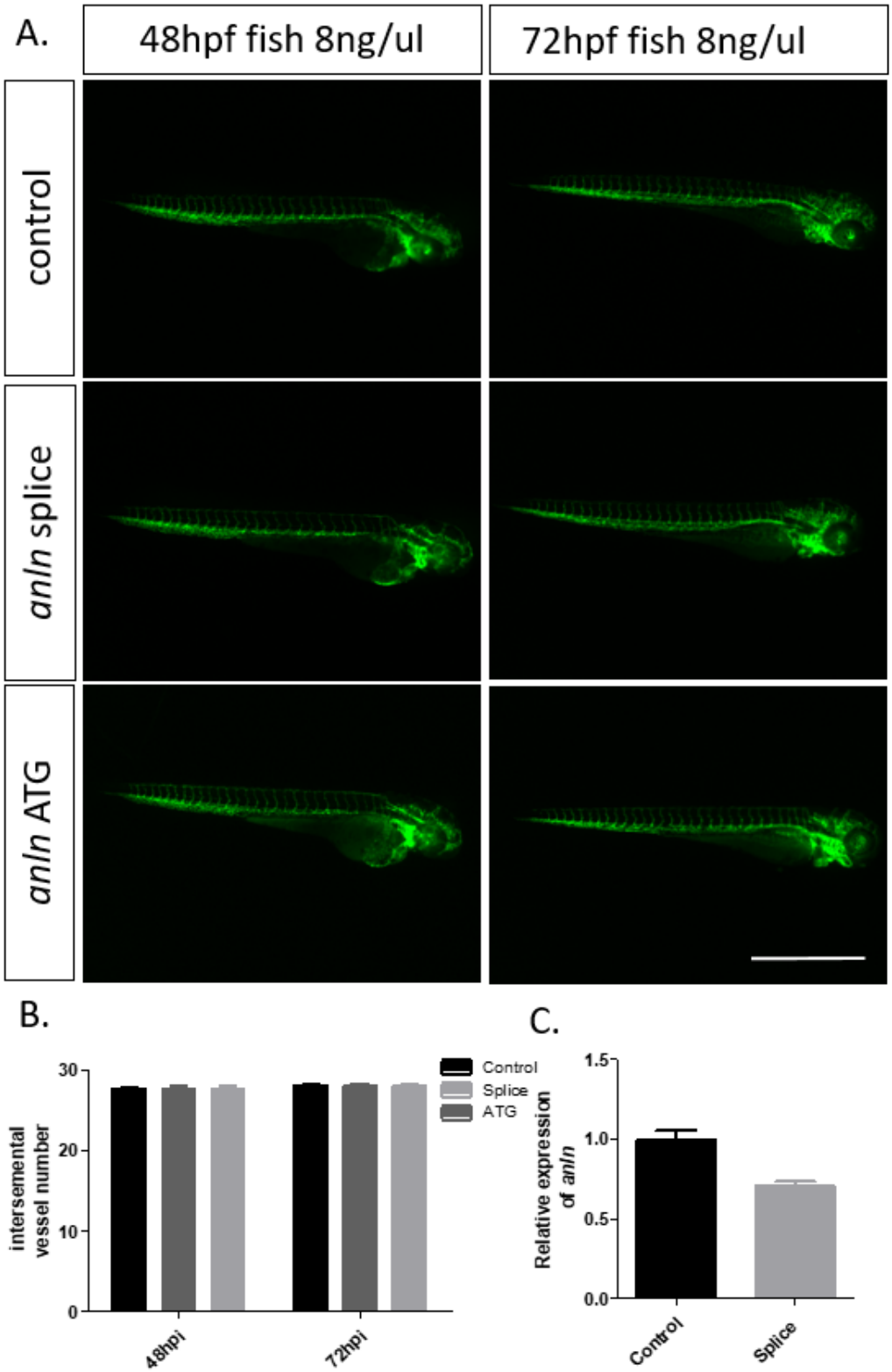

Figure 5.3.15: Partial silencing of *anln* with morpholinos does not affect ISV number:
(A) Images taken by epifluorescence show the lateral view of whole *flk:eGFP* zebrafish embryos after microinjection at the one cell stage with either control, splice or ATG blocking morpholinos (representative scale bars=1mm). (B) Quantification of ISV number along the zebrafish, morpholino treated groups showing no significant difference between groups (n=20, P>0.05 one way ANOVA with post-hoc Bonferroni) (C) qPCR analysis of whole zebrafish embryo mRNA 24 hpi detects a trend for a reduction in expression of *anln* mRNA after injection with splice blocking morphlino (n=2, ns unpaired t-test).

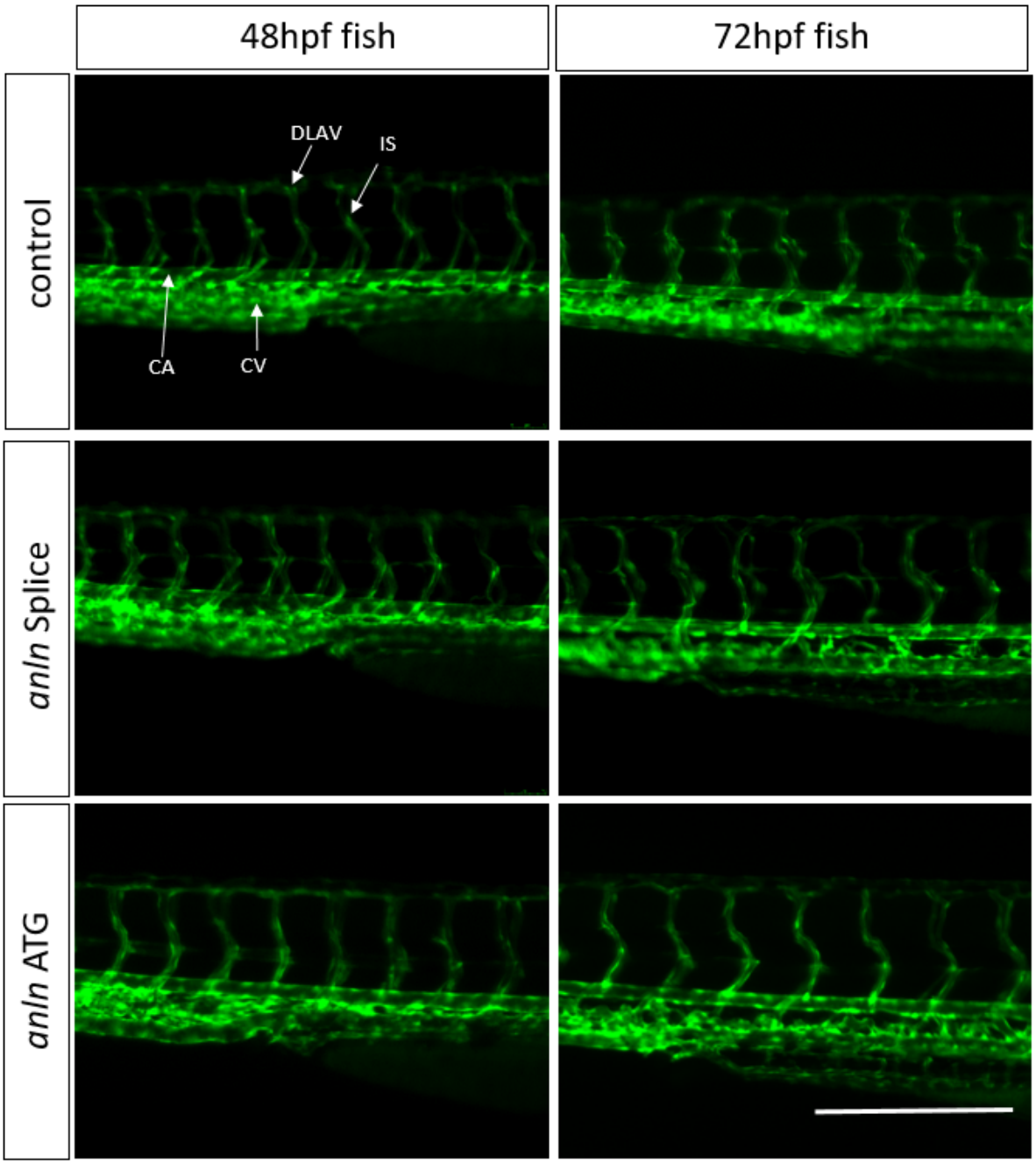

Figure 5.3.16: Partial silencing of *anln* with morpholino has no effect on the overall zebrafish vascular morphology:

Images taken by epifluorescence show the lateral view of *flk:eGFP* zebrafish ISVs after microinjection 24 and 48 hours post injection with 8pg of control, splice or ATG blocking morpholino. Arrows indicate the intersegmental vessels (ISV), dorsal longitudinal anastomotic vessel (DLAV), caudal vein (CV), and caudal artery (CA). No differences in morphology between control and morpholino treated groups were observed (scale bar= 200 µm).

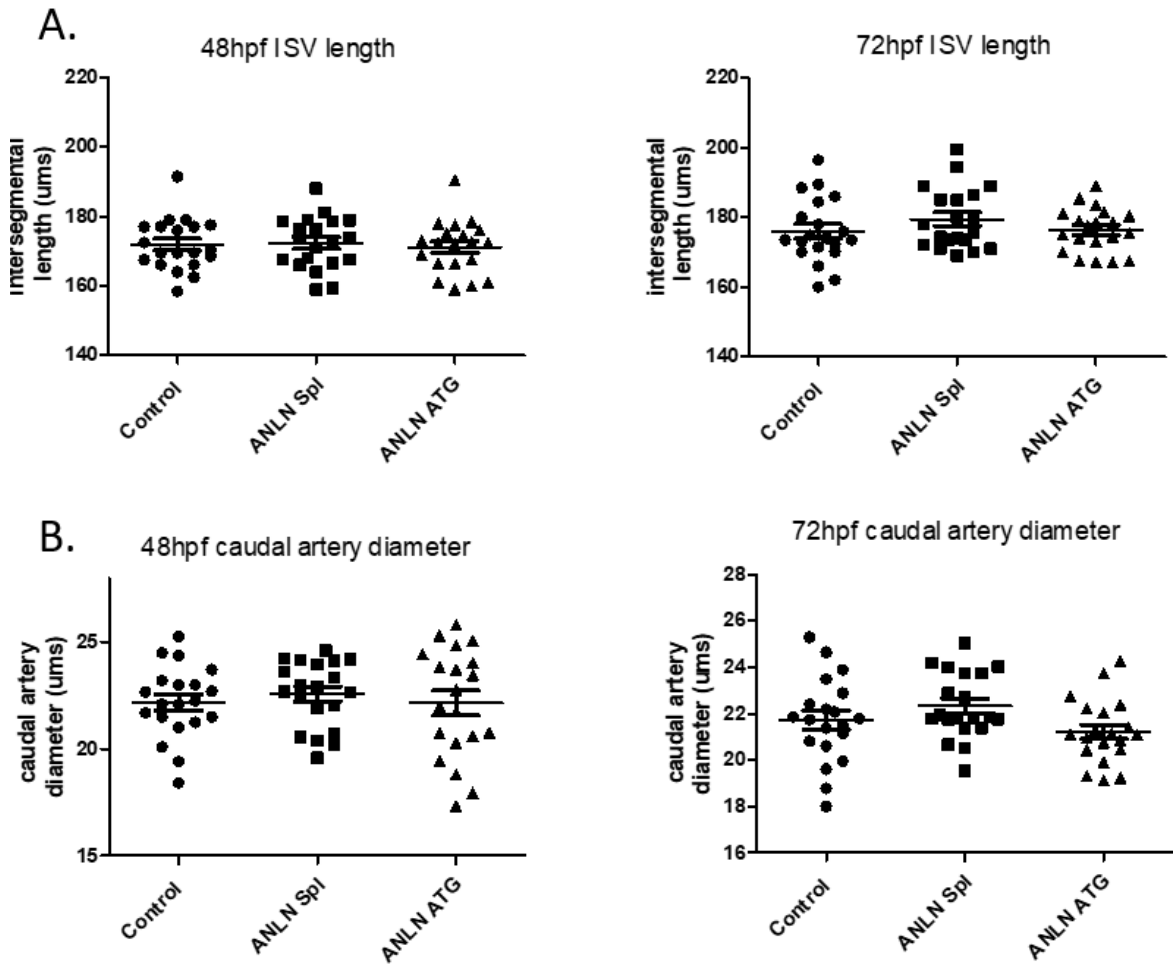

Figure 5.3.17: Morpholino-induced knockdown of Anln does not induce any obvious vascular abnormalities:
(A) The lengths of ISVs and (B) width of caudal artery of 48-72 hpf *flk:eGFP* zebrafish after morpholino injections between 48 and 72 hpf were not different between treatment groups. (n=20 error bars=SEM, ns= no significance by one way ANOVA with post hoc Bonferroni).

5.3.7 Generation of sgRNA guides for tissue specific *anln* CRISPR/CAS9 deletion:

There are difficulties associated with morpholino mediated *Anln* knockdown, these include severe overall embryonic phenotypes induced by complete knock out. I aimed to develop a tissue specific Anln knock-out fish to once more address the possibility that Anln might regulate angiogenesis/vascular development in the zebrafish. Unfortunately I failed to produce a CRISPR/Cas9 mediated knockout due to technical reasons that are laid out in the following.

The custom web tool CHOPCHOP was used to identify suitable sites for CRISPR CAS9 interference. This identified 201 potential sites with the NGG PAM motif in the zebrafish *anln* coding sequence, that would be suitable for sgRNA mediated CRISPR/CAS9 gene editing by injection into the one cell stage embryo as shown in *figure 5.3.18A-B*. The *in vitro* transcription of sgRNA guides was not producing detectable capped mRNA, therefore, the process had to be optimised to produce suitable capped sgRNA.

To confirm that sgRNA guides were being annealed successfully, a positive control annealed and non-annealed sgRNA guide template was received from Panna Tandon (Minchin group CVS, UoE). This positive control sgRNA template was annealed to the standard oligo alongside 3 sgRNA templates targeting the *anln* genomic sequence; the products of this reaction and the annealed positive control were ran on an agarose gel shown in *figure 5.3.19A*. This confirmed successful annealing of the sgRNA templates to the standard oligo. The annealed templates were used in an overnight T7 or SP6 reaction to produce capped sgRNA for CRISPR/CAS9 injection and the products were ran on an agarose gel as shown in *figure 5.3.19B*. No capped sgRNA was produced from the *anln* sgRNA templates via the T7 reaction whereas capped sgRNA was produced from both the preannealed positive control and the positive control template annealed in the same annealing reaction. This demonstrated that the failed capped sgRNA production was not related to the annealing reaction.

To investigate whether the *in vitro* transcription reaction was affected by the quality of the sgRNA oligonucleotide templates or the type of T7 reaction, two sgRNA were

produced using standard desalting and HPLC purification methods. They were annealed successfully and the products ran on an agarose gel as shown in figure *5.3.20A*; the annealed product was then used in an overnight T7 reaction which again produced no capped sgRNA from either standard desalted or HPLC purified annealed template as shown in *figure 5.3.20B*. This showed that the failure to produce capped sgRNA was not due to the method used to purify the sgRNA oligonucleotides.

Finally to investigate whether the reaction was due to the wrong concentration of sgRNA oligo template or by RNase contamination, the volume of annealed gRNA guides added to the T7 reactions were titrated with 1, 3 and 6 uls of gRNA template being added to reactions, and RNase inhibitor was added to duplicate reactions to inhibit potential RNase contamination within the T7 kit. The products of these reactions were ran on an agarose gel as shown in *figure 5.3.20C*. However this again did not produce capped sgRNA in any conditions except for the positive control.

A.

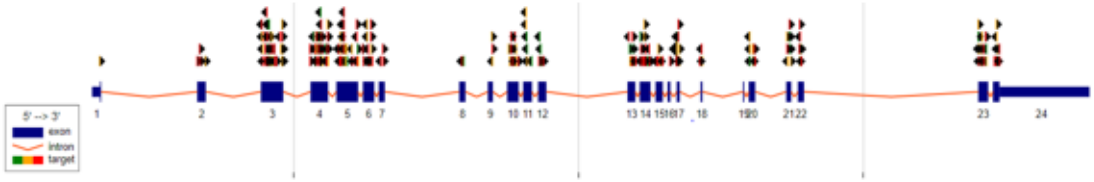

B.

Target	Sequence	Number of off targets		
		1 mismatch	2 mismatch	3 mismatch
SP6	ATTTAGGTGACACTATAGAAGGGGGATGGCTTGGAGGGTTTTAGAGCTAGAAATAGC	0	0	0
PH domain T7	TAATACGACTCACTATAGGACGCCTCTGTTAACTCTGTTTTAGAGCTAGAAATAGC	0	0	0
N terminal T7	TAATACGACTCACTATAGGGGTCGAGCACAGAACTCTGTTTTAGAGCTAGAAATAGC	0	0	0
N terminal T7	TAATACGACTCACTATAGGGGATGGATCCATTCACCGGTTTTAGAGCTAGAAATAGC	0	0	0

Figure 5.3.18; Bioinformatic analysis identifies multiple CRISPR/CAS9 target sites in the zebrafish *anln* gene.

(A) Shows the *anln* coding sequence containing the different sites targetable by CRISPR CAS9 whilst indicating the quality of each target site. Image taken from (CHOPCHOP.cbu.uib.no). (B) A selection of gRNA templates used during gRNA production optimisation showing the score of each template and target sequence location.

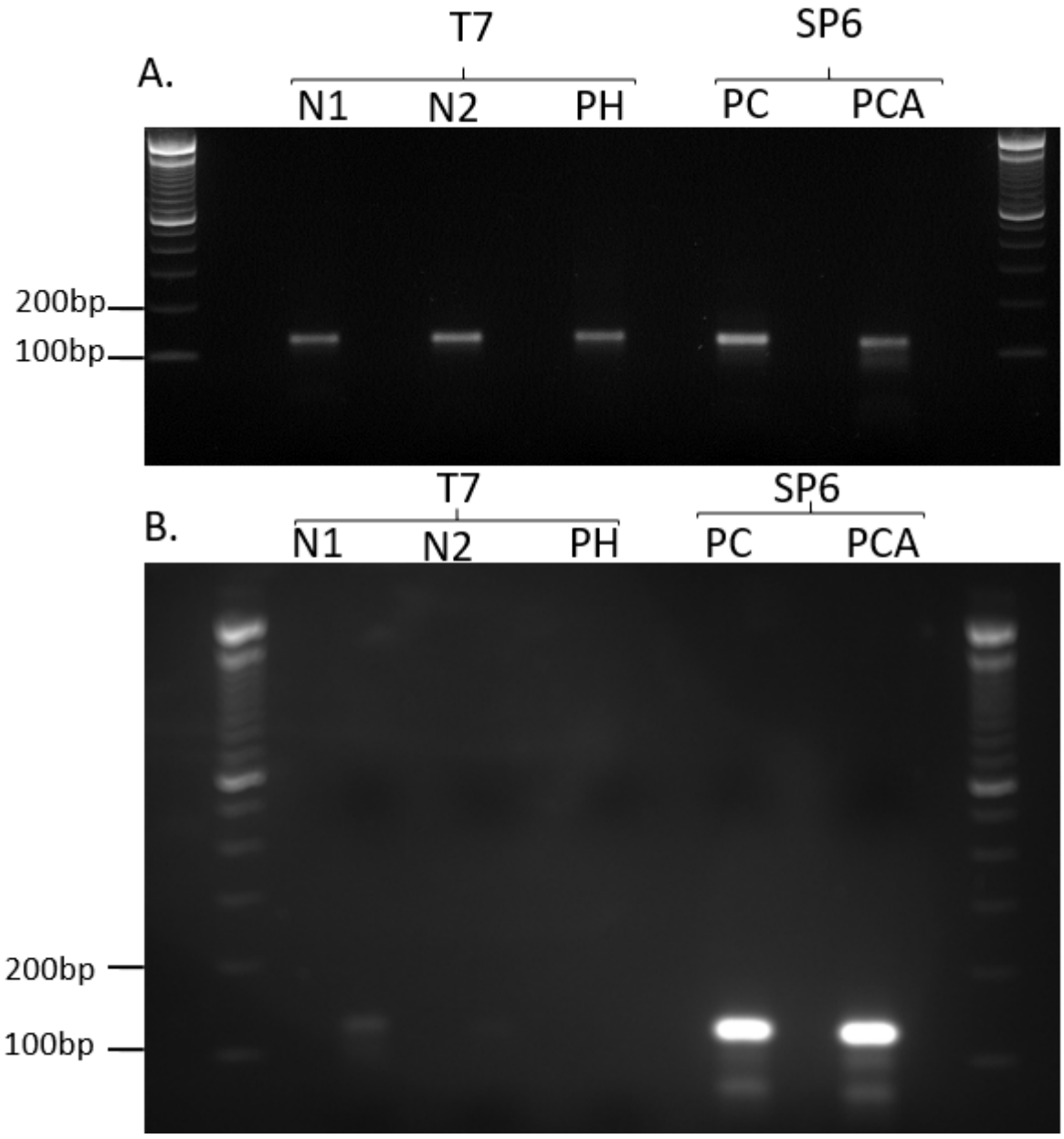

Figure 5.3.19: Low yield of Cas9 sgRNA is not due to faulty annealing reaction for T7 in vitro transcription:

(A) An agarose gel of gRNA guide oligos after being annealed to the universal TRACR oligo by Q5 polymerase. Guides target the N-terminal (N1-N2) region of ANLN and one of the PH domain (PH) for use in the T7 machine assay and a positive control gRNA guide annealed by myself and one preannealed are included. (B) Agarose gel of the products of an overnight T7 and SP6 reaction show that only the SP6 guide (PC) and pre-annealed guide (PCA) produced capped sgRNA (Ladder =100bp sizing; bp length is indicated)

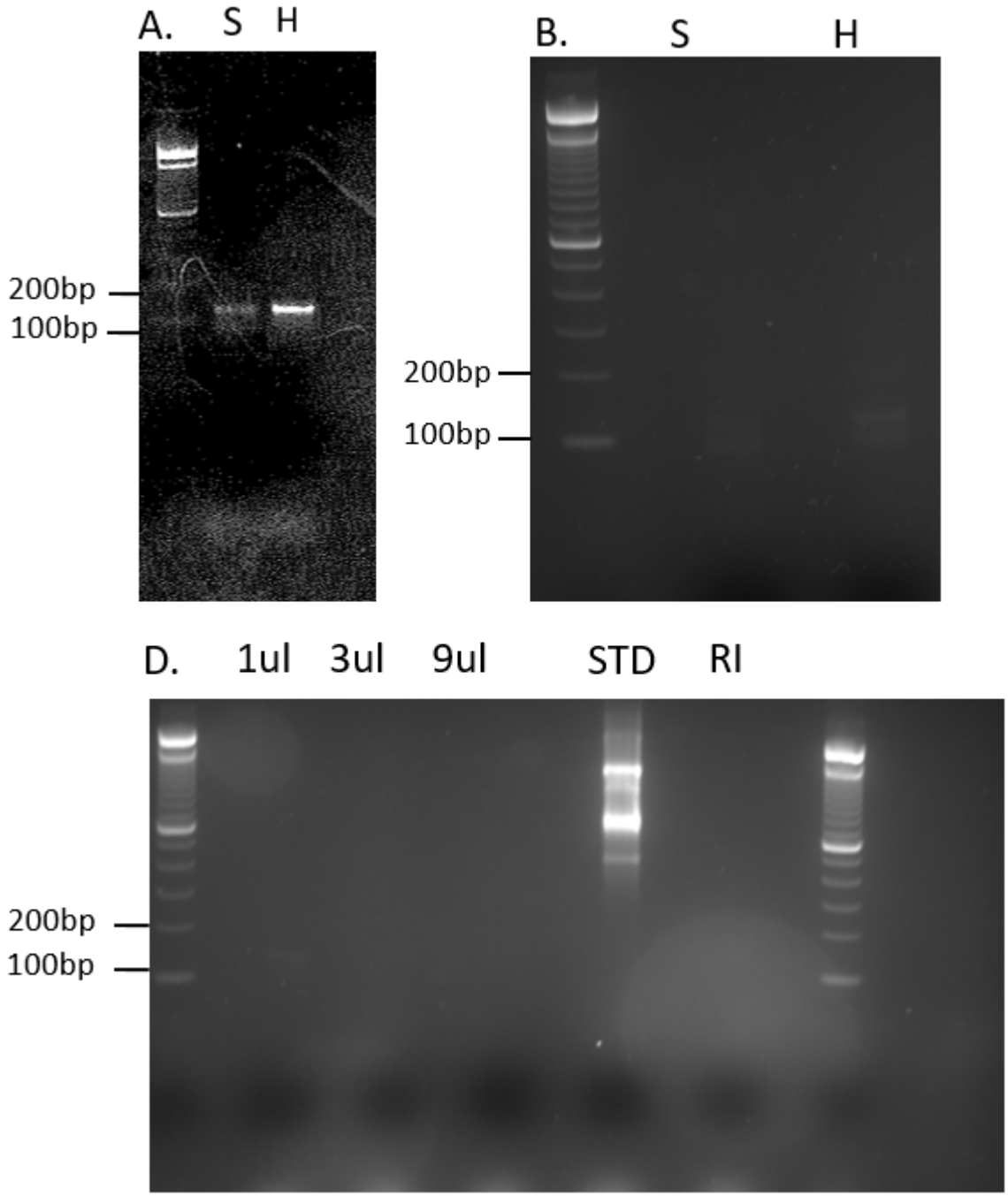

Figure 5.3.20: Low yield of Cas9 sgRNA is not due to poor oligo template quality, reaction mix or RNase contamination.

(A) Annealing of gRNA standard (S) and HPLC (H) templates show successful annealing of both gRNA templates. (B) Overnight T7 reaction of standard and HPLC purified annealed templates. (C) An agarose gel of products of T7 transcription reactions with increasing concentration of 1, 3 and 9 µls of annealed template, the positive control plasmid (STD) and a reaction containing RNAse inhibitor (RI) show no production of capped sgRNA except in the positive control (STD).

5.4 Discussion:

In this chapter, I investigated the expression of *anln* in the vascular development of the zebrafish embryo. Furthermore, I developed a novel method of vascular injury in the zebrafish embryo to address a potential association of *anln* with regenerating vasculature.

5.4.1 *Anln* is not associated with vascular development

The expression of Anln in early vascular development was investigated with the *anln:anln-eGFP* transgenic zebrafish line. Initial imaging of zebrafish embryos showed that the *anln:anln-eGFP* transgene was weakly expressed in early development and was detectable at the 32 cell, and shield stage of embryonic development by epifluorescence. There is a requirement for high Anln expression for the organisation of membrane contraction and cellularisation in non-vertebrate embryos like drosophila melanogaster (Straight et al. 2005). Anln is highly expressed in gametogenesis and is required for oogenesis so maternal inheritance of Anln to the zygote is expected (Dorn et al. 2010). By 24hpf, detection of signal in *anln:anln-eGFP* zebrafish however required light sheet or confocal level of microscopy. Therefore, a form of light sheet microscopy, "SPIM", was employed for further screening. Screening of 24 hpf to 48hpf embryos revealed *anln:anln-eGFP* signal in the head region, and particularly in the eye where, fluorescence was retained from 24-48hpf; this was previously characterised by Paolini *et al* (Paolini et al. 2015). In the trunk and tail, expression was visible in the dermis of both the 24-48hpf fish, with two strong bands of *Anln-eGFP*$^{+ve}$ cells observed ventrally and toward the midline of the trunk lost by 48 hpf. The mid line band appears to align anatomically with the developing notochord and CNS; these cell types in particular are highly proliferative at this time point (Stemple 2005). The notochord in particular has key roles in embryonic patterning by establishing the arterial venous border, assisting in early neurogenesis and allowing for rapid elongation of the trunk during embryonic development (Stemple 2005).

The ventral band of Anln positive cells observed at 24 hpf aligned with the developing trunk vasculature of the embryonic zebrafish (Isogai et al. 2001). The dorsal aorta and caudal artery/vein plexus undergo rapid maturation and development at this time point. These regions in particular were screened in the *anln:anln-eGFP* x *flk:mcherry* embryos (Isogai et al. 2001). I had hypothesised that Anln would co-localise with ECs and identify Anln distribution typical of either asymmetric cell division or, localising to the leading edge of migrating or sprouting ECs (Costa et al. 2016; Tian et al. 2015). Although there appeared to be an association of these *anln:anln-eGFP* positive cells with the developing vasculature at 24 hpf there was no evidence for Anln expression in ECs as judged by co-localisation of red and green fluorescence in these fish.

The identity of Anln-eGFP^{+ve} positive cells in close proximity to the vessels at 24 hpf is ambiguous; they are likely to be erythroid cells of the intermediate cell mass (ICM) which is surrounded by endothelium at this time-point (Willett et al. 1999). The 24 hpf ICM is located ventrally and superior to the yolk sac and is the source of primitive haematopoiesis. These cells form early erythrocytes that express *gata*1 stimulated by tissue secreted erythropoietin (Galloway et al. 2005). By crossing the *anln:anln-eGFP* line with fluorescent lines that mark primitive erythoid/myeloid markers such as the *gata1;dsRED*/*gata2;dsRED*/*scl-α;ds;RED* lines the association of *anln* with these cell lineages could be investigated (Zhen et al. 2013; Butko et al. 2015; Galloway et al. 2005). The early haematopoietic and EC precursors share a common lineage with haemangioblasts (Xiong 2008). It is therefore possible that populations of *Anln*$^{+ve}$ cells in the ICM may be EC precursor cells (Stainier et al. 1995). Flow cytometry on cell suspensions of collagenase digested pooled groups of *anln:anln-eGFP x flk:mcherry* 24hpf embryos could be used to detect Anln association with ECs and EC progenitors. If such an approach were successful, these cells could be enriched by FACS sorting for further analysis (Manoli & Driever 2012). Furthermore, we could fix and section 24-32 hpf embryos and stain them for *anln-eGFP* using an anti-eGFP antibody; this would allow for the detection of the localisation of *Anln in vivo*.

Signal intensity might be improved by injecting the *anln:anln-eGFP* BAC plasmid onto the *flk:mcherry* background to obtain a double reporter zebrafish line. However the

weak fluorescent intensity of the *anln:anln-eGFP* signal may be due to limitations of the transgene. Paolini et al demonstrated that the expression of the fluorescent *anln:anln-eGFP* transgene overlaps with an in situ hybridisation of endogenous *anln* mRNA in 28 hpf zebrafish embryos (Paolini et al. 2015). However the integration site or exact copy number of the BAC plasmid in the *anln:anln-eGFP* line genome was not investigated (Paolini et al. 2015). It is possible that several BACs integrated initially into distinct locations. If so, expression may have become diluted in subsequent generations due to copy number dilution in meiosis. The endogenous *anln* gene was not knocked out in this zebrafish line. It is conceivable that due to gene dosage effects endogenous Anln might reduce the expression of the *anln:anln-eGFP* transgene. Such factors would customarily be investigated in mice but with zebrafish it is less common to perform these validation steps (Chandler et al. 2007). Alternatively, weak expression of Anln-eGFP could be caused by the weakness of the anln promoter itself. Recently a mouse model expressing ANLN-eGFP under the flt1 promoter was described (Herz et al. 2018), where ANLN-eGFP expression was identified only in proliferating ECs of the mid gestation embryo (Herz et al. 2018). ANLN-eGFP^{+ve} cells are rare in adult tissues and only visible in mitotic cells; Anln-eGFP was found to be completely degraded through ubiquitination by APC^{cdh1} after the cell cycle (Herz et al. 2018; Zhao & Fang 2005). Anln-eGFP when expressed with the weaker *anln* promoter could accumulate slower than when expressed under the stronger flt1 promoter in ECs. Subsequent degradation by the APC^{cdh1} complex could further reduce the limit of detection of the *anln:anln-eGFP* transgene (Zhao & Fang 2005).

5.4.2 *Anln* is not associated with a laser induced vascular injury

To facilitate the investigation of Anln expression in injury of the zebrafish vasculature, a method of vascular injury had to be developed. Several methods are described in the literature for causing an insult to the vessels using an array of techniques. Physical injury has been used as a tool in both the adult and embryonic zebrafish to investigate angiogenesis, wound healing and immune cell migration and recruitment as laid out

in chapter 1 (Chassot et al. 2016). Two methods were of particular interest to injure an embryonic vessel. First, to tear of the caudal vein with a minutia pin to create an immediate vascular injury (Clay & Coughlin 2015), and second to use of a high energy laser system to induce a lesion or ablation of an area of a large vessel within the developing embryo (Matrone et al. 2014). Laser injury was chosen here, as it was considered to generate more reliable and reproducible injuries. Moreover, laser induced injuries were previously used to investigate vessel collateralisation, blood clot resolution and vessel repair in the zebrafish embryo (Matrone et al. 2013; Gray et al. 2007). Our data demonstrated that visible, yet not terminal injuries can be introduced in the zebrafish embryo using the 450nm wavelength micropoint laser system. The lack of lethality in laser injuries is likely due to the embryonic fish meeting their oxygen requirements through passive diffusion at these time points. Interestingly, the injuries induced in the two transgenic lines were not identical. The injury site appeared larger in the *flk:eGFP* line, likely due to a loss of fluorescence at the site of laser injury compared to injuries induced in the *flk:mcherry* zebrafish. It is possible that photo-bleaching contributes to the appearance of the injury; this is a known effect of laser injury and the 450 nm laser lies within the excitation spectra of eGFP (Saha et al. 2013). The excitation spectra of *flk:mcherry* does, however, not overlap with the laser wavelength. In line with this, I observed less loss of fluorescence at laser the injury sites with fish expressing the *flk:mcherry* than the *flk:eGFP* transgene. The loss of fluorescence may not necessarily be due only to the overlap of the laser and excitation spectra. Heat or reactive oxygen species generated by the laser can also cause denaturation and quenching of fluorescent proteins.

When the laser injury model was performed in *anln:anln-eGFP* x *flk:mcherry* zebrafish, no fluorescence was observed at the site of injury 1 or 10 hours post injury. There are multiple explanations why we may not have observed expression *of anln:anln-eGFP* at the wound site. Whether the vascular laser injury causes a severe enough injury to cause apoptosis and cell death to induce meaningful cell migration and proliferation is an issue that should be explored. Although it was shown that neutrophils associate with the site of the injury using the *mpx:mcherry* line,

macrophages were not analysed. An experiment with the *mpeg:eGFP* line would allow visualisation of macrophages in vascular injury. The migration and presence of these immune cells could be better explored via time-lapse microscopy or by simply adding more time-points and repeats to existing experiments. However such experiments would not necessarily show specifically why immune cell migration has occurred, as neutrophil migration could be initiated by alternative events such as thrombus formation or response to the injury of nearby tissues (Pfeiler et al. 2017). Therefore, to investigate the damage to the vessels itself, more specific techniques would be required. Electron microscopy can be used to further investigate the damage to the vessel ultrastructure caused by laser injury. This technique has been used widely to identify different cell types during myelopoesis and blood vessel formation (Armer et al. 2009; Lieschke et al. 2008). This would require fixation and resin mounting of zebrafish embryos, sectioning through the fish to the injury area and scanning electron microscopy used to investigate the morphology of the injured area. Investigation of the cellular response to damage can be investigated by either EDU of TUNEL staining and associated microscopy. EDU incorporation by treating laser injured embryos with EDU would identify if there are proliferating ECs as a regenerative response to the laser injury. Furthermore TUNEL staining would be able to identify the apoptotic cells in the laser injury site to measure the intensity of injury by quantification of cell death.

Contrasting with the results obtained in the laser injury model, tail fin injuries of *anln; anln-eGFP* embryonic zebrafish induced by scalpel identified an increase in *Anln* positive cells in the dermis at 4hpi. This suggested that the *anln:anln-egfp* transgene is expressed during the regenerative process of a mechanically induced injury model. Ideally, this experiment would be repeated with additional time points to identify the exact number of cycling mitotic cells over a 24 hour period post injury. Live imaging would require all fish to be embedded in agar over a 12 hour period which may impair the tail fin wound repair response. Given that the mechanical injury appeared to increase Anln expression, an equivalent mechanical vessel injury such as the minutia pin vessel tear injury described by Clay & Coughlin et al may generate a superior

regenerative response (Clay & Coughlin 2015). Mechanical injury of the somites of the developing embryo via a syringe has been shown to induce sprouting and anastomosis of ISVs that was mediated by macrophages (Gurevich et al. 2018). This model could also be used as analyse potential Anln expression in EC tip cell formation in regenerative angiogenesis. Furthermore introducing a known positive control line such as the *nfkb;eGFP* zebrafish might help with identifying a positive signal of injury response to validate both physical and laser injury models (Ogryzko et al. 2014).

5.4.4 *Anln* interference did not induce a strong vascular phenotype:

Knock-down of *anln* expression with morpholinos had no effect on the vascular morphology of 2-4 dpf zebrafish embryos. Modulating the expression of *anln* in the developing embryo requires a partial knockdown to prevent a severe general phenotype as was observed in other zebrafish morpholino studies (Gbadegesin et al. 2014). The partial knock down morpholino used in this study has been shown to produce cytokinetic defects by inhibiting asymmetric cell division in retinal cell division (Paolini et al. 2015). Therefore I hypothesized that the same partial *anln* knock down might affect asymmetric cell division during the development of the ISVs, thus leading to vascular defects. However at the selected time points of 48hpf-72hpf there was no impairment of ISVs vessel number or morphology. As there was no retardation of vessel development at the time points selected, it is possible that there is a recoverable phenotype at an earlier time-point. Investigating at 24-32 hpf as per Costa et al and investigating sprouting with live imaging would identify actual asymmetric cell division defects (Costa et al. 2016). It would also be useful to include the EC nuclear reporter (*flk:NLS-eGFP*) line to identify the nuclear midbody location of ECs after *anln* partial silencing.

The limitations of morpholino mediated interference may be a factor in our lack of an observed phenotype. Our morpholino injection at the dose specified by paolini et al produced a trend for a ~30% knockdown of *anln* mRNA 24 hpi; these injections should be repeated at a higher dose and over a longer time course (i.e. including 48hpi and 72hpi timepoints) to further optimise this experiment. A western blot using

the human anti-ANLN antibody did not work in zebrafish protein samples, therefore, I was unable to determine an efficiency of knockdown for the ATG morpholino. However, increasing the dose may cause an overall severe phenotype that may mask a cardiovascular phenotype. In addition to this, injected morpholinos are not consistently inherited equally during cell division and smaller doses can be diluted, this inheritance could be observed if our morpholinos were fluorescently tagged. CRISPR/Cas9 can be used to induce germ-line mutation at the single stage embryo. I aimed to use CRISPR/Cas9 mediated *anln* deletion, but struggled with the production of sgRNA guides despite extensive trouble shooting. Recently the interaction with *cd2ap* and *anln* was investigated as a mechanism of familial renal dysfunction (Gbadegesin et al. 2014). This study initially utilised morpholino interference of *anln* which produced severe phenotypes in zebrafish, whilst in a later follow-up study CRISPR/Cas9 interference was used to mutate the predicted *cd2ap/anln* interaction site(Hall et al. 2018; Gbadegesin et al. 2014). Hence, a point mutation could be incorporated to specifically mutate this site of *anln* to investigate the effect on the vascular phenotype of transgenic embryos. Any *C.Pyogenes* CAS9 mediated gene deletion would still result in a global knockout rather than a vascular specific mutation and so any phenotype observed could be caused by multiple different factors. Therefore, if CRISPR/Cas9 based interference of *anln* expression was used, one of two methods could be used. Either, the generation of a vascular specific CAS9 plasmid or, use of a vascular specific dCas9 *flk:gfp* zebrafish. The first option can be carried out as detailed by Ablain et al where plasmids were generated using gateway cloning containing a tissue specific promoter driven Cas9 and a sgRNA guide driven by the U6 promoter (Ablain et al. 2015). This generates a tissue specific CAS9 knockout that would express the sgRNA globally, producing a tissue specific mutation of your gene of interest. The second option utilises dCAS9, a mutant form of CAS9 which contains no active site for DNA cleavage (Ma et al. 2016). Therefore, when used in conjunction with a suitable gRNA guide, this would cause translational blocking of *anln* expression. Even with these methods generation of an ANLN knock out model may still be problematic. The mitotic requirement of ANLN would likely cause lethal

cytokinetic defects in knockout tissues (Piekny & Maddox 2010). A recent study in mice investigating a post mitotic role of ANLN in the septin organisation of oligodendrocytes successfully produced an ANLN conditional knockout mouse (Erwig et al. 2019). This used a Cre-Lox system where Cre recombinase was driven by the CNP promoter. CNP is only expressed in post-mitotic oligodendrocytes therefore removing a possible lethal ANLN knock out phenotype (Lappe-Siefke et al. 2003; Erwig et al. 2019).

In addition to improving modulation of *anln* expression, the quantification of vascular differences might also be improved. Using epifluorescence images to investigate and quantify vascular phenotypes can be achieved successfully (Watson et al. 2013). This technique can have more variation due to the orientation and mounting of individual fish in methyl-cellulose. Using confocal microscopy or light sheet microscopy to create 3D reconstructions of vascular networks can be employed to detect smaller differences by measuring branching or volumes of vessels. This was attempted using SPIM microscopy and IMARIS but limitations of the ability to obtain full 3D reconstructions reproducibly between samples was challenging. This could be improved by using the vertebrate automated screening technology (VAST) system for image acquisition, this uses spinning disk microscopy and an automated sample collection system to align and rapidly collect images of 2-7dpf embryos (Pulak 2016). Using the VAST system might remove variation in images as the fish are automatically aligned in the same orientation and then collected in at a 96 well plate for future acquisition of future time points (Pulak 2016).

5.5 Conclusion:

To conclude, the *anln:anln-eGFP* is a valid tool for investigating *anln* expression in zebrafish development and appears to mark different developing cell types, including potential developing haematopoietic cells. However, at the time points investigated *anln* was not visibly co-localised with the developing ECs. In response to laser-induced vascular injuries, *anln* was not expressed during repair of the injury. This may be due to insufficiencies with the method of injury, as suggested by the increased *Anln-eGFP*$^{+ve}$ cells observed with tail fish injuries in zebrafish embryos. *Anln* interference was not observed to affect vascular morphology of the 48-96hpf zebrafish. However, this experiment may be improved by using different methods for genetic interference and improved quantitative detection.

Chapter 6:

Final discussion and conclusions

6.1 Discussion and future directions:

In this thesis, I aimed to identify a role of ANLN in EC function and ischaemic angiogenesis. A post transcriptional regulatory mechanism of ANLN by ZFP36 RBPs was proposed. Unfortunately it proved impossible to obtain the relevant knockout mouse model, putting an end to this line of investigation. Instead I made use of a fluorescent zebrafish reporter model. This allowed me to characterise ANLN expression and localisation *in vivo* in developmental angiogenesis and to develop a new vascular injury model.

6.1.1 ANLN affects EC function *in vitro*:

My third chapter identified a potential role of ANLN in post ischaemic angiogenesis, but fell short of uncovering the exact mechanism by which ANLN affects EC function. In hind limb ischaemia ANLN was found to be specifically upregulated in ECs, suggesting a role for ANLN in pathological (post ischaemic) angiogenesis.

In agreement with such a function, the *in vitro* data demonstrated an involvement of ANLN in EC function. ANLN silencing experiments typically had a greater effect on the performance of EC *in vitro* than ANLN-EGFP overexpression. In particular, I observed a correlation between matrigel performance and ANLN expression which suggested an involvement of ANLN in sprouting angiogenesis. The localisation of ANLN observed in ECs reflected that previously described in the cell cycle, i.e. nuclear in interphase, and becoming associated with the cortex and cleavage furrow during cytokinesis (Piekny & Maddox 2010). I had hoped to observe endothelial ANLN localisation to the leading edge or to cell to cell contacts during tubulogenesis. Unfortunately, due to the high background and drift (likely due to shrinking of matrigel over time) I was unable to observe ANLN-EGFP localisation in tubulogenesis by live imaging. No changes in ANLN-EGFP localisation from the nucleus could be detected in fixed tubulogenesis assays. Using 2D co-cultures of ECs and fibroblasts would produce tubulogenesis without requiring the use of matrigel. These co-culture tubulogenesis assays would be easier to stain for other proteins of interest and could be imaged at multiple timepoints.

The localisation of ANLN with cytoskeletal structures may have helped with demonstrating a role of ANLN outside of cytokinesis. Other studies which have achieved this, and used these results as major justification for their entire study of ANLN. For example, ANLNs role in podocyte foot processes and its association with CD2AP-mediated PI3K signalling was identified in this way. Here overexpressed ANLN was seen to co-localise with CD2AP in foot process-like structures in HEK293 and immortalised podocytes *in vitro* (Gbadegesin et al. 2014; Hall et al. 2018). Altered ANLN distribution ameliorated concerns that increased ANLN expression in kidney injury was just a marker of podocyte entry into the cell cycle, because cell cycle entry is a marker of podocyte loss in renal disease (Gbadegesin et al. 2014). Similarly, in *C. elegans,* the ANLN homologue ani-1 was observed at the leading edges of migrating neurites, where it linked the cytoskeleton with RhoG (Tian et al. 2015). Importantly though, *C. elegans* ANLN homologues lack nuclear localisation sites, and are therefore characterised by distinct subcellular distribution to human ANLN (Maddox et al. 2005). The lack of altered ANLN localisation in ECs made it difficult to identify a specific mechanism of action in ECs outside of cytokinesis. Still, further *in vitro* experiments using EC spheroid cultures and fluorescent microscopy may more accurately identify ANLN distribution in EC sprouting.

It may be appropriate now to look at a role of ANLN in the regulation of nuclear actin as we only observed a typical nuclear distribution of ANLN *in vitro*. There is filamentous actin in the nucleus which has been shown to be able to support gene expression (Misu et al. 2017). This nuclear actin is supported by formins, including mDia2, a binding partner of ANLN (Liu et al. 2018). Therefore it may be of value to investigate the association of ANLN *in vitro* with nuclear actin being a potential mechanism of action in ECs.

It is possible that my initial *in vitro* assays did not reveal the true function of ANLN in EC function. As previously discussed (*section 3.4.1*), ANLN silencing can have adverse effects on the completion of cytokinesis, which may mask other functions (Piekny & Maddox 2010). It is therefore possible that the endothelial phenotype observed upon ANLN silencing may be the result of a cytokinetic defects rather than being specific

for ECs. We did not observe a cell cycle phase accumulation in HUVEC that ANLN had been silenced or overexpressed in, binucleation associated with the failure of cytokinesis would be expected in these conditions (Wang et al. 2015; Zhang et al. 2018; Zhao & Fang 2005). It is possible that there are other effects on the completion of cytokinesis that were not detected by these experiments, such as; asymmetric cell divisions or oscillation of the cleavage furrow (Zhao & Fang 2005; Piekny & Maddox 2010). The placement of the cleavage furrow could have been altered by ANLN depletion, this could result in different sized daughter cells (Paolini et al. 2015). We could investigate cell size after ANLN silencing or overexpression, this could be done by staining for VE-Cadherin and measuring the area of individual cells, or capturing individual cell divisions with live imaging and looking at placement of the cleavage furrow.

In addition, ANLN-EGFP overexpression required cell sorting, which may have caused ANLN-EGFP/EGFP overexpressing ECs to deteriorate. This conclusion is supported by the different base line of performance observed in some of the cell based functional experiments. To address this possibility, unsorted control groups of ECs could be included in future experiments aimed at identifying the reason for these differences in base line performance.

6.1.2 ZFP36 RBPs regulation of ANLN:

In my fourth chapter, a potential regulatory mechanism by ZFP36 RBPs was proposed due to the presence of ARE elements in the ANLN 3'UTR. These ARE elements can be targeted by ZFP36 RBPS. We showed a correlation between ANLN mRNA expression and ZFP36 RNA binding protein in an *in vivo* hind limb ischaemia model. *In vitro* we found an association between ZFP36L1 expression and ANLN mRNA expression in IL-1β-stimulated ECs. However silencing of ZFP36 RBPs in ECs did not result in the increased ANLN expression that would be typical of RBP based regulation. Binding of ZFP36 RBPs to the ANLN 3'UTR was supported by a luciferase assay. However, a RIP of ZFP36L1 did not show an enrichment of ANLN compared to the positive control VEGF. These experiments did not support the notion that ANLN is a target of ZFP36L1,

however, ANLN mRNA was enriched on a ZFP36 RIP. This has been observed with ZFP36 regulation of HIF-1α, where HIF-α mRNA is only enriched in ZFP36 silenced HUVEC after exposure of the ECs to hypoxia (Chamboredon et al. 2007). Therefore repeating the RIP and siRNA transfections with additional IL-1β stimulation to identify binding of the ANLN mRNA transcript to the ZFP36 RBPS under 'inflammatory conditions'.

It was initially intended to establish an inducible endothelial-specific knockout mouse model of either ZFP36 or ZFP36L1 in Edinburgh. This was to be used in hind limb ischemia experiments to determine the effect of ZFP36 knockout in post ischaemic angiogenesis and ANLN expression. Unfortunately, it was impossible to establish these lines for *in vivo* experiments due to difficulties with the import and time limitations. This limited how well we could determine an accurate phenotype of ZFP36 RBP knockout in angiogenesis. We considered performing functional EC based experiments such as those described in chapter 3 also with ECs in which ZFP36 family RBPs had been silenced. This would have informed on the role of ZFP36 RBPs in EC function *in vitro*. However, given the difficulties in obtaining the relevant ZFP36 RBP knockout mouse, we decided to focus on identifying a functional role of ANLN in ECs.

It is possible that the upregulation of ANLN in ECs in ischaemia is actually a marker of EC proliferation, this has been observed in reporter mouse models of ANLN (Herz et al. 2018; Hesse et al. 2012). If this is the case then the reason for ANLN expression in ischaemic ECs is to stabilise the contractile ring in EC cell division in proliferation to support angiogenesis. In this event the most likely regulatory mechanism of ANLN would be post translational by ubiquitination through the APC^{cdh1} complex rather than through a post transcriptional mechanism by RBPs (Zhao & Fang 2005). A caveat with this is that any treatment which affects the cell cycle may also affect ANLN expression. So, *in vitro* stimulation with cytokines or even the silencing/overexpression of RNA binding proteins may positively or negatively potentiate ANLN protein expression through altering APC^{cdh1} activity (Zhao & Fang 2005). Further experiments with the ANLN-EGFP lentivirus could determine if post translational regulation of ANLN is a significant factor in its degradation in ECs. In

skeletal muscle regeneration, muscle satellite cell proliferation and differentiation is in part controlled by ZFP36 RBP control of gene expression (Hausburg, et al. 2015). Therefore, it may be advantageous to identify if ANLN is upregulated in satellite cells in ischaemia and determine if ANLN's expression is regulated by ZFP36 RBPs in skeletal muscle regeneration. ANLN expression in this cell type in ischaemia would reinforce an association of ANLN with asymmetric cell division given the fact that satellite muscle cell division in regeneration is asymmetric (Gurevich et al. 2016).

6.1.3 There is no association of *Anln-eGFP* with zebrafish developmental angiogenesis:

In chapter 5 I imported and established an *anln:anln-eGFP* zebrafish from an external collaborator (Dr Lucia Poggi, University of Trento). I investigated Anln expression in the developing zebrafish vasculature. This was based on my initial *in vitro* results, where I hoped to observe a subcellular redistribution of the Anln-eGFP reporter in ECs during angiogenesis. The *anln:anln-eGFP* zebrafish had previously been used to identify asymmetric cell divisions in retinal neurogenesis. Asymmetric cell division has been suggested as a potential mechanism of angiogenesis in tip stalk cell designation (Costa et al. 2017). I therefore aimed to observe an association of Anln-eGFP with asymmetric cell division in early angiogenesis, or localisation of Anln-eGFP to the leading edge in EC migration.

Screening of initial *anln:anln-eGFP* embryos showed only very weak expression of the Anln-eGFP reporter past 24 hpf. Signal from *anln:anln-eGFP* was detected in the CNS, Retina, notochord and trunk. Outcrossing the *anln:anln-eGFP* fish with the *flk:mcherry* line allowed me to detect Anln expression and blood vessels simultaneously. Embryos were screened at 24 hpf, but, there was no association of Anln-eGFP with the developing vasculature. This was most likely due to a limit of detection or issue with the *anln:anln-eGFP* zebrafish. At ~24 hpf I noticed Anln-eGFP^{+ve} cells to be associated with the caudal artery/vein vascular plexus, these could be cells of the ICM. The ICM contains haematopoietic and endothelial progenitors, so it would be interesting to see if there is a population of Anln^{+ve} and *flk:mcherry*$^{+ve}$

cells. Furthermore, crossing the *anln:anln-eGFP* line with an erythrocyte marker such as *gata1/2* would enable visualisation of Anln^{+ve} haematopoietic progenitors. Haematopoietic primitive progenitors undergo asymmetric cell divisions to differentiate into different cell types. This would suggest why they would be Anln-eGFP^{+ve} as observed in retinal progenitor cells, before undergoing asymmetric cell division and differentiation into mature retinal ganglion cells (Paolini et al. 2015). The lack of Anln-eGFP association with the 24hpf blood vessels could be due to differences in pathological and developmental angiogenesis.

To address the function of Anln in pathological angiogenesis, I developed a laser induced injury of the caudal artery. This allowed me to study Anln expression in vascular repair. Laser wounding produced a highly reproducible lesion of the caudal artery which healed rapidly, inducing immune cell association with the injury site. I had anticipated to observe the induction of Anln-eGFP protein in ECs at the injury site, but there was no such association. This may be due to the low severity of the injury, or, the fact that these are embryos and surpass most other models in terms of their regenerative capacity. This possibility could be investigated by PI and TUNEL stain to detect cell death in injured tissues. Interestingly, I did observe the induction of Anln-eGFP^{+ve} cells at the site of tail fin injury which suggests that Anln-eGFP is induced upon tissue injury. This is supported by the expression of *Anln* at the injury border zone of adult zebrafish tail fin injury (Kang et al. 2016).

It would be useful to continue working with the laser injury by injuring the intersegmental vessels or the somites of the developing fish. This has been done before with mechanical injuries but utilising my newly developed laser injury model may be beneficial in terms of reproducibility (Gurevich et al. 2018; Clay & Coughlin 2015). When used in conjunction with fluorescent reporters of macrophages, the laser injury could be used to investigate vessel anastomoses and injury induced vessel sprouting (Liu et al. 2016; Gurevich et al. 2018).

To investigate a vascular phenotype of *anln* knockdown, I employed a partial knockdown of *anln* in *flk:eGFP* zebrafish, using ATG and splice targeting morpholinos

(Paolini et al. 2015). Using this approach, I did not identify any strong vascular phenotype in the vessels of the zebrafish trunk. This may be due to limitations of the knockdown or to a limit of detection issue with the quantification system I employed. This could be improved upon by using a better microscopy technique such as VAST microscopy, and/or by inducing a more efficient knockdown method, e.g. CRISPR/Cas9.

I began creating an *anln* CRISPR/Cas9 knockout zebrafish, but, due to technical issues and further consideration about its usefulness I stopped. A complete *Anln* knockout would not be helpful, because cytokinetic defects resulting from *anln* loss at the contractile ring are lethal. Even an inducible EC specific knockout would suffer from this issue. For example, if vascularisation of a tail fin injury of an adult inducible EC specific *anln* knockout was investigated, a potential phenotype may be observed. But, it would not be possible to determine if this was due to cytokinetic defects or a unique role of *anln* in EC migration in angiogenesis. Other studies have managed to avoid this by using conditional knockouts, for example there is an *anln* conditional knockout mouse in mature oligodendrocytes of the CNS (Erwig et al. 2019). The Cre employed (CNP) in this particular case functions only in mature oligodendrocytes, which are non-proliferating cells. There is therefore no mitotic element to the phenotype observed. However, ECs in angiogenesis, do not reach a stage at which they stop dividing for good. Unless it is possible to use a conditional knockout or viable mutation in ECs this approach may produce misleading data. Suitable viable mutations would be difficult to identify, as there are only few non-fatal pathogenic mutations of *anln* (Deng et al. 2018).

It would be interesting to use traditional ischaemic injuries such as hind limb ischaemia in a new ANLN reporter mouse line. The flt1-ANLN-EGFP mouse might be a suitable model for investigating ANLN in ischaemic angiogenesis and vascular development. In this mouse ANLN-EGFP is observed throughout development and including the vessels but is not present in the adult tissues. So if this direction was taken then this model should be established for future experiments *in vivo*. If

establishing this line is not possible then generating a *flk:anln-eGFP* zebrafish may be an improvement over the current *anln:anln-eGFP* zebrafish.

6.2 Conclusions:

To conclude, this thesis has highlighted the potential role of ANLN in ECs in angiogenesis.

Future experiments should focus on identifying a localisation of ANLN expression in ECs, particularly in an *in vitro* model of sprouting such as EC spheroid cultures. This would be required to attribute the initial phenotypes observed in *in vitro* ANLN silencing and overexpression studies to a unique role of ANLN in EC function. If no distribution can be identified then it would be beneficial to investigate a nuclear role of ANLN in ECs. Failing this then it should be considered that ANLN upregulation in angiogenesis may just mark mitotic cells that are progressing through the cell cycle.

The *anln:anln-eGFP* zebrafish did not mark asymmetric cell divisions or migrating angiogenic ECs, however, this line may be useful for studying early haematopoiesis. The vascular laser injury created in this thesis would be excellent for investigating angiogenesis in the zebrafish embryo at other time points and by targeting other vessels. However, some further optimisation of this injury would be useful to clarify the exact severity of these injuries. Further *in vivo* studies of ANLN in angiogenesis would benefit from the establishment of the flt1-ANLN-EGFP mouse or the generation of an *flt/flk:anln-eGFP* zebrafish.

Supplementary figures:

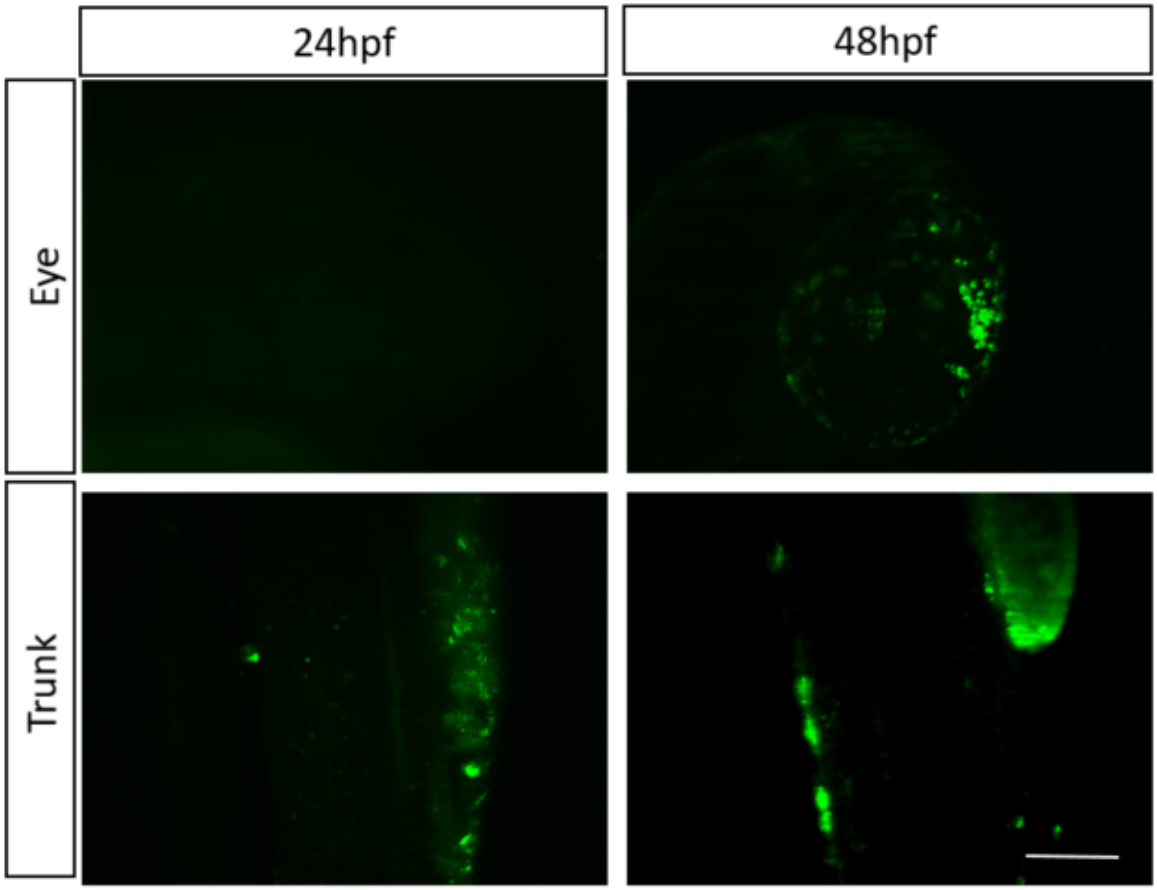

Negative control WIK zebrafish embryos at 24-48hpf show only weak auto fluorescence in the head and trunk:
SPIM imaging of 24-48 hpf *anln:anln-eGFP embryos* showing the head and trunk of 24-48 hpf embryos (scale bar= 100µms).

References:

Ablain, J. et al., 2015. A CRISPR/Cas9 Vector System for Tissue-Specific Gene Disruption in Zebrafish. *Developmental Cell*, 32(6), pp.756–764. Available at: http://www.sciencedirect.com/science/article/pii/S1534580715000751.

Adamis, A.P., Aiello, L.P. & D'amato, R.A., 1999. Angiogenesis and ophthalmic disease. *Angiogenesis*, 3(1), pp.9–14.

Allende, M.L. & Proia, R.L., 2002. Sphingosine-1-phosphate receptors and the development of the vascular system. *Biochimica et Biophysica Acta (BBA)-Molecular and Cell Biology of Lipids*, 1582(1–3), pp.222–227.

Ardi, V.C. et al., 2007. Human neutrophils uniquely release TIMP-free MMP-9 to provide a potent catalytic stimulator of angiogenesis. *Proceedings of the National Academy of Sciences*, 104(51), pp.20262–20267.

Armer, H.E.J. et al., 2009. Imaging transient blood vessel fusion events in zebrafish by correlative volume electron microscopy. *PLoS ONE*, 4(11).

Arroyo, A.G. & Iruela-Arispe, M.L., 2010. Extracellular matrix, inflammation, and the angiogenic response. *Cardiovascular Research*, 86(2), pp.226–235. Available at: https://doi.org/10.1093/cvr/cvq049.

AU - Davis, J., AU - Crampton, S.P. & AU - Hughes, C.C.W., 2007. Isolation of Human Umbilical Vein Endothelial Cells (HUVEC). *JoVE*, (3), p.e183. Available at: https://www.jove.com/video/183.

Augustin, H.G. et al., 2009. Control of vascular morphogenesis and homeostasis through the angiopoietin–Tie system. *Nature reviews Molecular cell biology*, 10(3), p.165.

Baarlink, C., Wang, H. & Grosse, R., 2013. Nuclear Actin Network Assembly by Formins Regulates the SRF Coactivator MAL. *Science*, 340(6134), p.864 LP-867. Available at: http://science.sciencemag.org/content/340/6134/864.abstract.

Barrangou, R. et al., 2007. CRISPR provides acquired resistance against viruses in prokaryotes. *Science*, 315(5819), pp.1709–1712.

Beaudet, D. et al., 2017. Active Ran regulates anillin function during cytokinesis. *Molecular Biology of the Cell*, 28(24), pp.3517–3531. Available at: https://doi.org/10.1091/mbc.e17-04-0253.

Bell, S.E. et al., 2006. The RNA binding protein Zfp36l1 is required for normal vascularisation and post-transcriptionally regulates VEGF expression. *Developmental Dynamics*, 235(11), pp.3144–3155.

Benjamin, D. et al., 2006. BRF1 protein turnover and mRNA decay activity are regulated by protein kinase B at the same phosphorylation sites. *Molecular and cellular biology*, 26(24), pp.9497–9507.

Berika, M., Elgayyar, M.E. & El-Hashash, A.H.K., 2014. Asymmetric cell division of stem cells in the lung and other systems. *Frontiers in Cell and Developmental Biology*, 2(July), pp.1–9. Available at: http://journal.frontiersin.org/article/10.3389/fcell.2014.00033/abstract.

Berika, M., Elgayyar, M.E. & El-Hashash, A.H.K., 2014. Asymmetric cell division of stem cells in the lung and other systems. *Frontiers in cell and developmental biology*, 2, p.33.

Bingham, S. et al., 2003. Neurogenic phenotype of mind bomb mutants leads to severe patterning defects in the zebrafish hindbrain. *Developmental dynamics: an official publication of the American Association of Anatomists*, 228(3), pp.451–463.

Blackshear, P.J. et al., 2003. Characteristics of the Interaction of a Synthetic Human Tristetraprolin Tandem Zinc Finger Peptide with AU-rich Element-containing RNA Substrates *. *Journal of Biological Chemistry*, 278(22), pp.19947–19955.

Blackshear, P.J., 2002. Tristetraprolin and other CCCH tandem zinc-finger proteins in the regulation of mRNA turnover. *Biochemical Society Transactions*, 30(6),

p.945 LP-952. Available at: http://www.biochemsoctrans.org/content/30/6/945.abstract.

Blackshear, P.J. et al., 2005. Zfp36l3, a Rodent X Chromosome Gene Encoding a Placenta-Specific Member of the Tristetraprolin Family of CCCH Tandem Zinc Finger Proteins. *Biology of Reproduction*, 73(2), pp.297–307. Available at: https://academic.oup.com/biolreprod/article/73/2/297/2666890/Zfp36l3-a-Rodent-X-Chromosome-Gene-Encoding-a.

Blanco, R. & Gerhardt, H., 2013. VEGF and Notch in tip and stalk cell selection. *Cold Spring Harbor perspectives in medicine*, 3(1), p.a006569.

Blasi, F. & Carmeliet, P., 2002. uPAR: a versatile signalling orchestrator. *Nature reviews Molecular cell biology*, 3(12), p.932.

Bollmann, F. et al., 2014. Endothelial dysfunction in tristetraprolin-deficient mice is not caused by enhanced tumor necrosis factor-α expression. *Journal of Biological Chemistry*, 289(22), pp.15653–15665.

Bologna-Molina, R. et al., 2013. Comparison of the value of PCNA and Ki-67 as markers of cell proliferation in ameloblastic tumors. *Medicina Oral, Patologia Oral y Cirugia Bucal*, 18(2).

Bosch-Marce, M. et al., 2007. Effects of aging and hypoxia-inducible factor-1 activity on angiogenic cell mobilization and recovery of perfusion after limb ischemia. *Circulation research*, 101(12), pp.1310–1318.

De Bruin, R.G. et al., 2016. The RNA-binding protein quaking maintains endothelial barrier function and affects VE-cadherin and β-catenin protein expression. *Scientific reports*, 6, p.21643.

Busse, M. et al., 2008. Strong induction of the Tis11B gene in myogenic differentiation. *European journal of cell biology*, 87(1), pp.31–38.

Bustin, S.A. et al., 1994. Cloning and characterization of ERF-1, a human member of the Tis11 family of early-response genes. *DNA and cell biology*, 13(5), pp.449–

459.

Butko, E. et al., 2015. Gata2b is a restricted early regulator of hemogenic endothelium in the zebrafish embryo. *Development (Cambridge, England)*, 142(6), pp.1050–1061. Available at: http://www.ncbi.nlm.nih.gov/pmc/articles/PMC4360177/.

Bye-A-Jee, H. et al., 2018. The RNA-binding proteins Zfp36l1 and Zfp36l2 act redundantly in myogenesis. *Skeletal Muscle*, 8(1), p.37. Available at: https://doi.org/10.1186/s13395-018-0183-9.

Campbell, E.L., 2015. Hypoxia-recruited angiogenic neutrophils. *Blood*, 126(17), p.1972 LP-1973. Available at: http://www.bloodjournal.org/content/126/17/1972.abstract.

Cao, H. et al., 2006. Identification of the anti-inflammatory protein tristetraprolin as a hyperphosphorylated protein by mass spectrometry and site-directed mutagenesis. *Biochemical Journal*, 394(1), p.285 LP-297. Available at: http://www.biochemj.org/content/394/1/285.abstract.

Caporali, A. et al., 2011. Deregulation of microRNA-503 contributes to diabetes mellitus-induced impairment of endothelial function and reparative angiogenesis after Limb Ischemia. *Circulation*, 123, pp.282–291.

Caporali, A. et al., 2018. Future directions for therapeutic strategies in post-ischaemic vascularization: a position paper from European Society of Cardiology Working Group on Atherosclerosis and Vascular Biology. *Cardiovascular Research*, 114(11), pp.1411–1421. Available at: https://dx.doi.org/10.1093/cvr/cvy184.

Caporali, A. et al., 2015. p75NTR-dependent activation of NF-[kappa] B regulates microRNA-503 transcription and pericyte-endothelial crosstalk in diabetes after limb ischaemia. *Nature communications*, 6.

Caporali, A. et al., 2012. Soluble ST2 is regulated by p75 neurotrophin receptor and

predicts mortality in diabetic patients with critical limb ischemia. *Arteriosclerosis, thrombosis, and vascular biology*, 32(12), pp.e149–e160.

Caporali, A. & Emanueli, C., 2011. MicroRNA-503 and the Extended MicroRNA-16 Family in Angiogenesis. *Trends in Cardiovascular Medicine*, 21(6), pp.162–166. Available at: http://dx.doi.org/10.1016/j.tcm.2012.05.003.

Carmeliet, P. & Jain, R.K., 2011. Molecular mechanisms and clinical applications of angiogenesis. *Nature*, 473(7347), p.298.

Cavazza, T. & Vernos, I., 2016. The RanGTP Pathway: From Nucleo-Cytoplasmic Transport to Spindle Assembly and Beyond . *Frontiers in Cell and Developmental Biology* , 3, p.82. Available at: https://www.frontiersin.org/article/10.3389/fcell.2015.00082.

Chamboredon, S. et al., 2007. Hypoxia-inducible factor-1 α mRNA : a new target for destabilization by tristetraprolin in endothelial cells. *Molecular biology of the cell*, 22, pp.3366–3378.

Chandler, K.J. et al., 2007. Relevance of BAC transgene copy number in mice: transgene copy number variation across multiple transgenic lines and correlations with transgene integrity and expression. *Mammalian Genome*, 18(10), pp.693–708.

Chappell, J.C. et al., 2009. Local guidance of emerging vessel sprouts requires soluble Flt-1. *Developmental cell*, 17(3), pp.377–386.

Chartier, N.T. et al., 2011. Article PAR-4 / LKB1 Mobilizes Nonmuscle Myosin through Anillin to Regulate C . elegans Embryonic Polarization and Cytokinesis. *Current biology : CB*, 21(4), pp.259–269.

Chassot, B., Pury, D. & Jaźwińska, A., 2016. Zebrafish fin regeneration after cryoinjury-induced tissue damage. *Biology Open*, 5(6), pp.819–828. Available at: http://bio.biologists.org/lookup/doi/10.1242/bio.016865.

Chen, A. et al., 2015. Importin β2 mediates the spatiotemporal regulation of anillin

through a non-canonical NLS. *Journal of Biological Chemistry*, p.jbc-M115.

Chrestensen, C.A. et al., 2004. MAPKAP Kinase 2 Phosphorylates Tristetraprolin on in Vivo Sites Including Ser 178 , a Site Required for 14-3-3 Binding *. , 279(11), pp.10176–10184.

Chu, H. & Wang, Y., 2012. Therapeutic angiogenesis: controlled delivery of angiogenic factors. *Therapeutic delivery*, 3(6), pp.693–714.

Ciais, D., Cherradi, N. & Feige, J.-J., 2013. Multiple functions of tristetraprolin/TIS11 RNA-binding proteins in the regulation of mRNA biogenesis and degradation. *Cellular and Molecular Life Sciences*, 70(12), pp.2031–2044. Available at: https://doi.org/10.1007/s00018-012-1150-y.

Clay, H. & Coughlin, S.R., 2015. Mechanical Vessel Injury in Zebrafish Embryos. *Journal of Visualized Experiments : JoVE*, (96), p.52460. Available at: http://www.ncbi.nlm.nih.gov/pmc/articles/PMC4354638/.

Coats, P. & Wadsworth, R., 2005. Marriage of resistance and conduit arteries breeds critical limb ischemia. *American Journal of Physiology-Heart and Circulatory Physiology*, 288(3), pp.H1044–H1050.

Cohn, J.N., 1996. The management of chronic heart failure. *New England Journal of Medicine*, 335(7), pp.490–498.

Collins, F. et al., 2009. Expression of oestrogen receptors, ERα, ERβ, and ERβ variants, in endometrial cancers and evidence that prostaglandin F may play a role in regulating expression of ERα. *BMC Cancer*, 9(1), p.330. Available at: https://doi.org/10.1186/1471-2407-9-330.

Costa, G. et al., 2016. Asymmetric division coordinates collective cell migration in angiogenesis. *Nature Cell Biology*, 18(12), pp.1292–1301.

Costa, G., Lovegrove, H.E. & Herbert, S.P., 2017. Endothelial cells divide unequally to sprout fairly. *Cell Cycle*, 16(7), pp.595–596. Available at: http://dx.doi.org/10.1080/15384101.2017.1294942.

Cougot, N., Babajko, S. & Séraphin, B., 2004. Cytoplasmic foci are sites of mRNA decay in human cells. *The Journal of cell biology*, 165(1), pp.31–40. Available at: https://www.ncbi.nlm.nih.gov/pubmed/15067023.

D'Avino, P.P., 2009. How to scaffold the contractile ring for a safe cytokinesis - lessons from Anillin-related proteins. *Journal of cell science*, 122(Pt 8), pp.1071–9. Available at: http://www.ncbi.nlm.nih.gov/pubmed/19339546 [Accessed December 29, 2014].

Dean, J.L. et al., 2001. The 3' untranslated region of tumor necrosis factor alpha mRNA is a target of the mRNA-stabilizing factor HuR. *Molecular and cellular biology*, 21(3), pp.721–730. Available at: https://www.ncbi.nlm.nih.gov/pubmed/11154260.

Deng, L. et al., 2018. Identification of ANLN as a new likely pathogenic gene of branchio-otic syndrome in a three-generation Chinese family. *Molecular genetics & genomic medicine*, 7(2), pp.e00525–e00525. Available at: https://www.ncbi.nlm.nih.gov/pubmed/30548429.

Desroches-castan, A. et al., 2011. A novel function of Tis11b / BRF1 as a regulator of Dll4 mRNA 3 ' -end processing. , 22, pp.3625–3633.

Dorn, J.F. et al., 2010. Actomyosin tube formation in polar body cytokinesis requires anillin in C. elegans. *Current Biology*, 20(22), pp.2046–2051.

Dragneva, G., Korpisalo, P. & Ylä-herttuala, S., 2013. Promoting blood vessel growth in ischemic diseases : challenges in translating preclinical potential into clinical success. *Disease models & mechanisms*, 322, pp.312–322.

Drake, C.J. & Fleming, P.A., 2000. Vasculogenesis in the day 6.5 to 9.5 mouse embryo. *Blood*, 95(5), pp.1671–1679.

Du, Y. et al., 2016. Three-dimensional characterization of mechanical interactions between endothelial cells and extracellular matrix during angiogenic sprouting. *Scientific reports*, 6, p.21362.

Dubreuil, V. et al., 2007. Midbody and primary cilium of neural progenitors release extracellular membrane particles enriched in the stem cell marker prominin-1. *Journal of Cell Biology*, 176(4), pp.483–495.

Duncan, A.W. et al., 2005. Integration of Notch and Wnt signaling in hematopoietic stem cell maintenance. *Nature immunology*, 6(3), p.314.

Eble, J.A. & Niland, S., 2009. The extracellular matrix of blood vessels. *Current pharmaceutical design*, 15(12), pp.1385–1400.

Ehling, M. et al., 2013. Notch controls retinal blood vessel maturation and quiescence. *Development*, p.dev-093351.

Eilken, H.M. & Adams, R.H., 2010. Dynamics of endothelial cell behavior in sprouting angiogenesis. *Current opinion in cell biology*, 22(5), pp.617–625.

Ellertsdóttir, E. et al., 2010. Vascular morphogenesis in the zebrafish embryo. *Developmental Biology*, 341(1), pp.56–65. Available at: http://www.sciencedirect.com/science/article/pii/S0012160609013116.

Ellett, F. et al., 2011. mpeg1 promoter transgenes direct macrophage-lineage expression in zebrafish. *Blood*, 117(4), pp.e49–e56.

Erwig, M.S. et al., 2019. Anillin facilitates septin assembly to prevent pathological outfoldings of central nervous system myelin. *eLife*, 8, p.e43888.

Ettinger, A.W. et al., 2011. Proliferating versus differentiating stem and cancer cells exhibit distinct midbody-release behaviour. *Nature Communications*, 2(1), pp.503–512. Available at: http://dx.doi.org/10.1038/ncomms1511.

Falk, E., 1992. Why do plaques rupture? *Circulation*, 86(6 Suppl), pp.III30-42.

Fallmann, J. et al., 2016. AREsite2: an enhanced database for the comprehensive investigation of AU/GU/U-rich elements. *Nucleic Acids Research*, 44(D1), pp.D90–D95. Available at: http://dx.doi.org/10.1093/nar/gkv1238.

Fantin, A. et al., 2010. Tissue macrophages act as cellular chaperones for vascular

anastomosis downstream of VEGF-mediated endothelial tip cell induction. *Blood*, p.blood-2009.

Ferrara, N. & Alitalo, K., 1999. Clinical applications of angiogenic growth factors and their inhibitors. *Nature medicine*, 5(12), p.1359.

Field, C.M. et al., 2005. Characterization of anillin mutants reveals essential roles in septin localization and plasma membrane integrity. *Development*, 132, pp.2849–2860.

Field, C.M. & Alberts, B.M., 1995. Anillin, a Contractile Ring Protein That Cycles from the Nucleus to the Cell Cortex. *The Journal of cell biology*, 131(1), pp.165–178.

Folkman, J., 1971. Tumor angiogenesis: therapeutic implications. *New england journal of medicine*, 285(21), pp.1182–1186.

Fotopoulos, N. et al., 2013. Caenorhabditis elegans anillin (ani-1) regulates neuroblast cytokinesis and epidermal morphogenesis during embryonic development. *Developmental Biology*, 383(1), pp.61–74. Available at: http://dx.doi.org/10.1016/j.ydbio.2013.08.024.

Fuster, V. et al., 1992. The pathogenesis of coronary artery disease and the acute coronary syndromes. *New England journal of medicine*, 326(5), pp.310–318.

Gaengel, K. et al., 2009. Endothelial-mural cell signaling in vascular development and angiogenesis. *Arteriosclerosis, thrombosis, and vascular biology*, 29(5), pp.630–638.

Galbán, S. et al., 2008. RNA-binding proteins HuR and PTB promote the translation of hypoxia-inducible factor 1α. *Molecular and cellular biology*, 28(1), pp.93–107.

Galloway, J.L. et al., 2005. Loss of Gata1 but not Gata2 converts erythropoiesis to myelopoiesis in zebrafish embryos. *Developmental Cell*, 8(1), pp.109–116.

Garneau, N.L., Wilusz, J. & Wilusz, C.J., 2007. The highways and byways of mRNA decay. *Nature Reviews Molecular Cell Biology*, 8, p.113. Available at:

https://doi.org/10.1038/nrm2104.

Gbadegesin, R.A. et al., 2014. Mutations in the Gene That Encodes the F-Actin Binding Protein Anillin Cause FSGS. *Journal of the American Society of Nephrology*, 25(9), pp.1991–2002. Available at: http://www.jasn.org/cgi/doi/10.1681/ASN.2013090976.

Gerhardt, H. et al., 2003. VEGF guides angiogenic sprouting utilizing endothelial tip cell filopodia. *The Journal of cell biology*, 161(6), pp.1163–1177.

Giannotta, M., Trani, M. & Dejana, E., 2013. VE-cadherin and endothelial adherens junctions: active guardians of vascular integrity. *Developmental cell*, 26(5), pp.441–454.

Gong, Y. & Koh, D.-R., 2010. Neutrophils promote inflammatory angiogenesis via release of preformed VEGF in an in vivo corneal model. *Cell and tissue research*, 339(2), pp.437–448.

González-Rosa, J.M. et al., 2011. Extensive scar formation and regression during heart regeneration after cryoinjury in zebrafish. *Development*, p.dev-060897.

Gray, C. et al., 2007. Ischemia is not required for arteriogenesis in zebrafish embryos. *Arteriosclerosis, thrombosis, and vascular biology*, 27(10), pp.2135–2141.

Grunwald, D.J. & Streisinger, G., 1992. Induction of recessive lethal and specific locus mutations in the zebrafish with ethyl nitrosourea. *Genetics Research*, 59(2), pp.103–116.

Gurevich, D.B. et al., 2016. Asymmetric division of clonal muscle stem cells coordinates muscle regeneration in vivo. *Science*, 353(6295), p.aad9969.

Gurevich, D.B. et al., 2018. Live imaging of wound angiogenesis reveals macrophage orchestrated vessel sprouting and regression. *The EMBO journal*, p.e97786.

Le Guyader, D. et al., 2008. Origins and unconventional behavior of neutrophils in developing zebrafish. *Blood*, 111(1), pp.132–141.

Hacker, C., Valchanova, R., Adams, S. & Munz, B., 2010. ZFP36L1 is regulated by growth factors and cytokines in keratinocytes and influences their VEGF production. *Growth Factors*, 28(3), pp.178–190.

Hacker, C., Valchanova, R., Adams, S., Munz, B., et al., 2010. ZFP36L1 is regulated by growth factors and cytokines in keratinocytes and influences their VEGF production. , 28(3)(june), pp.178–190.

Haffter, P. & Nusslein-Volhard, C., 2003. Large scale genetics in a small vertebrate, the zebrafish. *International Journal of Developmental Biology*, 40(1), pp.221–227.

Haglund, K. et al., 2010. Cindr Interacts with Anillin to Control Cytokinesis in Drosophila melanogaster. *Current Biology*, 20(10), pp.944–950.

Hall, G. et al., 2018. The Human FSGS-Causing ANLN R431C Mutation Induces Dysregulated PI3K/AKT/mTOR/Rac1 Signaling in Podocytes. *Journal of the American Society of Nephrology*, 29(8), p.2110 LP-2122. Available at: http://jasn.asnjournals.org/content/29/8/2110.abstract.

Hall, P.A. et al., 2005. Human Cancer Biology The Septin-Binding Protein Anillin Is Overexpressed in Diverse Human T umors. , 11(19), pp.6780–6787.

Hausburg, M.A., Doles, J.D., Clement, S.L., Cadwallader, A.B., Hall, M.N., Blackshear, P.J., Lykke-andersen, J., et al., 2015. Post-transcriptional regulation of satellite cell quiescence by TTP-mediated mRNA decay. *eLife*, 4, pp.1–18.

Hausburg, M.A., Doles, J.D., Clement, S.L., Cadwallader, A.B., Hall, M.N., Blackshear, P.J., Lykke-Andersen, J., et al., 2015. Post-transcriptional regulation of satellite cell quiescence by TTP-mediated mRNA decay M. Buckingham, ed. *eLife*, 4, p.e03390. Available at: https://dx.doi.org/10.7554/eLife.03390.

Heiss, M. et al., 2015. Endothelial cell spheroids as a versatile tool to study angiogenesis in vitro. *FASEB Journal*, 29(7), pp.3076–3084.

Hennekens, C.H. & Gaziano, J.M., 1993. Antioxidants and heart disease:

epidemiology and clinical evidence. *Clinical cardiology*, 16(S1), pp.10–15.

Henry, T.D. et al., 2013. Long-term survival in patients with refractory angina. *European heart journal*, 34(34), pp.2683–2688.

Henry, T.D., Satran, D. & Jolicoeur, E.M., 2014. Treatment of refractory angina in patients not suitable for revascularization. *Nature Reviews Cardiology*, 11(2), p.78.

Herbert, S.P. et al., 2009. Arterial-venous segregation by selective cell sprouting: an alternative mode of blood vessel formation. *Science*, 326(5950), pp.294–298.

Herz, K. et al., 2018. Visualization of endothelial cell cycle dynamics in mouse using the Flt - 1 / eGFP - anillin system. *Angiogenesis*, 21(2), pp.349–361. Available at: https://doi.org/10.1007/s10456-018-9601-1.

Hesse, M. et al., 2012. Direct visualization of cell division using high-resolution imaging of M-phase of the cell cycle. *Nature communications*, 3, p.1076.

Hlatky, M. a et al., 2004. Medical costs and quality of life 10 to 12 years after randomization to angioplasty or bypass surgery for multivessel coronary artery disease. *Circulation*, 110(14), pp.1960–6. Available at: http://www.ncbi.nlm.nih.gov/pubmed/15451795 [Accessed January 5, 2014].

Hlushchuk, R. et al., 2016. Zebrafish Caudal Fin Angiogenesis Assay—Advanced Quantitative Assessment Including 3-Way Correlative Microscopy. *PloS one*, 11(3), p.e0149281.

Hodson, D.J. et al., 2010. Deletion of the RNA-binding proteins ZFP36L1 and ZFP36L2 leads to perturbed thymic development and T lymphoblastic leukemia. *Nature immunology*, 11(8), pp.717–724.

Hofmann, W.A. et al., 2004. Actin is part of pre-initiation complexes and is necessary for transcription by RNA polymerase II. *Nature cell biology*, 6(11), p.1094.

Howe, K. et al., 2013. The zebrafish reference genome sequence and its relationship

to the human genome. *Nature*, 496(7446), p.498.

Hudson, B.P. et al., 2004. Recognition of the mRNA AU-rich element by the zinc finger domain of TIS11d. *Nature Structural and Molecular Biology*, 11(3), pp.257–264.

Isogai, S. et al., 2003. Angiogenic network formation in the developing vertebrate trunk. *Development*, 130(21), pp.5281–5290.

Isogai, S., Horiguchi, M. & Weinstein, B.M., 2001. The vascular anatomy of the developing zebrafish: an atlas of embryonic and early larval development. *Developmental biology*, 230(2), pp.278–301.

Itoh, M. et al., 2003. Mind bomb is a ubiquitin ligase that is essential for efficient activation of Notch signaling by Delta. *Developmental cell*, 4(1), pp.67–82.

Jia, Y. et al., 2011. Ultrahigh sensitive optical microangiography reveals depth-resolved microcirculation and its longitudinal response to prolonged ischemic event within skeletal muscles in mice. *Journal of biomedical optics*, 16(8), p.86004.

Jin, S.-W. et al., 2005. Cellular and molecular analyses of vascular tube and lumen formation in zebrafish. *Development*, 132(23), pp.5199–5209.

Kamei, M. et al., 2006. Endothelial tubes assemble from intracellular vacuoles in vivo. *Nature*, 442(7101), p.453.

Kamei, M. & Weinstein, B.M., 2005. Long-term time-lapse fluorescence imaging of developing zebrafish. *Zebrafish*, 2(2), pp.113–123.

Kamphuis, W. et al., 2007. Global gene expression profiling of ischemic preconditioning in the rat retina. *Molecular vision*, 13, pp.1020–1030. Available at: https://www.ncbi.nlm.nih.gov/pubmed/17653046.

Kang, J. et al., 2016a. Modulation of tissue repair by regeneration enhancer elements. *Nature*, 532(7598), pp.201–206. Available at: http://dx.doi.org/10.1038/nature17644.

Kang, J. et al., 2016b. Modulation of tissue repair by regeneration enhancer elements. *Nature*, 532(7598), pp.201–206. Available at: http://dx.doi.org/10.1038/nature17644.

Karsan, A., 2005. The role of notch in modeling and maintaining the vasculature. *Canadian journal of physiology and pharmacology*, 83(1), pp.14–23.

Kendall, R.L. & Thomas, K.A., 1993. Inhibition of vascular endothelial cell growth factor activity by an endogenously encoded soluble receptor. *Proceedings of the National Academy of Sciences*, 90(22), pp.10705–10709.

King, E.M. et al., 2009. Regulation of Tristetraprolin Expression by Interleukin-1 and Dexamethasone in Human Pulmonary Epithelial Cells: Roles for Nuclear Factor-B and p38 Mitogen-Activated Protein Kinase. *Journal of Pharmacology and Experimental Therapeutics*, 330(2), pp.575–585. Available at: http://jpet.aspetjournals.org/cgi/doi/10.1124/jpet.109.151423.

Kinoshita, M. et al., 2002. Self-and actin-templated assembly of mammalian septins. *Developmental cell*, 3(6), pp.791–802.

Klagsbrun, M. & D'amore, P.A., 1991. Regulators of angiogenesis. *Annual review of physiology*, 53(1), pp.217–239.

Knoblich, J.A., 2008. Mechanisms of asymmetric stem cell division. *Cell*, 132(4), pp.583–597.

Kobayashi, K. et al., 2017. Dynamics of angiogenesis in ischemic areas of the infarcted heart. *Scientific reports*, 7(1), p.7156.

Kofler, N.M. & Simons, M., 2015. Angiogenesis versus arteriogenesis: neuropilin 1 modulation of VEGF signaling. *F1000prime reports*, 7.

Krock, B.L., Skuli, N. & Simon, M.C., 2011. Hypoxia-induced angiogenesis: good and evil. *Genes & cancer*, 2(12), pp.1117–1133.

Krump-Konvalinkova, V. et al., 2005. Stable knock-down of the sphingosine 1-phosphate receptor S1P1 influences multiple functions of human endothelial

cells. *Arteriosclerosis, thrombosis, and vascular biology*, 25(3), pp.546–52. Available at: http://www.ncbi.nlm.nih.gov/pubmed/15618544 [Accessed January 16, 2014].

Lai, W.S. et al., 2014. Mutational and structural analysis of the tandem zinc finger domain of tristetraprolin. *Journal of Biological Chemistry*, 289(1), pp.565–580.

Lake, C.L., 1985. Cardiovascular anatomy and physiology. In *Cardiovascular Anesthesia*. Springer, pp. 1–14.

Lang, P.D. & Insull, W., 1970. Lipid droplets in atherosclerotic fatty streaks of human aorta. *The Journal of clinical investigation*, 49(8), pp.1479–1488.

Lappe-Siefke, C. et al., 2003. Disruption of Cnp1 uncouples oligodendroglial functions in axonal support and myelination. *Nature genetics*, 33(3), p.366.

Lawson, N.D., Vogel, A.M. & Weinstein, B.M., 2002. sonic hedgehog and vascular endothelial growth factor Act Upstream of the Notch Pathway during Arterial Endothelial Differentiation. *Developmental Cell*, 3(1), pp.127–136. Available at: http://www.sciencedirect.com/science/article/pii/S1534580702001983.

Lawson, N.D. & Weinstein, B.M., 2002. Arteries and veins: making a difference with zebrafish. *Nature Reviews Genetics*, 3(9), p.674.

Lazarous, D.F. et al., 1997. Pharmacodynamics of basic fibroblast growth factor: route of administration determines myocardial and systemic distribution. *Cardiovascular research*, 36(1), pp.78–85.

Lieschke, G.J. et al., 2008. macrophages in embryonic and adult zebrafish Morphologic and functional characterization of granulocytes and macrophages in embryonic and adult zebrafish. , 98(10), pp.3087–3096.

Lindblom, P. et al., 2003. Endothelial PDGF-B retention is required for proper investment of pericytes in the microvessel wall. *Genes and Development*, 17(15), pp.1835–1840.

Liu, C. et al., 2016. Macrophages Mediate the Repair of Brain Vascular Rupture

through Direct Physical Adhesion and Mechanical Traction. *Immunity*, 44(5), pp.1162–1176.

Liu, C., Zhu, R. & Mao, Y., 2018. Nuclear Actin Polymerized by mDia2 Confines Centromere Movement during CENP-A Loading. *iScience*, 9, pp.314–327. Available at: https://www.ncbi.nlm.nih.gov/pubmed/30448731.

Liu, J., Fairn, G.D., et al., 2012. Cleavage furrow organization requires PIP 2-mediated recruitment of anillin. *Current Biology*, 22(1), pp.64–69. Available at: http://dx.doi.org/10.1016/j.cub.2011.11.040.

Liu, J., Fairn, G.D., et al., 2012. Cleavage furrow organization requires PIP2-mediated recruitment of anillin. *Current biology*, 22(1), pp.64–69.

Livet, J. et al., 2007. Transgenic strategies for combinatorial expression of fluorescent proteins in the nervous system. *Nature*, 450(7166), pp.56–62.

Lobov, I.B. et al., 2007. Delta-like ligand 4 (Dll4) is induced by VEGF as a negative regulator of angiogenic sprouting. *Proceedings of the National Academy of Sciences of the United States of America*, 104(9), pp.3219–3224. Available at: https://www.ncbi.nlm.nih.gov/pubmed/17296940.

Ma, H. et al., 2016. Multiplexed labeling of genomic loci with dCas9 and engineered sgRNAs using CRISPRainbow. *Nature biotechnology*, 34(5), p.528.

Maddox, A.S. et al., 2005. Distinct roles for two C. elegans anillins in the gonad and early embryo. *Development*, 132(12), pp.2837–2848.

Magnusson, K. et al., 2016. ANLN is a prognostic biomarker independent of Ki-67 and essential for cell cycle progression in primary breast cancer. *BMC Cancer*, 16(1), p.904. Available at: https://doi.org/10.1186/s12885-016-2923-8.

Malo, M.C. et al., 2017. The Zebrafish Anillin-eGFP Reporter Marks Late Dividing Retinal Precursors and Stem Cells Entering Neuronal Lineages. , pp.1–15.

Manoli, M. & Driever, W., 2012. Fluorescence-activated cell sorting (FACS) of fluorescently tagged cells from zebrafish larvae for RNA isolation. *Cold Spring*

Harbor Protocols, 7(8), pp.879–886.

Manukyan, A. et al., 2015. A complex of p190RhoGAP-A and anillin modulates RhoA-GTP and the cytokinetic furrow in human cells. *Journal of Cell Science*, 128(1), pp.50–60. Available at: http://www.ncbi.nlm.nih.gov/pmc/articles/PMC4282047/.

Marín-Juez, R. et al., 2016. Fast revascularization of the injured area is essential to support zebrafish heart regeneration. *Proceedings of the National Academy of Sciences*, 113(40), p.11237 LP-11242. Available at: http://www.pnas.org/content/113/40/11237.abstract.

Matrone, G. et al., 2015. CDK9 and its repressor LARP7 modulate cardiomyocyte proliferation and response to injury in the zebrafish heart. *J Cell Sci*, 128(24), pp.4560–4571.

Matrone, G. et al., 2013. Laser-targeted ablation of the zebrafish embryonic ventricle: a novel model of cardiac injury and repair. *International journal of cardiology*, 168(4), pp.3913–3919.

Matrone, G. et al., 2014. Targeted Laser Ablation of the Zebrafish Larval Heart Induces Models of Heart Block, Valvular Regurgitation, and Outflow Tract Obstruction. *Zebrafish*, 11(6), pp.536–541.

Mattichak, S.J. et al., 2008. Failed percutaneous coronary intervention: a decade of experience in 21,000 patients. *Catheterization and Cardiovascular Interventions*, 71(2), pp.131–137.

McClelland, L., Jasper, H. & Biteau, B., 2017. Tis11 mediated mRNA decay promotes the reacquisition of Drosophila intestinal stem cell quiescence. *Developmental Biology*, 426(1), pp.8–16. Available at: http://dx.doi.org/10.1016/j.ydbio.2017.04.013.

McFaline-Figueroa, J.R. et al., 2011. Mitochondrial quality control during inheritance is associated with lifespan and mother-daughter age asymmetry in budding

yeast. *Aging Cell*, 10(5), pp.885–895.

Merhi-Soussi, F. et al., 2005. Interleukin-1 plays a major role in vascular inflammation and atherosclerosis in male apolipoprotein E-knockout mice. *Cardiovascular Research*, 66(3), pp.583–593. Available at: http://dx.doi.org/10.1016/j.cardiores.2005.01.008.

Mikawa, M., Su, L. & Parsons, S.J., 2008. Opposing Roles of p190RhoGAP and Ect2 RhoGEF in Regulating Cytokinesis. *Cell cycle (Georgetown, Tex.)*, 7(13), pp.2003–2012. Available at: http://www.ncbi.nlm.nih.gov/pmc/articles/PMC2791401/.

Miller, A.L., 2011. The contractile ring. *Current biology : CB*, 21(24), pp.R976–R978. Available at: https://www.ncbi.nlm.nih.gov/pubmed/22192825.

Miller, K.G., Field, C.M. & Alberts, B.M., 1989. Actin-binding proteins from Drosophila embryos: a complex network of interacting proteins detected by F-actin affinity chromatography. *The Journal of cell biology*, 109(6), pp.2963–2975.

Misu, S., Takebayashi, M. & Miyamoto, K., 2017. Nuclear Actin in Development and Transcriptional Reprogramming. *Frontiers in genetics*, 8, p.27. Available at: https://www.ncbi.nlm.nih.gov/pubmed/28326098.

Mitchell, P. & Tollervey, D., 2000. mRNA stability in eukaryotes. *Current opinion in genetics & development*, 10(2), pp.193–198.

Mohiuddin, M. et al., 2019. Critical Limb Ischemia Induces Remodeling of Skeletal Muscle Motor Unit, Myonuclear-, and Mitochondrial-Domains. *Scientific reports*, 9(1), p.9551.

Monahan-Earley, R., Dvorak, A.M. & Aird, W.C., 2013. Evolutionary origins of the blood vascular system and endothelium. *Journal of Thrombosis and Haemostasis*, 11, pp.46–66.

Montorsi, L. et al., 2016. Loss of zfp36 expression in colorectal cancer correlates to

wnt / ß-catenin activity and enhances epithelial-to-mesenchymal transition through upregulation of zeb1 , sox9 and macc1. *oncotarget*, 7(37).

Mukherjee, N. et al., 2014. Global target mRNA specification and regulation by the RNA-binding protein ZFP36. *Genome Biology*, 15(1), pp.1–16.

Newby, A.C. & Zaltsman, A.B., 1999. Fibrous cap formation or destruction—the critical importance of vascular smooth muscle cell proliferation, migration and matrix formation. *Cardiovascular research*, 41(2), pp.345–360.

Newman, R. et al., 2017. Maintenance of the marginal-zone B cell compartment specifically requires the RNA-binding protein ZFP36L1. *Nature Immunology*, 18(6), pp.683–693.

Ogryzko, N. V et al., 2014. Zebrafish tissue injury causes upregulation of interleukin-1 and caspase-dependent amplification of the inflammatory response. *Disease models & mechanisms*, 7(2), pp.259–264.

van Oostende Triplet, C. et al., 2014. Anillin interacts with microtubules and is part of the astral pathway that defines cortical domains. *Journal of Cell Science*, 127(17), pp.3699–3710. Available at: http://jcs.biologists.org/cgi/doi/10.1242/jcs.147504.

Ouriel, K., 2001. Peripheral arterial disease. *Lancet*, 358, pp.1257–1264.

Pacquelet, A. et al., 2015. PAR-4 and anillin regulate myosin to coordinate spindle and furrow position during asymmetric division. , 210(7), pp.1085–1099.

Paolini, A. et al., 2015. Asymmetric inheritance of the apical domain and self-renewal of retinal ganglion cell progenitors depend on Anillin function. , pp.832–839.

Pardali, E., Goumans, M.-J. & ten Dijke, P., 2010. Signaling by members of the TGF-β family in vascular morphogenesis and disease. *Trends in cell biology*, 20(9), pp.556–567.

Patel-Hett, S. & D'Amore, P.A., 2011. Signal transduction in vasculogenesis and

developmental angiogenesis. *The International journal of developmental biology*, 55, p.353.

Pfeiler, S. et al., 2017. Propagation of thrombosis by neutrophils and extracellular nucleosome networks. *Haematologica*, 102(2), pp.206–213.

Piekny, A.J. & Glotzer, M., 2008. Anillin is a scaffold protein that links RhoA, actin, and myosin during cytokinesis. *Current biology : CB*, 18(1), pp.30–6. Available at: http://www.ncbi.nlm.nih.gov/pubmed/18158243 [Accessed January 5, 2015].

Piekny, A.J. & Maddox, A.S., 2010. The myriad roles of Anillin during cytokinesis. *Seminars in Cell and Developmental Biology*, 21(9), pp.881–891. Available at: http://dx.doi.org/10.1016/j.semcdb.2010.08.002.

Pollack, A.L., Runyan, R.B. & Mostov, K.E., 1998. Morphogenetic mechanisms of epithelial tubulogenesis: MDCK cell polarity is transiently rearranged without loss of cell-cell contact during scatter factor/hepatocyte growth factor-induced tubulogenesis. *Developmental Biology*, 204(1), pp.64–79.

Postlethwait, J.H. et al., 1998. Vertebrate genome evolution and the zebrafish gene map. *Nature genetics*, 18(4), p.345.

Postlethwait, J.H. et al., 2000. Zebrafish comparative genomics and the origins of vertebrate chromosomes. *Genome research*, 10(12), pp.1890–1902.

Potente, M., Gerhardt, H. & Carmeliet, P., 2011. Basic and therapeutic aspects of angiogenesis. *Cell*, 146(6), pp.873–887. Available at: http://dx.doi.org/10.1016/j.cell.2011.08.039.

Pulak, R., 2016. Tools for automating the imaging of zebrafish larvae. *Methods*, 96, pp.118–126.

Rataj, F. et al., 2016. The cAMP pathway regulates mRNA decay through phosphorylation of the RNA-binding protein TIS11b/BRF1. *Molecular biology of the cell*, 27(24), pp.3841–3854.

Renshaw, S.A. et al., 2006. A transgenic zebrafish model of neutrophilic inflammation. *Blood*, 108(13), pp.3976–3978.

Reyes, C.C. et al., 2014. Anillin regulates cell-cell junction integrity by organizing junctional accumulation of Rho-GTP and actomyosin. *Current Biology*, 24(11), pp.1263–1270. Available at: http://dx.doi.org/10.1016/j.cub.2014.04.021.

Roberts, D.M. et al., 2004. The vascular endothelial growth factor (VEGF) receptor Flt-1 (VEGFR-1) modulates Flk-1 (VEGFR-2) signaling during blood vessel formation. *The American journal of pathology*, 164(5), pp.1531–1535.

Rogers, S.L. et al., 2003. Molecular requirements for actin-based lamella formation in Drosophila S2 cells. *The Journal of cell biology*, 162(6), pp.1079–1088.

Rosberger, D.F., 2013. Diabetic retinopathy: current concepts and emerging therapy. *Endocrinology and Metabolism Clinics*, 42(4), pp.721–745.

Ross, R., 1999. Atherosclerosis—an inflammatory disease. *New England journal of medicine*, 340(2), pp.115–126.

Saha, R. et al., 2013. Light driven ultrafast electron transfer in oxidative redding of Green Fluorescent Proteins. *Scientific Reports*, 3, pp.1–7.

Sandler, H. et al., 2011. Not1 mediates recruitment of the deadenylase Caf1 to mRNAs targeted for degradation by tristetraprolin. *Nucleic acids research*, 39(10), pp.4373–4386. Available at: https://www.ncbi.nlm.nih.gov/pubmed/21278420.

Sanduja, S. et al., 2012. The role of tristetraprolin in cancer and inflammation. *Frontiers in bioscience (Landmark edition)*, 17, pp.174–188. Available at: https://www.ncbi.nlm.nih.gov/pubmed/22201737.

Sasso, F.C. et al., 2005. Increased vascular endothelial growth factor expression but impaired vascular endothelial growth factor receptor signaling in the myocardium of type 2 diabetic patients with chronic coronary heart disease. *Journal of the American College of Cardiology*, 46(5), pp.827–834.

Scholz, D. et al., 2002. Contribution of arteriogenesis and angiogenesis to postocclusive hindlimb perfusion in mice. *Journal of molecular and cellular cardiology*, 34(7), pp.775–787.

Schroeder, T., 2007. Asymmetric cell division in normal and malignant hematopoietic precursor cells. *Cell stem cell*, 1(5), pp.479–481.

Schüpbach, T. & Wieschaus, E., 1991. Female sterile mutations on the second chromosome of Drosophila melanogaster. II. Mutations blocking oogenesis or altering egg morphology. *Genetics*, 129(4), pp.1119–1136.

Semenza, G.L., 2012. Hypoxia-inducible factors in physiology and medicine. *Cell*, 148(3), pp.399–408.

Shweiki, D. et al., 1992. Vascular endothelial growth factor induced by hypoxia may mediate hypoxia-initiated angiogenesis. *Nature*, 359(6398), p.843.

Siddall, M.E., 2004. Invertebrates.—R.C. Brusca and G. J. Brusca. 2003. Sinauer Associates, Sunderland, Massachusetts. xix + 936 pp. ISBN 0–87893–097–3. $109.95(cloth). *Systematic Biology*, 53(4), pp.664–666. Available at: http://dx.doi.org/10.1080/10635150490472968.

Silverman-Gavrila, R. V, Hales, K.G. & Wilde, A., 2008. Anillin-mediated targeting of peanut to pseudocleavage furrows is regulated by the GTPase Ran. *Molecular biology of the cell*, 19(9), pp.3735–3744.

Silvestre, J.-S., Smadja, D.M. & Levy, B.I., 2013. Postischemic revascularization: from cellular and molecular mechanisms to clinical applications. *Physiological reviews*, 93(4), pp.1743–1802.

De Smet, F. et al., 2009. Mechanisms of vessel branching: filopodia on endothelial tip cells lead the way. *Arteriosclerosis, thrombosis, and vascular biology*, 29(5), pp.639–649.

Soker, S. et al., 1998. Neuropilin-1 is expressed by endothelial and tumor cells as an isoform-specific receptor for vascular endothelial growth factor. *Cell*, 92(6),

pp.735–745.

Sotiropoulos, A. et al., 1999. Signal-regulated activation of serum response factor is mediated by changes in actin dynamics. *Cell*, 98(2), pp.159–169.

Stainier, D.Y. et al., 1995. Cloche, an early acting zebrafish gene, is required by both the endothelial and hematopoietic lineages. *Development (Cambridge, England)*, 121(10), pp.3141–3150.

Stark, K. et al., 2013. Capillary and arteriolar pericytes attract innate leukocytes exiting through venules and “instruct” them with pattern-recognition and motility programs. *Nature immunology*, 14(1), pp.41–51. Available at: http://www.ncbi.nlm.nih.gov/pubmed/23179077.

Staton, C.A., Reed, M.W.R. & Brown, N.J., 2009. A critical analysis of current in vitro and in vivo angiogenesis assays. *International journal of experimental pathology*, 90(3), pp.195–221.

Steinbrecher, U.P. et al., 1984. Modification of low density lipoprotein by endothelial cells involves lipid peroxidation and degradation of low density lipoprotein phospholipids. *Proceedings of the National Academy of Sciences*, 81(12), pp.3883–3887.

Stemple, D.L., 2005. Structure and function of the notochord: an essential organ for chordate development. *Development*, 132(11), p.2503 LP-2512. Available at: http://dev.biologists.org/content/132/11/2503.abstract.

Stetler-Stevenson, W.G. & Seo, D.-W., 2005. TIMP-2: an endogenous inhibitor of angiogenesis. *Trends in molecular medicine*, 11(3), pp.97–103.

Straight, A.F., Field, C.M. & Mitchison, T.J., 2005. Anillin binds nonmuscle myosin II and regulates the contractile ring. *Molecular biology of the cell*, 16(1), pp.193–201.

Strilić, B. et al., 2009. The molecular basis of vascular lumen formation in the developing mouse aorta. *Developmental cell*, 17(4), pp.505–515.

Stumpo, D.J. et al., 2004. Chorioallantoic Fusion Defects and Embryonic Lethality Resulting from Disruption of Zfp36L1 , a Gene Encoding a CCCH Tandem Zinc Finger Protein of the Tristetraprolin Family. *Molecular and cellular biology*, 24(14), pp.6445–6455.

Stüven, T., Hartmann, E. & Görlich, D., 2003. Exportin 6: a novel nuclear export receptor that is specific for profilin· actin complexes. *The EMBO journal*, 22(21), pp.5928–5940.

Suk, F.-M. et al., 2018. ZFP36L1 and ZFP36L2 inhibit cell proliferation in a cyclin D-dependent and p53-independent manner. *Scientific Reports*, 8(1), p.2742. Available at: http://www.nature.com/articles/s41598-018-21160-z.

Sun, L. et al., 2007. Tristetraprolin (TTP)-14-3-3 complex formation protects TTP from dephosphorylation by protein phosphatase 2a and stabilizes tumor necrosis factor-α mRNA. *Journal of Biological Chemistry*, 282(6), pp.3766–3777.

Suzuki, C. et al., 2005. ANLN plays a critical role in human lung carcinogenesis through the activation of RHOA and by involvement in the phosphoinositide 3-kinase/AKT pathway. *Cancer research*, 65(24), pp.11314–11325.

Taggart, D.P., 2013. CABG or stents in coronary artery disease: end of the debate? *The Lancet*, 381(9867), pp.605–607.

Taggart, D.P., 2012. Incomplete revascularization: appropriate and inappropriate. *European Journal of Cardio-Thoracic Surgery*, 41(3), pp.542–543. Available at: http://dx.doi.org/10.1093/ejcts/ezr298.

Taggart, D.P. et al., 2006. Protocol for the Arterial Revascularisation Trial (ART). A randomised trial to compare survival following bilateral versus single internal mammary grafting in coronary revascularisation [ISRCTN46552265]. *Trials*, 7(1), p.7.

Takahashi, H. & Shibuya, M., 2005. The vascular endothelial growth factor (VEGF)/VEGF receptor system and its role under physiological and pathological

conditions. *Clinical science*, 109(3), pp.227–241.

Taylor, G. a. et al., 1996. A pathogenetic role for TNFα in the syndrome of cachexia, arthritis, and autoimmunity resulting from tristetraprolin (TTP) deficiency. *Immunity*, 4(5), pp.445–454.

Tian, D. et al., 2015. Anillin Regulates Neuronal Migration and Neurite Growth by Linking RhoG to the Actin Cytoskeleton Article Anillin Regulates Neuronal Migration and Neurite Growth by Linking RhoG to the Actin Cytoskeleton. *Current Biology*, 25(9), pp.1135–1145. Available at: http://dx.doi.org/10.1016/j.cub.2015.02.072.

Timme-Laragy, A.R., Karchner, S.I. & Hahn, M.E., 2012. Gene knockdown by morpholino-modified oligonucleotides in the zebrafish (Danio rerio) model: applications for developmental toxicology. In *Developmental Toxicology*. Springer, pp. 51–71.

Tischer, E. et al., 1991. The human gene for vascular endothelial growth factor. Multiple protein forms are encoded through alternative exon splicing. *Journal of Biological Chemistry*, 266(18), pp.11947–11954.

Varnum, B.C. et al., 1991. The TIS11 primary response gene is a member of a gene family that encodes proteins with a highly conserved sequence containing an unusual Cys-His repeat. *Molecular and cellular biology*, 11(3), pp.1754–8. Available at: http://www.pubmedcentral.nih.gov/articlerender.fcgi?artid=369492&tool=pmcentrez&rendertype=abstract.

Vlodaver, Z. & Edwards, J.E., 1971. Pathology of coronary atherosclerosis. *Progress in cardiovascular diseases*, 14(3), pp.256–274.

Vogel, K.U. et al., 2016. The RNA-Binding Proteins Zfp36l1 and Zfp36l2 Enforce the Thymic β-Selection Checkpoint by Limiting DNA Damage Response Signaling and Cell Cycle Progression. *Journal of immunology (Baltimore, Md. : 1950)*, 197(7), pp.2673–2685. Available at:

https://www.ncbi.nlm.nih.gov/pubmed/27566829.

De Vries, M.R. et al., 2016. Vein graft failure: from pathophysiology to clinical outcomes. *Nature Reviews Cardiology*, 13(8), p.451.

Waltenberger, J. et al., 1994. Different signal transduction properties of KDR and Flt1, two receptors for vascular endothelial growth factor. *Journal of Biological Chemistry*, 269(43), pp.26988–26995.

Waltenberger, J., Lange, J. & Kranz, A., 2000. Vascular endothelial growth factor-A–induced chemotaxis of monocytes is attenuated in patients with diabetes mellitus: a potential predictor for the individual capacity to develop collaterals. *Circulation*, 102(2), pp.185–190.

Wang, D. et al., 2015. F-actin binding protein, anillin, regulates integrity of intercellular junctions in human epithelial cells. *Cellular and Molecular Life Sciences*, 72(16), pp.3185–3200.

Wang, J. et al., 2010. Müller cell-derived VEGF is essential for diabetes-induced retinal inflammation and vascular leakage. *Diabetes*.

Wang, Y. et al., 2010. Moesin1 and Ve-cadherin are required in endothelial cells during in vivo tubulogenesis. *Development*, 137(18), pp.3119–3128.

Watanabe, S. et al., 2008. mDia2 Induces the Actin Scaffold for the Contractile Ring and Stabilizes Its Position during Cytokinesis in NIH 3T3 Cells. *Molecular biology of the cell*, 19(May), pp.2328–2338.

Watanabe, S. et al., 2010. Rho and Anillin-dependent Control of mDia2 Localization and Function in Cytokinesis F. Chang, ed. *Molecular Biology of the Cell*, 21(18), pp.3193–3204. Available at: http://www.ncbi.nlm.nih.gov/pmc/articles/PMC2938385/.

Watson, O. et al., 2013. Blood flow suppresses vascular Notch signalling via dll4 and is required for angiogenesis in response to hypoxic signalling. *Cardiovascular Research*, 100(2), pp.252–261.

Weavers, H. & Skaer, H., 2014. Tip cells: master regulators of tubulogenesis? *Seminars in cell & developmental biology*, 31(100), pp.91–99. Available at: https://www.ncbi.nlm.nih.gov/pubmed/24721475.

Wegmüller, D. et al., 2007. A Cassette System to Study Embryonic Stem Cell Differentiation by Inducible RNA Interference. *STEM CELLS*, 25(5), pp.1178–1185. Available at: http://dx.doi.org/10.1634/stemcells.2006-0106.

Weis, S.M. & Cheresh, D.A., 2005. Pathophysiological consequences of VEGF-induced vascular permeability. *Nature*, 437(7058), p.497.

Welch, E.M. et al., 2009. Targeting post-transcriptional control for drug discovery AU - Peltz, Stuart W. *RNA Biology*, 6(3), pp.329–334. Available at: https://doi.org/10.4161/rna.6.3.8953.

Willett, C.E. et al., 1999. Early hematopoiesis and developing lymphoid organs in the zebrafish. *Developmental Dynamics*, 214(4), pp.323–336.

Xiong, J., 2008. Molecular and developmental biology of the hemangioblast. *Developmental dynamics: an official publication of the American Association of Anatomists*, 237(5), pp.1218–1231.

Xu, H. et al., 2015. Sequence determinants of improved CRISPR sgRNA design. *Genome Research*, 25(8), pp.1147–1157.

Yoo, K.-W. et al., 2006. Snx5, as a Mind bomb-binding protein, is expressed in hematopoietic and endothelial precursor cells in zebrafish. *FEBS letters*, 580(18), pp.4409–4416.

Zeeb, M., Strilic, B. & Lammert, E., 2010. Resolving cell–cell junctions: lumen formation in blood vessels. *Current opinion in cell biology*, 22(5), pp.626–632.

Zhang, S. et al., 2018. Knockdown of Anillin Actin Binding Protein Blocks Cytokinesis in Hepatocytes and Reduces Liver Tumor Development in Mice Without Affecting Regeneration. *Gastroenterology*, 154(5), pp.1421–1434. Available at: https://doi.org/10.1053/j.gastro.2017.12.013.

Zhao, W. & Fang, G., 2005. Anillin is a substrate of anaphase-promoting complex/cyclosome (APC/C) that controls spatial contractility of myosin during late cytokinesis. *Journal of Biological Chemistry*, 280(39), pp.33516–33524.

Zhen, F. et al., 2013. Hemogenic endothelium specification and hematopoietic stem cell maintenance employ distinct Scl isoforms. *Development*, 140(19), pp.3977–3985. Available at: http://dev.biologists.org/lookup/doi/10.1242/dev.097071.

Zhou, W., Wang, Z. & Shen, N., 2015. Knockdown of ANLN by lentivirus inhibits cell growth and migration in human breast cancer. *Mol Cell Biochem*, 398, pp.11–19.

Ziegler, M.A. et al., 2010. Marvels, mysteries, and misconceptions of vascular compensation to peripheral artery occlusion. *Microcirculation*, 17(1), pp.3–20.

Ziyadeh, F.N. et al., 2000. Long-term prevention of renal insufficiency, excess matrix gene expression, and glomerular mesangial matrix expansion by treatment with monoclonal antitransforming growth factor-β antibody in db/db diabetic mice. *Proceedings of the National Academy of Sciences*, 97(14), pp.8015–8020.